GERMANY

VDC (Verband der Cigarettenindustrie)

DRAFT RESEARCH PROGRAM OF THE VDC

Promotion of research by the VdC is based on the public discussion on the impact of smoking and so-called passive smoking on human health. The health hazards attributed to smoking by epidemiological studies are to be further explored (on molecular and cellular levels) and be brought into relation with risks of life in general. In order to make researc has effective as possible the funds provided are to be concentrated on the following areas:

1.) Investigation on the effect of nicotine alone or in correlation with other substances in tobacco smoke on human health.

2.) Investigation of the effect of the so-called passive smoking (ETS) on human health in the light of endogenous and exogenous influential factors.

3.) Research into the metabolism of the tobacco plant and development of methods for influencing it.

009881/PWB/EE
2nd September 1992

VdC RESEARCH PROGRAM 1992

1. **THEME:** **PLANT RESEARCH**
   - Effect of nitrate concentration in tobacco on smoke composition
   - Nitrates in tobacco plant
   - Genetic engineering in tobacco growing

2. **THEME:** **POSSIBLE HEALTH/RELATED EFFECTS**
   - Chromosome aberrations in smokers and non-smokers
   - Levels of methylnitroso pyridyl butyric acid in urine
   - Skin wrinkling in smokers and non-smokers

3. **THEME:** **ETS AND ITS EFFECT ON MEN**
   - Serum cotinine in populations
   - Confounding variables
   - Asthma in children, acute reaction of ETS
   - DNA adducts in monocytes after exposure to MS
   - Blood biochemistry survey of smokers
     - pooled analytical results
   - Asthma medium/long term reaction to ETS

2023251918

4. **THEME:** **ENDOGENOUS/EXOGENOUS FACTORS - BASIC MEDICAL RESEARCH**

- Steroids in serum
- Dioxin distribution
- Benzene levels on the work place (Halle)
- Diet and lung cancer in the mouse model
- Lipoprotein levels in general population

5. **THEME:** **SMOKING/PASSIVE SMOKING AND LIFESTYLE RISKS**

- Benzene levels and road traffic
- Benzene levels - non occupation
- Lung cancer epidemiology (workplace and general environment)
- Longitudinal epidemiological survey on pregnancy outcome and lifestyle in smoking and non-smoking women
- Lung cancer epidemiology US/Japan

6. **THEME:** **MOTIVATION**

- Social-psychological effects of smoking

TOTAL BUDGET: DM 4 538 960

2023251919

Holland

SSI (Dutch Cigarette Industry)
and
VNK (Dutch Roll Your Own Industry)
through the Scientific Advisory Council.

The Dutch NMA's Budget for 1993 has been reserved for the following studies :

ANTONIE VAN LEEUWENHOEKHUIS

Basic Cancer Research

CIVO/TNO

Research re influence of cigarettes smoke on bronchial tubes and influence of vitamin A.

Prof. SNOW

Genotoxic factors regarding the arising of head and neck cancer.

Prof. RAMAECKERS

Biological research to identify genetic predisposition of lung cancer patients.

2023251921

LIST OF PUBLICATIONS

RESULTING

FROM ASFC

(ASSOCIATION OF SWISS CIGARETTE MANUFACTURERS)

SUPPORTED

RESEARCH

1964 - 1992

PR E. GRANDJEAN

WEBER-A, FISCHER-T, GRANDJEAN-E	PASSIVRAUCHEN UNTER EXPERIMENTELLEN BEDINGUNGEN UND IN FELDVERSUCHEN.	SOZIAL- UND PRAEVENTIVMED. 23, (261-262), 1978
WEBER-A, FISCHER-T, GIERER-R, GRANDJEAN-E	EXPERIMENTELLE REIZWIRKUNGEN VON ACROLEIN AUF DAS RAUCHEN	INT ARCH OCCUP ENVIRON HEALTH, 1977, 40 (117-130)
FISCHER-T, WEBER-A, GRANDJEAN-E	LUFTVERUNREINIGUNG DURCH TABAKRAUCH IN GASTSTAETTEN	INT ARCH OCCUP ENVIRON HEALTH, 1977, 40 (117-130)
WEBER-A, JERMINI-E, GRANDJEAN-E	LUFTVERUNREINIGUNG UND BELAESTIGUNGEN DURCH ZIGARETTENRAUCH	SOZIAL UND PREVENTIVMEDIZIN, 1976, 21 (101-106)
WEBER-A, FISCHER-T, GRANDJEAN-E	WIRKUNG VON NEBENSTROMRAUCH AUF PHYSIOLOGISCHE FUNKTIONEN	INT ARCH OCCUP ENVIRON HEALTH, 1976, 37 (277-288)
WEBER-A, JERMINI-C, GRANDJEAN-E	BEZIEHUNG ZWISCHEN OBJEKTIVEN UND SUBJEKTIVEN MESSMETHODEN BEI EXPERIMENTELL ERZEUGTER "ERMÜDUNG	PRAEVENTIMEDIZINE NO 18, 1973 "
WEBER-A, JERMINE-C, MARTIN-E, UDRIS-I, GRANDJEAN-E	OBJEKTIVE UND SUBJEKTIVE ERMÜDUNG IN EXPRERIMENTELLEN MONOTONIE-SITUATIONEN	PRAEVENTIVMEDIZIN 1973
DRISCOLL-P, DEUBER-A, BÄTTIG-K, GRANDJEAN-E	EFFECT OF FILTERED CIGARETTE SMOKE ON RATS	NATURE 237, 1972
PHILIPPIN-CL, GILGEN-A, GRANDJEAN-E	ETUDE TOXICOLOGIQUE ET PHYSIOLOGIQUE DE L'ACROLEINE CHEZ LA SOURIS	INTERNAT. ARCH. ARBEITSMEDIZIN NO 26, 1970
GILGEN-A, PHILIPPIN-CL, GRANDJEAN-E	DIE TOXIZITAET VON ACROLEIN. SCHRIFTENREIHE ARBEITSMEDIZIN, SOZIALMEDIZIN,	ARBEITSHYGIENE NR 41, 1970
PHILIPPIN-CL, GRANDJEAN-E, GILGEN-A	ACTION PHYSIOLOGIQUE DE L'ACROLEINE CHEZ LA SOIURIS	REV. MED. PREV. NO 14, 1969
GRANDJEAN-E, CAPITAINE-CL, GILGEN-A	TOXIKOLOGISCHE WIRKUNGEN DURCH INHALATION VON NO2 BEI DER MAUS.	PRAEVENTIVMEDIZIN NO 13, 1968
CAPITAINE-CL	ACTION PHYSIOLOGIQUE ET TOXICOLOGIQUE DE L'ACETALDEHYDE CHEZ LA SOURIS	REV. MED. PREV. NO 13, 1968

LEUCHTENBERGER-C, LEUCHTENBERGER-R	ABNORMALITIES OF MITOSIS, DNA METABOLISM AND GROWTH IN HUMAN LUNG CULTURES, EXPOSED TO SMOKE FROM MARIJUANA CIGARETTES, AND THEIR SIMILARITY WITH ALTERATIONS EVOKED BY TOBACCO CIGARETTE SMOKE	UNITED NATIONS BULLETIN, NOVEMBER 1972
LEUCHENTENBERGER-C, LEUCHTENBERGER-R, SCHNEIDER-A	EFFECTS OF FRESH SMOKE FROM MARIJUANA AND KENTUCKY CIGARETTES ON FIBROLASTIC CELLS OF ADULT HUMAN LUNG EXPLANTS	PROC. OF 63RD ANNUAL MEETING OF AMER ASSOC. FOR CANCER RES., VOL. 13, 1972
LEUCHTENBERGER-C, LEUCHTENBERGER-R	THE BEHAVIOUR OF MACROPHAGES IN LUNG CULTURES AFTER EXPOSURE TO CIGARETTE SMOKE	EVIDENCE FOR SELECTIVE INHIBITION BY PARTICULATE MATTER AND STIMULATION BY THE GAS PHASE OF CELL METABOLISM OF ALVEOLAR MACROPHAGES; THE RETICULOENDOTHELIAL SYSTEM & IMMUNE PHENOMENA N.R. DILUZIO 1971
LEUCHTENBERGER-C, LEUCHTENBERGER-R	MORPHOLOGICAL AND CYTOCHEMINCAL EFFECTS OF MARIJUANA CIGARETTE SMOKE ON EPITHELIOID CELLS OF LUNG EXPLANTS FROM MICE	NATURE, VOL. 234 1971
LEUCHTENBERGER-C, LEUCHTENBERGER-R	EINFLUSS VON FRISCHEM ZIGARETTENRAUCH AUF DIE ENTWICKLUNG VON LUNGENTUMOREN UND AUF LUNGENKULTUREN BEI DER SNELL-MAUS	SCHWEIZ. MEDIZIN NO 38, 1971
LEUCHTENBERGER-C, LEUCHTENBERGER-R	ENHANCEMENT OF ABNORMAL CELL PROLIFERATION IN LUNG EXPLANTS AFTER MARIJUANA CIGARETTE SMOKE	EXPERIENTIA NO 27, 1971
LEUCHTENBERGER-C, LEUCHTENBERGER-R	DIFFERENTIAL CYTOLOGICAL AND CYTOCHEMICAL RESPONSES OF VARIOUS CULTURES FROM MOUSE TISSUES TO REPEATED EXPOSURES TO PUFFS FROM THE GAS VAPOUR PHASE OF CHARCOAL-FILTERED CIGARETTE SMOKE	EXPERIMENTAL CELL RESEARCH NO 62, 1970
LEUCHTENBERGER-C	MODERN APPROACHES TO EXPERIMENTAL CANCER RESEARCH	SURGICAL ONCOLOGY - F-SAEGESSER & J-PETTAVEL, HANS HUBER PUBL., BERN, 1970
LEUCHTENBERGER-C, LEUCHTENBERGER-R	EFFECT OF CHRONIC INHALATION OF WHOLE FRESH CIGARETTE SMOKE AN OF ITS GAS PHASE ON PULMONARY TUMORIGENESIS IN SNELL'S MICE. IN: MORPHOLOGY OF EXPERIMENTAL RESPIRATORY CARCINOGENESES	21ST AEC SYMPOSIUM SERIES GATLINBURG, US ATOMIC ENERGIY COMMISSION, 1970
LEUCHTENBERGER-C, LEUCHTENBERGER-R, BLANCHARD-J, DECKERT-M	ABNORMAL PROLIFERATIVE EFFECTS OF THE GAS PHASE OF CHARCOAL FILTERED FRESH CIGARETTE SMOKE ON 3T3 CELLS	PROC. OF FED. AMER. SOC. FOR EXPERIMENTAL BIOLOGIY, 1969.
LEUCHTENBERGER-C, LEUCHTENBERGER-R	CYTOLOGIC AND CYTOCHEMICAL EFFECTS ON PRIMARY MOUSE KIDNEY TISSUE AND LUNG ORGAN CULTURES AFTER EXPOSURE TO WHOLE, FRESH SMOKE AN ITS GAS PHASE FROM UNFILTERED, CHARCOAL-FILTERED, AND CIGAR TABACCO CIGARETTES	CANCER RES. 29, 1969
LEUCHTENBERGER-C, SCHUMACHER-M, HALDIMANN-T	FURTHER CYTOLOGICAL AN CYTOCHEMICAL STUDIES ON THE BIOLOGICAL SIGNIFICANCE OF THE GAS PHASE OF FRESH CIGARETTE SMOKE	PRÄVENTIVMEDIZIN NO 13, 1968

2023251924

C. . .EUC NBE R

LEUCHTENBERGER-C, LEUCHTENBERGER-R	PROTECTION OF HAMSTER LUNG CULTURES BY L-CYSTEINE OR VITAMIN C AGAINST CARCINOGENIC EFFECTS OF FRESH SMOKE FROM TOBACCO OR MARIHUANA CIGARETTES	BR J EXP PATH, 1977, 58 (625-634)
LEUCHTENBERGER-C, LEUCHTENBERGER-R	L-CYSTEINE OR VITAMINE C INFLUENCE, CELLULAR GROWTH AND PROLONG SURVIVAL OF NORMAL ADULT HUMAN LUNG TISSUE IN CULTURE	CELL BIOLOGY INT. REPORTS, 1977, 1/4 (317-324)
LEUCHTENBERGER-C, LEUCHTENBERGER-R	SH REACTIVITY OF CIGARETTE SMOKE AND ITS CORRELATION WITH CARCINOGENIC EFFECTS ON HAMSTER LUNG CULTURES	SOZIAL UND PREVENTIVMEDIZIN, 1976, 21 (47-50)
LEUCHTENBERGER-C, LEUCHTENBERGER-R, ZBINDEN-I, SCHLEH-E	SH REACTIVITY OF CIGARETTE SMOKE AND ITS CORRELATION WITH CARCINOGENIC EFFECTS ON HAMSTER LUNG CULURES	SOZIAL- UND PRÄVENTIVMEDIZIN 21, 1976
LEUCHTENBERGER-C, LEUCHTENBERGER-R, ZBINDEN-I, SCHLEH-E	CYTOLOGICAL AND CYTOCHEMICAL EFFECTS OF WHOLE SMOKE AND OF THE GAS VAPOR PHASE FROM MARIHUANA CIGARETTES ON GROWTH AND DNA METABOLISM OF CULTURED MAMMALIAN CELLS	IN MARIHUANA: CHEMISTRY, BIOCHEMISTRY, AND CELLULAR EFFECTS, ED. G.G.NAHAS, SPRINGER-VERLAG NEW YORK INC., 1976
LEUCHTENBERGER-C, LEUCHTENBERGER-R	CYTOLOGICAL AND CYTOCHEMICAL STUDIES OF THE EFFECTS OF FRESH MARIHUANA CIGARETTE SMOKE ON GROWTH AND DNA METABOLISM OF ANIMAL AND HUMAN LUNG CULTURES	THE PHARMACOLOGY OF MARIHUANA, ED. M.C. BRUADE AND S.SZARA, RAVEN PRESS, NEW YORK, 1976
LEUCHTENBERGER-C, LEUCHTENBERGER-R	PROTECTION OF HAMSTER LUNG CULTURES BY L-CYSTEINE AGAINST CARCINOGENIC EFFECTS OF FRESH SMOKE FROM TOBACCO OR MARIHUANA CIGARETTES	ABSTRACT IN THE JOURNAL OFF CELL BIOLOGY, VOL. 70, 1976
DAVIES-P, KISTLER-GS, LEUCHTENBERGER-C, LEUCHTENBERGER-R	ULTRASTRUCTURAL STUDIES ON CELLS OF HAMSTER LUNG CULTURES AFTER CHRONIC EXPOSURE TO WHOLE SMOKE OR THE GAS VAPOUR PHASE OF CIGARETTES.	BEITR.PATH.BD. 155, 1975
LEUCHTENBERGER-C, LEUCHTENBERGER-R, ZBINDEN-I	GAS VAPOUR PHASE CONSTITUENTS AND SH REACTIVITY OF CIGARETTE SMOKE INFLUENCE LUNG CULTURES	NATURE, VOL. 247, 1974
LEUCHENTENBERGER-C, LEUCHTENBERGER-R	THE EXPERIMENTAL EXPLORATION OF HEALTH DAMAGING FACTORS IN CIGARETTE SMOKE	SOZIAL UND PREVENTIVMEDIZIN, 1974, 19 (41-45)
LEUCHTENBERGER-C, LEUCHTENBERGER-R	DIFFERENTIAL RESPONSE OF SNELL'S AND C57 BLACK MICE TO CHRONIC INHALATION OF CIGARETTTE SMOKE.	ONCOLOGY 29, 1974
LEUCHTENBERGER-C, LEUCHTENBERGER-R, SCHNEIDER-A	EFFECT OF MARIJUANA AND TOBACCO SMOKE ON HUMAN LUNG PHYSIOLOGY	NATURE, VOL 241, 1973
LEUCHTENBERGER-C, LEUCHTENBERGER-R, RITTER-U, INUI-N	EFFECTS OF MARIJUANA AND TOBACCO SMOKE ON DNA AN CHROMOSOMAL COMPLEMENT IN HUMAN LUNG EXLANTS	NATURE, VOL 242, 1973

2023251925

ROTH-N, LUTIGER-B, HASENFRATZ-M, BATTIG-K, KNYE-M.	SMOKING DEPRIVATION IN EARLY AND LATE SMOKERS AND MEMORY FUNCTIONS.	PSYCHOPHARMACOLOGY, 1992, V106, N2, P253-260
HASENFRATZ-M, THUT-G, BATTIG-K.	24-HOUR MONITORING OF HEART-RATE, MOTOR-ACTIVITY AND SMOKING-BEHAVIOR INCLUDING COMPARISONS BETWEEN SMOKERS AND NONSMOKERS.	PSYCHOPHARMACOLOGY, 1992, V106, N1, P39-44.
HASENFRATZ-M, JAQUET-F, AESCHBACH-D, BATTIG-K.	INTERACTIONS OF SMOKING AND LUNCH WITH THE EFFECTS OF CAFFEINE ON CARDIOVASCULAR FUNCTIONS AND INFORMATION-PROCESSING.	HUMAN-PSYCHOPHARMACOLOGY-CLINICAL-AND-EXPERIMENTAL, 1991, V6, N4, P277-284.
HOFER-I, NIL-R, BATTIG-K.	NICOTINE YIELD AS DETERMINANT OF SMOKE EXPOSURE INDICATORS AND PUFFING BEHAVIOR.	PHARMACOLOGY-BIOCHEMISTRY-AND-BEHAVIOR, 1991, V40, N1, P139-149.
HOFER-I, NIL-R, BATTIG-K.	ULTRALOW-YIELD CIGARETTES AND TYPE OF VENTILATION - THE ROLE OF VENTILATION BLOCKING.	PHARMACOLOGY-BIOCHEMISTRY-AND-BEHAVIOR, 1991, V40, N4, P907-914
COHEN-C, WELZL-H, BATTIG-K.	EFFECTS OF NICOTINE, CAFFEINE, AND THEIR COMBINATION ON LOCOMOTOR- ACTIVITY IN RATS.	PHARMACOLOGY-BIOCHEMISTRY-AND-BEHAVIOR, 1991, V40, N1, P121-123.
HASENFRATZ-M, BATTIG-K.	NICOTINE ABSORPTION AND THE SUBJECTIVE AND PHYSIOLOGICAL-EFFECTS OF NICOTINE TOOTHPICKS.	CLINICAL-PHARMACOLOGY-AND-THERAPEUTICS, 1991, V50, N4, P456-461.
ROTH-N, BATTIG-K.	EFFECTS OF CIGARETTE-SMOKING UPON FREQUENCIES OF EEG ALPHA-RHYTHM AND FINGER TAPPING.	PSYCHOPHARMACOLOGY, 1991, V105, N2, P186-190.
BATTIG-K.	CARDIOVASCULAR AND PERFORMANCE EFFECTS OF COFFEE AND SMOKING.	INTERNATIONAL-JOURNAL-OF-PSYCHOPHYSIOLOGY, 1991, V11, N1, P10-10.
HASENFRATZ-M, BATTIG-K.	PSYCHOPHYSIOLOGICAL REACTIONS DURING ACTIVE AND PASSIVE STRESS COPING FOLLOWING SMOKING CESSATION.	PSYCHOPHARMACOLOGY, 1991, V104, N3, P356-362.
WELZL-H, BATTIG-K, BERZ-S.	ACUTE EFFECTS OF NICOTINE INJECTION INTO THE NUCLEUS-ACCUMBENS ON LOCOMOTOR-ACTIVITY IN NICOTINE-NAIVE AND NICOTINE-TOLERANT RATS.	PHARMACOLOGY-BIOCHEMISTRY-AND-BEHAVIOR, 1990, V37, N4, P743-746.
HASENFRATZ-M, NIL-R, BATTIG-K.	DEVELOPMENT OF CENTRAL AND PERIPHERAL SMOKING EFFECTS OVER TIME.	PSYCHOPHARMACOLOGY, 1990, V101, N3, P359-365.
HASENFRATZ-M, PFIFFNER-D, PELLAUD-K, BATTIG-K.	POSTLUNCH SMOKING FOR PLEASURE SEEKING OR AROUSAL MAINTENANCE.	PHARMACOLOGY-BIOCHEMISTRY-AND-BEHAVIOR, 1989, V34, N3, P631-639.
HASENFRATZ-M, MICHEL-C, NIL-R, BATTIG-K.	EFFECTS OF SMOKING AND NOISE ON INFORMATION-PROCESSING - ELECTROCORTICAL, PSYCHOPHYSIOLOGICAL AND ENDOCRINOLOGICAL CONCOMITANTS.	INTERNATIONAL-JOURNAL-OF-PSYCHOPHYSIOLOGY, 1989, V7, N2-4, P229-230.
NIL-R, BATTIG-K.	SEPARATE EFFECTS OF CIGARETTE-SMOKE YIELD AND SMOKE TASTE ON SMOKING- BEHAVIOR.	PSYCHOPHARMACOLOGY, 1989, V99, N1, P54-59.
HASENFRATZ-M, MICHEL-C, NIL-R, BATTIG-K.	CAN SMOKING INCREASE ATTENTION IN RAPID INFORMATION-PROCESSING DURING NOISE - ELECTROCORTICAL, PHYSIOLOGICAL AND BEHAVIORAL-EFFECTS.	PSYCHOPHARMACOLOGY, 1989, V98, N1, P75-80.
MICHEL-C, BATTIG-K.	SEPARATE AND COMBINED PSYCHOPHYSIOLOGICAL EFFECTS OF CIGARETTE- SMOKING AND ALCOHOL-CONSUMPTION.	PSYCHOPHARMACOLOGY, 1989, V97, N1, P65-73.
WELZL-H, ALESSANDRI-B, OETTINGER-R, BATTIG-K.	THE EFFECTS OF LONG-TERM NICOTINE TREATMENT ON LOCOMOTION, EXPLORATION AND MEMORY IN YOUNG AND OLD RATS.	PSYCHOPHARMACOLOGY, 1988, V96, N3, P317-323.

MICHEL-C, HASENFRATZ-M, NIL-R, BATTIG-K.	CARDIOVASCULAR, ELECTROCORTICAL, AND BEHAVIORAL-EFFECTS OF NICOTINE CHEWING GUM.	KLINISCHE-WOCHENSCHRIFT, 1988, V66, S11, P72-79.
NIL-R, WOODSON-P-P, MICHEL-C, BATTIG-K.	EFFECTS OF SMOKING ON MENTAL PERFORMANCE AND VEGETATIVE FUNCTIONS IN HIGH AND LOW CO ABSORBING SMOKERS.	KLINISCHE-WOCHENSCHRIFT, 1988, V66, S11, P66-71.
MICHEL-G, BATTIG-K.	SEPARATE AND JOINT EFFECTS OF CIGARETTE-SMOKING AND ALCOHOL- CONSUMPTION ON MENTAL PERFORMANCE AND PHYSIOLOGICAL FUNCTIONS.	ACTIVITAS-NERVOSA-SUPERIOR, 1988, V30, N2, P107-109.
BATTIG-K, NIL-R.	PSYCHOPHYSIOLOGICAL EFFECTS OF SMOKING AND INTERACTIONS WITH STRESS.	ACTIVITAS-NERVOSA-SUPERIOR, 1988, V30, N2, P103-105.
MICHEL-C, NIL-R, BUZZI-R, WOODSON-P-P, BATTIG-K.	RAPID INFORMATION-PROCESSING AND CONCOMITANT EVENT-RELATED BRAIN POTENTIALS IN SMOKERS DIFFERING IN CO ABSORPTION.	NEUROPSYCHOBIOLOGY, 1987, V17, N3, P161-168.
NIL-R, WOODSON-P-P, BATTIG-K.	EFFECTS OF SMOKING ON PSYCHOPHYSIOLOGICAL REACTIVITY TO ENVIRONMENTAL NOISE STRESS IN HIGH AND LOW CO ABSORBING SMOKERS.	PSYCHOPHYSIOLOGY, 1987, V24, N5, P603-603.
NIL-R, WOODSON-P-P, BATTIG-K.	EFFECTS OF SMOKING DEPRIVATION ON SMOKING-BEHAVIOR AND HEART-RATE RESPONSE IN HIGH AND LOW CO ABSORBING SMOKERS.	PSYCHOPHARMACOLOGY, 1987, V92, N4, P465-469.
HASENFRATZ-M, MICHEL-C, NIL-R, BATTIG-K.	CARDIOVASCULAR, ELECTROCORTICAL AND BEHAVIORAL-EFFECTS OF NICOTINE.	EXPERIENTIA, 1987, V43, N6, P714-714.
NIL-R, MICHEL-C, WOODSON-P-P, BATTIG-K.	PSYCHOPHYSIOLOGICAL EFFECTS OF PRESMOKING AND POSTSMOKING RAPID INFORMATION-PROCESSING.	EXPERIENTIA, 1987, V43, N6, P707-707.
NIL-R, BATTIG-K.	SMOKING BEHAVIOR: A MULTIVARIATE PROCESS	SMOKING AND HUMAN BEHAVIOR, EDS T. NEY & A. GALE, JOHN WILEY & SONS LTD, 1989
NIL-R, WOODSON-P-P, BATTIG-K.	EFFECTS OF SMOKING DEPRIVATION ON SMOKING BEHAVIOR AND HEART RATE RESPONSE IN HIGH AND LOW CO ABSORBING SMOKERS.	PSYCHOPHARMACOLOGY, 1987, 92/4 (465-469).
WOODSON-P-P, BUZZI-R, NIL-R, BATTIG-K	.EFFECTS OF SMOKING ON VEGETATIVE REACTIVITY TO NOISE IN WOMEN.	PSYCHOPHYSIOLOGY, 1986, 23/3 (272-282).
NIL-R, WOODSON-P-P, BATTIG-K.	SMOKING BEHAVIOUR AND PERSONALITY PATTERNS OF SMOKERS WITH LOW AND HIGH CO ABSORPTION.	CLIN-SCI, 1986, 71/5 (595-603).
WOODSON-P, BUZZI-R, NIL-R, BATTIG-K	EFFECTS OF SMOKING ON VEGETATIVE REACTIVITY TO NOISE IN LIGHT VERSUS DEEP INHALERS	
NIL-R, BUZZI-R, BATTIG-K.	EFFECTS OF DIFFERENT CIGARETTE SMOKE YIELDS ON PUFFING AND INHALATION: IS THE MEASUREMENT OF INHALATION VOLUMES RELEVANT FOR SMOKE ABSORPTION?	PHARMACOL-BIOCHEM-BEHAV, 1986, 24/3 (587-595).
FITZGERALD-R-E, OETTINGER-R, BATTIG-K.	REDUCTION OF NICOTINE-INDUCED HYPERACTIVITY BY PCPA.	PHARMACOL-BIOCHEM-BEHAV, 1985, 23/2 (279-284).
BUZZI-R, NIL-R, BATTIG-K.	DEVELOPMENT OF PUFFING BEHAVIOUR ALONG BURNING TIME OF A CIGARETTE. NO RELATION TO ALVEOLAR INHALATION OR NICOTINE DELIVERY OF THE CIGARETTES?	PSYCHOPHARMACOLOGY, 1985, 86/1-2 (102-107).
MICHEL-C, NIL-R, BUZZI-R, WOODSON-P, BÄTTIG-K	EFFECTS OF SMOKING ON VISUAL EVOKED POTENTIALS IN RAPID INFORMATION PROCESSING	EXPERENTIA, 1985, 41 (832)

BÄTTIG-K, NIL-R	RAUCHEN UND STRESS	PROC OF THE EUROP ASS FOR BEHAVIOUR THERAPY, 15TH MEETING, MUNICH, 1985
BÄTTIG-K	DIE PSYCHOPHARMAKOLOGIE VON RAUCHEN UND NIKOTINNEUERE FROSCHUNGSERGEBNISSE. I	N J.C. BRENGELMANN (ED.), GRUNDLAGEN UND PRAXIS DER RAUCHERENTWÖHNUNG. MÜNCHEN: GEHARD RÖTTGER VERLAG, 1984, 85-102
NIL-R. BÄTTIG-K	ZIGARETTENSTÄRKE, RAUCHVERHALTEN UND RAUCHAUFNAHME. I	N J.C. BRENGELMANN (ED.), GRUNDLAGEN VERLAG, 1984, PP 117-130
WOODSON-PP,	THE NEUROPHARMACOLOGICAL DOUBLE ACTION OF NICOTINE: MEDIATION OF CIGARETTE SMOKE'S ENERGIZING YET STABILIZING EFFECTS ON PSYCHOLOGICAL FUNCTION.	DISSERTATION. ETH ZÜRICH, 1984
EFFECTS OF SINGLE DOSES OF ALCOHOL AND CAFFEINE ON CIGARETTE SMOKE PUFFING BEHAVIOR.	NIL-R. BUZZI-R, BATTIG-K.	PHARMACOL-BIOCHEM-BEHAV, 1984. 20/4 (583-590).
NIL-R, BÄTTIG-R	RELATION OF CIGARETTE PUFFING AND INHALATION TO SMOKE YIELDS OF CIGARETTES	EXPERIENTIA. 39, 638, 1983
NIL-R. BUZZI-R, BÄTTIG-K	PERSÖNLICHKEIT, TYP A/B-VERHALTEN UND LEBENSGEWOHNHEITEN BEI RAUCHERN UND NICHTRAUCHERN.	SOZIAL- UND PRÄVENTIVMEDIZIN, 28, 242-243. 1983
SUTER-TH-W. BUZZI-R. WOODSON-PP. BÄTTIG-K.	PSYCHOPHYSIOLOGICAL CORRELATES OF CONFLICT SOLVING AND CIGARETTE SMOKING	ACTIVITAS NERVOSA SUPERIOR (PRAHA), 25(4). 261-272. 1983
WOODSON-PP. BUZZI-R. BÄTTIG-K	EFFECTS OF SMOKING ON VEGETATIVE REACTIVITY TO NOISE.	SOZIAL- UND PRÄVENTIVMEDIZIN. 28. 240-241. 1983
WOODSON-PP. SUTER-TH-W. BUZZI-R. BÄTTIG-K	EFFECTS OF SMOKING ON VEGETATIVE REACTIVITY TO NOISE	EXPERIENTIA, 39, 643, 1983
WOODSON-PP, BÄTTI-K. KALLMAN-WM. HARRY-GJ. KALLMANN-MJ. MASECRANS-JA	EFFECTS OF NICOTINE ON THE VISUAL EVOKED RESPONSES.	PHARMACOL. BIOCHEM. & BAHV.. 17. 1982. 915-920
SUTER-TH-W. BUZZI-R. BATTIG-K.	CARDIOVASCULAR EFFECTS OF SMOKING CIGARETTES WITH DIFFERENT NICOTINE DELIVERIES. A STUDY USING MULTILEAD PLETHYSMOGRAPHY.	PSYCHOPHARMACOLOGY, 1983, 80/2 (106-112).
EFFECTS OF NICOTINE ON THE AVERAGED VISUAL EVOKED RESPONSE.	WOODSON-P-P. BATTIG-K. ROSECRANS-J-A.	SOZ-PRAVENTIVMED. 1982, 27/5 (242-243).
EFFECTS OF ETHANOL AND CAFFEINE ON CIGARETTE PUFFING AND INHALATION.	NIL-R. BUZZI-R, BATTIG-K.	SOZ-PRAVENTIVMED, 1982. 27/5 (238-239).
SMOKE YIELD OF CIGARETTES AND PUFFING BEHAVIOR IN MEN AND WOMEN.	BATTIG-K, BUZZI-R. NIL-R.	PSYCHOPHARMACOLOGY, 1982, 76/2 (139-148).
KALLMAN-WM, RASECRANS-JA. KALLMAN-MJ. HARRY-GJ. WOODSON-PP	NICOTINE AS A DISCRIMINATIVE STIMULUS IN HUMAN SUBJECTS	PSYCHOPHARMACOLOGY, 76, 1982
NIL-R, BUZZI-R, BÄTTIG-K,	EFFEKTE VON AETHYLALKOHOL UND KOFFEIN AUF DIE INTENSITÄT DES ZIGARETTENRAUCHENS	SOZIAL- UND PRÄVENTIVMEDIZIN, 27, (238-239). 1982

NIL-R, WOODSON-PP, BÄTTIG-K	DER RAUCHER. SEIN RAUCHVERHALTEN UND SEINE RAUCHMOTIVATIONS	SCHWEIZERISCHE ZEITSCHRIFT FÜR PSYCHOLOGIE. 41. (217-229), 1982
SUTER-THW. FEIERABEND-JM. BÄTTIG-K	PHYSIOLOGISCHE KORRELATE VON ZWEI VERSCHIEDENEN MENTALEN TÄTIGKEITEN: KONFLIKTLÖSEN UND KONZEPTLERNEN	SCHWEIZERISCHE ZEITSCHRIFT FÜR PSYCHOLOGIE, (203-216). 1982
WOODSON-PP, BÄTTIG-K. ROSECRANS-JA	NIKOTINWIRKUNGEN AUF VISUELLE EVOZIERTE EEG POTENTIALE	SOZIAL- UND PRÄVENTIVMEDIZIN, 27. (242-243). 1982
SCHLATTER-J. BATTIG-K.	THE ADRENERGIC ROLE IN THE MANIFESTATION OF NICOTINE EFFECTS ON MAZE AMBULATION IN ROMAN HIGH AND ROMAN LOW AVOIDANCE RATS.	BR-J-ADDICT. 1981. 76/2 (199-209).
DRISCOLL-P, BÄTTIG-K	"SELECTIVE INHIBITION BY NICOTONIE OF SHOCK-INDUCED FIGHTING IN THE RAT"	PHARMACOLOGY BIOCHEMISTRY & BEHAVIOR, 14 (175-179) 1981
BATTIG-K.	THE SMOKING HABIT AND PSYCHOPHARMACOLOGICAL EFFECTS OF NICOTINE.	ACT-NERV-SUPER-(PRAHA), 1980, 22/4 (274-288).
BÄTTIG-K, MARTIN-JR. CLASSEN-W	NICOTINE AND AMPHETAMINE: DIFFERENTIAL TOLERANCE AND NO CROSS-TOLERANCE FOR INGESTIVE EFFECTS	PHARMACOLOGY BIOCHEMISTRY & BEHAVIOR, VOL. 12. (107-111), 1980
DRISCOLL-P. WOODSON-P. FUEMM-H. BÄTTIGK	SELECTION FOR TWO-WAY AVOIDANCE DEFICIT INHIBIT SCHOCK-INDUCED FIGHTING IN THE RAT	PHYSIOL. BEHAV, VOL. 24. (793-795). 1980
KAESERMANN-HP. DRISCOLL-P	DIFFERENTIAL SENSITIVITY TO ETHER ANAESTHESIA IN RHA/VERH AND RLA/VERH RATS.	VII SYMPOSIUM ICLA - ANIMAL QUALITY AND MODELS IN BIOMEDICAL RESEARCH. GUSTAV FISCHER VERLAG. STUTTGART. 1980
MARTIN-JR. DRISCOLL-P. BÄTTIG-K	FURTHER BEHAVIORAL CHARACTERIZATION OF TWO PSYCHOGENETICALLY-SELECTED LINES OF RATS (RHA/VERH AND RLA/VERH)	VII SYMPOSIUM ICLA - ANIMAL QUALITY AND MODELS IN BIOMEDICAL RESEARCH. GUTAV FISCHER VERLAG. STUTTGART. 1980
SCHLATTER-J. BÄTTIG-K	THE ADRENERGIC ROLE IN THE MANIFESTATION OF NICOTINE EFFECTS ON MAZE AMBULATION IN ROMAN HIGH AND LOW AVOIDANCE RATS.	BRIT. J. OF ADDICTION RESEARCH. 1980
BÄTTIG-K	RUCHGEWOHNHEIT UND PSXCHOPHARMAKOLOGIE DES NIKOTINS	NATURW. RUNDSCHAU. 33 JAHRG. HEFT 9. 1980
NIL-R	ANALYSE DES RAUCHVERHALTENS UND IHALIERENS BEI ZIGARETTENRUCHERN	AUSSTELLUNGSKATALOG: FORSCHUNGS- UND INNOVATIONSAUSTELLUNG. NR. 43. 85-85. 1980
DRISCOLL-P. DEDEK-J. MARTIN-J-R.. BÄTTIG-K	REGIONAL 5--HT ANALYSIS IN ROMAN HIGH- AND LOW-ADVOIDANCE RATS FOLLOWING MAO INHIBITION	ERO. JOURNAL OF PHARMACOLOGY, 68 (373-376) 1980
SCHLATTER-J. BATTIG-K.	DIFFERENTIAL EFFECTS OF NICOTINE AND AMPHETAMINE ON LOCOMOTOR ACTIVITY AND MAZE EXPLORATION IN TWO RAT LINES.	PSYCHOPHARMACOLOGY, 1979, 64/2 (155-161).
DRISCOLL-P. BÄTTIG-K	DOSE-TIME-EFFECT-RELATION.	BEHAVIORAL AN DPHYSIOLOGICAL CORRELATES OF PSYCHOGENETIC SELECTION (RHA/VERH VS RLA/VERH RATS). SYPOSIUM "THE LABORATORY ANIMAL IN THE SERVICE OF MANKIND"; LYON, COLLECTION FOND. MÉRIEUX. (477-487). 1979

KELLER-HH, DRISCOLL-P, DA PRADA-M, BÄTTIG-K	MONOAMINE SYSTEM ANALYSIS IN ROMAN HIGH- AND LOW-AVOIDANCE RATS.	NEUROSCI- LETTERS SUPPL. 3, 245, 1979
SCHLATTER-J, BÄTTIG-K, .	MENTAL MAZE LEARNING IN HUMANS	EXPERIENTIA 35 (7), 1979
BÄTTI-K, SCHLATTER-J	EFFECTS OF SEX AND STAIN ON EXPLORATORY LOCOMOTION AND EVELOPMENT OF NONREINFORCED MAZE PATROLLING	ANIMAL LEARNING AND BEHAVIOUR 7, (99-105), 1979
DRISCOLL-P, BÄTTIGK	DIE HEMMUNG SCHOCK-INDUZIERTEN KÄMPFENS DURCH NIKOTIN BEI RATTEN.	BEITRÄGE ZUR 21 TAGUNG EXPERIMENTELL ARBEITENDER PSYCHOLOGEN, HEIDELBERG, (62), 1979
DRISCOLL-P, FUEMM-H, BÄTTIG-K	MATERNAL BEHAVIOR IN TWO RAT LINES SELECTED FOR DIFFERENCES IN THE ACQUISITION OF TWO-WAY AVOIDANCE.	EXPERIENTIA, (786-788), 1979
DRISCOLL-P	INHIBITION OF SCHOCK-INDUCED FIGHTING BY NICOTINE	EXPERIENTIA, (948), 1979
DRISCOLL-	THE ELECTROCARDIOGRAM OF ROMAN HIGH- AND LOW-AVOIDANCE RATS UNDER PENTOBARBITAL SODIUM ANESTHESIA	ARZNEIHM FORSCH , 1979, 29 (897-900)
BÄTTIG-K	NICOTINE AND MOTIVATION OF SMOKING	RIVISTA DI TOSSICOLOGIA ROMA, 1977, 3-4 (145-160)
DRISCOLL-P	ACUTE NICOTINE TOXICITY IN MICE: OBSERVATIONS CONCERNING PH MANIPULATION AND INTERACTION WITH MECAMYLAMINE	RIVISTA DI TASSICOLOGIA: SPERIMENTALE E CLINICA FASC. 3-4 1977 (161-170)
DÜTSCH-HR, BÄTTIG-K	PSYCHOGENETISCHE UNTERSCHIEDE (RHA-VS RLA-RATTEN) IM VERMEIDUNGSLERNEN, OFFENFELDVERHALTEN, HEBB-WILLIAMS-INTELLIGENZTEST UND BEI DER LABYRINTHEXPLORATION	ZEITSCHRIFT FÜR EXPERIMENTELLE UND ANGEWANDTE PSYCHOLOGIE, 1977, 2 (230-423)
DRISCOLL-P, KÄSERMANN-HP	DIFFERENCES IN THE RESPONSE TO PENTOBARBITAL SODIUM OF ROMAN HIGH- UND LOW-AVOIDANCE RATS	ARZNEIMITTEL-FORSCHUNG/DRUG RESEARCH 27, 1977
CLASSEN-W, BÄTTIG-K,	WIRKUNG VON NIKOTIN UND AMPHETAMINE AUF DIE REGULATION DES KÖPERGEWICHTS	SOZ.- UND PRÄVENTIVMEDIZIN, 22, 1977 (197-198)
SCHLATTER-J, BÄTTIG-K	EFFECTS OF ALPHA METHYL-P-TYROSINE ON EXPLORATORY BEHAVIOR IN TWO RAT STRAINS	EXPERIENTIA 33, (809) 1977
DRISCOLL-P.	NICOTINE-LIKE BEHAVIORAL EFFECT AFTER SMALL DOSE OF MECAMYLAMINE IN ROMAN HIGH-ADVOIDANCE RATS	PSYCHOPHARMACOLOGIA 47, 1976
BÄTTIG-K, DRISCOLL-P, SCHLATTER-J, USTER-HJ	EFFECTS OF NICOTINE AND THE EXPLORATORY LOCOMOTION PATTERNS OF FEMALE ROMAN HIGH- AND LOW-AVOIDANCE RATS	PHARMACOL. BIOCHEM. BEHAV. 4, 1976
DRISCOLL-P	INHALATION OF SMOKE FROM HIGH- AND LOW-NICOTINE CIGARETTES BY GUINEA PIGS:	BEHAVIORAL AND ECG-EFFECTS IN: (HORVATH-M.) "ADVERSE EFFECTS OF ENCIROMENTAL CHEMICALS AND PSYCHOTROPIC DRUGS VOL. 2. NEUROPHYSIOLOGICAL AND BEHAVIORAL TESTS." :ELSEVIER. AMSTERDAM. 1976
SCHLATTER-J, BÄTTIG-K	EFFECTS OF MAZE HABITUATION AND HABITUATION TO NICOTINE AND AMPHETAMINE ON EXPLORATORY LOCOMOTION PATTERNS IN RATS.	BEHAVIORAL EFFECTS OF NICOTINE. SEPT. 1976
BÄTTIG-K, SCHLATTER-J	EFFECTS OF NICOTINE AND AMPHETAMINE ON EXPLORATION AND ON MAZE MEMORY BY RHA AND RLA RATS.	BEHAVIORAL EFFECTS OF NICOTINE. SEPT. 1976

DRISCOLL-P	INHALATION OF SMOKE FROM HIGH- AND LOW-NICOTINE CIGARETTES BY GUINEA PIGS. BEHAVIORAL AND EGG EFFECTS	ADV. EFF. ENV. CHEM. AND PSYCH. DRUGS. 2, NEUCHROPHYSIOLOGICAL AND BEHAVIOURAL TESTS, 1976 (241-256)
MÜNSTER-G, BÄTTIG-K	NICOTINE-INDUCED HYPOPHAGIA AND HYPODIPSIA IN DEPRIVATED AND IN HYPOTHALAMICALLY STIMULATED RATS	PSYCHOPHARMACOLOGIA, 1975, 41 (211-217)
DRISCOLL-P, BÄTTIG-K	THE EFFECT OF SMALL DOSES OF MECAMYLAMINE ON SHUTTLE BOX BEHAVIOR IN THE GUINEA PIG	EXPERIENTIA NO 29, 1973
SCHLATTER-J	DIE WIRKUNG VON NIKOTIN AUF DAS EXPLORATIONSVERHALTEN VON ROMAN HIGH AVOIDANCE UND ROMAN LOW AVOIDANCE RATTEN	DIPLOM THESIS NO 690262N, SCHWISS FEDERAL INSTITUTE OF TECHNOLOGY, ZURICH, 1973
DRISCOLL-P, BÄTTIG-K	CIGARETTE SMOKE AND BEHAVIOR: SOME RECENT DEVELOPMENTS.	REV. ENVIR. HEALTH 1, 1973
BÄTTIG-K, DRISCOLL-P	EFFECTS OF THE INHALATION OF CIGARETTE SMOKE ON SWIMMING ENDURANCE AND AVOIDANCE BEHAVIOR IN THE RAT.	PLENUM PRESS 1974, 5TH ROCHESTER INT. CONF. ENVIRONM. TOXICITY 1972
DEUBER-A, BÄTTIG-K, GRANDJEAN-E	EFFECT OF FILTERED CIGARETTE SMOKE ON RATS	NATURE NO 237, 1972
BÄTTIG-K, DRISCOLL-P	DIFFERENTIAL EFFECTS OF FILTERED AND UNFILTERED CIGARETTE SMOKE ON TWO BEHAVIOR TESTS WITH RATS	ABSTRACT, 5TH INTERNATIONAL CONG. PHARMACOL., 1972
DRISCOLL-P	THE COMPARATIVE TOXICITY FOR MICE OF FIVE COMMONLY USED NICOTINE PREPARATIONS	PRÄVENTIVMEDIZIN NO 17, 1972
BÄTTIG-K, HRUBES-V	THE EFFECT OF FILTRATE FRACTIONS OF TOBACCO SMOKE ON SWIMMING ENDURANCE IN THE RAT	PRÄVENTIVMEDIZIN NO 16, 1971
BÄTTIG-K, PERRET-CH	BEZIEHUNGEN VON ALKOHOL- UND TABAKKONSUM ZU SOZIALSTATUS, PERSÖNLICHKEIT UND POLITISCHEN EINSTELLUNGEN BEI STUDENTEN	PRÄVENTIMEDIZIN NO 16, 1971
DRISCOLL-P, BÄTTIG-K	THE EFFECT OF FILTRATE FRECTIONS OF TOBACCO SMOKE ON THE AVOIDANCE BEHAVIOR OF RATS UND EXTINCTION PROCEDURE	PRÄVENTIVMEDIZIN NO 16, 1971
BÄTTIG-K	PERSÖNLICHKEITSASPEKTE UND SUBJEKTIVE EINSTELLUNGEN BEI RAUCHERN UND NICHTRAUCHERN, ABSTINENTEN UND ALKOHOLKONSUMENTEN	PRÄVENTIVMEDIZIN NO 16, 1971
DRISCOLL-P, DEUBER-A	DIE WIRKUNGEN VON FILTRIERTEM ZIGARETTENRAUCH AUF DEN KOHLENMONOXID-HÄMOGLOBIN-SPIEGEL UND DIE ATMUNGSFREQUENZ DER RATTE.	PRÄVENTIVMEDIZING NO 16, 1971
BÄTTIG-K	THE EFFECT OF PRE- AND POST-TRIAL APPLICATION OF NICOTINE ON THE 12 PROBLEMS OF THE HEBB-WILLIAMS-TEST IN THE RAT	PSYCHOPHARMACOLOGIA NO 18, 1970
BÄTTIG-K	DIFFERENTIAL EFFECTS OF NICOTINE AND TOBACCO SMOKE ALKALOIDS ON SWIMMING ENDURANCE IN THE RAT.	PSYCHOPHARMACOLOGIA NO 18, 1970
DRISCOLL-P, BÄTTIG-K	THE EFFECT OF NICOTINE AND TOTAL ALKALOIDS EXTRACTED FROM CIGARETTE SMOKE AND AVOIDANCE BEHAVIOR IN RATS UNDER EXTINCTION PROCEDURE.	PSYCHOPHARMACOLOGIA NO 18, 1970
HRUBES-V, BÄTTIG-K	EFFECT OF INHALED CIGARETTE SMOKE ON SWIMMING ENDURANCE IN THE RAT	ARCH. ENVIRON. HEALTH NO 21, 1970
DRISCOLL-P	THE EFFECT OF FILTERED AND UNFILTERED CIGARETTE SMOKE ON THE AVOIDANCE BEHAVIOR OF RATS UNDER EXTINCTION PROCEDURE.	PRÄVENTIVMEDIZIN NO 15, 1970

BÄTTIG-K	THE EFFECT OF NICOTINE ON THE SWIMMING SPEED OF PRETRAINED RATS THROUGH A WATER ALLEY	PSYCHOPHARMACOLOGIA NO 15, 1969
HRUBES-V, BÄTTIG-K	DER EINFLUSS DES ZIGARETTENRAUCHES AUF DIE SCHWIMMLEISTUNG DER RATTEN	PRÄVENTIMEDIZIN NO 14, 1969
BÄTTIG-K	DIE WIRKUNG VON NIKOTIN AUF DIE SCHWIMMAUSDAUERTESTGEWÖHNTER RATTEN.	PRÄVENTIVMEDIZIN NO 13, 1968
WANNER-H-U, BÄTTIG-K	DIE WIRKUNG VON NIKOTIN UND AMPHETAMIN AUF DIE SUBKORTIKALE SELBSTREIZUNG BEI DER RATTE	PRÄVENTIVMEDIZIN NO 13, 1968
WANNER-H-U, BÄTTIG-K	DIE WIRKUNG VON NIKOTIN UND AMPHETAMIN AUF DIE SELBSTREIZUNG BEI DER RATTE	HELV. PHYSIOL, ACTA 24, 1966

PR G. KISTLER

PETER-H-J, KISTLER-G-S	ISOLATION UND IN VITRO-KULTIVATION VON TUMORZELLEN AUS MENSCHLICHEN, IN DER NU/NU MAUS TRANSPLANTIERTEN BRONCHUSKARZINOMEN	SCHWEIZ MED WOCHENSCHRIFT, 1979, 109 (830-832)
KISTLER-G-S, PETER-H-J O (NU/NU MAUS) UND IN VITRO	WIRKUNG VON 2 RETINOIDEN (VITAMIN A-ANALOGEN) AUF MENSCHLICHE BRONCHUSKARZINOME IN VIVO UND IN VITRO	SCHWEIZ MED WOCHENSCHRIFT,1979, 109 (847-850)
PETER-H-J, KISTLER-G-S, SAUTER-C	ISOLATION MENSCHLICHER TUMORZELLEN: VORAUSSETZUNG FÜR DIAGNOSTISCHE UND THERAPEUTISCHE UNTERSUCHUNGEN IN VITRO	SCHWEIZ MED WOCHENSCHRIFT, 1978, 108 , 1607
WALT-H, KISTLER-GS	HETEROGENICITY OF THE EPITHELIUM AT THE BIFURCATIONS OF THE TRACHEO-BRONCHIAL TREE. A SCANNING- AND TRANSMISSION ELECTRON MICROSCOPICAL STUDY IN MACACA FASCICULARIS.	ABSTRACT, 10TH ANNUAL MEETING OF THE USGEB, MAI 1978, DAVOS
GROSCURTH-P, FLEMING-N, KISTLER-G-S	ACTIVITY AND DISTRIBUTION OF GAMMA-GLUTAMYL-TRANS-PEPTIDASE (Y-GT) IN HUMAN LUNG CANCERS SERIALLY TRANSPLANTED IN NUDE MICE	HISTOCHEMISTRY, 1977, 53 (135-142)
FLEMING-N, KISTLER-G-S	MORPHOLOGY, CYTOCHEMISTRY AND ISOZYMES OF MONKEY KIDNEY CULTURE CELLS DURING LONG-TERM EXPOSURE TO CIGARETTE SMOKE	ACTA HISTOCHEM, 1977, 60 (132-145)
GROSCURTH-P, KISTLER-G-S	LANGZEIT-BEOBACHTUNGEN ÜBER DAS VERHALTEN MENSCHLICHER MALIGNOME IN DER NU/NU MAUS: I. HYPERNEPHROIDE NIERENKARZINOME	BEITR PATH, 1977, 160 (337-360)
FLEMING-N, GROSCURTH-P, KISTLER-G-S	THE ACTIVITY AND DISTRIBUTION OF GAMMA-GLUTAMYL TRANSPEPTIDASE (Y-GT) IN HUMAN FOETAL ORGANS	HISTOCHEMISTRY, 1977, 51 (209-218)
DAVIES-P, KISTLER-G	THE ASSESSMENT OF TOBACCO SMOKE TOXICITY AND ORGAN CULTURE: AN ARRANGEMENT FOR EXPOSURE UNDER DEFINED CONDITIONS	EXPERIENTIA,1974.
KISTLER-G-S, GROSCURTH-P, FLEMING-N	MORPHOLOGY UND BIOCHEMIE MENSCHLICHER BRONCHIAL-TUMOREN IN DER THYMUS-DYSGENETISCHEN (NU/NU) MAUS	?

PR G. KISTLER

PETER-H-J, KISTLER-G-S	ISOLATION UND IN VITRO-KULTIVATION VON TUMORZELLEN AUS MENSCHLICHEN, IN DER NU/NU MAUS TRANSPLANTIERTEN BRONCHUSKARZINOMEN	SCHWEIZ MED WOCHENSCHRIFT, 1979, 109 (830-832)
KISTLER-G-S. PETER-H-J O (NU/NU MAUS) UND IN VITRO	WIRKUNG VON 2 RETINOIDEN (VITAMIN A-ANALOGEN) AUF MENSCHLICHE BRONCHUSKARZINOME IN VIV	SCHWEIZ MED WOCHENSCHRIFT,1979, 109 (847-850)
PETER-H-J, KISTLER-G-S. SAUTER-C	ISOLATION MENSCHLICHER TUMORZELLEN: VORAUSSETZUNG FÜR DIAGNOSTISCHE UND THERAPEUTISCHE UNTERSUCHUNGEN IN VITRO	SCHWEIZ MED WOCHENSCHRIFT, 1978, 108 , 1607
WALT-H. KISTLER-GS	HETEROGENICITY OF THE EPITHELIUM AT THE BIFURCATIONS OF THE TRACHEO-BRONCHIAL TREE. A SCANNING- AND TRANSMISSION ELECTRON MICROSCOPICAL STUDY IN MACACA FASCICULARIS.	ABSTRACT, 10TH ANNUAL MEETING OF THE USGEB, MAI 1978, DAVOS
GROSCURTH-P, FLEMING-N, KISTLER-G-S	ACTIVITY AND DISTRIBUTION OF GAMMA-GLUTAMYL-TRANS-PEPTIDASE (Y-GT) IN HUMAN LUNG CANCERS SERIALLY TRANSPLANTED IN NUDE MICE	HISTOCHEMISTRY, 1977, 53 (135-142)
FLEMING-N, KISTLER-G-S	MORPHOLOGY, CYTOCHEMISTRY AND ISOZYMES OF MONKEY KIDNEY CULTURE CELLS DURING LONG-TERM EXPOSURE TO CIGARETTE SMOKE	ACTA HISTOCHEM, 1977, 60 (132-145)
GROSCURTH-P. KISTLER-G-S	LANGZEIT-BEOBACHTUNGEN ÜBER DAS VERHALTEN MENSCHLICHER MALIGNOME IN DER NU/NU MAUS: I. HYPERNEPHROIDE NIERENKARZINOME	BEITR PATH, 1977, 160 (337-360)
FLEMING-N. GROSCURTH-P, KISTLER-G-S	THE ACTIVITY AND DISTRIBUTION OF GAMMA-GLUTAMYL TRANSPEPTIDASE (Y-GT) IN HUMAN FOETAL ORGANS	HISTOCHEMISTRY, 1977, 51 (209-218)
DAVIES-P, KISTLER-G	THE ASSESSMENT OF TOBACCO SMOKE TOXICITY AND ORGAN CULTURE: AN ARRANGEMENT FOR EXPOSURE UNDER DEFINED CONDITIONS	EXPERIENTIA,1974.
KISTLER-G-S. GROSCURTH-P. FLEMING-N	MORPHOLOGY UND BIOCHEMIE MENSCHLICHER BRONCHIAL-TUMOREN IN DER THYMUS-DYSGENETISCHEN (NU/NU) MAUS	?

PR G. KISTLER

PETER-H-J, KISTLER-G-S	ISOLATION UND IN VITRO-KULTIVATION VON TUMORZELLEN AUS MENSCHLICHEN, IN DER NU/NU MAUS TRANSPLANTIERTEN BRONCHUSKARZINOMEN	SCHWEIZ MED WOCHENSCHRIFT, 1979, 109 (830-832)
KISTLER-G-S, PETER-H-J O (NU/NU MAUS) UND IN VITRO	WIRKUNG VON 2 RETINOIDEN (VITAMIN A-ANALOGEN) AUF MENSCHLICHE BRONCHUSKARZINOME IN VIVO UND IN VITRO	SCHWEIZ MED WOCHENSCHRIFT,1979, 109 (847-850)
PETER-H-J, KISTLER-G-S, SAUTER-C	ISOLATION MENSCHLICHER TUMORZELLEN: VORAUSSETZUNG FÜR DIAGNOSTISCHE UND THERAPEUTISCHE UNTERSUCHUNGEN IN VITRO	SCHWEIZ MED WOCHENSCHRIFT, 1978, 108 , 1607
WALT-H, KISTLER-GS	HETEROGENICITY OF THE EPITHELIUM AT THE BIFURCATIONS OF THE TRACHEO-BRONCHIAL TREE. A SCANNING- AND TRANSMISSION ELECTRON MICROSCOPICAL STUDY IN MACACA FASCICULARIS.	ABSTRACT, 10TH ANNUAL MEETING OF THE USGEB, MAI 1978, DAVOS
GROSCURTH-P, FLEMING-N, KISTLER-G-S	ACTIVITY AND DISTRIBUTION OF GAMMA-GLUTAMYL-TRANS-PEPTIDASE (Y-GT) IN HUMAN LUNG CANCERS SERIALLY TRANSPLANTED IN NUDE MICE	HISTOCHEMISTRY, 1977, 53 (135-142)
FLEMING-N, KISTLER-G-S	MORPHOLOGY, CYTOCHEMISTRY AND ISOZYMES OF MONKEY KIDNEY CULTURE CELLS DURING LONG-TERM EXPOSURE TO CIGARETTE SMOKE	ACTA HISTOCHEM, 1977, 60 (132-145)
GROSCURTH-P, KISTLER-G-S	LANGZEIT-BEOBACHTUNGEN ÜBER DAS VERHALTEN MENSCHLICHER MALIGNOME IN DER NU/NU MAUS: I. HYPERNEPHROIDE NIERENKARZINOME	BEITR PATH, 1977, 160 (337-360)
FLEMING-N, GROSCURTH-P, KISTLER-G-S	THE ACTIVITY AND DISTRIBUTION OF GAMMA-GLUTAMYL TRANSPEPTIDASE (Y-GT) IN HUMAN FOETAL ORGANS	HISTOCHEMISTRY, 1977, 51 (209-218)
DAVIES-P, KISTLER-G	THE ASSESSMENT OF TOBACCO SMOKE TOXICITY AND ORGAN CULTURE: AN ARRANGEMENT FOR EXPOSURE UNDER DEFINED CONDITIONS	EXPERIENTIA,1974.
KISTLER-G-S, GROSCURTH-P, FLEMING-N	MORPHOLOGY UND BIOCHEMIE MENSCHLICHER BRONCHIAL-TUMOREN IN DER THYMUS-DYSGENETISCHEN (NU/NU) MAUS	?

CERUTTI-P-A.	RESPONSE MODIFICATION IN CARCINOGENESIS.	ENVIRONMENTAL-HEALTH-PERSPECTIVES, 1989, V81, MAY, P39-43.
KRUPITZA-G, CERUTTI-P.	POLY(ADP-RIBOSYLATION) OF HISTONES IN INTACT HUMAN KERATINOCYTES.	BIOCHEMISTRY, 1989, V28, N9, P4054-4060.
KRUPITZA-G, CERUTTI-P.	ADP-RIBOSYLATION OF ADPR-TRANSFERASE AND TOPOISOMERASE-I IN INTACT MOUSE EPIDERMAL-CELLS JB6.	BIOCHEMISTRY, 1989, V28, N5, P2034-2040.
LARSSON-R, CERUTTI-P.	OXIDANTS INDUCE PHOSPHORYLATION OF RIBOSOMAL PROTEIN-S6.	JOURNAL-OF-BIOLOGICAL-CHEMISTRY, 1988, V263, N33, P17452-17458.
CRAWFORD-D, ZBINDEN-I, AMSTAD-P, CERUTTI-P.	OXIDANT STRESS INDUCES THE PROTO-ONCOGENES CIS-FOS AND CIS-MYC IN MOUSE EPIDERMAL-CELLS.	ONCOGENE, 1988, V3, N1, P27-32.
CERUTTI-P.	OXIDANT TUMOR PROMOTERS	GROWTH FACTORS, TUMOR PROMOTERS, AND CANCER GENES 239-247 , 1988.
CRAWFORD-D-R, MIRAULT-M-E, MORET-R, ZBINDEN-I, CERUTTI-P-A.	MOLECULAR DEFECT IN HUMAN ACATALASIA FIBROBLASTS.	BIOCHEMICAL-AND-BIOPHYSICAL-RESEARCH-COMMUNICATIONS, 1988, V153, N1, P59-66.
CERUTTI-P-A.	RESPONSE MODIFICATION CREATES PROMOTABILITY IN MULTISTAGE CARCINOGENESIS.	CARCINOGENESIS, 1988, V9, N4, P519-526.
CRAWFORD-D, ZBINDEN-I, MORET-R, CERUTTI-P.	ANTIOXIDANT ENZYMES IN XERODERMA PIGMENTOSUM FIBROBLASTS.	CANCER-RESEARCH, 1988, V48, N8, P2132-2134.
MUEHLEMATTER-D, LARSSON-R, CERUTTI-P.	ACTIVE OXYGEN INDUCED DNA STRAND BREAKAGE AND POLY ADP-RIBOSYLATION IN PROMOTABLE AND NON-PROMOTABLE JB6 MOUSE EPIDERMAL-CELLS.	CARCINOGENESIS, 1988, V9, N2, P239-245.
CERUTTI-P, LARSSON-R, KRUPITZA-G, MUEHLEMATTER-D, CRAWFORD-D, AMSTAD- P.	PATHOPHYSIOLOGICAL MECHANISMS OF OXIDANTS	OXY-RADICALS IN MOLECULAR BIOLOGY AND PATHOLOGY, PP. 493-507, ALAN R. LISS, 1988.
CERUTTI-P, KRUPITZA-G, LARSSON-R, MUEHLEMATTER-D, CRAWFORD-D, AMSTAD- P.	PHYSIOLOGICAL AND PATHOLOGIC EFFECTS OF OXIDANTS IN MOUSE EPIDERMAL CELLS	MEMBRANE IN CANCER CELLS, ANNALS OF THE NEW-YORK ACADEMY OF SCIENCES, DEC. 30, 1988
KOZUMBO-W-J, MUEHLEMATTER-D, JORG-A, EMERIT-I, CERUTTI-P.	PHORBOL ESTER-INDUCED FORMATION OF CLASTOGENIC FACTOR FROM HUMAN- MONOCYTES.	CARCINOGENESIS, 1987, V8, N4, P521-526.
OCHI-T, CERUTTI-P-A.	CLASTOGENIC ACTION OF HYDROPEROXY-5.8.11.13-ICOSATETRAENOIC ACIDS ON THE MOUSE EMBRYO FIBROBLASTS C3H-10T1/2.	PROCEEDINGS-OF-THE-NATIONAL-ACADEMY-OF-SCIENCES-OF-THE-UNITED-STATES- OF-AMERICA, 1987, V84, N4, P990-994.
KOZUMBO-W-J, HARRIS-D-T, GROMKOWSKI-S, CEROTTINI-J-C, CERUTTI-P-A.	MOLECULAR MECHANISMS INVOLVED IN T-CELL ACTIVATION .2. THE PHOSPHATIDYLINOSITOL SIGNAL-TRANSDUCING MECHANISM MEDIATES ANTIGEN- INDUCED LYMPHOKINE PRODUCTION BUT NOT INTERLEUKIN-2-INDUCED PROLIFERATION IN CLONED CYTO-TOXIC LYMPHOCYTES-T.	JOURNAL-OF-IMMUNOLOGY, 1987, V138, N2, P606-612.
CERUTTI-P.	THE ROLE OF DNA DAMAGE AND ITS REPAIR IN AGING: FUTURE DIRECTIONS OF RESEARCH	MODERN BIOLOGICAL THEORIES OF AGING. H.R. WARNER ET AL., RAVEN PRESS, 1987
CERUTTI-P.	GENOTOXIC OXIDANT TUMOR PROMOTERS	BANBURRY REPORT 25: NONGENOTOXIC MECHANISM IN CARCINOGENESIS, COLD SPRING HARBOR LAB., 1987

PROFESSEUR PETER A. CERUTTI

AMSTAD-P, PESKIN-A, SHAH-G, MIRAULT-M-E, MORET-R, ZBINDEN-I, CERUTTI- P.	THE BALANCE BETWEEN CU, ZN-SUPEROXIDE DISMUTASE AND CATALASE AFFECTS THE SENSITIVITY OF MOUSE EPIDERMAL-CELLS TO OXIDATIVE STRESS.	BIOCHEMISTRY, 1991, V30, N38, P9305-9313.
FELLEYBOSCO-E, POURZAND-C, ZIJLSTRA-J, AMSTAD-P, CERUTTI-P.	A GENOTYPIC MUTATION SYSTEM MEASURING MUTATIONS IN RESTRICTION RECOGNITION SEQUENCES.	NUCLEIC-ACIDS-RESEARCH, 1991, V19, N11, P2913-2919.
CERUTTI-P-A.	OXIDANT STRESS AND CARCINOGENESIS.	EUROPEAN-JOURNAL-OF-CLINICAL-INVESTIGATION, 1991, V21, N1, P1-5.
CERUTTI-P-A, TRUMP-B-F.	INFLAMMATION AND OXIDATIVE STRESS IN CARCINOGENESIS.	CANCER-CELLS-A-MONTHLY-REVIEW, 1991, V3, N1, P1-7.
AMSTAD-P, CERUTTI-P.	GENETIC MODULATION OF THE CELLULAR ANTIOXIDANT DEFENSE CAPACITY.	ENVIRONMENTAL-HEALTH-PERSPECTIVES, 1990, V88, AUG, P77-82.
CERUTTI-P, LARSSON-R, KRUPITZA-G.	MECHANISM OF OXIDANTS CARCINOGENESIS	GENETIC MECHANISM IN CARCINOGENESIS AND TUMOR PROGRESSION, P. 69-82, 1990
CERUTTI-P.	MECHANISM OF ACTION OF OXIDANT CARCINOGENS	DETECTION AND PREVENTION, CRC PRESS, VOL. 14. PP. 281-284, 1990
ZIMMERMAN-P, CERUTTI-P,LITTLE-J-B.	BIOLOGICAL CHARACTERIZATION AND QUANTIATION OF MARKERS OF TRANSFORMATION OF HUMAN FIBROPLASTS	G. MILO AND B. CASTRO, CRC HANDBOOK 113-117, 1990
ZIJLSTRA-J. FELLEYBOSCO-E. AMSTAD-P. CERUTTI-P.	A MAMALIAN MUTATION SYSTEM AVOIDING PHENOTIC SELECTION: THE RFLP/PCR APPROACH	CARCINOGENS AND MUTAGENS IN THE DIET EDS. M. PARIZA & H.U. AESCHBACHER. WILEY-LYSS INC. PP. 187-200, 1990
OCHI-T. CERUTTI-P-A.	DIFFERENTIAL-EFFECTS OF GLUTATHIONE DEPLETION AND METALLOTHIONEIN INDUCTION ON THE INDUCTION OF DNA SINGLE-STRAND BREAKS AND CYTOTOXICITY BY TERT-BUTYL HYDROPEROXIDE IN CULTURED-MAMMALIAN-CELLS.	CHEMICO-BIOLOGICAL-INTERACTIONS, 1989, V72, N3, P335-345.
MUEHLEMATTER-D. OCHI-T. CERUTTI-P.	EFFECTS OF TERT-BUTYL HYDROPEROXIDE ON PROMOTABLE AND NON-PROMOTABLE JB6 MOUSE EPIDERMAL-CELLS.	CHEMICO-BIOLOGICAL-INTERACTIONS, 1989, V71, N4, P339-352.
CANTONI-O. CATTABENI-F, STOCCHI-V. MEYN-R-E, CERUTTI-P, MURRAY-D.	HYDROGEN-PEROXIDE INSULT IN CULTURED MAMMALIAN-CELLS - RELATIONSHIPS BETWEEN DNA SINGLE-STRAND BREAKAGE, POLY(ADP-RIBOSE) METABOLISM AND CELL KILLING.	BIOCHIMICA-ET-BIOPHYSICA-ACTA. 1989. V1014, N1, P1-7.
LARSSON-R. CERUTTI-P.	TRANSLOCATION AND ENHANCEMENT OF PHOSPHOTRANSFERASE ACTIVITY OF PROTEIN KINASE-C FOLLOWING EXPOSURE IN MOUSE EPIDERMAL-CELLS TO OXIDANTS.	CANCER-RESEARCH. 1989, V49, N20, P5627-5632.
CRAWFORD-D-R, AMSTAD-P-A, FOO-D-D-Y, CERUTTI-P-A.	CONSTITUTIVE AND PHORBOL-MYRISTATE-ACETATE REGULATED ANTIOXIDANT DEFENSE OF MOUSE EPIDERMAL JB6 CELLS.	MOLECULAR-CARCINOGENESIS, 1989, V2, N3, P136-143.
CERUTTI-P, LARSSON-R, KRUPITZA-G, MUEHLEMATTER-D, CRAWFORD-D, AMSTAD- P.	PATHOPHYSIOLOGICAL MECHANISMS OF ACTIVE OXYGEN.	MUTATION-RESEARCH. 1989, V214, N1, P81-88.
CANTONI-O, SESTILI-P, CATTABENI-F, BELLOMO-G, POU-S, COHEN-M, CERUTTI-P.	CALCIUM CHELATOR QUIN-2 PREVENTS HYDROGEN-PEROXIDE-INDUCED DNA BREAKAGE AND CYTO-TOXICITY.	EUROPEAN-JOURNAL-OF-BIOCHEMISTRY, 1989, V182, N2, P209-212.

CRAWFORD-D, CERUTTI-P.	EXPRESSION OF OXIDANT STRESS-RELATED GENES IN TUMOR PROMOTION OF MOUSE EPIDERMAL CELLS	ANTICARCINOGENESIS AND RADIATION PROTECTION, EDS P. CERUTTI, PLENUM PUBLISHING CORP., 1987
CERUTTI-P-A	THE ROLE OF ACTIVE OXYGEN IN TUMOR PROMOTION	BIOCHEMICAL AND MOLECULAR EPIDEMIOLOGY OF CANCER, 1986, 167-176
BROWN-T-C, CERUTTI-P-A	ULTRAVIOLET RADIATION INACTIVATES SV40 BY DISRUPTING AT LEAST FOUR GENETIC FUNCTIONS	THE EMBO JOURNAL, 1986, VOL. 5, PP. 197-203
SINGH-N, CERUTTI-P	POLY ADP-RIBOSYLATION OF HISTONES IN TUMOR PROMOTER PHORBOL-12-MYRISTATE-13-ACETATE TREATED MOUSE EMBRYO FIBROPLASTS C3H10T1/2	BIOCHEMICAL AND BIOPHYSICAL RESEARCH COMMUNICATIONS , 1985, VOL. 132, PP. 811-819
SINGH-N, LEDUC-Y, POIRIER-G, CERUTTI-P.	NON-HISTONE CHROMOSOMAL PROTEIN ACCEPTORS FOR POLY(ADP)-RIBOSE IN PHORBOL-12-MYRISTATE-13-ACETATE TREATED MOUSE EMBRYO FIBROBLASTS (C3H10T1/2).	CARCINOGENESIS, 1985, 6/10 (1489-1494).
POIRIER-G-G, BROWN-T-C, CERUTTI-P-A.	POLY ADP-RIBOSYLATION AND DNA STRAND BREAKAGE IN SV 40 MINICHROMOSOMES.	CARCINOGENESIS, 1985, 6/2 (283-287).
SINGH-N, POIRIER-G, CERUTTI-P.	TUMOR PROMOTER PHORBOL-12-MYRISTATE-13-ACETATE INDUCES POLY ADP- RIBOSYLATION IN HUMAN MONOCYTES.	BIOCHEM-BIOPHYS-RES-COMMUN, 1985, 126/3 (1208-1214).
CERUTTI-P-A.	PROOXIDANT STATES AND TUMOR PROMOTION.	SCIENCE, 1985, 227/4685 (375-381).
SINGH-N, POIRIER-G, CERUTTI-P.	TUMOR PROMOTER PHORBOL-12-MYRISTATE-13-ACETATE INDUCES POLY ADP-RIBOSYLATION IN FIBROBLASTS	EMBO JOURNAL, 1985, 4, PP. 1491-1494
RUDIGER-H-W, NOWAK-D, HARTMANN-K, CERUTTI-P.	ENHANCED FORMATION OF BENZO(A)PYRENE:DNA ADDUCTS IN MONOCYTES OF PATIENTS WITH A PRESUMED PREDISPOSITION TO LUNG CANCER.	CANCER-RES, 1985, 45/11II (5890-5894).
AMSTAD-P, LEVY-A, EMERIT-I, CERUTTI-P.	EVIDENCE FOR MEMBRANE-MEDIATED CHROMOSOMAL DAMAGE BY AFLATOXIN BSUB 1 IN HUMAN LYMPHOCYTES.	CARCINOGENESIS, 1984, 5/6 (719-723).
ZIMMERMAN-R, CERUTTI-P.	ACTIVE OXYGEN ACTS AS A PROMOTER OF TRANSFORMATION IN MOUSE EMBRYO C3H/10T.5/C18 FIBROBLASTS.	PROC-NATL-ACAD-SCI-U-S-A, 1984, 81/7I (2085-2087).
CERUTTI-P-A, EMERIT-I, AMSTAD-P	MEMBRANE-MEDIATED CHROMOSOMAL DAMAGE	GENES AND PROTEINS IN ONCOGENESIS, ACADEMIC PRESS, 1983
CERUTTI-P-A, EMERIT-I, AMSTAD-P	TUMOR PROMOTER PHORBOL -MYRISTATE ACETATE INDUCES MEMBRANE-MEDIATED CHROMOSOMAL DAMAGE	RADIOPROTECTORS AND ANTICARCINOGENS, ACADEMIC PRESS, 1983
BROWN-T-C, AMSTAD-P-A, NIGGLI-J, CERUTTI-P-A	CELLULAR RESPONSES TO DAMAGE IN DNA	HUMAN CARCINOGENESIS, ACADEMIC PRESS, 1983
EMERIT-I, CERUTTI-P.	CLASTOGENIC ACTION OF TUMOR PROMOTER PHORBOL-12-MYRISTATE-13 ACETATE IN MIXED HUMAN LEUKOCYTE CULTURES.	CARCINOGENESIS, 1983, 4/10 (1313-1316).
EMERIT-I, CERUTTI-P-A.	TUMOR PROMOTER PHORBOL 12-MYRISTATE 13-ACETATE INDUCES A CLASTOGENIC FACTOR IN HUMAN LYMPHOCYTES.	PROC-NATL-ACAD-SCI-U-S-A, 1982, 79/23I (7509-7513).
CERUTTI-P-A	DNA LESIONS : NATURE AND GENESIS	CHEMICAL CARCINOGENESIS, 1982

KANEKO-M, CERUTTI-P-A.	EXCISION OF BENZO(A)PYRENE DIOL EPOXIDE I ADDUCTS FROM NUCLEOSOMAL DNA OF CONFLUENT NORMAL HUMAN FIBROBLASTS.	CHEM-BIOL-INTERACT, 1982, 38/3 (261-274).
KOOTSTRA-A, CERUTTI-P-A.	EFFECT OF HISTONE ACETYLATION ON THE FORMATION AND REMOVAL OF COVALENT BENZO(A)PYRENE CHROMATIN ADDUCTS.	J-SUPRAMOL-STRUCT-CELL-BIOCHEM, 1981, 15/SUPPL.5 (NO. 501).
KOOTSTRA-A, CERUTTI-P-A.	EFFECT OF HISTONE ACETYLATION ON THE FORMATION AND REMOVAL OF COVALENT BENZO(A)PYRENE CHROMATIN ADDUCTS.	J-SUPRAMOL-STRUCT-CELL-BIOCHEM, 1981, 15/SUPPL.5 (NO. 501).
EMERIT-I, CERUTTI-P-A.	TUMOUR PROMOTER PHORBOL-12-MYRISTATE-13-ACETATE INDUCES CHROMOSOMAL DAMAGE VIA INDIRECT ACTION.	NATURE-(LONDON), 1981, 293/5828 (144-146).
FELDMAN-G, REMSEN-J, WANG-T-V, CERUTTI-P.	FORMATION AND EXCISION OF COVALENT DEOXYRIBONUCLEIC ACID ADDUCTS OF BENZO(A)PYRENE 4,5-EPOXIDE AND BENZO(A)PYRENEDIOL EPOXIDE I IN HUMAN LUNG CELLS A549.	BIOCHEMISTRY (WASH.), 1980, 19/6 (1095-1101).
CERUTTI-P, KANEKO-M, BEARD-P	NUCLEOSOMAL STRUCTURE CHROMATIN: DISTRIBUTION AND EXCISION OF DNA DAMAGE.	PROCEEDINGS NATO/EMBO LECTURE COURSE ON "CHROMOSOME DAMAGE AND REPAIR", NORWAY MAI 27-JUNE 5, 1980

PR MEDICI

UNGER-S	BEEINFLUSST DIE RAUCHWEISE VON ZIGARETTEN DIE CHRONISCHE OBSTRUKTIVEN ATEMWEGESERKRANKUNGEN UND DEN BRONCHIALKREBS	INAUGURAL - DISSERTATION, MEDIZINISCHE POLIKLINIK DER UNIVERSITÄT ZÜRICH, 1982 SCHWEIZ MED WOCHENSCHRIFT, 1983, 113 (104)
MEDICI-C	"SMALL AIRWAYS DISEASE": FAKTEN ODER FIKTION	SCHWEIZ MED WOCHENSCHRIFT, 1985, 115 (592-596)
MEDICI-T-C, UNGER-S, RUEGGER-M	SMOKING PATTERN OF SMOKERS WITH AND WITHOUT TOBACCO-SMOKE-RELATED LUNG DISEASES	AM REV RESPIR DIS, 1985, 131 (385-388)

PROFESSEUR P. HAAB

PIIPER-J, HAAB-P.	OXYGEN-SUPPLY AND UPTAKE IN TISSUE MODELS WITH UNEQUAL DISTRIBUTION OF BLOOD-FLOW AND SHUNT.	RESPIRATION-PHYSIOLOGY, 1991, V84, N2, P261-271.
BETTICHER-D, GEISER-J, TEMPINI-A	LUNG DIFUSING CAPACITY AND RED BLOOD CEL VOLUME	RESPIRATION PHYSIOLOGIY 89, PP. 271-278, 1991
HAAB-P-E, DURAND-ARCZYNSKA-W-Y	CARBON MONOXYDE EFFECTS ON OXYGEN TRANSPORT	THE LUNG: SCIENTIFIC FOUNDATIONS, ED. R.G. CRYSTAL AND J.B. WEST, RAVEN PRESS, NEW YORK, 1991
SCHUWEY-D, TEMPINI-A, HAAB-P-E.	CARBON MONOXIDE EQUILIBRIUM CURVE OF HUMAN UMBILICAL CORD BLOOD	OXYGEN TRANSPORT TO TISSUE XII ; ED. PIIPER ET AL., PLENUM PRESS, NEW YORK, 1990
HAAB-P.	THE EFFECT OF CARBON-MONOXIDE ON RESPIRATION.	EXPERIENTIA. 1990. V46. N11-1. P1202-1206.
HOGAN-M-C, BEBOUT-D-E, GRAY-A-T, WAGNER-P-D, WEST-J-B, HAAB-P-E.	MUSCLE MAXIMAL O-2 UPTAKE AT CONSTANT O-2 DELIVERY WITH AND WITHOUT CO IN THE BLOOD.	JOURNAL-OF-APPLIED-PHYSIOLOGY, 1990, V69, N3, P830-836.
UNGERSBOECK-I, TEMPINI-A, HAAB-P. SAVOY-J.	RESPIRATORY RESPONSE TO INDUCED BRONCHOSPASM IN HYPOXIA	EUROPEAN RESPIRATORY JOURNAL, 2 SUPPL. 2, P. 314, 1989.
HAAB-P-E, HOGAN-M-C, BEBOUT-D-E, GRAY-A, WAGNER-P-D, WEST-J-B.	LIMITATION OF O-2 UPTAKE IN WORKING MUSCLE DUE TO THE PRESENCE OF CARBON-MONOXIDE IN BLOOD.	FASEB-JOURNAL, 1988, V2, N4, P760-760.
SCHUWEY-D, KEHTARI-G, TEMPINI-A, HAAB-P-E.	EQUALITY OF CO AFFINITY IN FETAL AND MATERNAL BLOOD.	EXPERIENTIA. 1987. V43. N6. P720-720.
HAAB-P, TEMPINI-A, SCHUWEY-D.	CO EQUILIBRIUM CURVE OF WHOLE FETAL BLOOD AT BIRTH.	FEDERATION-PROCEEDINGS, 1987, V46, N3, P512-512.
HAAB-P, KEHTARI-G, TEMPINI-A, HAAG-R.	ISOMORPHISM OF O_2 AND CO EQUILIBRIUM CURVES OF HUMAN WHOLE BLOOD	THE PHYSIOLOGIST 30, 231, 1987
SPAHR-I, TEMPINI-A, HAAB-P	COMPARISON OF ROTATING AND BUBBLE TONOMETERS FOR THEIR EFFICIENCY	TOPICS IN RESPIRATORY AND COMPARATIVE PHYSIOLOGY, GUSTAV FISCHER VERLAG, 1986, SYSTEME 16 (23-32)
HAAB-P, SPAHR-I	WHOLE BLOOD DIFFUSIVE CONDUCTANCE FOR O2 AND CO IN OPEN TONOMETERS	PROG RESP RES. 1986, 21 (79-81)
WERLEN-C, PY-P, HAAB-P	ALVEOLAR-ARTERIAL EQUILIBRATION IN THE LUNG OF SHEEP	RESPIRATION PHYSIOLOGY, 1984, 55 (205-221)
HAAG-R, TEMPINI-A, TSCHOPP-M, HAAB-P	MESURES SIMULTANÉES DES CONCENTRATIONS SANGUINES EN O2 ET EN CO À L'APPAREIL DE VAN SLYKE	J PHYSIOL, 1982-1983, 78 (843-847)
KEHTARI-G, TEMPINI-A, SPAHR-I, HAAB-P	EFFECT OF 2-3 DPG ON CO EQUILIBRIUM CURVE OF HUMAN ADULT BLOOD	EN VOIE DE PUBLICATION
SCHUWEY-D, KEHTARI-G, TEMPINI-A, HAAB-P	THE CO AFFINITY OF HUMAN FOETAL BLOOD	EN VOIE DE PUBLICATION
SCHUWEY-D, HAAB-P	DOES THE FOETUS CONCENTRATE CO ?	EN VOIE DE PUBLICATION

2023251941

PROFESSEUR H.R. BRUNNER

TARDY-Y, MEISTER-J-J, WAEBER-B, BRUNNER-H- R.	NON_INVASIVE ESTIMATE OF THE MECHANICAL PROPERTIES OF PERIPHERAL ARTERIES FROM ULTRASONIC AND PHOTOPLETHYSMOGRAPHICS MEASUREMENTS	CLIN. PHYS. PHYSIOL MEAS, 1991, 12 (39-54)
PERRET-F, MOOSER-V, HAYOZ-D, TARDY-Y, MEISTER-J-J, ETIENNE-J-D, FARINE-P-A, MARAZZI-A, BURNIER-M, NUSSBERGER-J, WAEBER-B, BRUNNER-H-R.	EVALUATION OF ARTERIAL COMPLIANCE-PRESSURE CURVES: EFFECT OF ANTIHYPERTENSIVE DRUGS	HYPERTENSION, 18 SUPPL. II, 1991, II (77-83)
TARDY-Y, MEISTER-J-J, PERRET-F, BRUNNER-H- R., ARDITI-M	NON-INVASIVE ASSESSMENT OF ARTERIAL COMPLIANCE-PRESSURE CURVES	ABSTRACT OF FOURTH EUROPEAN MEETING ON HYPERTENSION, MILAN, JUNE 1989.
PERRET-F, WAEBER-B, TARDY-Y, MEISTER-J-J, BURNIER-M, NUSSBERGER-J, BRUNNER-H- R.	COMPLIANCE-PRESSURE CURVES OF THE RADIAL ARTERY IN NORMAL SUBJECTS UNDER PROLONGED ADMINISTRATION OF ATENOLOL, LISINOPRIL, NITRENDIPINE AND PLACEBO	ABSTRACT OF FOURTH EUROPEAN MEETING ON HYPERTENSION, MILAN, JUNE 1989.
MOOSER-V, BURNIER-M, NUSSBERGER-J, JUILLERAT-L, WAEBER-B, BRUNNER-H- R.	EFFECTS OF SMOKING AND PHYSICAL EXERCISE ON PLATELET FREE CYTOSOLIC CALCIUM IN HEALTHY NORMOTENSIVE VOLUNTEERS.	JOURNAL-OF-HYPERTENSION, 1989, V7, N3, P211-216.
MOOSER-V, ETIENNE-J-D, FARINE-P-A, MONNEY-P, PERRET-F, CECCHINI-M, GAGNEBIN-E, BORNOZ-C, TARDY-Y, ARDITI-M, MEISTER-J-J, LEUENBERGER-C-E, SAURER-E, MOOSER-E, WAEBER-B, BRUNNER-H-R.	NON-INVASIVE MEASUREMENT OF INTERNAL DIAMETER OF PERIPHERAL ARTERIES DURING THE CARDIAC CYCLE.	JOURNAL-OF-HYPERTENSION, 1988, V6, S4, P179-181.
BURGENER-E, MOOSER-V, WAEBER-B, PORCHET-M, GARDAZ-J-P, NUSSBERGER-J, BRUNNER-H-R.	CALCIUM ENTRY BLOCKADE ATTENUATES THE ACUTE BLOOD-PRESSURE RISE INDUCED BY CIGARETTE-SMOKING.	JOURNAL-OF-CARDIOVASCULAR-PHARMACOLOGY, 1988, V12, S6, P126-130.
AUBERT-J-F, BURNIER-M, WAEBER-B, NUSSBERGER-J, BRUNNER-H-R.	NICOTINE-INDUCED RELEASE OF VASOPRESSIN IN THE CONSCIOUS RAT - ROLE OF OPIOID-PEPTIDES AND HEMODYNAMIC-EFFECTS.	JOURNAL-OF-PHARMACOLOGY-AND-EXPERIMENTAL-THERAPEUTICS. 1987, V243, N2, P681-685.
BUHLER-F-R, BERGLUND-G, ANDERSON-O-K, BRUNNER-H-R, SCHERRER-U, VANBRUMMELEN-P, DISTLER-A, PHILIPP-T, FOGARI-R, MIMRAN-A, FOURCADE-J, DALPALU-C, PRICHARD-B-N-C, BACKHOUSE-C-I, REID-J-L, ELLIOTT-H, ZANCHETTI-A.	SMOKING STATUS AND CARDIOSELECTIVE BETA-BLOCKADE IN ANTIHYPERTENSIVE THERAPY - THE BISOPROLOL INTERNATIONAL MULTICENTER STUDY (BIMS).	JOURNAL-OF-HYPERTENSION, 1986, V4, S6, P144-146.
WAEBER-B, SCHALLER-M-D, NUSSBERGER-J, BUSSIEN-J-P, HOFBAUER-K-G, BRUNNER-H-R.	SKIN BLOOD FLOW REDUCTION INDUCED BY CIGARETTE SMOKING: ROLE OF VASOPRESSIN	AM-J-PHYSIOL, HEART-CIRC-PHYSIOL, 1984, 247, (H895-H901)

BURNIER-M, BRUNNER-H-R.	PRESSOR RESPONSES OF RATS TO VASOPRESSIN: EFFECT OF SODIUM, ANGIOTENSIN, AND CATECHOLAMINES.	AM-J-PHYSIOL, HEART-CIRC-PHYSIOL, 1983, 13/2 (H253-H258).
BURNIER-J, BIOLLAZ-D, BRUNNER-D-B, GAVRAS,-H BRUNNER-H-R	BLOCKADE IN NORMOTENSIVE AND DEOXYCORTICOSTERONE (DOC)-HYPERTENSIVE RATS PLASMA VASOPRESSIN AND VASOPRESSIN PRESSOR EFFECT	J-PHARMACOL-EXP-THER, 1983, 224 (222-).
WAEBER-B, NUSSBERGER-J, BRUNNER-H-R.	BLOOD PRESSURE DEPENDENCY ON VASOPRESSIN AND ANGIOTENSIN II IN PRAZOSIN-TREATED CONSCIOUS NORMOTENSIVE RATS.	J-PHARMACOL-EXP-THER, 1983, 225/2 (442-446).
BURNIER-M, BIOLLAZ-J, BRUNNER-D-B, BRUNNER-H-R.	BLOOD PRESSURE MAINTENANCE IN AWAKE DEHYDRATED RATS: RENIN, VASOPRESSIN, AND SYMPATHETIC ACTIVITY.	AM-J-PHYSIOL, HEART-CIRC-PHYSIOL, 1983, 14/2 (H203-H209).
WAEBER-B, GAVRAS-H, BRESNAHAN-R, GAVRAS-I, BRUNNER-H-R.	THE ROLE OF VASOCONSTRICTOR SYSTEMS IN EXPERIMENTAL GLUCOCORTICOID-HYPERTENSION IN RATS	CLIN-SCI, 1983, 65 (255-261).
WAEBER-H, NUSSBERGER-J, BRUNNER-H-R.	BLOOD PRESSURE AND HEART RATE EFFECT OF A VASOPRESSIN ANTAGONIST IN CONSCIOUS NORMOTENSIVE RATS PRETREATED WITH EXOGENOUS VASOPRESSIN.	EUR-J-PHARMACOL, 1983, 91/1 (135-137).
BRUNNER-D-B, BURNIER-M, BRUNNER-H-R.	PLASMA VASOPRESSIN IN RATS: EFFECT OF SODIUM, ANGIOTENSIN, AND CATECHOLAMINES.	AM-J-PHYSIOL, HEART-CIRC-PHYSIOL, 1983, 13/2 (H259-H265).

UNITED KINGDOM

TAC / TPRT
(Tobacco Advisory Council)
(Tobacco Products Research Trust)

U.K. Via TPRT

Under the terms of the Voluntary Agreements on Product Modification concluded between the Government and the tobacco industry in 1980 and in 1984, sums of up to £1m per annum over the period 1981 to 1987 were made available to the Independent Scientific Committee on Smoking and Health by the industry to promote research on the effects of modified products on human health. A charitable trust, the Tobacco Products Research Trust, was set up to administer the funds, each project being considered by the Committee and outside referees.

TOBACCO PRODUCTS RESEARCH TRUST

Report to the Tobacco Advisory Council on the Research Programme to August 1992.

SUMMARY

1. The research programme continues to proceed well and a total of 22 out of 31 projects have now completed their experimental phases; eighteen final reports have been received, some of which have been written up for publication. One major extension to a project (Oxford) has been agreed this year and three new projects have been approved for funding, the first of which (a small pilot study) is already complete. One further new application is still under consideration. Remaining uncommitted funds now stand at approximately £100,000 and thus there is little capacity to fund any other major studies in the estimated final two years of the Trust.

PROGRESS

2. A full list of all the projects funded is at Appendix I. Final reports have now been received on 18 projects (numbers 1-7, 10-13, 15, 18, 19 21-23 and 29), four projects are completed and in the report writing stage (numbers 16,20, 24 and 27), seven projects are ongoing (numbers 8, 9,14,17,25,26 and 28) and two are about to commence (numbers 30 and 31). Completion schedules are as follows:

1992 : projects 9,17
1993 : projects 8,14,25,28
1994 : projects 26,30,31.

3. Of the ongoing projects that at Oxford **(project 8)** has been extended to the end of 1993. Recruitment into the case control study from the ISIS - 3 phase far exceeded all expectations, yielding 23,000 each of cases and controls. Consequently existing funds were exhausted in completing the collection, separation and storage of bloods, and the collection, checking, coding and preliminary statistical analysis of the questionnaires. Work outstanding includes all cotinine assays, assays for potential confounders of the association between smoking and heart disease (including cholesterol, apo B, apo Al and maybe one or two others) as well as completion of the results from the questionnaire data, the latter which should be available towards the end of 1992.

4. The further statistical analysis on the Pooling Study at St.Bartholomew's **(project 9)** should by now be almost complete. This investigated confounding variables such as social class, which differed greatly in the four studies summarised, as well as the rate of change of tar yields within each study. On **project 14** at Charing Cross the longitudinal study is now completed and data analysis has just commenced. This part of the study will be written up and presented together with the M.Phil. thesis of one of the research assistants employed. Admission of cases into the case-control study is below that anticipated and recruitment has been extended to December 1992. Final data analysis should be complete by August 1993. **Project 17** at Guy's is nearing completion, the experimental phase almost finalised. Surplus cigarettes are being returned to the individual companies and their assistance is acknowledged.

5. Final reports are imminently awaited from **project 20** at St.Bartholomew's and **project 24** at the Sunley Research Centre. **Project 25** at St.Thomas's has now passed the half-way stage. Recruitment will be completed towards the end of 1992 and all is reported to be proceeding well. Some additional funding has been provided to cover the cost of cotinine analyses. The study at Aberdeen University **(project 26)** has just successfully completed its first year. A helpful site visit was made in May. Whilst numbers of placentae obtained are slightly lower than expected, the capacity exists to collect more although since at present they cannot be processed any more quickly, greater numbers might delay other analyses. All analytical methods are now fully functioning and a small additional grant has covered the cost of cotinine analyses. A CO analyser has also been made available which has assisted in patients' honesty in self-reporting of smoking status.

6. A final report is in preparation from Swansea **(project 27).** Results from part of the study were presented at the June 1992 meeting of the IARC and a paper will be included in the proceedings of the meeting. A further paper is being written up for "Carcinogenesis". The study at the Rowett Research Institute **(project 28)** is proceeding well. The recruitment and supplementation trial is now complete and now all biochemical analyses have to be performed, together with nutritional analyses based on the questionnaire data.

FINAL REPORTS

7. Since the last report to TAC final reports have been received on two projects (18 and 29). That from **project 18** at BIBRA, the abstract of which is reproduced below, concluded that of the markers investigated none could be used to specifically predict long-term smoking-induced pulmonary damage.

"Abstract

We have shown that Sprague-Dawley rats exposed to tobacco smoke via inhalation to a high tar cigarette, Capstan Full Strength, for 4 hours/day over a 14 day period showed measurable changes in lung pathology, specific biochemical and immunological markers of lung injury when compared to control rats exposed to clean dry air. We found epithelial layer thickening, increased lung permeability as measured by hexose and protein exudation and decreased IgA levels in the lung. In addition altered responsiveness of alveolar macrophages as measured by increased spontaneous interleukin-1β mRNA production but decreased lipopolysaccaride sensitivity resulting in inhibition of the production of this cytokine was also observed. As part of this study we tested the effect of tobacco smoke inhalation from two brands of medium tar cigarettes. These medium yield cigarettes did not show the wide spectrum of effects seen with the high yield brand. The only change observed with all the cigarette types tested was a small increase in the number of cells recovered by broncoalveolar lavage.

From these results we can see that high yield cigarettes can lead to disfunctional changes in immune systems. However as we could only show these specific changes with Capstan Full Strength (the high tar brand),

with no reproducible changes being seen using the lower yield cigarette smoke, we have to conclude that, as yet, there is no universal marker that can be used that will specifically predict long term pulmonary damage induced by smoking."

8. The final report from **project 29** at Liverpool, a one month pilot study, has formed part of the grant application for a two year study of the effects of neuropeptide Y on rat hypothalamus in relation to the effects of nicotine and its withdrawal on energy balance. The pilot study confirmed the involvement of nicotine treatment on NPY levels in both the arcuate and paraventricular nuclei independently of changes in food intake.

FINANCE

9. The Trust's Annual Accounts for the period 1st June 1991 to 31st May 1992 should be finalised at the next meeting of Trustees on 25th November and a copy will then be forwarded. With the recent agreement to fund a further two projects (see paras. 11 & 12) remaining uncommitted funds now stand at approximately £100,000 and there is now little scope for funding major new projects.

PUBLICATION

10. A full list of publications, recently updated, is attached as Appendix II. As and when papers are published, copies (if provided) will be sent to TAC also.

NEW PROJECTS

11. Three new grants have been awarded since the last report to TAC (numbers 29-31 in Appendix I). The results of the short pilot study **(project 29)** are outlined in para. 8 above. **Project 30** from Professor Caro (Imperial College, London) has been developed over the course of the past few months. Entitled "Non-invasive ultrasound study of the effects of nicotine on arterial haemodynamics in healthy young adult human subjects" the study aims to establish the acute changes induced by nicotine (administered as Nicorette) in some arterial haemodynamic quantities believed to be involved in the aetiology of atherosclerosis. It will examine changes in the diameter, velocity profile, flow rate and flow pulsatility in the femoral artery, pulse wave transit time between the transverse aorta and femoral artery, arterial blood pressure, heart rate, stroke volume and the manner of cardiac ejection. As well as a group of healthy smokers of a range of brands, control groups will include non-smokers and groups administered a placebo gum. The study is due to start imminently.

12. The latest project to be funded is **project 31** from Dr.Higenbottam at Cambridge. Entitled "Reaction of nitric oxide in air and in tobacco smoke with aqueous solutions and confluent cell cultures" it aims to learn more of the behaviour of NO at an air-liquid interface to predict the outcome of inhalation of nitrogen oxides in tobacco smoke.

To do this a study of the rate of oxidation of NO in vitro is planned. Using a "headspace" design, the concentration of NO above an air-liquid interface and within aqueous solutions or cultured human nasal epithelial cells will be measured with a chemiluminescent analyser and a new voltametric sensor respectively. Tobacco smoke (from a range of brands) and NO in air will be compared. This two-year study is due to start imminently.

13. One further application is still under consideration, the results of a short pilot supporting it **(project 29)** having been funded already. Of the potential applications mentioned in the previous report to TAC and not already covered above, that planning to investigate NO yields on oxidative stress in endothelial cells was rejected and it is unlikely that any follow-up of morbidity and mortality from the Scottish Smoking Survey **(project 5)** can be completed either within the remaining timescale of the Trust (approximately two years) or remaining funds.

Mrs. C.A.Swann
10th September, 1992.

TOBACCO PRODUCTS RESEARCH TRUST

PUBLICATIONS

Professor Holland - Projects 1,3 & 7

1. Peach,H., Hayward,D.M., Shah,D. & Ellard,G.A. A double blind randomised controlled trial of the effect of a low vs a middle tar cigarette on respiratory symptoms - a feasibility study. Proc. Int. Meeting on Cancer Control & Prevention. Tobacco, a major issue. IARC Scientific Monographs, Moscow, June 1985.

2. Peach,H., Ellard,G.A., Jenner,P.J. & Morris,R.W. A simple inexpensive urine test of smoking. Thorax (1985) 40 : 351-357.

3. Peach,H., Hayward,D.M., Ellard,D.R., Morris,R.W. & Shah,D. Phlegm production and lung function among cigarette smokers changing tar groups during the 1970s. J.Epidemiol.Community Health (1986), 40 : 110-116.

4. Peach,H., Shah,D. & Morris,R. Validity of smokers answers about present and past cigarette brands - implication for epidemiological studies. Thorax (1986) 41 : 203-7.

5. Holland,W.W., Colley,J.R.T., North,F. (1986). Low tar cigarettes put to the test. Lancet 2 : 156.

6. Withey et al. Respiratory effects of lowering tar and nicotine levels of cigarettes smoked by young male middle tar smokers. I. Design of a randomised controlled trial. J.Epidemiol.Community Health 1992, 46 , 274-280.

7. Withey et al. Respiratory effects of lowering tar and nicotine levels of cigarettes smoked by young male middle tar smokers. II. Results of a randomised controlled trial. J. Epidemiol.Community Health,1992, 46, 281-285.

1. Barlow,R.D., Stone,R.B., Wald,N.J., Puhakainin,E.V.J. The direct barbituric acid method for the determination of urine nicotine matabolites. A simple colourimetric test for the routine assessment of smoking status and cigarette smoke intake. Clin. Chim.Acta. (1987) 165 : 45-52.

2. Puhakainen,E.V.J., Barlow,R.D., Sulonen,J.T. An automated colourimetric assay for urine nicotine metabolites. A suitable alternative to cotinine assays for the assessment of smoking status and cigarette smoke intake. Clin.Chim.Acta (1987) 170 : 255-262.

3. Barlow,R.D., Thompson,P.A., Stone,R.B. Simultaneous determination of nicotine, cotinine and five additional metabolites in the urine of smokers using precolumn derivatisation and isocratic high performance liquid chromatography. J.Chromat. (1987) 419 : 375-80.

4. Parviainen,M.T., Barlow,R.D. Assessment of exposure to environmental tobacco smoke using a high performance liquid chromatographic method for the simultaneous determination of nicotine and two of its metabolites in urine. Journal of Chromatography (1988) 431: 216-221.

5. Barlow,R.D., Parviainen,M.T. et al. 3-Pyridyl carbinol : a major nicotine metabolite in the urine of smokers. (In preparation).

6. Ellard, G.A., Tucker,D.R., Poolim,Y.L., Wang,D.Y., Barlow,R.D., Stone,R. Serum placental-like alkaline phosphatase levels and nicotine intake in smokers. British Journal of Cancer (1988) 58: 219-221.

7. Thompson,S.G., Stone,R., Nanchahal,K., Wald,N. The relationship of urinary cotinine concentrations with cigarette smoking and the exposure to other people's smoke. Thorax 45 (S), 356-361 (1990).

8. Barlow,R.D., Thompson,S.G., Wald,N.J., Van-Vunakis, H. How should urinary cotinine concentrations be adjusted for urinary creatinine concentration? Clin.Chim.Acta. 187, 289-296 (1990).

9. Barlow,R.D. (Ph.D. Thesis, University of London, 1988). Studies on biochemical markers of oral medicine compliance and cigarette smoke intake.

1. Woodward,M., Tunstall-Pedoe,H., Smith,W.C.S. & Tavendale,R. Smoking characteristics and inhalation biochemistry in the Scottish population. J.Clin.Epidemiol. 1991; 44:1405-1410.

2. Tunstall-Pedoe,H., Woodward,M. & Brown,C.A. Tea drinking, passive smoking and serum cotinine in the Scottish Heart Health Study. J.Clin.Epidemiol. 1991; 44: 1411-1414.

3. Woodward,M. and Tunstall-Pedoe,H. Do smokers of lower tar cigarettes consume lower amounts of smoke components? Results from the Scottish Heart Health Study. Br.J.Addiction 1992; 87: 921-928.

4. Brown,C.A., Crombie,I.K., Smith,W.C.S. and Tunstall-Pedoe,H. Cigarette tar content and symptoms of chronic bronchitis: results of the Scottish Heart Health Study. J.of Epidemiol. and Comm.Health 1991; 45: 287-290.

5. Brown,C.A., Crombie,I.K., Smith,W.C.S., and Tunstall-Pedoe,H. The impact of quitting smoking on symptoms of chronic bronchitis : results of the Scottish Heart Health Study. Thorax 1991; 46 : 112-116.

6. Tunstall-Pedoe,H., Smith,W.C.S., Crombie,I.K., Tavendale,R. Coronary risk factor and lifestyle variation across Scotland : results from the Scottish Heart Health Study. Scot.Med.J. 1989: 34 : 556-560.

7. Smith,W.C.S., Tunstall-Pedoe,H., Crombie,I.K., Tavendale,R. Concomitants of excess coronary deaths - major risk factor and lifestyle findings from 10,359 men and women in the Scottish Heart Health Study. Scot.Med.J. 1989; 34 : 550-555.

Dr. J. Pritchard - Project 6

1. Ph.D. Thesis - J.Pritchard, University of Essex, Colchester (1987).

2. Pritchard, J.N., McAughey,J.J. & Black,A. A technique for radio-labelling tar particulate material in cigarette smoke. J.Aerosol.Sci. 19 : 715-724, 1989.

3. McAughey,J.J., Pritchard,J.N. & Black,A. Relative lung cancer risk from exposure to mainstream and sidestream smoke particulates.

   (i) Proc.Int.Conf. on Present and Future of Indoor Air Quality, Brussels, 1989.

   (ii) "Aerosols; their generation, behaviour and application". Proc. 3rd Ann.Conf. of Aerosol Soc., Birmingham, 1989, pp 231-234, ISBN 0 951 2216 Z 0.

Professor Parry (Project 10)

1. Lafi,A. & Parry, J.M. Cytogenetic activities of tobacco particulate matter derived from a low to middle tar British cigarette. Mutat. Res. 201 : 365-74. 1988.

Mr. Martin Jarvis - Project 11

1. Factors determining exposure to passive smoking in young adults living at home: quantitative analysis using saliva cotinine concentrations. Jarvis,M.J., McNeill,A.D., Bryant,A. & Russell,M.A.H. International Journal of Epidemiology, 1991, 20: 126-131.

2023251953

Dr. Waters - Project 13

1. Fielding,S., Short,C., Davies,K., Wald,N., Bridges,B.A. & Waters, R. Studies on the ability of smoke from different types of cigarettes to induce DNA single strand breaks in cultured human cells. Mutation Research (1989) 214, 147-151.

2. Jones,N.J., Kadhim,M.A., Hodkins,P.L., Parry,J.M. & Waters,R. P-Postlabelling analysis and micronuclei induction in primary Chinese hamster lung cells exposed to tobacco particulate matter. Carcinogenesis (1991) 12(8) 1507-1514.

Professor Neville Woolf - Project 16

1. Noronha-Dutra,A.A., Epperlein,M.M. & Woolf,N. Nitric oxide reacts with hydrogen peroxide to produce potentially cytotoxic singlet oxygen. Submitted to Science 1992.

2. Epperlein,M.M., Noronha-Dutra,A.A. & Woolf,N. The effect of cigarette smoke on cultured human endothelial cells. (In preparation)

Dr. Mary Seller - Project 17

1. Seller,M.J., Bnait,R.S., Cairns,N.J. Effects of maternal tobacco smoke inhalation on early embryonic growth. In "Effects of Smoking on the fetus, neonate and child", Ch.4, p.45-59. OUP 1992 (Sept.)

2023251954

Dr. Humphries & Dr.Thomas - Project 24

1. Thomas,A.E., Green,F.R., Kelleher,C.H., Wilkes,H.C., Brennan,P.J., Meade,T.W. and Humphries,S.E.(1991) Variation in the promoter region of the Fibrinogen gene is associated with plasma fibrinogen levels in smokers and non-smokers. Thrombosis & Haemostasis. 65(5) 487-490.

Professor R. Waters - Project 27

1. Jones, J.J., McGregor,A.D., Hoskins,P.L. and Waters,R. (1993). ^{32}P-postlabelling analysis in human tissues and their potential usage for biomonitoring. In Phillips,D.H., Castegnaro,M. and Bartsch,H. (Eds.) Postlabelling methods for the detection of DNA damage, IARC Scientific Publications No.124, Lyon, in press.

2. Jones,N.J., Hoskins,P.L., McGregor,A.D. and Waters,R. Detection of DNA adducts in human oral tissue: correlation of adduct levels with tobacco smoking and differential enhancement of adducts using the butanol extraction and nuclease P1 versions of ^{32}P-postlabelling. In preparation for submission to Carcinogenesis.

PROJECTS FUNDED BY THE

TOBACCO PRODUCTS RESEARCH TRUST

Project No.	GRANTHOLDER	TITLE	GRANT		DURATION
			Initial	As at 3.9.1992	
			£	£	
1	Prof. Holland (St.Thomas)	Tar content of cigarettes on respiratory symptoms	24,652	24,652	1 year (completed)
	Prof. Holland (St.Thomas)	Effect of tar yield of cigarettes on respiratory symptoms (pre pilot study)	66,160	55,994 (saved 10,166)	do.
3	Prof.Holland (St.Thomas)	Validate questions about brand of cigarettes smoked and effect of changing to lower tar brands on respiratory symptoms and lung function.	15,540	9,185 (saved 6,355)	do.
4	Prof. Wald (St.Bartholomews)	Biochemical & epidemiological research into health effects of low tar cigarettes	303,243* (amalgamated with 9 below)		1/6/84 - 30/5/87
5	Prof.Tunstall Pedoe (Dundee)	Scottish Smoking Study	266,164	370,754* (saved 11,769)	1/4/85 - 31/3/88 extended to 30/9/89 (completed)
6	Dr.Pritchard (Harwell)	Measurement of tar retention in smokers switching to products with lower tar yields	226,164	308,698* (saved £77)	1/2/86 - 31/1/88 extended to 31/7/88 (completed)
7	Prof.Holland (St.Thomas)	Effect of different cigarettes on respiratory health	1,317,964 (excluding cost of cigarettes)	1,398,151* (saved 18,239)	1/12/85 - 31/12/87 extended to 31/1/89 (completed)
8	Mr.Peto (Oxford)	Isis epidemiology enquiry	791,314	1,122,546	1/4/86 - 31/3/89 extended to 31/12/93
9	Prof. Wald (St.Bartholomews)	Tar reduction study (incorporates 4)	336,829	848,705	1/1/86 - 30/6/88 analytical service extended to 31/12/90 6 month extension 1992
10	Prof.Parry (Swansea)	Ability of tobacco condensates to induce aberrations of chromosome number and structure in cultured primary fibroblasts	89,878	124,523* (saved 5,243)	1/10/86 - 30/9/89 (completed)

*These are actual sums paid out; the "saving" represents the difference between the sum finally agreed and that paid out.

PROJECTS FUNDED BY THE

TOBACCO PRODUCTS RESEARCH TRUST

Pro-ject No.	GRANTHOLDER	TITLE	GRANT		DURATION
			Initial	As at 3.9.1992	
			£	£	
	Mr.Jarvis (Institute of Psychiatry)	Development of smoke intakes in novice smokers in relation to brand smoked	30,578	45,136* (saved 2,109)	1/9/86 - 31/8/88 (completed)
12	Dr.Powell (Charing Cross)	Smoking profile of patients with symptomatic peripheral arterial disease. (Pilot)	7,263	6,048* (saved 1,215)	1/9/86 - 30/3/87 (completed)
3	Dr.Waters (Swansea)	Correlation between lung cancer and ability of smoke to induce DNA damage in cultured human cells or mutation in a bacterial assay.	66,478	69,020* (saved 1,951)	12/10/87 - 11/10/90 (completed)
	Dr.Powell (Charing Cross)	Does the tar brush paint the artery wall.	219,166	258,059	1/5/88 - 31/5/93
5	Prof.Rosen (Cardiff)	Effect of switching cigarettes on post-operative pulmonary complications in middle tar smokers.	84,366	91,635* (saved nil.)	4/7/88 - 3/7/89 (completed)
6	Prof.Woolf (Middlesex)	Use of models of cigarette smoke related vascular damage in comparing smoking materials.	108,303	121,687	1/7/88 - 30/6/91
17	r.Seller (Guy's)	Effect of tar yield on developing embryos using curly tail mice, a model for human neural tube defects.	147,254	207,154	1/6/88 - 31/10/91 (extended to 31/10/92)
18	Dr.Miller (BIBRA)	Tobacco smoke constituents on pulmonary surfactant system (in vitro studies)	183,518	180,575* (saved 6,488)	1/10/88 - 30/9/91 (completed)
9	Dr.Duthie (Rowett)	Functional antioxidant status and heart disease in smokers and non-smokers	127,950	167,348* (saved £407)	2/5/88 - 1/6/90 (extended to 1/3/91) (completed)
20	Dr.Law (St.Bartholomews)	Cigarette smoking, nicotine/tar yield and bone density	176,492	266,165	1/7/88 - 30/6/90 (extended to 31/12/91)

*These are actual sums paid out; the "saving" represents the difference between the sum finally agreed and that paid out.

PROJECTS FUNDED BY THE

TOBACCO PRODUCTS RESEARCH TRUST

Project No.	GRANTHOLDER	TITLE	GRANT		DURATION
			Initial	As at 3.9.1992	
			£	£	
21	Dr.Pritchard (Harwell)	Reducing tar, but maintaining delivery on tar retention (Males)	116,495	118,191* (saved nil.)	Nov.88 - 1 year (completed)
22	Dr.Pritchard	Deposition of tar in female smokers	114,655	116,351* (saved nil)	Apr. 88 - 1 year (completed)
23	Dr.Pritchard (Harwell)	Comparison of cigarette smoke intake in men and women	11,730	11,669* (saved £60)	Oct.89 - 6 months (completed)
24	Dr.Humphries (Sunley Research)	Interaction between smoking fibrinogen levels and fibrinogen gene haplotype: comparison between low yield and higher yield brand cigarettes.	11,096	19,512	Nov. 90 - Oct. 91
25	Professor Milner (St.Thomas's)	Pregnancy smoking and the lower respiratory tract in infancy.	182,543	185,993	1/12/90 - 30/11/93
26	Dr.Page (Aberdeen)	Human placental function in relation to tar yield and cadmium content in cigarettes smoked by pregnant women.	99,828	103,629	19/8/91 - 18/8/94
27	Dr.Waters	Smoking related DNA damage in normal oral tissue from patients suffering with oral cancer.	11,700	12,411	March 91 - Feb.92
28	Dr.Duthie (Aberdeen)	Effects of vitamin E supplementation on plasma cholesterol concentration and free radical-mediated damage in smokers.	62,794	65,794	1/10/91 - 31/3/93
29	Dr.Williams (Liverpool)	Effects of nicotine and its withdrawal on energy balance: the role of neuropeptide Y in the rat hypothalamus.	2,010		1 month (May 1992) pilot

* These are actual sums paid out; the "saving" represents the difference between the sum finally agreed and that paid out.

PROJECTS FUNDED BY THE

TOBACCO PRODUCTS RESEARCH TRUST

ro-c-o	GRANTHOLDER	TITLE	GRANT		DURATION
			Initial	As at 3.9.1992	
			£	£	
30	Professor Caro (London I.C.)	Non-invasive ultrasound study of the effects of nicotine on arterial haemodynamics in healthy young adult human subjects.	47,450		2 years
31	Dr.Higenbottam (Cambridge)	Reaction of nitric oxide in air and in tobacco smoke with aqueous solutions and confluent cell cultures.	66,200		2 years

2023251959

BATTIG, K.

Laboratory for Compared Physiology and Behavioural Biology
ETH
ZURICH

POSTERS PRESENTED AT :

25TH ANNUAL MEETING OF THE SWISS SOCIETIES FOR EXPERIMENTAL BIOLOGY (USGEB / USSBE)

PUBLISHED IN : EXPERIENTIA - VOLUME 49 / 1993

340

A NEW METHOD FOR ASSESSING DIETARY HABITS AND STROOP PERFORMANCE UNDER FIELD CONDITIONS

Jiri Kos, Markus Hasenfratz and Karl Bättig, Behavioral Biology Laboratory, Swiss Federal Institute of Technology, ETH-Zentrum, CH-8092 Zurich

The assessment of dietary or subjective behavioural data has traditionally been done by paper-and-pencil methods which have certain disadvantages (absence of a time protocol, bias of earlier answers, time consuming handling of the data). Our method uses a pocketcomputer for all data inputs. Also, a version of the Stroop task was implemented. The PSION II Organiser LZ 64 pocketcomputer (142 x 78 x 29mm, 250g) offers 32Kbyte of working memory and up to 256 KByte of storage capacity using 2 EPROM cartridges. Programs and data can be transferred to a PC/AT and vice versa. The software so far consists of 3 program modules: assessment of dietary intake, presenting of questions using analouge-like scales and a numerical version of the Stroop task. On the PC side our software offers quick viewing of the data immediately after finishing the experiment. Every data input is stored with time and date so that the subject's compliance can easily be checked. The method is now being used in an experiment with 80 smokers and nonsmokers. Differences regarding dietary habits and Stroop performance are being investigated under field conditions. So far the computer and software have been well accepted by the subjects and appear to deliver reliable results.

468

SOCIAL RANK DETERMINED IN A COMPETITIVE SITUATION AND ITS RELATION TO VOLUNTARY ALCOHOL CONSUMPTION IN RATS.

Kessler, M., Welzl, H., Bättig, K., Lab. Behavioral Biology, ETH Zürich, CH-8092 Zürich

The present experiment investigated a possible relationship between dominance and alcohol consumption in male Wistar rats. Rats were housed in groups of 3 animals per cage (triads) and competed daily for a limited number of food-pellets after being food deprived for 22 hrs. Based on each individual's competition-score (number of food pellets gained per session), rats were either labeled as being dominant (D), intermediate, or subordinate (S). Clear and stable rank orders developed in 10 out of 15 triads (1). After 32 days of adaptation to alcohol drinking (alcohol in increasing concentrations was substituted in place of water every other day), alcohol (9% v/v) consumption was measured in a free-choice, two bottle situation during 6 days in single-housed D- and S-rats. Dominant rats consumed significantly ($p \leq 0.05$) more alcohol (3.56 g/kg/day) than subordinate rats (2.14 g/kg/day). This finding is in agreement with neurochemical data indicating that dominant behavior is inversely related to the activity of brain 5-HT-systems. On the other hand, low 5-HT activity is related to increased chronic alcohol drinking. Our result suggests that social rank is a non-pharmacological factor which influences alcohol consumption.
(1) Gentsch et al. (1988). *Behav. Brain Research* **27**:37.

524

THE INFLUENCE OF NICOTINE AND TAR YIELD ON COMPENSATORY CIGARETTE SMOKING

Beatrice Baldinger, Markus Hasenfratz and Karl Bättig, Behavioral Biology Laboratory, Swiss Federal Institute of Technology, ETH-Zentrum, 8092 Zurich, Switzerland

As found in an earlier study with cigarettes of varying nicotine and tar yields, tar yield seemed to be more important for regulating smoke intake than nicotine yield, since the smokers compensated only while smoking low tar/low nicotine cigarettes (ultra-light) but not medium tar/low nicotine cigarettes (test cigarette). Hypothesizing compensatory intensification of puffing and inhaling, the present study examined puffing behavior. Twelve female smokers participated in the experiment smoking cigarettes with tar and nicotine yields of 11.4 and 0.9 (habitual); 2.0 and 0.21 (ultra-light); and 9.3 and 0.08 mg/cigarette (test), respectively, resulting in tar/nicotine ratios of 12.6, 9.5, and 116.25. Physiological parameters and subjective ratings confirmed the results of a former switching study. Whereas the test cigarettes produced only weak physiological effects and low taste scores, the effects of the habitual cigarettes were in the expected range and those of the ultra-light cigarettes about halfway in between. The present puffing behavior measurements revealed a greater number of puffs and greater total puff volumes for ultra-light than for habitual and test cigarettes while puff interval was longest for the habitual cigarettes, shorter and similar for the test and the ultra-light cigarettes. These results support the earlier conclusion that ultra-light cigarettes were smoked compensatorily whereas the test cigarettes with a very high tar/nicotine ratio did not produce a comparable behavior.

525

CIGARETTE SMOKING RELATED VARIATIONS OF PULSE AND ACTIVITY UNDER FIELD CONDITIONS

Albert Jacober, Markus Hasenfratz & Karl Bättig
Behavioural Biology Laboratory, Swiss Federal Institute of Technology, ETH-Zentrum, CH-8092 Zurich, Switzerland

Small portable devices were used to record 30-sec averages of heart rate and motor activity over 2 consecutive days and nights. On smoking days, subjects had to press a marker button whenever they lit a cigarette. On abstinence days, when smoking was not allowed, the moments of strong desire to smoke had to be marked. Smoking related pulse (SRP) and activity (SRA) were computed by averaging the 30-sec data across all cigarettes for the 10 minutes preceding and the 10 minutes following the lighting of the cigarettes. The grand means of SRP and SRA started to increase 5 minutes before and reached a maximum with lighting the cigarettes, dropped immediately after lighting to an absolute minimum and while SRA remained at prelighting levels, SRP recovered continuously from 5 minutes after lighting onwards to a maximum. Qualitatively equal curves were obtained for both sexes, for workdays and days off and for subjects with different professions, suggesting an ubiquitous presence of the phenomenon. In contrast to the SRP and SRA of the first 5 cigarettes of the day, which showed the same pattern with even more pronounced increases of SRP 5 minutes after lighting, the SRP of the last 5 cigarettes of the day remained at prelighting levels after cigarette lighting. These findings support the concept of nicotine induced heart rate increases which disappear during the day, and the SRP and SRA of the markings of smoking desire on abstinence days confirmed this view since no SRP increases after these markings occurred. The pronounced increases of SRP and SRA before the lighting of the cigarettes might be interpreted as conditioned unrest, preceding the lighting of a cigarette.

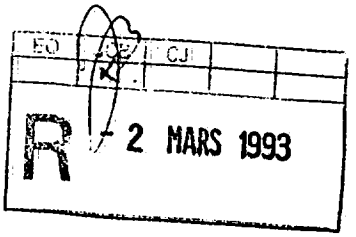

Verband Schweiz. Zigarettenfabrikanten
Association suisse des
fabricants de cigarettes
Pérolles 5a - 1701 Fribourg
C.P. 212

ZWISCHENBERICHT ☐ (Nur einreichen, wenn ein Gesuch für die Fortsetzung in der nächstfolgenden Jahresperiode gestellt wird)

RAPPORT INTERMEDIAIRE *(A soumettre seulement lors d'une requête de prolongation pour la période annuelle suivante)*

oder
ou

SCHLUSSBERICHT ☒ X
RAPPORT FINAL

für die Zeit von 1.1.1992 bis 31.12.1992
pour la période du *au*

Titel des Projektes Psychopharmakologische Effekte des Rauchens
Titre du projet

Name des Beitragsempfängers Bättig Vorname Karl
Nom du bénéficiaire du crédit *Prénom*

Akademischer Grad oder Titel, Stellung Prof. Dr. med.
Degré académique ou titre, position

Genaue Adresse Arbeitsort, mit Postleitzahl
Adresse professionnelle exacte, avec no postal
Laboratorium für Verhaltensbiologie, Turnerstr. 1, ETH-Zentrum, CH-8092 Zürich

Telephon während der Arbeitszeit 01/ 256 5840
No de téléphone professionnel

Datum der Berichtseinreichung 25.2.1993
Date de la soumission du rapport

Weitere Bemerkungen :
Observations :

2023251966

1. WISSENSCHAFTLICHER BERICHT
RAPPORT SCIENTIFIQUE

1.1. Darstellung der Forschungsarbeit, die während der Berichtsperiode geleistet wurde und Zusammenfassung der Ergebnisse, in Form einer Kurzfassung von 10-15 Zeilen auf deutsch oder französisch und einer detaillierten Beschreibung auf englisch.

Exposé des travaux de recherche accomplis pendant la période sous rapport et résumé des résultats sous forme d'un condensé de 10 à 15 lignes en allemand ou en français, et d'une description détaillée en anglais.

EFFEKTE VON RAUCHEN AUF KOGNITIVE LEISTUNG UND PSYCHOPHYSIOLOGISCHE PARAMETER IN ABHÄNGIGKEIT VOM RAUCHZUSTAND

Die Wirkung des Rauchens auf die kognitive Leistungsfähigkeit, auf physiologische Parameter und auf die Befindlichkeit wurden in einem vollständigen 2 x 2 Versuchsprotokoll im "normalen Rauch-" sowie im "Deprivationszustand" untersucht. Verglichen mit "normalem" Rauchen führte Rauchabstinenz vor der Sitzung zu reduzierter kognitiver Leistung sowie zu reduziertem kardiovaskulärem und elektrokortikalem Arousal. Rauchen in der Sitzung führte zu genau entgegengesetzten Effekten, wie dies auch schon früher berichtet wurde. Generell bewirkte die morgendliche Rauchabstinenz eine Verstärkung der Raucheffekte.

2023251967

EFFECTS OF SMOKING ON COGNITIVE PERFORMANCE AND PSYCHOPHYSIOLOGICAL PARAMETERS AS A FUNCTION OF SMOKING STATE

The effects of smoking on cognitive, physiological and subjective parameters were investigated in a "normal" smoking state as well as during smoking deprivation according to a complete 2 x 2 cross-over design.

METHODS

Subjects

Twenty female regular smokers with a mean age of 27.9 years (range 21 - 34) participated in the study. They all reported being in good health and smoking 26.8 cigarettes per day (range 23 - 33). They weighed 58.1 kg (range 45 - 82) and had a mean height of 167.5 cm (range 155 - 180). The subjects were selected responders to an advertisement in a local newspaper and their fee consisted of a fixed sum plus an efficiency bonus.

Design

According to a 2 x 2 cross-over design the pre/post treatment changes of all dependent variables were compared for smoking vs non-smoking as treatment and presession smoking vs abstinence as predisposing condition.

RIP task

The rapid information processing task (RIP) was used as in earlier studies (Hasenfratz and Bättig, 1991, 1992), but without any additional stressor.

Physiological recordings

The physiological parameters were the same as described in the ASFC final report of March 1992.

Subjective parameters

In order to assess anxiety, the German version of the State-Trait-Anxiety-Inventory questionnaire (Laux et al., 1981) was used. The following questions were presented one after the other at the top of the screen and the subjects had to answer by adjusting a pointer on

an 18-cm long horizontal analog scale in the middle of the screen (operating a Logitech trackball with their dominant hand). The first two questions were answered after the rest phase following each RIP-trial (two times in a session), the latter six once after the smoking period. Subjective performance: "How would you judge your task performance?" (left end labelled with: poor - right end labelled with: good); craving to smoke: "How much would you like to smoke now?" (not at all - very much); pleasure of smoking: "How was the pleasure of smoking?" (minimal - maximal); strength of cigarette: "How was the strength of the cigarette?" (weak - strong); taste of tobacco: "How was the taste of the tobacco?" (bad - good); stimulation: "Did smoking stimulate you?" (not at all - very much); nausea: "Do you feel sick?" (not at all - very much); dizziness: "Do you feel dizzy?" (not at all - very much).

The positions of the cursor were transformed to a 0 - 100-mm scale.

Procedure

In a training session the subjects were familiarized with the laboratory situation and allowed to practise the RIP task three times. No physiological parameters were recorded. After that, each subject took part in four test sessions according to a 2 x 2 (abstinent - non-abstinent x smoking - non-smoking) cross-over design. The test sessions started in the early afternoon and the subjects were required to abstain from smoking from bedtime until the beginning of the experiment for two of the four experimental sessions (abstinence condition), whereas preceding the other two experimental sessions they were required to smoke as usual before coming to the lab (non-abstinence condition).

After the subject's arrival at the laboratory the electrodes were attached and carbon monoxide in the expiratory air was measured in order to check compliance with the abstinence instruction. Continuous recordings of the physiological parameters started with a first 5-min rest period. Then the first 20-min RIP task period was started, which was followed by a second 5-min rest period. Then subjective performance and craving to smoke were rated, respiratory CO was measured and subsequently a cigarette was lighted in the smoking condition. After the subject had finished with the cigarette, the six questions concerning the effects of smoking were answered. Thereafter, or after a corresponding time lag in the case of the non-smoking condition, respiratory CO was measured and the same sequence as before the treatment period (5-min rest, 20-min task, 5-min rest) was repeated. After the last rest phase the subjective performance and craving to smoke were rated, respiratory CO was measured and then the electrodes were detached.

Data processing and statistics

All continuously recorded cardiovascular data were analyzed off-line so as to obtain the mean values and standard deviations for each successive 10-sec period. After a visual artefact control carried out under blind conditions, the 10-sec averages were aggregated to means for each experimental period or to consecutive 5-min means.

From the EEG data, the relative power of the delta (1.0 - 3.9 Hz), theta (4.0 - 7.8 Hz), alpha (7.9 - 11.7 Hz) and beta bands (11.8 - 24.7 Hz) as well as the mean peak frequencies of the alpha and beta bands were determined for each 5-min rest period. The remaining EEG recordings during the RIP trials were used for computing event related potentials (ERPs) to the third digits of the correctly detected triads. The averaging period lasted 500 ms after the onset of the stimulus. These ERPs were characterized by a late positive wave (LP) after the correct answer to the third digit. The latency and amplitude of this LP were determined in a window between 250 and 500 ms after the stimulus onset.

These reduced data sets were then statistically analyzed using analyses of variance (ANOVAs, BMDP 2V) with the factors Abstinence in the morning (A), Smoking during the session (S), Prepost smoking (P) and Block (B: experimental phases or subtrials, depending on the respective parameters). For all significance levels Greenhouse-Geisser probabilities were considered where appropriate.

RESULTS

RIP performance **(Fig. 1)**

Presession smoking abstinence, as compared to the normal smoking condition, was followed by a lower level in RIP performance (processing rate: $F(1,19) = 5.86$, $p < 0.05$). On the other hand, the smoking of a cigarette during the session led to an increase in processing rate (interaction S x P: $F(1,19) = 5.11$, $p < 0.05$). Moreover, this significant smoking-induced increase was greater after presession abstinence than after presession smoking, as supported by the significant A x S x P interaction ($F(1,19) = 4.62$, $p < 0.05$).

For reaction time, only the interaction A x P reached significance ($F(1,19) = 6.03$, $p < 0.05$), indicating a greater decrease throughout the session after presession abstinence than after presession smoking.

The frequencies of hits and commission errors were not significantly affected either by presession abstinence nor by smoking during the session.

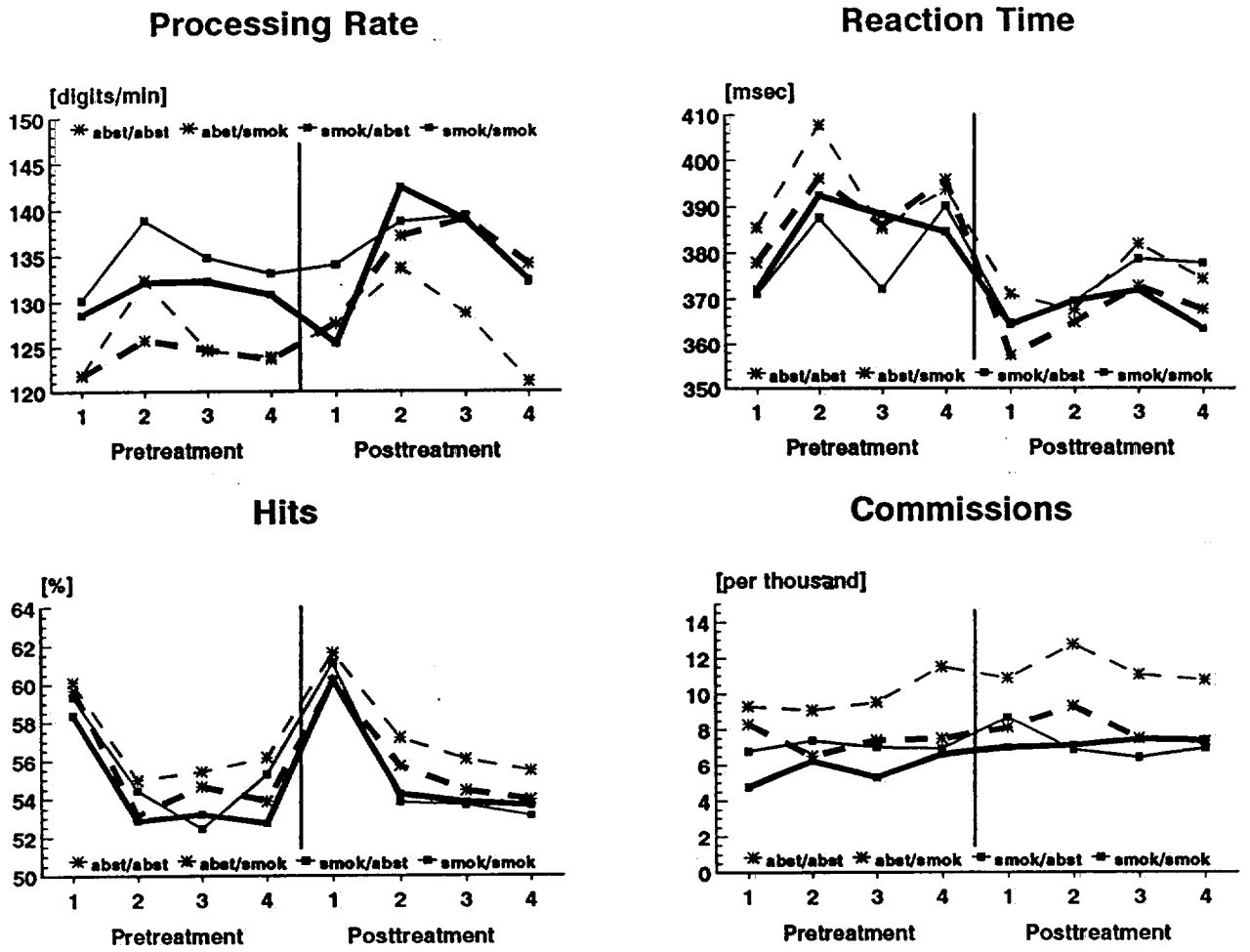

Figure 1. Performance parameters for consecutive 5-min means of the pre- and posttreatment trials of the RIP task. Solid lines: subjects were not smoking-deprived; broken lines: subjects were smoking-deprived; thin lines: no smoking in the session; bold lines: smoking in the session.

EEG, ERP (Fig. 2)

Generally, presession abstinence produced greater effects on the resting EEG parameters than did the smoking of a cigarette in the session. After presession abstinence, EEG arousal was lower than after presession smoking. Beta power ($F(1,19) = 16.70$, $p < 0.001$) and dominant alpha ($F(1,19) = 14.61$, $p < 0.01$) and beta frequencies ($F(1,19) = 6.41$, $p < 0.05$) were lower after presession abstinence than after presession smoking, whereas the inverse was true for delta ($F(1,19) = 5.68$, $p < 0.05$) and theta power ($F(1,19) = 15.31$, $p < 0.001$).

Smoking in the session, on the other hand, tended to decrease delta power to a non-significant extent ($F(1,19) = 3.46$, $p = 0.078$) but significantly increased beta power ($F(1,19) = 20.03$, $p < 0.001$) and the dominant alpha frequency ($F(1,19) = 7.80$, $p < 0.05$).

A nearly significant interaction between presession abstinence and smoking in the session was found for dominant beta frequency only, indicating that smoking increased it only after presession abstinence ($F(1,19) = 4.05$, $p = 0.059$).

Neither LP latency nor the LP amplitude was affected by either of the manipulations.

Peripheral physiology (Fig. 3)

The results of the cardiovascular parameters were very similar to those of the EEG parameters and the processing rate. Whereas presession abstinence led to lower heart rate and blood pressure levels than after presession smoking (HR: $F(1,19) = 137.61$, $p < 0.001$; SBP: $F(1,19) = 4.38$, $p = 0.0509$; DBP: $F(1,19) = 5.10$, $p < 0.05$), the inverse was true for the finger and ear pulse amplitudes (FPA: $F(1,19) = 5.54$, $p < 0.05$; EPA: $F(1,19) = 5.94$, $p < 0.05$) and the left ventricular ejection time ($F(1,10) = 17.90$, $p < 0.01$).

Smoking in the session, on the other hand, led to significant increases in heart rate, blood pressure and cardiac output (interaction S x P: HR: $F(1,19) = 60.06$, $p < 0.001$; SBP: $F(1,19) = 14.78$, $p < 0.01$; DBP: $F(1,19) = 7.89$, $p < 0.05$; CO: $F(1,10) = 5.94$, $p < 0.05$) and decreases in finger pulse amplitude ($F(1,19) = 26.54$, $p < 0.001$) and left ventricular ejection time ($F(1,10) = 20.89$, $p < 0.001$) and non-significant decreases in pre-ejection period ($F(1,10) = 3.87$, $p = 0.078$) and stroke volume ($F(1,10) = 3.55$, $p = 0.089$).

Significant interactions between presession abstinence and acute smoking, indicating greater smoking effects after presession abstinence than after presession smoking, were obtained for the following effects: increases in heart rate (interaction A x S x P:

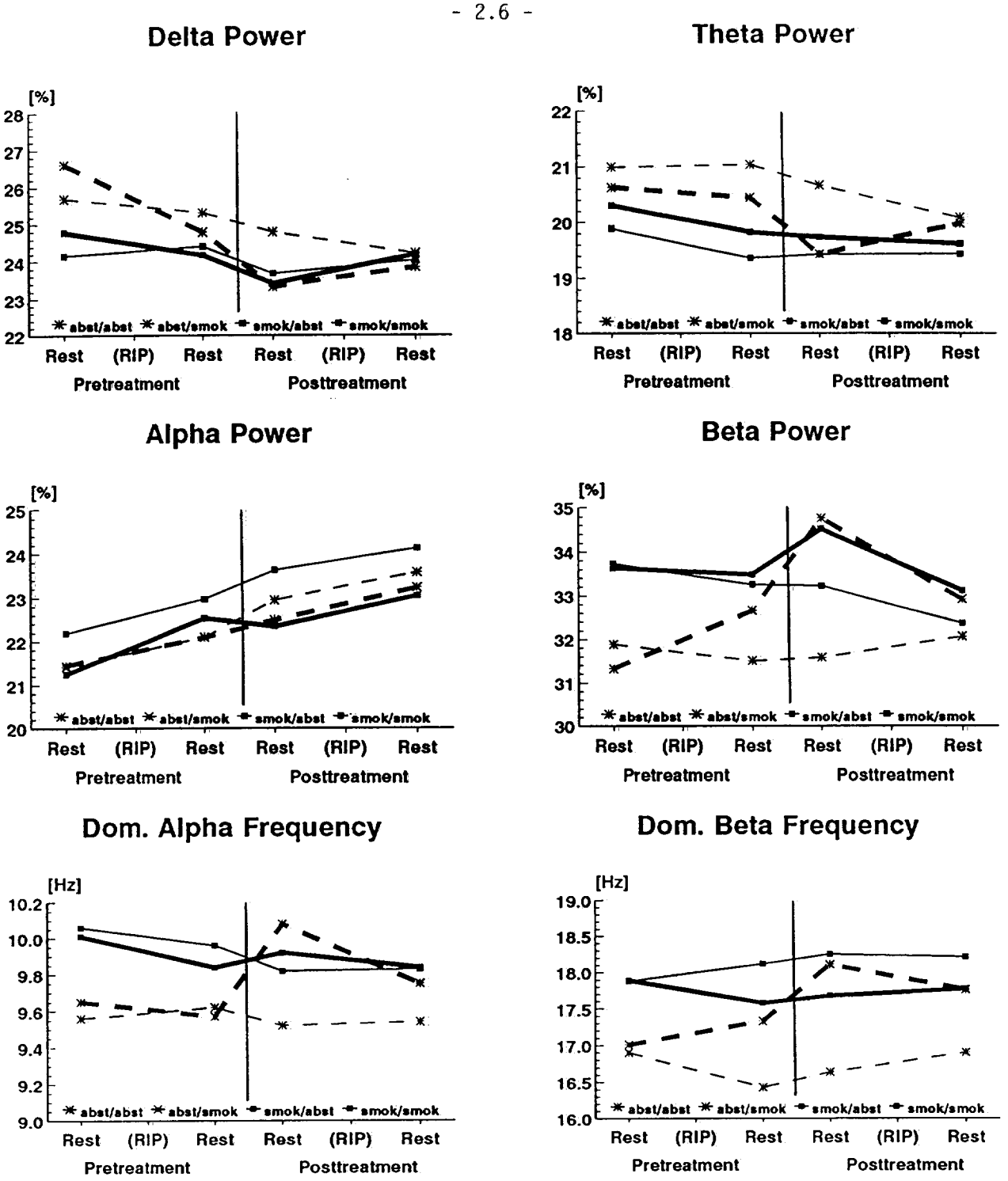

Figure 2. EEG parameters during the rest phases. Solid lines: subjects were not smoking-deprived; broken lines: subjects were smoking-deprived; thin lines: no smoking in the session; bold lines: smoking in the session.

Figure 3. (Next page). Phase means of the cardiovascular parameters. Solid lines: subjects were not smoking-deprived; broken lines: subjects were smoking-deprived; thin lines: no smoking in the session; bold lines: smoking in the session.

Heart Rate

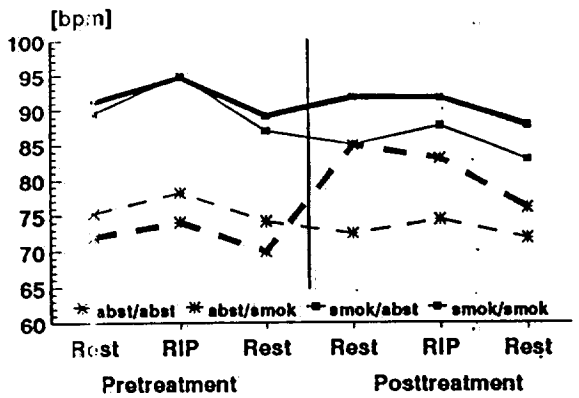

Systolic Blood Pressure

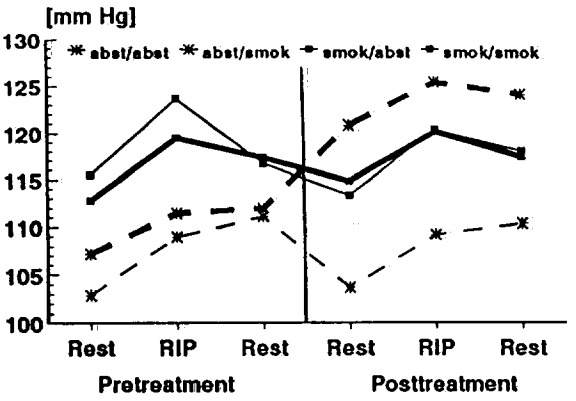

Finger Pulse Amplitude

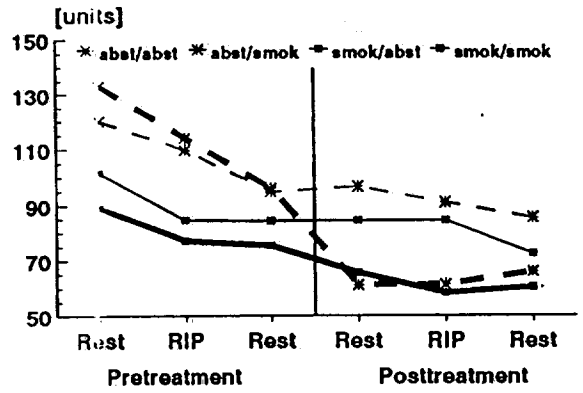

Diastolic Blood Pressure

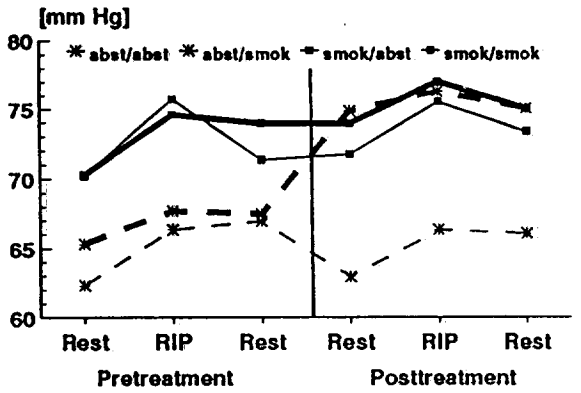

Pre-ejection Period

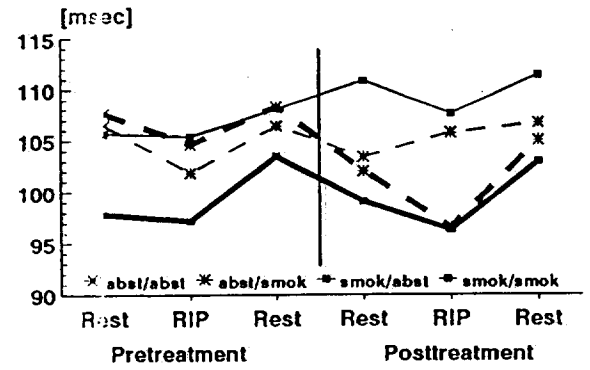

(n=11)

Left Ventricular Ejection Time

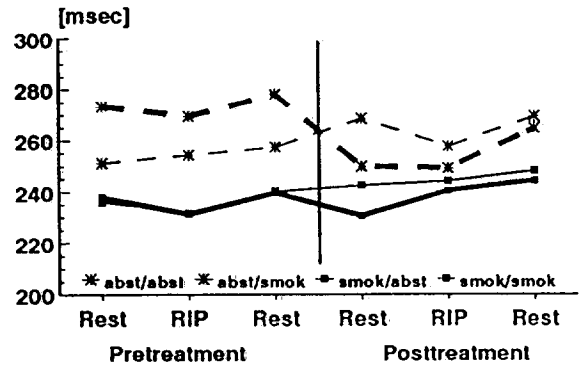

(n=11)

Stroke Volume

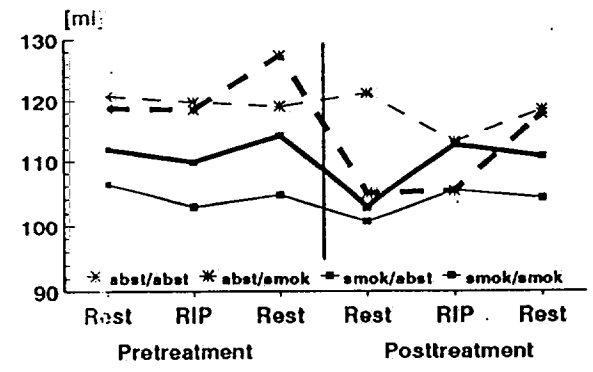

(n=11)

Cardiac Output

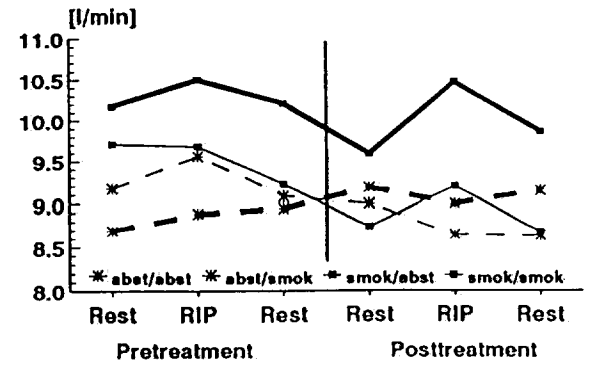

(n=11)

2023251974

$F(1,19) = 28.29$, $p < 0.001$) and an upward trend in cardiac output ($F(1,19) = 3.77$, $p = 0.081$) and significant decreases in finger pulse amplitude ($F(1,19) = 6.48$, $p < 0.05$), left ventricular ejection time ($F(1,10) = 20.20$, $p < 0.001$) and stroke volume ($F(1,10) = 6.15$, $p < 0.05$).

All other peripheral physiological parameters were not affected by either of the manipulations.

In order to investigate the interactions between smoking/smoking state and the physiological reactions to the RIP-task stress, the differences between the means of the RIP phases and the preceding rest phases were computed and analyzed with separate A x S x P ANOVAs. Significant reactions to RIP stress were found for increases in systolic ($F(1,19) = 19.52$, $p < 0.001$) and diastolic ($F(1,19) = 14.29$, $p < 0.01$) blood pressure, physical activity ($F(1,19) = 19.11$, $p < 0.001$) and EMG ($F(1,19) = 7.17$, $p < 0.05$) and decreases in finger pulse amplitude ($F(1,19) = 7.90$, $p < 0.05$) and arrival time ($F(1,19) = 10.19$, $p < 0.01$). The increases in heart rate just failed significance ($F(1,18) = 4.34$, $p = 0.052$). However, there were but two significant interactions with smoking and smoking state. The stress-induced increases in diastolic blood pressure were significantly greater after presession smoking than after presession abstinence ($F(1,19) = 5.19$, $p < 0.05$) and the stress-induced increases in physical activity decreased after smoking, but increased when the subjects were not allowed to smoke in the session ($F(1,19) = 4.59$, $p < 0.05$).

Subjective parameters **(Fig. 4)**

Anxiety was significantly greater after presession abstinence than after presession smoking ($F(1,19) = 10.09$, $p < 0.01$), but was reduced after smoking during the session (interaction A x S x P: $F(1,19) = 4.84$, $p < 0.05$).

The judgement of the individual performance was, similar to that of the processing rate, initially lower after presession abstinence (interaction A x P: $F(1,19) = 14.41$, $p < 0.01$) but increased after smoking in the session (interaction S x P: $F(1,19) = 5.26$, $p < 0.05$).

The craving for smoking a cigarette was higher after presession abstinence than after presession smoking ($F(1,19) = 4.67$, $p < 0.05$), above all before the smoking period (interaction A x P: $F(1,19) = 7.66$, $p < 0.05$), and decreased significantly after the smoking of a cigarette (interaction S x P: $F(1,19) = 18.65$, $p < 0.001$).

Among the other ratings concerning liking and effects of the cigarette, strength of the cigarette ($F(1,19) = 16.05$, $p < 0.001$), nausea ($F(1,19) = 17.01$, $p < 0.001$) and dizziness ($F(1,19) = 16.45$, $p < 0.001$) all were rated significantly higher after presession ab-

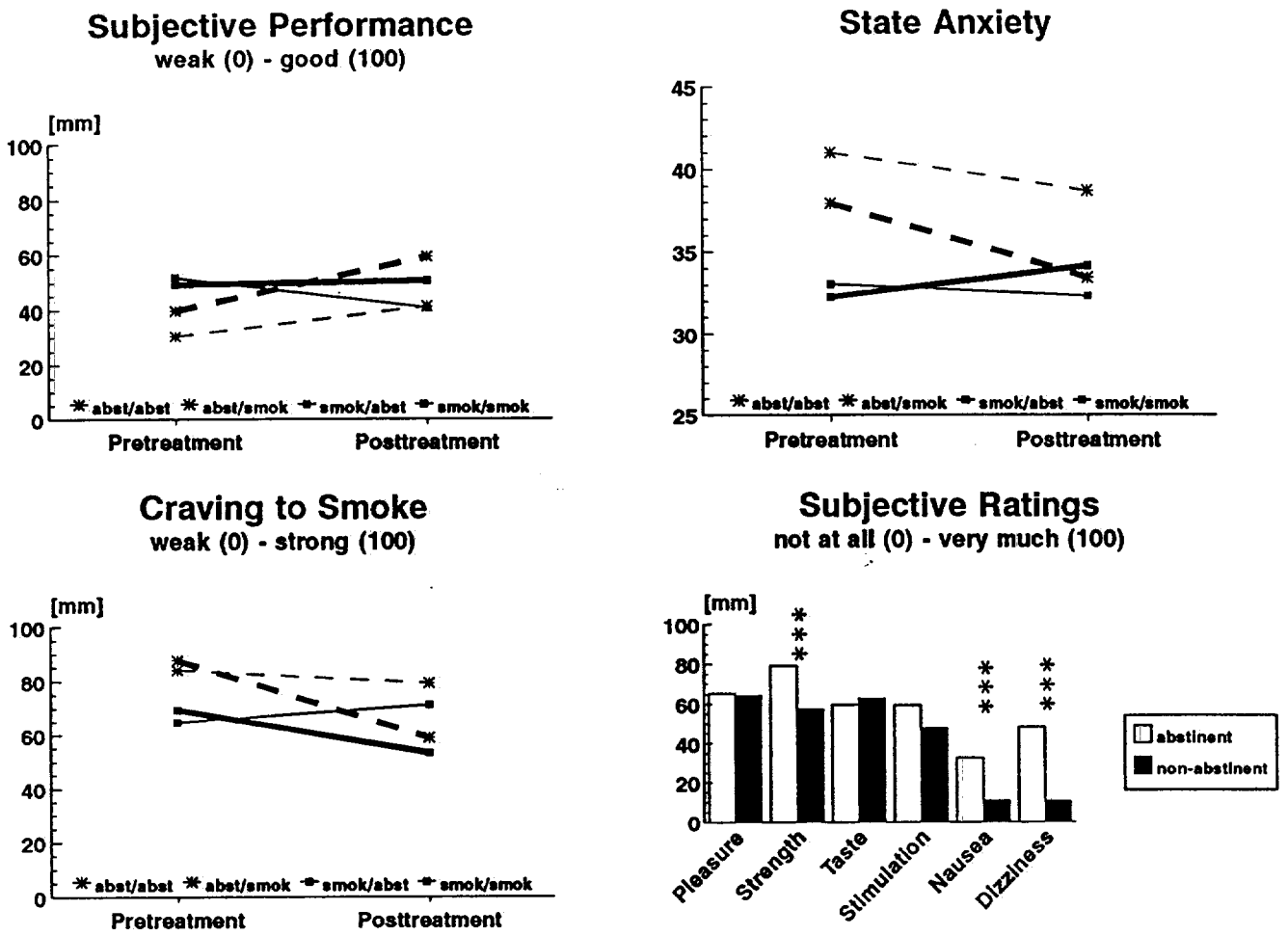

Figure 4. Means of different subjective ratings. Solid lines: subjects were not smoking-deprived; broken lines: subjects were smoking-deprived; thin lines: no smoking in the session; bold lines: smoking in the session.

stinence than after presession smoking. Pleasure, taste and stimulation were not affected by either manipulation.

CONCLUSIONS

The study aimed to investigate to what extent the hypothesis is correct that smoking can alleviate withdrawal symptoms and in addition, whether smoking can have additional positive effects.

Presession abstinence, as compared to presession smoking, decreased cognitive performance, electrocortical and cardiovascular arousal but increased presession anxiety and the magnitude of some averse effects of the cigarette smoked during the session. All these effects contribute to a homogenous withdrawal syndrome.

Smoking during the session, as compared to non-smoking, increased cognitive performance, electrocortical and cardiovascular arousal, as found in earlier studies (Hasenfratz et al., 1989, 1990). However, there were also some significant interactions between presession abstinence and smoking during the session, indicating that the effects of smoking were greater after presession abstinence than after presession smoking or that smoking effects reached significance only after preceding abstinence. This was true for the increases in processing rate, heart rate and stroke volume and the decreases in finger pulse amplitude, LVET and anxiety.

Thus, summing up, it may be said that for most of the parameters presession abstinence led to more pronounced smoking effects. And finally, the smoking manipulations led only exceptionally to significant effects on the stress-induced physiological reactions, suggesting that smoking as a coping aid is only of restricted value for controlling physiological stress reactions.

REFERENCES

Hasenfratz M, Michel C, Nil R, Bättig K (1989) Can smoking increase attention in rapid information processing during noise? Electrocortical, physiological and behavioral effects. Psychopharmacology 98: 75 - 80.

Hasenfratz M, Nil R, Bättig K (1990) Development of central and peripheral smoking effects over time. Psychopharmacology 101: 359 - 365.

Hasenfratz M, Bättig K (1991) Psychophysiological reactions during active and passive stress coping following smoking cessation. Psychopharmacology 104: 356 - 362.

Hasenfratz M, Bättig K (1992) No psychophysiological interactions between caffeine and stress? Psychopharmacology 109: 283 - 290.

Laux L, Glanzmann P, Schaffner P, Spielberger CD (1981) Das State-Trait-Angstinventar. Beltz, Weinheim.

1.2. Verzeichnis der im Rahmen des Forschungsprojektes erfolgten und diesem Bericht in je 20 Exemplaren beigelegten Veröffentlichungen.

Liste des publications parues dans le contexte du projet de recherche et dont 20 exemplaires de chacune sont joints au présent rapport.

1.3. Im Druck befindliche Publikationen, die später nachgeliefert werden.

Publications en voie d'impression et qui seront remises plus tard.

1.4. Sind noch weitere Veröffentlichungen vorgesehen ?

D'autres publications sont-elles envisagées ?

ja	nein
[X]	[ ]
oui	*non*

1.5. Mitteilung, ob sich die Forschungsergebnisse zur Anmeldung von Schutzrechten eignen und ob bereits Schutzrechte angemeldet worden sind :

Les résultats de recherche donnent-ils lieu à des dépôts de brevets, et des demandes dans ce sens ont-elles déjà été faites ?

1.6. Eventual-Vorschlag * zur Weiterverwendung des Materials von bleibendem Wert (nur ausfüllen, falls es sich um einen Schlussbericht handelt).

*Proposition éventuelle * pour l'utilisation ultérieure du matériel de valeur durable (ne remplir que s'il s'agit d'un rapport final).*

Inventar-Nr. *No d'inventaire*	Gegenstand *Objet*	Vorschlag zur Weiterverwendung : Institut, Bibliothek, juristische Person *Proposition pour utilisation ultérieure : Institut, bibliothèque, personne morale*

* Im Prinzip bleibt die ASFC Besitzerin des Materials von bleibendem Wert

* *L'ASFC reste en principe propriétaire du matériel de valeur durable*

2023251982

BRUNNER, H.R.

Division of Hypertension
Faculty of Medicine, Lausanne

Evaluation of Arterial Compliance–Pressure Curves

Effect of Antihypertensive Drugs

François Perret, Vincent Mooser, Daniel Hayoz, Yanik Tardy, Jean-J. Meister, Jean-D. Etienne, Pierre-A. Farine, Alfio Marazzi, Michel Burnier, Jürg Nussberger, Bernard Waeber, and Hans-R. Brunner

A new high-precision ultrasonic device was developed to determine noninvasively arterial compliance as a function of blood pressure. Because of the nonlinear elastic properties of arterial walls, measurements of compliance can be appropriately compared only if obtained over a range of pressures. This apparatus was used to evaluate in a double-blind, parallel fashion the effect of three different antihypertensive drugs and of a placebo on radial artery compliance. Thirty-two normotensive volunteers were randomly allocated to an 8-day, once-a-day oral treatment with either a placebo, 100 mg atenolol, 20 mg nitrendipine, or 20 mg lisinopril. Blood pressure, heart rate, radial artery diameter, and arterial compliance were measured immediately before as well as 6 hours after dosing on the first and last days of the study. On the eighth day of administration, within 6 hours after dosing, lisinopril induced an acute increase in radial artery diameter, from 2.99±0.06 to 3.28±0.09 mm (mean±SEM, $p<0.01$). The compliance–pressure curve was shifted upward on day 1 ($p<0.01$) as well as on day 8 ($p<0.05$). None of the other drugs induced any significant modification of these parameters. Arterial compliance has a strong nonlinear dependency on intra-arterial pressure and therefore has to be defined as a function of pressure. Antihypertensive drugs acting by different mechanisms may have different effects on the mechanical properties of large arteries.
(*Hypertension* 1991;18[suppl II]:II-77–II-83)

During recent years, interest in the mechanical properties of the arterial system has grown considerably. Hypertension has been reported to decrease arterial elasticity due to thickening of the arterial wall.[1-3] The resulting impairment in the buffering function of the arteries seems to exert some untoward effects on cardiovascular homeostasis by increasing cardiac afterload, enhancing arterial cyclic stress, and possibly modifying the pattern of arterial blood flow.[4,5] It therefore seems highly desirable to treat hypertensive patients with drugs that not only decrease blood pressure but also correct arterial compliance. Accordingly, a great need exists for accurate and reliable measurements of arterial compliance using noninvasive methods.

This prompted us to develop a new device that makes it possible to determine noninvasively the compliance of peripheral arteries in humans. The measurement is based on the simultaneous quantitation of changes in arterial volume (reflected by changes in arterial cross section) as related to changes in blood pressure. By establishing this relation over the whole range of pressures prevailing during one cardiac cycle, a compliance–pressure curve characterizing the particular artery studied is obtained and becomes a suitable parameter for vessel comparison.

In the present investigation, we used this device to evaluate the effects of three different antihypertensive drugs and of a placebo on arterial compliance of young normotensive volunteers. Clearly, different effects on the compliance–pressure curves were observed with the three compounds representing three different classes of antihypertensive drugs.

Methods

Subjects and Study Protocol

Thirty-two healthy male subjects aged 20–44 (mean, 26) years were recruited for this study. All of them were

From the Division of Hypertension (F.P., V.M., D.H., M.B., J.N., B.W., H.-R.B.), University Hospital, and the Federal Institute of Technology (Y.T., J.-J.M.), Lausanne, Switzerland; Asulab SA (J.-D.E., P.-A.F.), Research Laboratories of the SMH Group, Neuchâtel, Switzerland; and the Institute of Social and Preventive Medicine (A.M.), University of Lausanne, Lausanne, Switzerland.

Supported by grants from the Commission Suisse pour l'Encouragement de la Recherche Scientifique (C.E.R.S.) and the Swiss Association of Cigarette Manufacturers (A.S.F.C.).

Address for correspondence: H.R. Brunner, MD, Hypertension Division, CHUV, 1011 Lausanne, Switzerland.

normotensive (blood pressure <140/90 mm Hg) and considered healthy based on a medical history, a complete physical examination, and routine laboratory tests. The study protocol was reviewed and approved by the institutional ethics committee. All volunteers signed a consent form before entering the trial.

The investigation was carried out in double-blind fashion according to a parallel design. Treatment periods lasted 8 days. On days 1 and 8, the fasting volunteers came at 8 AM to the clinical research facility, where they were installed in a supine position. Coffee, alcohol, and cigarette consumption had been discontinued for the previous 12 hours. After a 30-minute resting period, the initial measurement (H0) of arterial compliance was carried out as outlined below. At 9 AM, the volunteers swallowed the test medication with a glass of water. At 3 PM (H6), a second determination of arterial compliance was obtained following the same procedure. Blood pressure and heart rate were measured using the Finapres system (see below).

Investigational medications consisted of either atenolol (100 mg p.o. daily) (Tenormine, ICI, Luzern, Switzerland), nitrendipine (20 mg p.o. daily) (Baypress, Bayer, Zurich, Switzerland), or lisinopril (20 mg p.o. daily) (kindly provided by Merck Sharp & Dohme, Glattbrugg, Switzerland). The volunteers were randomly assigned to one of the four study groups (n=8 per group). There was no statistically significant difference in age, weight, or blood pressure between the groups. All subjects completed the study, with the exception of one from the placebo group who was excluded because he did not strictly adhere to the study protocol.

Measurement of Arterial Compliance

Compliance describes the elasticity of volumic structures. In the case of an artery, it defines the blood volume that can be stored or released given a specific change in blood pressure (compliance=δ volume/δ pressure) and is expressed in cubic millimeters per millimeter of mercury. Because changes in arterial volume are mainly due to changes in arterial cross section, compliance also may be defined as the change in arterial cross section induced by a change in arterial pressure and is expressed in square millimeters per millimeter of mercury. The elastic properties of the arterial wall being a function of blood pressure,[6] compliance is determined over a wide range of pressures (e.g., pulse pressure). As a consequence, it is characterized by a compliance–pressure curve.

A new A-mode ultrasonic echo-tracking device[7] was used to record displacement of arterial walls over the whole cardiac cycle. This device was developed by Asulab SA (Research Laboratories of the SMH Group, Neuchâtel, Switzerland) in collaboration with the Swiss Federal Institute of Technology (EPFL, Lausanne, Switzerland) and our laboratory. Briefly, a 10-MHz focalized transducer is stereotaxically positioned over the radial artery without direct contact with the skin using gel as a transmitting medium. Doppler mode is used to place the probe perpendicularly to the arterial axis, in its largest cross-sectional dimension. After the transducer is switched to A-mode, the backscattered echoes from both inner anterior and posterior walls are visualized on an oscilloscopic screen (Figure 1). The electric signals of both walls exhibiting a high signal-to-noise ratio then are easily tagged by an electronic tracer so that their movement can be continuously tracked. Recording of the tracer's displacements allows a digitalized signal of diameter variation to be derived. The internal diameter of the pulsating artery is measured 5,000 times per second. This extremely high frequency of data acquisition makes it possible to average a short series of diameter measurements to further increase instrument precision. Calibration of the device on artificial targets revealed a resolution of close to 1 μm. Simultaneously, blood pressure is measured noninvasively by a commercially available photoplethysmograph (Finapres system, Ohmeda, BOC Group Inc., Engelwood, Colo.). The principle of the method was described in the early 1970s by Penaz.[8] It is based on the volume-clamp method and provides accurate continuous blood pressure measurements very comparable to intra-arterial blood pressure recordings, as has been shown previously.[8–11] Because our technique rests on the concept that arterial compliance is a function of blood pressure, it is also critical to demonstrate similitude between the pressure wave shapes recorded intra-arterially and those obtained at the same time noninvasively at the finger. For this reason, simultaneous photoplethysmographic (finger) and intra-arterial (brachial artery) recordings were compared in three patients included in a different protocol. Figure 2 illustrates in a representative patient that the two pressure tracings are superimposable.

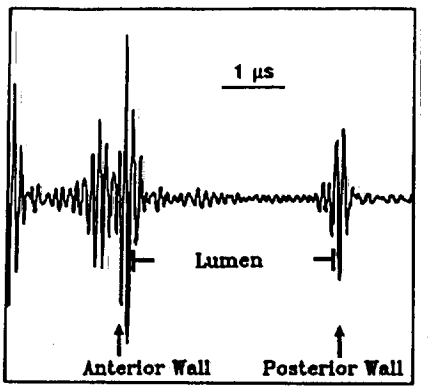

FIGURE 1. *A-mode image of a radial artery.*

From the two simultaneous and continuous signals of arterial diameter and blood pressure (Figure 3), the computerized acquisition system fits the cross section–pressure curve (Figure 4) using an arctangent model with three independent parameters[7] adapted from previously reported work[12–14] and then calculates the compliance–pressure curve.

The oscillographic display of arterial wall echoes on the screen is recorded on Polaroid film. This

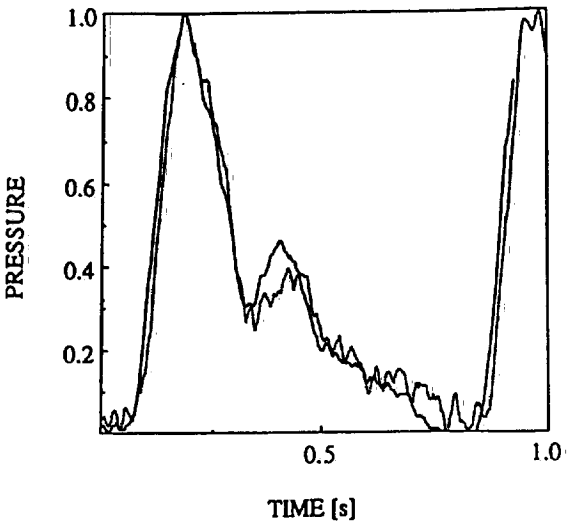

FIGURE 2. *Comparison of the blood pressure wave shape recorded invasively (solid line) in the brachial artery with the noninvasive (dotted line) obtained at the middle finger. Curves were normalized for a difference in amplitude.*

facilitates repositioning of the transducer on the same spot from session to session. The reproducibility of compliance measurements was studied in 10 normotensive volunteers aged 22–67 years. The two sessions took place during the same time of day within a 9-day period. Measurements were performed by a single investigator. The data presented in Figure 5 indicate that in this group of volunteers, compliance–pressure curves measured with this echo-tracking device are highly reproducible.

Statistical Analysis

As mentioned above, the function used to fit the cross section–pressure data and the compliance–pressure curve is based on an arctangent relation with three independent parameters. Three separate points of such a curve are sufficient to characterize the whole relation. To perform a statistical analysis of a compliance–pressure curve, a set of three compliance values at three different pressures (P1, P2, P3) is selected over the range of pulse pressure (Figure 6). A multivariate test based on Hotelling's T^2 statistics[15] then is used to compare matched samples of these sets, in two different sessions.

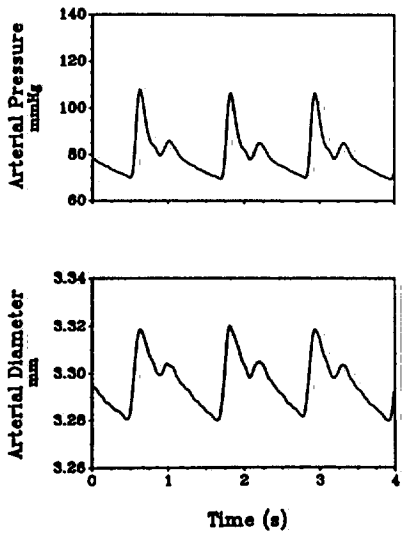

FIGURE 3. *Simultaneous recordings of finger arterial pressure* (top panel) *and radial artery diameter* (bottom panel).

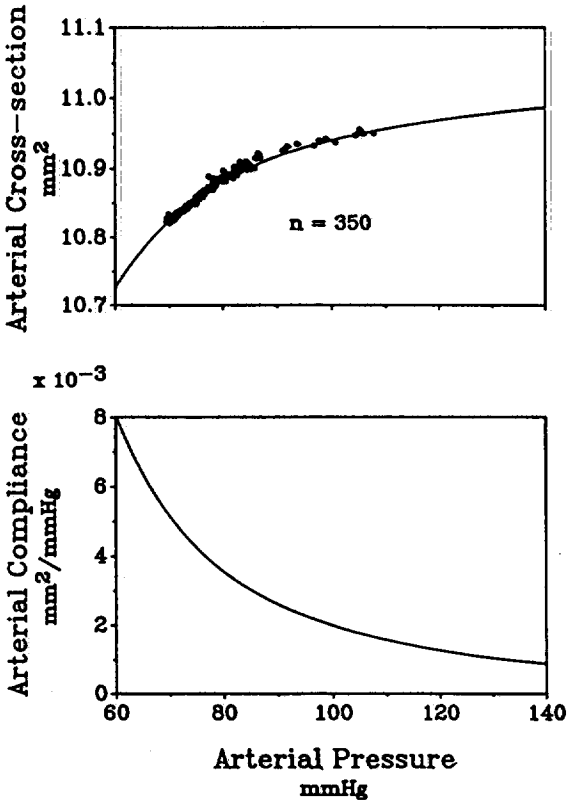

FIGURE 4. *Cross-section–pressure and compliance–pressure curves fitted on data from Figure 3.*

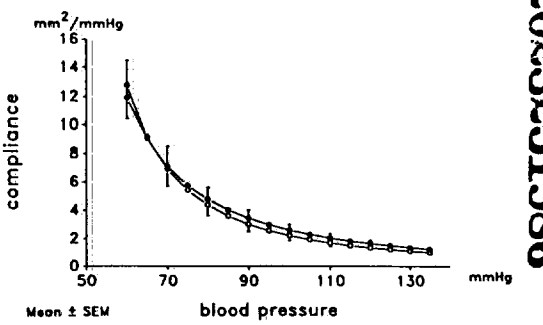

FIGURE 5. *Mean compliance–pressure curve of 10 volunteers studied under similar conditions on two different sessions 9 days apart.* ○, *Session one;* ●, *session two. Compliance values are given in mm²/mm Hg×1,000.*

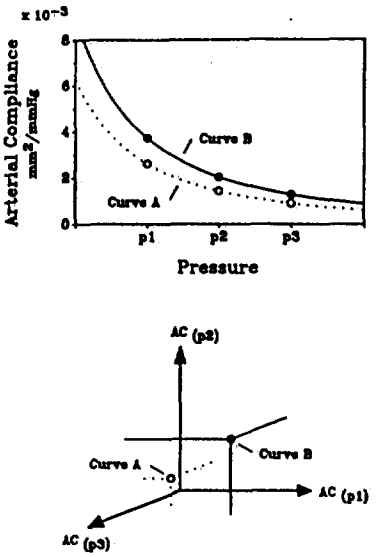

FIGURE 6. Top panel: *Schematic representation of two arterial compliance–pressure curves (A and B). Each is characterized by three points chosen arbitrarily (p1, p2, p3) over the pulse pressure range.* Bottom panel: *Three-dimensional graph of the spatial position (illustrated by points A and B) of the two curves as defined by their respective three compliance values (AC) measured at p1, p2, and p3.*

A one-way analysis of variance followed by a least significant difference test was used to evaluate changes in blood pressure, heart rate, and arterial diameter. Differences were considered significant at values of $p<0.05$. Results are expressed as mean±SEM.

Results

Blood Pressure, Heart Rate, and Arterial Diameter

Table 1 shows the time course of blood pressure, heart rate, and arterial diameter (at a pressure of 100 mm Hg) and its change during a cardiac cycle. Values measured on the first and eighth day of treatment before H0 and 6 hours after H6 dosing are given. Neither placebo nor nitrendipine induced significant changes in any of the three variables. Atenolol administration caused a significant decrease in both systolic and diastolic blood pressures within the first 6 hours of treatment, and this effect persisted until day 8. As expected, β-adrenoceptor blockade reduced heart rate. Despite these changes, neither diastolic arterial diameter nor its variations during the cardiac cycle were altered by atenolol. A similar trend toward blood pressure reduction was observed in the group treated with lisinopril. However, the blood pressure fall did not reach statistical significance except for the diastolic blood pressure on day 8, 6 hours after the drug. This was accompanied by a significant rise in arterial diameter ($p<0.05$).

Compliance–Pressure Curves

On day 1 of drug administration, the compliance–pressure curves were not changed by placebo,

TABLE 1. Changes in Blood Pressure, Heart Rate, and Radial Artery Diameter During Study Course

Time	Systolic pressure (mm Hg)	Diastolic pressure (mm Hg)	Heart rate (beats/min)	Diameter at 100 mm Hg (mm)	Pulsatile changes in diameter (μm)
Placebo					
D1H0	105±5	53±2	57±3	2.92±0.14	49±9
D1H6	105±4	52±3	59±3	3.03±0.15	42±7
D8H0	105±3	54±2	61±3	3.03±0.16	43±5
D8H6	110±3	56±1	63±3	3.10±0.17	46±7
Atenolol					
D1H0	113±4	60±2	63±2	3.04±0.14	37±4
D1H6	96±3*	51±2*	54±2†	3.15±0.15	47±5
D8H0	103±2‡	52±1*	53±1†	2.97±0.12	44±5
D8H6	100±3†	49±1†	53±1†	3.00±0.12	47±6
Nitrendipine					
D1H0	99±4	54±2	59±3	2.99±0.09	43±5
D1H6	96±5	50±3	62±3	3.13±0.09	55±8
D8H0	100±5	53±3	59±4	2.96±0.11	45±5
D8H6	103±3	55±2	62±3	3.10±0.13	49±6
Lisinopril					
D1H0	107±4	58±2	62±3	2.99±0.06	34±2
D1H6	102±4	54±2	64±3	3.04±0.07	43±4
D8H0	99±4	55±2	62±4	3.00±0.05	36±3
D8H6	97±2	52±2‡	68±4	3.28±0.09*	48±5‡

Values are mean±SEM. D1, day 1; D8, day 8; H0, before dosing; H6, 6 hours after dosing.
*$p<0.01$, †$p<0.001$, ‡$p<0.05$ vs. D1H0.

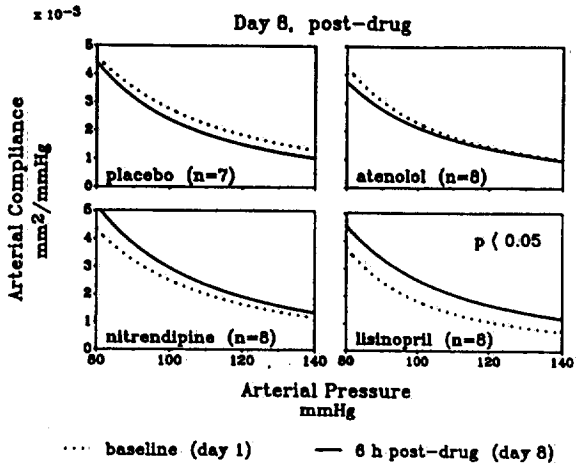

FIGURE 7. *Compliance–pressure curves on the first day before dosing (D1H0) and the eighth day of treatment 6 hours after dosing (D8H6).*

atenolol, or nitrendipine, but in lisinopril-treated subjects, a shift upward of the curve was apparent 6 hours after dosing (D1H6 versus D1H0, $p<0.01$). When the curves between days 1 and 8 established before drug intake (D1H0 versus D8H0) are compared, none of the drugs induced any lasting shift in the compliance–pressure curves. However, after lisinopril administration, on the eighth day, 6 hours after the drug (D8H6 versus D1H0), a significant shift ($p<0.05$) of the compliance–pressure curve was still apparent (Figure 7). A similar but nonsignificant trend was observed after nitrendipine, but this was not statistically significant in this small number of volunteers.

Discussion

This report describes a new and original approach to the measurement of arterial compliance of peripheral arteries in humans. The most important aspects of this new methodology are the following: First, the method is completely noninvasive, using A-mode ultrasound for the measurement of internal diameter of the arteries and photoplethysmography for the continuous recording of blood pressure. As a consequence, the measurements can be repeated many times in the same subject. Furthermore, the method is characterized by an extremely high precision of the measurements of the internal arterial diameter, that is, its cross section. This precision is indispensable for tracking changes in arterial geometry occurring within the cardiac cycle. Most important, because arterial compliance is inherently dependent on blood pressure and indeed easily doubles when the pressure falls from a systolic pressure of 120 mm Hg to a diastolic pressure of 80 mm Hg, this method has the advantage of providing noninvasively compliance–pressure curves. In this preliminary study, it has been possible to demonstrate that the angiotensin converting enzyme inhibitor lisinopril can actually enhance the arterial compliance of the radial artery of normal volunteers.

Some researchers have tried to characterize the physical properties of arteries by measuring vascular elasticity[16] or stiffness.[17] Compliance is the physical parameter most often used to quantify arterial elasticity. Much work already has been carried out attempting to evaluate this parameter noninvasively, by using pulse wave velocity,[18,19] by analyzing the diastolic pressure decay,[20–23] or by determining the stroke volume/pulse pressure index.[3,24] These different approaches allow investigation of arteries of major clinical interest at the cost of their inability to determine arterial compliance as a function of pressure. This makes it impossible to compare measurements of arterial compliance in any situations in which blood pressure is not equal. Thus, increases in arterial compliance occurring in the face of a blood pressure decrease cannot be interpreted if compliance–pressure curves are not available. Similarly, comparison of the arterial compliance of hypertensive patients to that of normotensive subjects can provide valid results only if it is based on overlapping compliance–pressure curves determined in the two populations.

Megerman and coworkers[13] have determined in vivo some compliance–pressure curves in animals using a similar ultrasonic approach with an invasive blood pressure recording. The new system used in the present study now allows determination of compliance–pressure curves totally noninvasively in humans, as well as providing a higher degree of precision.

We chose to work on the radial artery, a medium-sized muscular artery, because it has the advantage of being quite superficial and close to the digital artery where the pressure signal is recorded.[7] It still remains to be determined how precisely the diameter of deeper arteries can be tracked. Even more problematic is the distance between the ultrasound probe and the site where the pressure is recorded. Ideally, the pressure and arterial cross section should be determined at exactly the same place. For the moment, this is technically unfeasible. The physical separation of the two probes results in a hysteresis of the diameter–pressure curve. Hysteresis related to intrinsic properties of the radial artery wall is negligible compared with the effect of distance mismatch. Indeed, based on a hemodynamic model developed by Tardy et al[7] and taking into account only the time delay between the two signals, it is possible to eliminate the hysteresis.

The choice of a muscular artery could be criticized for two reasons. First, these muscular-type arteries do not have a major role in the buffering capacity of the arterial tree. Second, because the radial artery is rarely affected by severe atherosclerosis, it could exhibit particular characteristics that might not reflect the physiology or pathophysiology of the whole arterial tree, particularly of large elastic arteries. It has been suggested, however, that in hypertensive subjects, the distal arterial compliance may be de-

creased more than the proximal one, which could imply greater changes in the medium-sized muscular than in predominantly elastic arteries.[25] Moreover, the short-term effects of vasoactive drugs on arterial compliance most probably are mediated by changes in muscular tone rather than alterations in wall structure. More importantly, animal studies have shown that hypertension seems to induce diffuse and rather homogeneous thickening of the arterial wall, which could be reflected by altered compliance–pressure curves involving also the radial artery. This artery therefore should be an interesting model of the peripheral arteries worth investigating.

The three different compounds evaluated in this study represent three major drug classes, and they exert different actions. Therefore, these compounds also may have different effects on arteries. For instance, depending on whether β-adrenoceptor antagonists are selective β_1-blockers or not, they appear either to have no effect or to produce vasoconstriction. On the other hand, β-blockers with intrinsic sympathomimetic activity may induce vasodilation.[26–28] Calcium channel antagonists[29–33] and converting enzyme inhibitors[26,34–37] have been reported to produce vasodilation of large arteries. All these previous measurements were carried out with a pulsed Doppler device that provides only a mean arterial diameter.

As one might have expected with a cardioselective compound lacking any intrinsic sympathomimetic activity, in the present studies atenolol did not change radial artery diameter or compliance. Nitrendipine produced acutely a slight increase in arterial diameter. Likewise, a trend toward enhancing arterial compliance was noted after dosing, especially after the first administration of this calcium antagonist. However, because of the disparity of the responses, this tendency did not reach statistical significance. In contrast, lisinopril increased both arterial diameter and compliance 6 hours after dosing. The effect on compliance was already seen on the first day of treatment, but it was not apparent 24 hours after dosing, at a time when plasma angiotensin II levels are known to have returned to baseline.[38] It seems most unlikely that a change in wall structure could account for these acute modifications. Furthermore, because of the technique we used, the concomitant decrease in diastolic blood pressure cannot explain the enhanced arterial compliance. Thus, the upward shift of the compliance–pressure curve we observed in the lisinopril-treated group is highly suggestive of a transient decrease in vascular tone consecutive to the fall in plasma angiotensin II levels. Longer follow-up will be necessary to detect potential benefit of this drug on arterial wall structure.

In conclusion, the present data, obtained with a new ultrasonic device, demonstrate for the first time that it is possible to determine noninvasively and with a high degree of precision arterial compliance of a peripheral artery as a function of pressure. Lack of data on compliance–pressure curves still renders their interpretation difficult. Nevertheless, this new technique opens a new field in the study of dynamic arterial wall behavior. It allows researchers to follow changes in arterial compliance resulting from changes in wall elasticity independently of passive changes caused by variations in arterial pressure. The results observed during a few days of administration of lisinopril, atenolol, and nitrendipine strongly suggest that antihypertensive drugs acting by different mechanisms may display quite different effects on arterial compliance of normal volunteers.

References

1. Gribbin B, Pickering TG, Sleight P: Arterial distensibility in normal and hypertensive man. *Clin Sci* 1979;56:413–417
2. Safar ME, Simon AC, Levenson JA: Structural changes in large arteries in sustained essential hypertension. *Hypertension* 1984;6(suppl III):III-117–III-121
3. Ventura H, Messerli FH, Oigman W, Suarez DH, Dreslinski GR, Dunn FG, Reisin E, Frohlich ED: Impaired systemic arterial compliance in borderline hypertension. *Am Heart J* 1984;108:132–136
4. O'Rourke MF: *Arterial Function in Health and Disease.* Edinburgh, Churchill Livingstone, 1982, pp 196–252
5. O'Rourke MF: Basic concepts for the understanding of large arteries in hypertension. *J Cardiovasc Pharmacol* 1985;7(suppl 2):S14–S21
6. Bergel DH: The dynamic elastic properties of the arterial wall. *J Physiol* (Lond) 1961;156:458–469
7. Tardy Y, Meister JJ, Perret F, Waeber B, Brunner HR: Assessment of the elastic behaviour of peripheral arteries from a non-invasive measurement of their diameter–pressure curves. *Clin Phys Physiol Meas* 1991;12:39–54
8. Penaz J, Voigt A, Teichmann W: Beitrag zur fortlaufenden blutdruckmessung. *Zeitschrift Innere Med* 1976;31:1030–1033
9. Wesseling KH, Settels JJ, De Wit B: The measurement of continuous finger arterial pressure non-invasively in stationary subjects, in: *Biological and Psychological Factors in Cardiovascular Disease.* Berlin, Springer-Verlag, 1986, pp 355–375
10. Parati G, Casadei R, Groppelli A, Di Rienzo M, Mancia G: Comparison of finger and intra-arterial blood pressure monitoring at rest and during laboratory testing. *Hypertension* 1989;13:647–655
11. Burgener E, Mooser V, Waeber B, Porchet M, Gardaz JP, Nussberger J, Brunner HR: Calcium entry blockade attenuates the acute blood pressure rise induced by cigarette smoking. *J Cardiovasc Pharmacol* 1988;12(suppl 6):126–130
12. Langewouters GJ, Wesseling KH, Godehard WJA: The static elastic properties of 45 human thoracic and 20 abdominal aortas in vitro and the parameters of a new model. *J Biomech* 1984;17:425–435
13. Megerman J, Hasson JE, Warnock DF, L'Italien GJ, Abbott WM: Noninvasive measurements of nonlinear arterial elasticity. *Am J Physiol* 1986;250:H181–H188
14. Langewouters GJ, Zwart A, Busse R, Wesseling KH: Pressure–diameter relationships of segments of human finger arteries. *Clin Phys Physiol Meas* 1986;7:43–56
15. Morrison DF: *Multivariate Statistical Methods.* New York, McGraw-Hill Book Co, 1976, pp 128–141
16. Peterson LH, Jensen RE, Parnell J: Mechanical properties of arteries in vivo. *Circ Res* 1960;8:622–639
17. Kawasaki T, Sasayama S, Yagi SI, Asakawa T, Hirai T: Non-invasive assessment of the age related changes in stiffness of major branches of human arteries. *Cardiovasc Res* 1987;21:678–687
18. Bramwell JC, Hill AV: The velocity of the pulse wave in man. *Proc Soc Exp Biol Med* 1922;93:298–306
19. Gribbin B, Pickering TG, Sleight P: Methodology: Pulse wave velocity as a measure of blood change. *Psychophysiology* 1976;13:90–95

20. Simon AC, Safar ME, Levenson JA, London GM, Levy BI, Chau NP: An evaluation of large arteries compliance in man. *Am J Physiol* 1979;237:H550–H554
21. Simon AC, Laurent S, Levenson JA, Bouthier JA, Safar ME: Estimation of forearm arterial compliance in normal and hypertensive men from simultaneous pressure and flow measurements in the brachial artery, using a pulsed Doppler device and a first-order arterial model during diastole. *Cardiovasc Res* 1983;17:331–338
22. Randall OS, Esler MD, Calfee RV, Buloch GF, Maisel AS, Culp B: Arterial compliance in hypertension (abstract). *Aust N Z J Med* 1976;6(suppl 2):49
23. Zobel LR, Finkelstein SM, Carlyle PF, Cohn JN: Pressure pulse contour analysis in determining the effect of vasodilatator drugs on vascular hemodynamics impedence characteristics in dogs. *Am Heart J* 1980;100:81–88
24. Tarazi RC, Magrini F, Dustan HP: The role of aortic distensibility in hypertension, in Milliez P, Safar ME (eds): *International Symposium on Hypertension.* Ingelheim, FRG, Boehringer Ingelheim, 1975, pp 133–142
25. Finkelstein SM, Feske W, Mock J, Carlyle P, Rector T, Kubo S, Cohn JN: Vascular compliance in hypertension. *10th Annual International Conference Proceedings.*, IEEE Engineering in Medicine & Biology Society, 1988, pp 241–242
26. Simon AC, Levenson JA, Bouthier JD, Benetos A, Achimastos A, Fouchard M, Maarek B, Safar ME: Comparison of oral MK 421 and propranolol in mild to moderate essential hypertension and their effects on arterial and venous vessels of the forearm. *Am J Cardiol* 1984;53:781–785
27. Maarek B, Simon AC, Levenson JA, Merli I, Bouthier JD: Chronic effects of pindolol on the arterioles, large arteries, and veins of the forearm in mild to moderate essential hypertension. *Clin Pharmacol Ther* 1986;39:403–408
28. Levenson JA, Le Quan Sang KH, Devynck MA, Gitel R, Simon AC: The role of antihypertensive drugs in counteracting adverse influence on large arteries. *Am Heart J* 1987;114:992–997
29. Safar ME, Simon AC, Levenson JA, Cazor JL: Hemodynamic effects of diltiazem in hypertension. *Circ Res* 1983;52(suppl I):I-169–I-173
30. Thuillez C, Duhaze P, Fournier C, Lapierre V, Giudicelli JF: Arterial and venous effects of verapamil in normal volunteers. *Fundam Clin Pharmacol* 1987;1:35–44
31. Thuillez C, Gueret M, Duhaze P, Lhoste F, Kiechel JR, Giudicelli JF: Nicardipine: Pharmacokinetics and effects on carotid and brachial blood flows in normal volunteers. *Br J Clin Pharmacol* 1984;18:837–847
32. Levenson J, Simon AC, Safar ME, Bouthier J, Maarek BC: Large arteries in hypertension: Acute effects of a new calcium entry blocker, nitrendipine. *J Cardiovasc Pharmacol* 1984;6:S1006–S1010
33. Levenson J, Simon AC, Bouthier J, Maarek BC, Safar ME: The effect of acute and chronic nicardipine therapy on forearm arterial haemodynamics in essential hypertension. *Br J Clin Pharmacol* 1984;20:107S–113S
34. Thuillez C, Richer C, Giudicelli JF: Pharmacokinetics, converting enzyme inhibition and peripheral arterial hemodynamics of ramipril in healthy volunteers. *Am J Cardiol* 1987;59:38D–44D
35. Richer C, Thuillez C, Giudicelli JF: Perindopril, converting enzyme blockade, and peripheral arterial hemodynamics in the healthy volunteer. *J Cardiovasc Pharmacol* 1987;9:94–102
36. Simon AC, Levenson JA, Bouthier J, Maarek B, Safar ME: Effects of acute and chronic angiotensin-converting enzyme inhibition on large arteries in human hypertension. *J Cardiovasc Pharmacol* 1985;7:S45–S51
37. Asmar RG, Pannier B, Santoni JP, Laurent S, London GM, Levy BI, Safar ME: Reversion of cardiac hypertrophy and reduced arterial compliance after converting enzyme inhibition in essential hypertension. *Circulation* 1988;78:941–950
38. Brunner DB, Desponds G, Biollaz J, Keller I, Ferber F, Gavras H, Brunner HR, Schelling JL: Effect of a new angiotensin converting enzyme inhibitor MK421 and its lysine analogue on the components of the renin system in healthy subjects. *Br J Clin Pharmacol* 1981;11:461–467

KEY WORDS • antihypertensive therapy • vascular elasticity • ultrasonic diagnosis • lisinopril • nitrendipine • atenolol

Conduit Artery Compliance and Distensibility Are Not Necessarily Reduced in Hypertension

Daniel Hayoz, Blaise Rutschmann, François Perret, Michel Niederberger, Yanik Tardy, Vincent Mooser, Jürg Nussberger, Bernard Waeber, and Hans R. Brunner

The goal of this study was to investigate whether the elastic behavior of conduit arteries of humans or rats is altered as a result of concomitant hypertension. Forearm arterial cross-sectional compliance–pressure curves were determined noninvasively by means of a high precision ultrasonic echo-tracking device coupled to a photoplethysmograph (Finapres system) allowing simultaneous arterial diameter and finger blood pressure monitoring. Seventeen newly diagnosed hypertensive patients with a humeral blood pressure of 163/103±4.4/2.2 mm Hg (mean±SEM) and 17 age- and sex-matched normotensive controls with a humeral blood pressure of 121/77±3.2/1.9 mm Hg were included in the study. Compliance–pressure curves were also established at the carotid artery of 16-week-old anesthetized spontaneously hypertensive rats (n=14) as well as Wistar-Kyoto normotensive animals (n=15) using the same echo-tracking device. In these animals, intra-arterial pressure was monitored in the contralateral carotid artery. Mean blood pressures averaged 197±4 and 140±3 mm Hg in the hypertensive and normotensive rats, respectively. Despite the considerable differences in blood pressure, the diameter–pressure and cross-sectional compliance–pressure and distensibility–pressure curves were not different when hypertensive patients or animals were compared with their respective controls. These results suggest that the elastic behavior of a medium size muscular artery (radial) in humans and of an elastic artery (carotid) in rats is not necessarily altered by an increase in blood pressure. (*Hypertension* 1992;20:1–6)

KEY WORDS • **elasticity** • **arteries** • **essential hypertension** • **ultrasonography** • **spontaneously hypertensive rats**

The structural changes of arterial wall observed in hypertensive patients may reflect either a primary defect or a consequence of an elevated blood pressure.[1–5] Increased vascular thickness is thought to be a key determinant of the mechanical behavior of conduit vessels. Several physical parameters have been used in an attempt to assess the influence of morphological changes on arterial impedance. Pulse wave velocity per se[6] or in combination with mean arterial diameter measurements,[7,8] arterial stiffness,[9] exponential diastolic pressure wave decay analysis,[10–13] and invasive compliance recordings[14–16] are among the approaches used to characterize the mechanical properties of the arterial wall associated with hypertension.

Arterial compliance, which can be defined as the blood volume stored or released given a specific change in intraluminal blood pressure, as well as the cross-section adjusted distensibility, decreases in close relation with blood pressure when this latter increases. Because the pressure–volume relation is clearly nonlinear,[17] compliance changes dramatically with variations in blood pressure. Therefore, pressure has to be accounted for as a variable. This has not always been possible in the past due to methodological difficulties.

In the present study, variations in the internal diameter of the radial artery and in finger blood pressure were recorded simultaneously and continuously by means of a noninvasive, high-precision echo-tracking device coupled to a commercially available photoplethysmograph. Seventeen newly diagnosed hypertensive patients and an equal number of sex- and age-matched normotensive subjects were investigated. Additional measurements were performed in anesthetized spontaneously hypertensive rats (SHR) and normotensive Wistar-Kyoto (WKY) control rats. In these animals, the internal diameter of the external carotid artery was tracked using the same device, and intra-arterial blood pressure was monitored via a catheter placed in the contralateral carotid artery.

Methods

Human Studies

Seventeen newly diagnosed and untreated hypertensive patients (office blood pressure was more than 160 mm Hg or diastolic blood pressure more than 95 mm Hg, or both, on at least three occasions) and 17 normotensive subjects were included in the current study. The protocol for this study was approved by the institutional ethics committee. Informed consent was obtained from all participants for entry into the study.

From the Hypertension Division and Cardiovascular Research Group (D.H., B.R., F.P., M.N., V.M., J.N., B.W., H.R.B.), University Hospital (CHUV) and the Department of Physics (Y.T.), Federal Swiss Institute of Technology, Lausanne, Switzerland.

Supported by grants from the Swiss Association of Cigarette Manufacturers, the Cardiovascular Research Fund, and the Swiss National Science Foundation.

Address for correspondence: H.R. Brunner, MD, Division d'hypertension, CHUV 1011 Lausanne, Switzerland.

Received May 14, 1991; accepted in revised form November 1, 1991.

TABLE 1. Characteristics of the Human Study Groups

Variables	Normotensive (n=17)	Hypertensive (n=17)
Sex (F/M)	7/10	7/10
Age (yr)	47.5 (23–65)	49.7 (24–67)
Office humeral blood pressure (mm Hg)*		
Systolic	121±3.2	163±4.4†
Diastolic	77±1.9	103±2.2†
Finger blood pressure (mm Hg)*		
Systolic	121±5.2	148±4.2†
Diastolic	68±2.1	82±2.6†
Internal diameter of radial artery (mm)		
Systolic	2.807±0.134	2.866±0.081
Diastolic	2.767±0.133	2.830±0.081
Plasma cholesterol (mmol/l)	4.45±0.16	5.60±0.27†
Smokers (No.)	8	11

Values are mean±SEM.
*Blood pressure was measured with different techniques on different days: office humeral blood pressure was measured with subject in seated position, and finger blood pressure was measured after the subject had been in the supine position for 15 minutes.
†$p<0.01$ vs. normotensive group.

The two groups were age- and sex-matched. Secondary hypertension was excluded on the basis of medical history, physical examination, and laboratory tests. The control group consisted of normotensive subjects recruited from the medical, nursing, and technical hospital staff. The clinical characteristics of both study groups are presented in Table 1.

Technique of Arterial Diameter and Pressure Measurement

All subjects were studied in supine position after 15 minutes of rest in a room with a constant temperature of 23°C. Arterial measurements were carried out on the right radial artery. For this purpose the right supinated arm was placed in a gutter to avoid involuntary movements. The measurements were always performed at the same time of the day by a single operator. The description of the measuring device as well as preliminary observations made in humans using this new system have been reported previously.[18,19] Briefly, the apparatus consists of an A-Mode, ultrasonic echo-tracking device that measures internal radial artery diameter variations with a precision close to 1 μm. The degree of resolution is made possible by oversampling (5,000 arterial diameter measurements per second) and averaging 16 consecutive values. For the recordings, a 10-MHz probe is positioned perpendicularly over the artery without direct contact with the skin. The Doppler technique is used for guidance of the probe and an ultrasonic gel is used for signal transduction.

In the present study, measurements were obtained at three different locations evenly spaced (2 cm) along the radial artery starting from the wrist. Five arterial recordings were performed at each position, the whole procedure being accomplished within a 15-minute period. The cross-sectional compliance–pressure (C–P) curves obtained at these three different positions along the radial artery axis were averaged for each subject. This latter C–P relation was used for calculating the mean C–P curve for the different study groups. In each group, the mean of systolic and diastolic pressure was taken as cut point for the upper and lower limit of the curves. The backscattered echoes from inner walls are visualized on an oscilloscope and a Polaroid picture of the analog display is taken for the record. The ultrasound device is coupled to a photoplethysmograph (Finapres system, Ohmeda, BOC Group Inc., Engelwood, Colo.), which measures blood pressure continuously and noninvasively at the middle finger. This latter instrument based on a volume-clamp method has been shown previously to provide accurate blood pressure measurements as compared with blood pressure measured intra-arterially.[20–24] The simultaneous and continuous acquisitions of internal arterial diameter and blood pressure (Figure 1A) are processed on line to compute a cross-section–pressure relation (Figure 1B). This latter is subsequently converted into a compliance–pressure curve (Figure 1C), which is fully characterized over the whole range of blood pressure. This curve fits best with an arctangent function described by Lang-

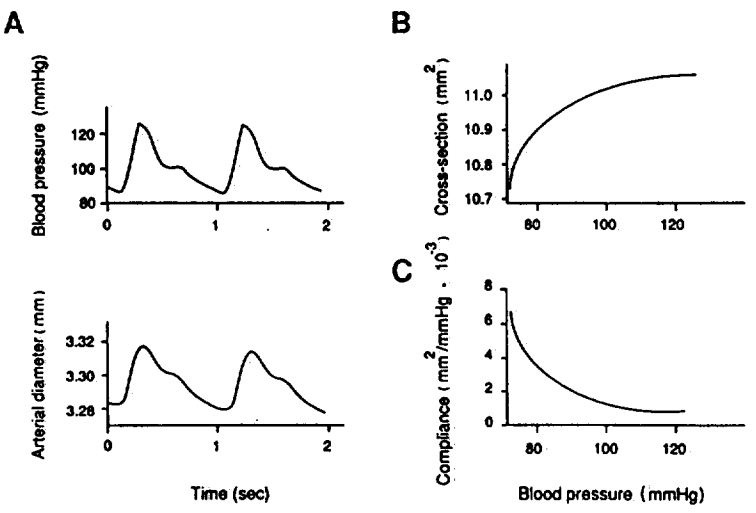

FIGURE 1. Panel A: *Tracings of a simultaneous recording of finger arterial pressure and radial artery diameter in a normal subject. Continuous measurement of these two parameters allows establishment of a cross-section* (panel B) *and compliance–pressure* (panel C) *relation.*

TABLE 2. Characteristics of the Rats

Variables	WKY (n=15)	SHR (n=14)
Body weight (g)	325±3	327±6
Blood pressure during anesthesia (mm Hg)		
Systolic	131±3	192±1*
Diastolic	88±3	133±2*
Heart rate (bpm)	431±10	405±14
Internal diameter of carotid artery (mm)		
Systolic	1.195±0.06	1.304±0.10
Diastolic	1.037±0.05	1.190±0.10

Values are mean±SEM. WKY, Wistar-Kyoto rats; SHR, spontaneously hypertensive rats; bpm, beats per minute.
*p<0.01 vs. WKY rats.

ewouters et al.[25] Cross-sectional compliance (C) in the case of a cylindrical vessel is given by

$$C=\delta s/\delta p \quad (1)$$

where δs is change in cross-section and δp is change in blood pressure. Arterial cross-sectional distensibility (D) is the inverse of the Peterson elastic modulus,[26] i.e., the compliance value normalized for the cross-section (s). It is defined by

$$D=(1/s)*(\delta s/\delta p) \quad (2)$$

Animal Experiments

Fifteen 16-week-old normotensive male WKY rats and 14 age- and sex-matched SHR were obtained from IFFA-CREDO, Lyon, France. They were housed in a room at a constant temperature of 23°C. Ordinary rat chow (UAR, A04, Villemoisson-sur-Orge, France) containing 100 μmol sodium per gram and tap water were given ad libitum. On the day of the experiment, anesthesia was induced with ether and then maintained with fluothane at a concentration of 1.5%. The left external carotid artery was cannulated with a catheter (PE-50) filled with a heparinized 0.9% NaCl solution. Intra-arterial pressure and heart rate were monitored as described previously using a computerized data acquisition system.[27] The internal diameter of the right external carotid artery was measured at the same time using our new ultrasonic device. The whole procedure lasted 15–20 minutes. The different curves were established over the range of pressures actually measured in the two groups of rats, the mean diastolic and systolic values serving as lower and upper limits. The characteristics of the two groups of animals are summarized in Table 2.

Statistical Analysis

Student's t test for unpaired data was used to compare the general baseline characteristics of the two clinical and experimental groups. Differences were considered significant for values of p<0.05. Data are reported as mean±SEM. Statistical analysis of compliance–pressure and distensibility–pressure curves obtained in humans were done using a multivariate analysis based on Hotelling's T^2 considering compliance values at three arbitrary defined blood pressures in the proximity of measured values (80, 100, and 120 mm Hg).

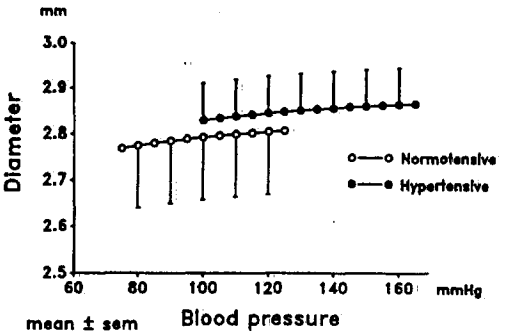

FIGURE 2. *Line plot shows relation between blood pressure and internal diameter of the right radial artery.*

Results

Human Studies

Figure 2 depicts the diameter–pressure curves established in the hypertensive patients and the normotensive subjects. There was a more than 5 mm Hg overlap between the finger pressures measured in the two groups. The internal diameter of the radial artery increased in parallel with blood pressure and tended to be larger in hypertensive patients than in normotensive subjects (Table 1). Due to the widespread distribution of this parameter, however, no significant difference was observed between the two study populations. There was no relation between age and arterial diameter.

The compliance–pressure curves are shown in Figure 3 (upper panel). The behavior of the arterial wall was very similar in the two groups. No significant difference in cross-sectional arterial compliance was found between

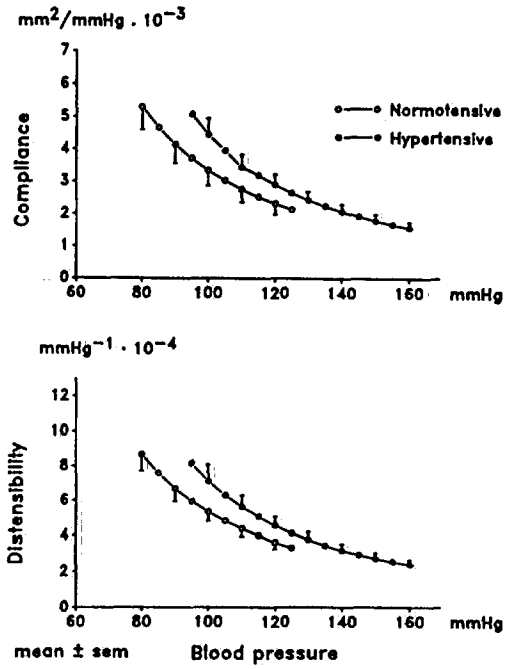

FIGURE 3. *Cross-sectional compliance–pressure curves* (upper panel) *and cross-sectional distensibility–pressure curves* (lower panel) *established in hypertensive patients and normotensive subjects.*

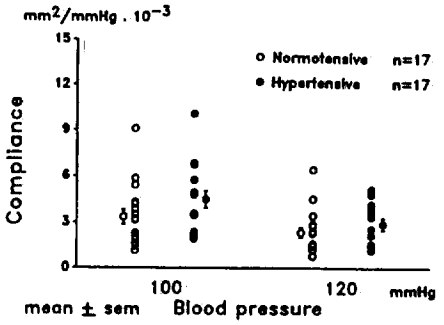

FIGURE 4. *Individual values of compliance values measured at 100 and 120 mm Hg in hypertensive patients and normotensive subjects.*

hypertensive patients and normotensive subjects. Actually, there was a considerable scatter of individual compliance–pressure curves in each group. This is illustrated by the cross-sectional compliance values measured in each hypertensive patient and normotensive subject at pressures of 100 and 120 mm Hg, i.e., at pressures common to both populations (Figure 4). Similarly, there was no difference in the cross-sectional distensibility–pressure curves between the two groups (Figure 3, lower panel). The stiffness index β defined by Kawasaki et al,[9] which compensates for the nonlinear relation between the elastic modulus and the diameter, was also comparable in hypertensive patients (42.89±6.94) and normotensive subjects (40.37±3.10).

Animal Experiments

Because the SHR exhibited quite severe hypertension, their pressures hardly overlapped with those of normotensive rats (Table 2). Figure 5 illustrates the diameter–pressure relations determined in the two groups of animals. The curve obtained in hypertensive rats appeared to be the direct continuation of that established in normotensive animals. Figure 6 depicts the compliance– and distensibility–pressure curves. There exists a slight difference between hypertensive and normotensive animals in the small range of near overlapping pressures. If anything, cross-sectional arterial compliance and distensibility are higher in SHR than in WKY rats.

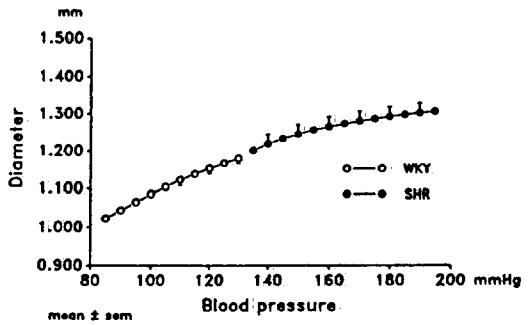

FIGURE 5. *Line plot shows relation between blood pressure and internal diameter carotid artery in spontaneously hypertensive rats (SHR) and normotensive Wistar-Kyoto (WKY) rats.*

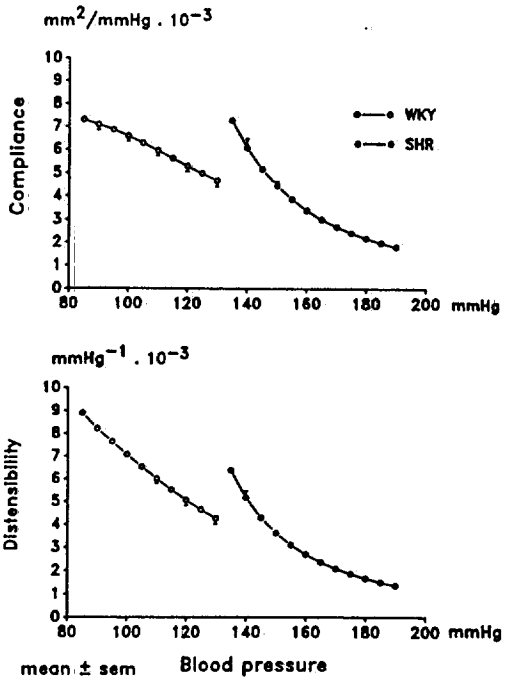

FIGURE 6. *Line plots show cross-sectional compliance–pressure curves* (upper panel) *and cross-sectional distensibility–pressure curves* (lower panel) *established in spontaneously hypertensive rats (SHR) and normotensive Wistar-Kyoto (WKY) rats.*

Discussion

In the present study, cross-sectional compliance of the radial artery was measured noninvasively in newly diagnosed, untreated hypertensive patients and age- and sex-matched normotensive control subjects. The measured compliance could be related to the simultaneously determined finger blood pressure using a recently developed technique. The hypertensive patients exhibited a forearm arterial cross-sectional compliance–pressure curve similar to that of the normotensive control subjects. The same was true for the carotid artery diameter–pressure relation established in hypertensive rats, which did not differ from that observed in normotensive controls. In this latter experiment, diameter and blood pressure variations were both recorded at the carotid arteries, thus eliminating the need for correction of the diameter–pressure curve phase shift, which we face in the clinical situation because the sites for arterial diameter and blood pressure measurements differ.[18]

The present data obtained in humans as well as in rats confirm the nonlinear internal diameter–pressure relation (and thus nonlinear cross-sectional compliance– and distensibility–pressure relation) that has been described previously for various muscular and elastic arteries.[14–16] The results demonstrate a considerable scatter of individual compliance–pressure curves in the normal and the hypertensive subjects. The radial artery is a medium-sized muscular artery. This is important since the physical characteristics of the arterial wall in predominantly muscular arteries have been shown to be much more variable than in elastic arteries because of a

greater influence of vasoactive stimuli.[9] Arteries with less physiological variability of the mechanical characteristics might exhibit more important changes resulting from modifications of their environment[28] such as hypertension or drug-related modifications. For this reason and because of their major clinical implications, elastic arteries with a smaller quantity of smooth muscle cells, e.g., carotid and femoral arteries, could appear more appropriate candidates. At present, in human subjects there is yet a strong limitation to continuous and accurate noninvasive monitoring of blood pressure in these arteries.

When compared at their respective different mean arterial blood pressures, hypertensive patients exhibit a lower arterial compliance than normotensive control subjects.[8,11,12,29,30] This is inherent to the compliance–pressure relation, as shown in Figure 1C, with increasing pressure compliance decreases or, in other words, the arterial wall becomes stiffer. Because of this relation, arterial compliance should therefore not be given as a single independent variable.

It is possible to calculate arterial cross-sectional compliance based on the Bramwell and Hill equation[31] by using pulse wave velocity as an index of arterial stiffness and measuring intra-arterial blood pressure. With this approach, taking blood pressure into account as a variable, other investigators have actually come to conclusions similar to those presented in this report,[6,14,15] i.e., there is no difference in forearm arterial compliance between hypertensive and normotensive subjects.

As already stressed, mechanical properties of muscular arteries such as the radial artery do not necessarily reflect the behavior of proximal elastic arteries. This may be particularly true in hypertensive patients. Indeed, the large elastic arteries are the preferential site of the deleterious effects of high blood pressure, leading to an increase in cardiovascular morbidity and mortality.[32–34] Therefore, further comparative compliance measurements were needed in elastic arteries. The observations made in rats, in contrast to those obtained in humans, concerned the elastic carotid arteries. Furthermore, the hypertensive animals exhibited a quite severe blood pressure elevation compared with the normotensive controls without any overlap between the groups. Notwithstanding, in these experimental animals, no difference in the diameter–pressure relation could be detected between the normotensive and hypertensive groups. At near-matching blood pressures, the arterial compliance and distensibility were actually higher in the hypertensive than in the normotensive rats. These findings are in good agreement with the results regarding arterial distensibility in stroke-prone SHR.[35] This is certainly not yet understood. Unlike normotensive and hypertensive subjects, who are members of a continuous blood pressure distribution, WKY rats and SHR belong to different populations with distinct blood pressure distributions. It may therefore not be surprising if some small differences exist between the two strains in terms of arterial compliance and distensibility.

The results of the present investigations, with use of a novel, high-precision echo-tracking device, provide no evidence for a difference in arterial cross-sectional compliance or distensibility in the forearm between newly diagnosed hypertensive and normotensive subjects as well as between young hypertensive and normotensive rats at the carotid artery. These results suggest that mechanical alterations of these conduit vessels are not causal in the development of hypertension.

References

1. Mulvany MJ: Determinants of vascular hemodynamic characteristics. *Hypertension* 1984;6(suppl III):III-13–III-18
2. Lever AF: Slow pressor mechanisms in hypertension: A role for hypertrophy of resistance vessels? *J Hypertens* 1986;5:514–524
3. Olivetti G, Melissari M, Marchetti G, Anversa P: Quantitative structural changes of the rat thoracic aorta in early spontaneous hypertension. *Circ Res* 1982;51:19–26
4. Folkow B: The hemodynamic consequence of adaptative structural changes of the resistance vessels in hypertension. *Clin Sci* 1971;41: 1–12
5. Folkow B: Physiological aspects of primary hypertension. *Physiol Rev* 1982;62:347–351
6. Gribbin B, Pickering TG, Sleight P: Arterial distensibility in normal and hypertensive man. *Clin Sci* 1979;56:413–417
7. Safar ME, Peronneau PA, Levenson JA, Toto-Moukouo JA, Simon AC: Pulsed Doppler: Diameter, blood flow velocity and volumic flow of the brachial artery in sustained essential hypertension. *Circulation* 1981;63:393–400
8. Simon AC, Laurent S, Levenson JA, Bouthier JA, Safar ME: Estimation of forearm arterial compliance in normal and hypertensive men from simultaneous pressure and flow measurements in the brachial artery, using a pulsed Doppler device and a first-order arterial model during diastole. *Cardiovasc Res* 1983;17:331–338
9. Kawasaki T, Sasayama S, Yagi SI, Asakawa T, Hirai T: Noninvasive assessment of the age related changes in stiffness of major branches of human arteries. *Cardiovasc Res* 1987;21:678–687
10. Goldwyn RM, Watt TB: Arterial pressure pulse contour analysis via a mathematical model for clinical quantification of human vascular properties. *IEEE Trans Biomed Eng* 1967;14:11–17
11. Watt TB, Burrus CS: Arterial pressure contour analysis for estimating human vascular properties. *J Appl Physiol* 1976;40:171–176
12. Simon AC, Safar ME, Levenson JA, Kheder AM, Levy BI: Systolic hypertension: Hemodynamic mechanism and choice of antihypertensive treatment. *Am J Cardiol* 1979;44:505–511
13. Zobel LF, Finkelstein SM, Carlyle PF, Cohn JN: Pressure pulse contour analysis in determining the effect of vasodilator drugs on vascular hemodynamic impedance in congestive heart failure. *Am Heart J* 1980;100:81–88
14. Smulyan H, Vardan S, Griffiths A, Gribbin B: Forearm arterial distensibility in systolic hypertension. *JAMA* 1984;3:387–393
15. Westling H, Jansson L, Johnson B, Nilsen R: Vasoactive drugs and elastic properties of human arteries in vivo, with special reference to the action of nitroglycerine. *Eur Heart J* 1980;1:445–452
16. Megerman J, Hasson JE, Warnock DF, L'Italien GD, Abbot WM: Noninvasive measurements of nonlinear arterial elasticity. *Am J Physiol* 1986;250:H181–H188
17. Hallock P, Benson IC: Studies on the elastic properties of human isolated aorta. *J Clin Invest* 1937;16:595–602
18. Tardy Y, Meister JJ, Perret F, Brunner HR, Arditi M: Noninvasive estimate of mechanical properties of peripheral arteries from ultrasonic and photoplethysmographic measurements. *Clin Phys Physiol Meas* 1991;12:39–54
19. Perret F, Mooser V, Hayoz D, Tardy Y, Meister JJ, Etienne JD, Farine PA, Marazzi A, Burnier M, Nussberger J, Waeber B, Brunner HR: Evaluation of arterial compliance-pressure curves: Effect of antihypertensive drugs. *Hypertension* 1991;18(suppl II): II-77–II-83
20. Penaz J: Photoelectric measurement of blood pressure, volume and flow in the finger, in: *Digest of the 10th International Conference on Medical and Biological Engineering*. Dresden, 1973, pp 104
21. Wesseling KH, Settels JJ, De Wit B: The measurement of continuous finger arterial pressure non-invasively in stationary subjects, in: *Biological and Psychological Factors in Cardiovascular Disease*. Berlin, Springer Verlag, 1986, pp 355–375
22. Parati G, Casadei R, Groppelli A, Di Rienzo M, Mancia G: Comparison of finger and intra-arterial blood pressure monitoring at rest and during laboratory testing. *Hypertension* 1989;13:647–655
23. Burgener E, Mooser V, Waeber B, Porchet M, Gardaz JP, Nussberger J, Brunner HR: Calcium entry blockade attenuates the acute blood pressure rise induced by cigarette smoking. *J Cardiovasc Pharmacol* 1988;12(suppl 6):126–130

24. Imholz BPM, Settels JJ, Van der Meiracker AH, Weeseling KH, Wieling W: Non-invasive continuous finger blood pressure measurement during orthostatic stress compared to intra-arterial pressure. *Cardiovasc Res* 1990;24:214–221
25. Langewouters GJ, Wesseling KH, Godehard WJA: The static elastic properties of 45 human thoracic and 20 abdominal aortas in vitro and the parameters of a new model. *J Biomechanics* 1984;17:425–435
26. Peterson LH, Jensen RE, Parnell J: Mechanical properties of arteries in vivo. *Circ Res* 1960;8:622–639
27. Flückiger JP, Gremaud G, Waeber B, Kulik A, Ichino A, Nussberger J, Brunner HR: Measurement of sympathetic nerve activity in the unanesthetized rat. *J Appl Physiol* 1989;67:250–255
28. Kontis S, Gosling RG: On-line Doppler ultrasound measurement of aortic compliance and its repeatability in normal subjects. *Clin Phys Physiol Meas* 1989;10:127–135
29. Ventura H, Messerli FH, Oigman W, Suarez DH, Dreslinski GR, Dunn FG, Reisin E, Frohlich ED: Impaired systemic arterial compliance in borderline hypertension. *Am Heart J* 1984;108: 132–136
30. Collins VR, Finkelstein SM, Cohn JN: Evaluation of a pulse contour technique for measuring arterial elasticity. (abstract) *Circulation* 1980;62(suppl II):II-1120
31. Bramwell JC, Hill AV: The velocity of the pulse wave in man. *Proc Soc Exp Biol Med* 1922;93:298–306
32. Pickering GW: *High Blood Pressure.* New York, Grune & Stratton, Inc, 1968, p 291
33. Kannel WB, Dawber TR, McGee DL: Perspectives on systolic hypertension: The Framingham study. *Circulation* 1980;6: 1179–1182
34. O'Rourke MF: *Arterial Function in Health and Disease.* Churchill Livingstone, Inc, Edinburgh, Scotland, 1982, p 185
35. Heistad DD, Lopez JAG, Baumbach GL: Hemodynamic determinant of vascular changes in hypertension and atherosclerosis. *Hypertension* 1991;17(suppl III):III-7–III-11

Endothelial Function in Chronic Congestive Heart Failure

Helmut Drexler, MD, Daniel Hayoz, MD, Thomas Münzel, MD, Burckhardt Hornig, MD, Hanjörg Just, MD, Hans R. Brunner, MD, and Robert Zelis, MD

There is evidence that the endothelium plays an important role in the control of human vascular tone by releasing endothelium-derived nitric oxide. The hypothesis that an impairment of this mechanism is involved in the increased peripheral vasoconstriction of patients with chronic congestive heart failure (CHF) was tested. Acetylcholine and N-monomethyl-L-arginine (L-NMMA), a specific inhibitor of nitric oxide synthesis from L-arginine, were infused in the brachial artery of healthy volunteer subjects (controls) and patients with severe CHF. The radial artery diameter was determined by a high-precision A-mode ultrasound device, using a 10 MHz probe. Forearm blood flow was calculated from vessel diameter and blood flow velocity measured simultaneously by Doppler. The blood flow response to acetylcholine was blunted in patients with CHF compared with that in control subjects. In contrast, the decrease in blood flow induced by L-NMMA was exaggerated in CHF, and the blood flow response to nitroglycerin was preserved. The changes in radial artery diameter induced by acetylcholine and L-NMMA were not significant in control subjects and CHF patients, but dilation of the radial artery by nitroglycerin was significantly reduced in CHF. The results demonstrate an impaired endothelium-dependent dilation of forearm resistance vessels in CHF, suggesting a reduced release of nitric oxide on stimulation. In contrast, the basal release of nitric oxide from endothelium of forearm resistance vessels is preserved or may even be enhanced, and may play an important compensatory role in chronic CHF by antagonizing neurohumoral vasoconstrictor forces in CHF.

(Am J Cardiol 1992;69:1596–1601)

Systemic vasoconstriction is a hallmark of advanced chronic congestive heart failure (CHF) and appears to be due to several compensatory mechanisms such as neural, hormonal and local vascular factors.[1] Whereas the neurohumoral factors involved in this impaired vasodilation were studied extensively in the past, the impact of local factors regulating peripheral vasomotor tone and tissue perfusion in CHF are poorly defined. Experimental data suggest that CHF impairs endothelial-dependent dilation of femoral arteries and hind-limb resistance vessels in response to acetylcholine.[2,3] Thus, depression of endothelium-dependent vasodilation may represent 1 local mechanism involved in the impaired metabolic vasodilation in patients with CHF.

The release of endothelium-derived relaxing factor in humans is stimulated by acetylcholine.[4] Basal release of nitric oxide that accounts for the biologic activity of endothelium-derived relaxing factor[5] has been shown to contribute to the control of regional blood flow in humans[6] by using N-monomethyl-L-arginine (L-NMMA), a selective inhibitor of nitric oxide from L-arginine.[7] In the absence of marked vasoconstriction of conduit vessels, changes in blood flow indicate the response of resistance vessels. However, both acetylcholine and L-NMMA have been shown to markedly constrict diseased human conduit arteries, thereby limiting blood flow.[8–10] Therefore, the differential effects of these agents on conduit versus resistance vessels in patients with endothelial dysfunction cannot be assessed by simply measuring blood flow. To identify the endothelium-dependent vasomotor response of large forearm conduit versus small resistance vessels we used a novel ultrasound device to accurately determine forearm arterial diameter, measuring blood flow velocity simultaneously in this vessel. By this approach, the effects of intraarterial infusion of acetylcholine, L-NMMA and nitroglycerin on forearm conduit and resistance vessels were examined in patients with chronic CHF and in age-matched healthy volunteers.

METHODS

Subjects: The control group in this study included 9 normal subjects (3 men and 6 women, aged 30 to 63 years). Subjects with systemic hypertension, diabetes mellitus, hypercholesterolemia, and hematologic, renal and hepatic dysfunction were excluded by a careful history, physical examination, electrocardiogram and laboratory analysis. Nine patients with chronic CHF in New York Heart Association functional class III (Table I) with clinical, radiologic and echocardiographic signs of cardiomegaly and CHF despite treatment with digi-

From the Medizinische Klinik III, University of Freiburg, Freiburg, Germany, and Centre Hospital Universitaire Vaudois, Lausanne, Switzerland. This study was supported in part by the Deutsche Forschungsgemeinschaft (DFG, Dr 148/5-1), and the Swiss Association of Cigarette Manufacturers. Manuscript received November 26, 1991; revised manuscript received and accepted February 24, 1992.

Address for reprints: Helmut Drexler, MD, Medizinische Klinik III, Hugstetterstr. 55, 7800 Freiburg, Germany.

alis, converting enzyme inhibitors and diuretics were studied. In 3 patients, the etiology of CHF was coronary artery disease, and in 5 it was idiopathic dilated cardiomyopathy. One patient had severe left ventricular dysfunction and cardiomegaly after mitral valve replacement, but normal coronary arteries. No patient had history or clinical evidence of hypertension, diabetes, claudication or peripheral arterial occlusive disease. Increased serum and low-density lipoprotein cholesterol levels were found in 3 patients, whereas these levels were within normal range (low-density lipoprotein cholesterol <140 mg/dl) in the remaining 6. No control subject was receiving medication. Patients with CHF were treated with diuretics, converting enzyme inhibitors and digoxin (n = 7), but none received other vasoactive therapy. Digoxin and captopril were stopped 24 hours (48 hours for enalapril) and diuretics ≥12 hours before beginning measurements. Alcohol, caffeine and cigarettes were all prohibited within 8 hours of the study. Written informed consent was obtained from all subjects, and the protocol was approved by the ethical committee of the University of Freiburg.

Determination of arterial diameter: To measure the diameter of conduit arteries we used a recently developed high-resolution A-mode ultrasonic echo-tracking device (Asulab, Neuchatel, Switzerland) that allows measurements of the arterial diameter with a resolution of ±2.5 μm.[11,12] Recordings of the arterial diameter (8 cm proximal to wrist) were obtained with a focalized 10 MHz transducer positioned perpendicularly to the vessel by Doppler guidance without direct skin contact, using ultrasonic gel as a transmitting medium.[12]

Determination of blood flow velocity: Forearm blood flow velocity was measured by Duplex sonography imaging (5 MHz Doppler and 7.5 MHz 2-dimensional probe, ATL, Ultramark 8) just distal to the 10 MHz device that was used for diameter measurements. After adjusting the Doppler sample to the width of the vessel, mean blood flow velocity was determined by means of standard software of the Duplex scanner after angle correction for the Doppler ultrasonic beam. Arterial blood flow (ml/min) at mid-forearm level was calculated as the product of blood flow velocity and arterial cross-sectional area, obtained from the arterial diameter (measured simultaneously at the time of flow velocity recording) assuming a circular vessel area. Forearm vascular resistance was calculated from arterial pressure (determined invasively; see later) and blood flow. Blood flow velocity was obtained as a mean of 5 consecutive beats (15 beats in 2 patients with atrial fibrillation). Baseline values were calculated from 2 sets of measurements.

Experimental protocol: After insertion of a polyethylene catheter in a brachial artery, blood flow velocity was recorded continuously until stable baseline conditions were obtained (approximately 30 minutes), and arterial blood pressure was measured at baseline and at the end of each drug infusion. Increasing dosages of acetylcholine (10^{-8}, 10^{-7} and 5×10^{-6} M/min) (Dispersa Company, Germering, Germany) were infused in the brachial artery at a rate of 1.7 ml/min, lasting 5 minutes for each concentration. After a second control period to reestablish basal conditions, L-NMMA (Calbiochem, Lucerne, Switzerland) was infused in 6 subjects of both groups over 5 minutes at a dose of 12 nmol/min (infusion rate 1.7 ml/min). The solution was passed through a FlowPore D26 bacterial filter immediately before use. The selection of this dose was based on the report of Vallance et al[6] and on our observations in 5 normal subjects and 3 patients with CHF. Because 4 nmol/min (as used by Vallance et al)[6] did not consistently attenuate the arteriolar dilator response to acetylcholine in our preliminary studies, a threefold higher dose was used. This reduced the blood flow response to acetylcholine by 42 ± 6% compared with that at control, which was consistent with the findings of Vallance et al.[6] To distinguish abnormalities in endothelial function from those of vascular smooth muscle, all subjects received a final intraarterial infusion of nitroglycerin at 5 nmol/min over 5 minutes (rate 1.7 ml/min). Blood flow and diameter data reported for acetylcholine, L-NMMA and nitroglycerin represent the measurements during the last minute of infusion. Radial artery blood flow depends on the variable blood flow distribution pattern of the radial artery. Thus, the relative changes by different interventions should be emphasized, rather than the comparison of absolute values.

Statistical analysis: All data are expressed as mean ± SEM. Statistical comparisons of vessel diameter and blood flow before and during administration of drugs were obtained by analysis of variance for repeated measures, followed by the Student-Newman Keuls test. The statistical significance of differences between groups was determined by Student's *t* test. A p value <0.05 was considered statistically significant.

TABLE I Characteristics of the Study Cohort

	Normal	CHF
Sex (men/women)	3/6	7/2
Age	52 ± 4	58 ± 4
LV ejection fraction (%)	—	30 ± 3
Peak oxygen consumption (ml/min/kg)	—	15 ± 1
Hemoglobin (g/dl)	14 ± 0.4	15 ± 0.5
Serum sodium (mmol/L)	140 ± 0.9	141 ± 0.7
Resting heart rate (beats/min)	71 ± 6	81 ± 6
Body height (cm)	168 ± 3	169 ± 2
Body weight (kg)	68 ± 4	66 ± 3
Resting forearm blood flow (ml/min)	30 ± 6	27 ± 5
Resting forearm vascular resistance (mm Hg/ml/min)	5 ± 1	6 ± 3
Mean blood pressure	96 ± 4	88 ± 3

CHF = congestive heart failure; LV = left ventricular.

RESULTS

Patient characteristics: Baseline characteristics of control subjects and patients with CHF were similar for all variables (Table I). Vascular responses to the various interventions did not differ between women and men.

Blood flow response to acetylcholine: Mean blood pressure and heart rate at baseline (before administration of drugs) did not differ between the 2 groups (Table I). The incremental intraarterial infusion of acetylcholine caused no significant changes in systemic blood pressure or heart rate in either group. Forearm blood

flow response to acetylcholine in control subjects and CHF patients is illustrated in Figure 1, demonstrating a blunted arteriolar dilator response in patients compared with that in controls. Similarly, forearm vascular resistance did not change with acetylcholine in CHF patients, but decreased in control subjects (Figures 1 and 2). The acetylcholine-induced change in forearm blood flow was not related to baseline vascular resistance.

Blood flow response to nitroglycerin: To determine whether CHF affects smooth muscle reactivity directly, the vasodilator response to a high dose of nitroglycerin was examined. Intraarterial infusion of nitroglycerin did not significantly change mean blood pressure or heart rate in either group. Forearm blood flow response to nitroglycerin in control subjects and CHF patients did not differ significantly (Figure 1). Similarly, forearm vascular resistance during nitroglycerin was not significantly different in CHF patients and control subjects (Figures 1 and 2). To exclude hypercholesterolemia as a potential confounding factor,[13] a separate analysis was performed in 6 CHF patients with idiopathic dilated cardiomyopathy and a normal lipid profile (serum cholesterol 196 ± 4 mg%, low-density lipoprotein 124 ± 2 mg% and high-density lipoprotein 60 ± 5 mg%). Blood flow response to acetylcholine was blunted in this subset of patients (baseline 27 ± 7 ml/min and maximal acetylcholine response 34 ± 9 ml/min; p = not significant vs baseline, but $p < 0.05$ vs response to acetylcholine in control subjects), and the blood flow response to nitroglycerin was preserved (68 ± 19 ml/min). In further support of the impaired receptor-mediated arteriolar dilator response, the ratio of blood flow elicited by the maximal dose of acetylcholine and nitroglycerin was calculated in these CHF patients with a normal lipid profile. This ratio serves as a means to differentiate impaired endothelium-dependent dilation and vascular smooth muscle reactivity, and was significantly reduced in CHF patients (control subjects 0.6 ± 0.1 and patients 0.3 ± 0.09; $p < 0.05$).

Blood flow response to N-monomethyl-L-arginine: L-NMMA was administered to 6 control subjects and 6 CHF patients. The comparative percent changes obtained in the 6 subjects of each group receiving all 3 drugs in forearm blood flow and vascular resistance during acetylcholine, L-NMMA and nitroglycerin are illustrated in Figure 2. Forearm blood flow response to acetylcholine was blunted, but the response to nitroglycerin was preserved in CHF patients. L-NMMA de-

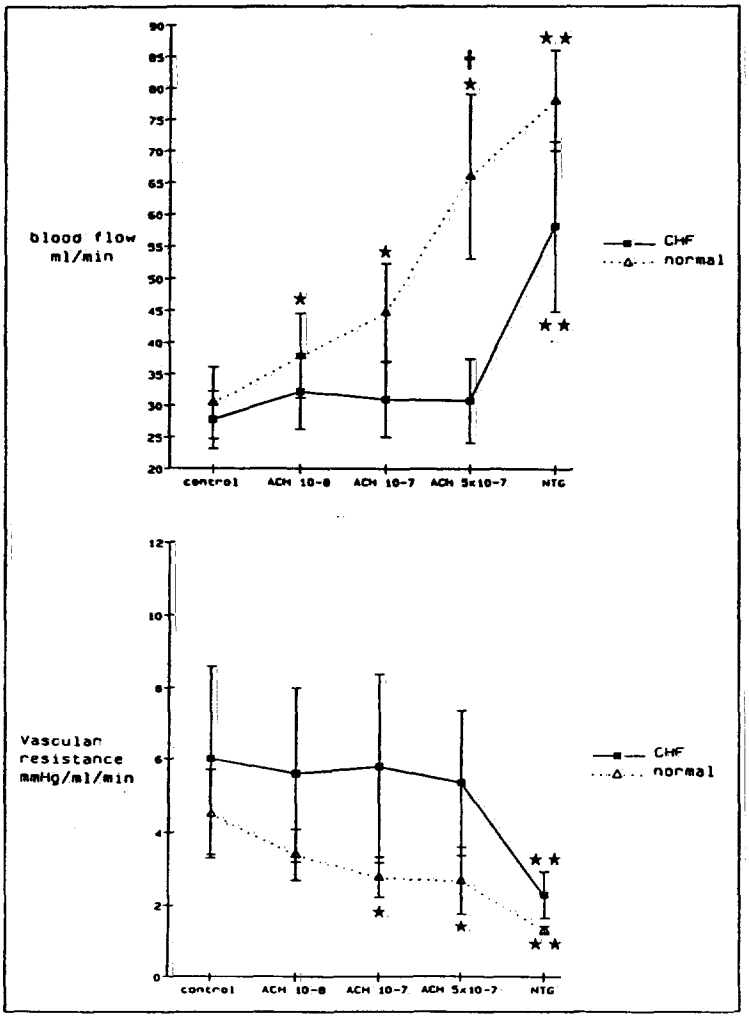

FIGURE 1. Response of forearm blood flow and vascular resistance to increasing doses of acetylcholine (ACH) (10^{-8}, 10^{-7} and 5×10^{-6} M) and to nitroglycerin (NTG) (5 nM/min) infused in brachial artery in control subjects (n = 9) and all patients with severe congestive heart failure (CHF) (n = 9). Data are mean ± SEM. *p <0.01 versus control; **p <0.001 versus control; †p <0.02, control subjects versus heart failure patients.

reased forearm blood flow from 26 ± 6 ml/min at baseline to 14 ± 4 ml/min ($p < 0.01$) in CHF patients. L-NMMA decreased forearm blood flow from 32 ± 9 ml/min at baseline to 20 ± 6 ml/min ($p < 0.05$) in control subjects. The percent change was significantly different in control subjects compared with that in CHF patients (Figure 2). Similarly, the percent change in forearm vascular resistance elicited by L-NMMA was more prominent in CHF patients than in control subjects (Figure 2).

Effects of acetylcholine, N-monomethyl-L-arginine and nitroglycerin on radial diameter: Table II summarizes the data of all patients and those with normal serum lipids. The endothelium-mediated dilation of large conduit vessels (radial artery) in response to acetylcholine was modest and not significant in control subjects and CHF patients. Nitroglycerin dilated radial diameter in both groups. The percent change in diameter elicited by nitroglycerin was more prominent in control subjects ($p < 0.01$) (Table II). Figure 3 depicts the results of 6 subjects in each group receiving all 3 agents. No significant changes in arterial diameters were noted with L-NMMA in either group.

Plasma levels of digoxin were undetectable in 2 CHF patients, and no inverse correlation was found between the plasma levels of digoxin and the endothelium-dependent response to acetylcholine in the remaining 7.

DISCUSSION

The results of our present study led to 2 major conclusions. First, the endothelium-dependent dilation in response to acetylcholine is blunted. Second, the basal release of nitric oxide derived from L-arginine is preserved or may even be enhanced in forearm resistance vessels in CHF patients.

Blood flow response to acetylcholine was substantially inhibited by L-NMMA, indicating that the vascular effect of acetylcholine can (at least in part) be attributed to the release of nitric oxide, which is consistent with previous studies.[4,6] In contrast to the blunted response

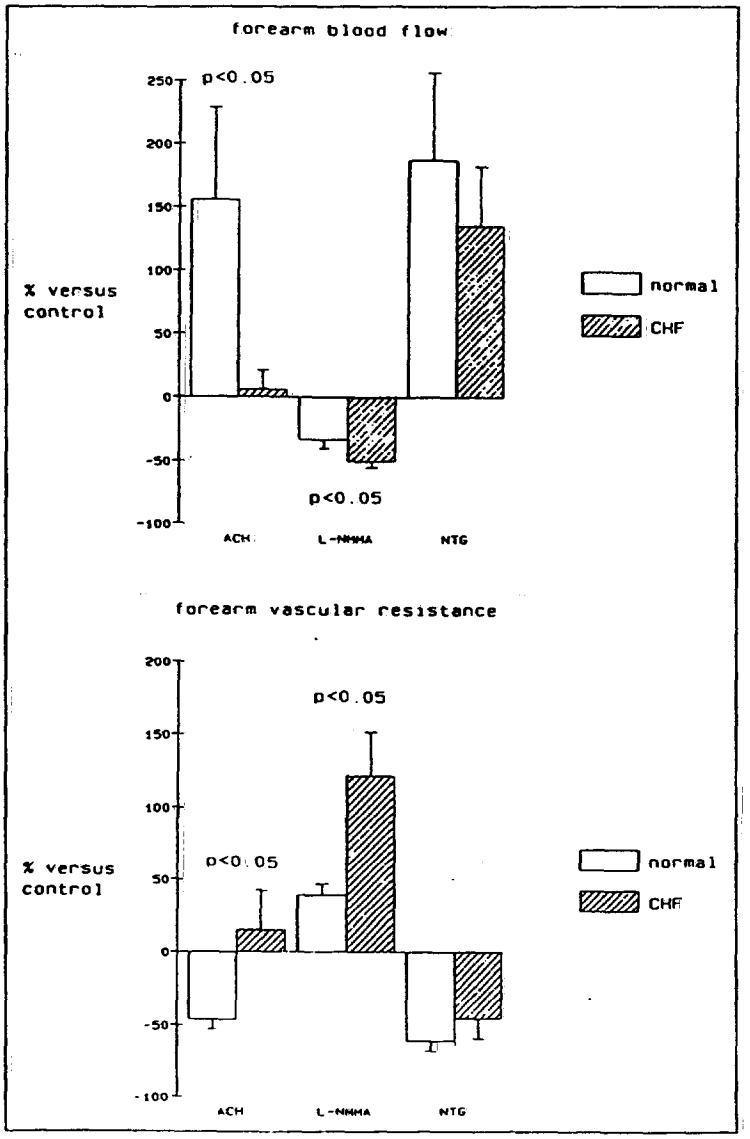

FIGURE 2. Maximal percent change in forearm blood flow and vascular resistance versus control induced by acetylcholine (ACH) (endothelium-dependent), N-monomethyl-L-arginine (L-NMMA) (inhibitor of nitric oxide synthesis) and nitroglycerin (NTG) (endothelium-independent) in control subjects (n = 6) and patients with congestive heart failure (CHF) (n = 6). Data are mean ± SEM. p values denote statistical significance between percent changes in control subjects and patients with heart failure.

TABLE II Effect of Acetylcholine and Nitroglycerin on Arterial Diameter (mm)

	Normal Subjects (n = 9)	CHF (n = 9)	CHF (LDL <140 mg%) (n = 6)
Control	2.81 ± 0.1	2.84 ± 0.19	2.94 ± 0.28
ACH (10^{-8} M)	2.80 ± 0.13	2.85 ± 0.18	2.96 ± 0.26
ACH (10^{-7} M)	2.78 ± 0.13	2.83 ± 0.18	2.96 ± 0.26
ACH (5×10^{-7} M)	2.98 ± 0.12	2.88 ± 0.18	3.00 ± 0.26
NTG	3.50 ± 0.17*	3.23 ± 0.27*	3.38 ± 0.23*
ACH % change	6.7 ± 3.8	2.0 ± 1.4	2.8 ± 2.0
NTG % change	24.3 ± 0.8	14.8 ± 2.9†	16.6 ± 4.0

*p <0.001 versus corresponding control values; †p <0.01 versus normal subjects.
Data are mean ± SEM.
ACH = acetylcholine; CHF = congestive heart failure; LDL = low-density lipoprotein; NTG = nitroglycerin.

to acetylcholine, the increase in forearm blood flow caused by nitroglycerin was similar in CHF patients and control subjects, which is consistent with recent observations.[14] Because the dilator response to both acetylcholine and nitroglycerin involves the activation of the guanylate cyclase system (or a nonspecific effect of opposing constrictor forces), a generalized defect within the guanylate cyclase system cannot account for the present findings. Thus, in CHF patients, the stimulated release of endothelium-derived relaxing factor appears to be attenuated, resulting in an impaired endothelium-dependent relaxation of resistance vessels, which is consistent with a recent report.[15] However, this does not establish a general impairment of endothelial function, and specifically, an impairment of the basal release of nitric oxide synthetized from L-arginine. Indeed, the striking reduction in blood flow in control subjects seen after a high dose of L-NMMA was intensified rather than impaired in CHF patients, which is consistent with preliminary experimental data.[16]

This study suggests a dissociation of stimulated and basal release of nitric oxide in CHF patients (i.e., the basal release of nitric oxide appears to be preserved or may even be enhanced in the peripheral circulation, whereas the stimulated endothelial-dependent dilation exerted by acetylcholine is blunted). The observation that a substantial reduction in forearm blood flow occurred with L-NMMA in the absence of significant changes in diameters of large conductance vessels in normal subjects suggests a preferential release or activity of nitric oxide in forearm resistance vessels as compared with large conductance vessels in humans. Thus, the basal release of nitric oxide appears to have an important role in modulating tissue perfusion at the levels of distal resistance vessels in the forearm and hand, but may be negligible in conduit vessels, or alternatively, its effect on vasomotor tone in large arteries is overridden by other factors.

To establish CHF as a causal factor, other conditions associated with endothelial dysfunction such as atherosclerosis, hypercholesterolemia, hypertension and diabetes[17] should be considered. Therefore, patients with history of hypertension or diabetes were excluded. Moreover, a subgroup analysis confirmed the blunted endothelium-dependent dilation in patients with pure dilated cardiomyopathy, normal lipid profile and absence of coronary artery disease. Furthermore, the drug regimen in the CHF group (although withheld for 12 to 24 hours) may have affected endothelial function. Digoxin has been shown to impair acetylcholine-induced, endothelium-dependent relaxation.[18] However, endothelium-dependent dilation was blunted in 2 patients not receiving digoxin; furthermore, endothelium-dependent responses were not inversely related to plasma levels of digoxin. Thus, although digoxin may have contributed to the impaired endothelium-dependent dilation in some CHF patients it cannot account for the completely blunted effect of acetylcholine in these patients. To the contrary, experimental data suggest that converting enzyme inhibitors improve receptor-mediated endothelium-dependent relaxation,[19] and therefore, any residual effect of converting enzyme inhibition would tend to restore endothelial function. Indeed, it is possible that

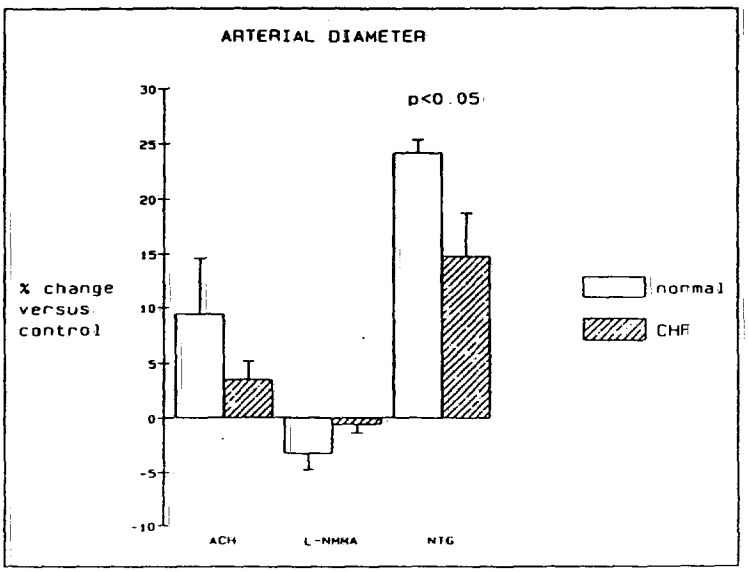

FIGURE 3. Percent change in radial arterial diameters (vs control) produced by acetylcholine (ACH) (5×10^{-7} M/min), N-monomethyl-L-arginine (L-NMMA) and nitroglycerin (NTG) in control subjects (n = 6) and patients with congestive heart failure (CHF) (n = 6). Data are mean ± SEM. p values denote statistical significance between control subjects and patients with heart failure.

long-term withdrawal of converting enzyme inhibitors would reveal a more markedly impaired endothelium-dependent relaxation in response to acetylcholine. Conceivably, specific CHF-related factors may be involved in the endothelial dysfunction of patients with CHF. Chronically reduced blood flow or tumor necrosis factor can decrease the release of endothelium-derived relaxing factor.[20,21] Thus, chronically reduced blood flow associated with limited physical activity may contribute to endothelial dysfunction in CHF patients. Plasma levels of tumor necrosis factor have been shown to be increased in patients with severe CHF[22] and, therefore, may adversely affect the vascular response to acetylcholine.[21]

The clinical feasibility of multiple interventions is limited in these patients, and, therefore, only 1 high dose of L-NMMA was administered in an attempt to achieve a maximal inhibitory effect. Significantly, the effect of L-NMMA on blood flow (−33%), and its ability to inhibit acetylcholine-induced increases in blood flow in normal subjects were similar to the maximal effects with the highest dose of L-NMMA (−32% in blood flow) used by Vallance et al[6] who noted a dose-dependent reduction in forearm blood flow with increasing doses of L-NMMA. This indicates that a high level of inhibition of nitric oxide formation was achieved in the present study by L-NMMA. The higher dose of L-NMMA in this study than that needed by Vallance may be related to the hand circulation that was not excluded to avoid movement artifacts by wrist-cuff inflation during diameter measurements.

Clinical implications: The results suggest that changes in local endothelial function may be involved in the impaired vasodilator response of the peripheral vasculature in CHF patients. The increased basal release of nitric oxide from resistance vessels may help (in a compensatory manner) to maintain adequate tissue perfusion at rest, thereby providing an important local "endogenous" vasodilator system to antagonize neurohumoral vasoconstrictor forces. However, the stimulated release of nitric oxide (i.e., during exercise) may be limited. Indeed, improvement of endothelial function could be 1 potential mechanism by which long-term converting enzyme inhibitors improve blood flow to working muscle during exercise in this setting.[23]

Acknowledgment: We are most grateful to Wolfgang Heiss, MD, for providing the ATL Doppler device for this study.

REFERENCES

1. Zelis R, Flaim SF. Alterations in vasomotor tone in congestive heart failure. *Prog Cardiovasc Dis* 1982;24:437–459.
2. Kaiser L, Spickard RC, Olivier NB. Heart failure depresses endothelium-dependent responses in canine femoral artery. *Am J Physiol* 1989;256: H962–H967.
3. Drexler H, Lu W. Endothelial dysfunction of hindquarter resistance vessels in experimental heart failure. *Am J Physiol* 1992 (in press).
4. Linder L, Kiowski W, Bühler FR, Lüscher TF. Indirect evidence for release of endothelium-derived relaxing factors in human forearm circulation in vivo. Blunted response in essential hypertension. *Circulation* 1990;81:1762–1767.
5. Palmer RMJ, Ferrige AG, Moncada S. Nitric oxide release accounts for the biological activity of endothelium-derived relaxing factor. *Nature* 1987;327: 524–526.
6. Vallance P, Collier J, Moncada S. Effects of endothelium-derived nitric oxide on peripheral arteriolar tone in man. *Lancet* 1989:997–1000.
7. Moncada S, Palmer MRJ, Higgs EA. Biosynthesis of nitric oxide from L-arginine. A pathway for the regulation of cell function and communication. *Biochem Pharmacol* 1989;38:1709–1715.
8. Ludmer PL, Selwyn AP, Shook TL, Wayne RR, Mudge GH, Alexander RW, Ganz P. Paradoxical vasoconstriction induced by acetylcholine in atherosclerotic coronary arteries. *N Engl J Med* 1986;315:1046–1051.
9. Zeiher AM, Drexler H, Wollschläger H, Just H. Modulation of coronary vasomotor tone in humans. Progressive endothelial dysfunction with different early stages of coronary atherosclerosis. *Circulation* 1991;83:391–401.
10. Chester AH, O'Neil GS, Moncada S, Tajkarimi K, Yacoub MH. Low basal and stimulated release of nitric oxide in atherosclerotic epicardial coronary arteries. *Lancet* 1990;336:897–900.
11. Tardy Y, Meister JJ, Perret F, Brunner HR, Arditi M. Non-invasive estimate of the mechanical properties of peripheral arteries from ultrasonic and photoplethysmographic measurements. *Clin Phys Physiol Meas* 1991;12:39–54.
12. Perret F, Mooser V, Hayoz D, Tardy Y, Meister JJ, Etienne JD, Farine PA, Marazzi A, Burnier M, Nussberger J, Waeber B, Brunner HR. Evaluation of arterial compliance–pressure curves: effect of antihypertensive drugs. *Hypertension* 1991;18:II-77–II-83.
13. Creager MA, Cooke JP, Mendelsohn ME, Gallagher SJ, Coleman SM, Loscalzo J, Dzau VJ. Impaired vasodilation of forearm resistance vessels in hypercholesterolemic humans. *J Clin Invest* 1990;86:228–234.
14. Hirooka Y, Takeshita A, Imaizumi T, Suzuki S, Yoshida M, Ando S, Nakamura M. Attenuated forearm vasodilative response to intra-arterial natriuretic peptide in patients with heart failure. *Circulation* 1990;82:147–153.
15. Kubo SH, Rector TS, Bank AJ, Williams RE, Heifetz SM. Endothelium-dependent vasodilation is attenuated in patients with heart failure. *Circulation* 1991;84:1589–1596.
16. Hildebrand FL, Perella MA, Burnett JC. The role of endothelium-derived relaxing factor in experimental congestive heart failure (abstr). *J Am Coll Cardiol* 1991;17:281A.
17. Henderson AH. Endothelium in control. *Br Heart J* 1991;65:116–125.
18. Woolfson RG, Post NL. Effect of ouabain on endothelium-dependent relaxation of human resistance arteries. *Hypertension* 1991;17:619–625.
19. Clozel M, Kuhn H, Hefti F. Effects of angiotensin converting enzyme inhibitors and of hydralazine on endothelial function in hypertensive rats. *Hypertension* 1990;16:532–540.
20. Miller VM, Vanhoutte PM. Enhanced release of endothelium-derived factor(s) by chronic increases in blood flow. *Am J Physiol* 1988;255:H446–H451.
21. Aoki N, Siegfried M, Lefer AM. Anti-EDRF effect of tumor necrosis factor in isolated, perfused cat carotid arteries. *Am J Physiol* 1989;256:H1509–H1512.
22. Levine B, Kalman J, Mayer L, Fillit HM, Packer M. Elevated circulating levels of tumor necrosis factor in severe chronic heart failure. *N Engl J Med* 1990;323:236–241.
23. Drexler H, Banhardt U, Meinertz T, Wollschläger H, Lehmann M, Just H. Contrasting peripheral short-term and long-term effects of converting enzyme inhibition in patients with congestive heart failure. A double-blind, placebo-controlled trial. *Circulation* 1989;79:491–502.

Clin. Phys. Physiol. Meas., 1991, Vol. 12, No. 1, 39–54. Printed in the UK

Non-invasive estimate of the mechanical properties of peripheral arteries from ultrasonic and photoplethysmographic measurements

Y Tardy†, J J Meister†, F Perret‡, H R Brunner‡ and M Arditi§

† Department of Physics, Swiss Federal Institute of Technology, Champs-Courbes 1, CH-1024 Ecublens, Switzerland

‡ Division of Hypertension, University Hospital, Lausanne, Switzerland

§ Asulab SA, Research Laboratories of the SMH, Neuchâtel, Switzerland

Received 17 July 1990, in final form 15 November 1990

Abstract. The non-linear elastic response of arteries implies that their mechanical properties depend strongly on blood pressure. Thus, dynamic measurements of both the diameter and pressure curves over the whole cardiac cycle are necessary to characterise properly the elastic behaviour of an artery. We propose a novel method of estimating these mechanical properties based on the analysis of the arterial diameter against pressure curves derived from ultrasonic and photoplethysmographic measurements. An ultrasonic echo tracking device has been developed that allows continuous recording of the internal diameter of peripheral arteries. It measures the diameter 300 times per second with a resolution of 2.5 μm. This system is linked to a commercially available light-plethysmograph which continuously records the finger arterial pressure (0.25 kPa accuracy). Because of the finite pulse wave velocity, the separation between the diameter and the pressure measurement sites causes a hysteresis to appear in the recorded diameter-pressure curve. Using a model based on haemodynamic considerations, the delay between the diameter variations and the finger arterial pressure is first eliminated. As the pulse wave velocity depends on the pressure, the delay is determined for each pressure value. The relationship between pressure and diameter is then described by a non-linear mathematical expression with three parameters, which best fits the recorded data. The dynamic local behaviour of the vessel is fully characterised by these parameters. Compliance, distensibility and pulse wave velocity can then be calculated at each pressure level. Thus, the mechanical behaviour of peripheral human arteries can now be characterised non-invasively over the pressure range of the whole cardiac cycle . The results obtained *in vivo* on human radial and brachial arteries show that a thorough analysis of the compliance-pressure curves and their modifications (curving, shift) is needed in order to compare two different vessels in a meaningful way.

1. Introduction

One of the biggest unsolved challenges in modern medicine is atherosclerosis and its consequences such as myocardial infarction, stroke and peripheral vascular obstruction. Up to the present time, all available methods for investigating the state of arteries are either too invasive or not accurate enough to be practically useful.

Due to the non-linear elastic and, to some extent, viscoelastic nature of the vessel wall constituents, mechanical properties of arteries vary markedly with blood pressure. The behaviour of a vessel consequently cannot be characterised by a single elastic parameter (such as compliance, elastic modulus or distensibility), but must take into account the pressure dependence.

0143-0815/91/010039 + 16 $02.50

Much work has been done to assess vessel wall properties, but most of the data have been obtained *in vitro* or *in vivo* following surgical exposure of the vessel (King 1946, Peterson *et al* 1960, Bergel 1961, Simon 1971, Histand and Anliker 1973, van Loon *et al* 1977, Ghista *et al* 1978, Busse *et al* 1979, Oddou 1980, Stettler *et al* 1981, Langewouters *et al* 1984, Finkelstein *et al* 1988). Hasson *et al* (1984) have shown that invasive methods clearly affect the elastic behaviour of the artery.

By using an ultrasonic probe and a photoplethysmograph to measure the diameter and the pressure, respectively, it is possible to avoid these problems. This prompted us to develop a new method which makes it possible to obtain, non-invasively and continuously, the internal diameter and pressure of forearm arteries (patent pending). This allows suitable elastic parameters for vessel characterisation to be calculated.

Arndt *et al* (1968) first reported completely non-invasive measurement of arterial diameter by means of a pulsed ultrasound technique. The echoes backscattered by the arterial walls were tracked by a gated threshold detector. Later, Hokanson *et al* (1972) developed a phase locked tracking device which permitted the selection and tracking of a particular zero crossing within the vessel wall echoes. Recent improvements of the original technique have been proposed: digital tracking (Groves *et al* 1982), prior inverse filtering (Eriksen 1987), coupling with B-mode imaging (e.g. Imura *et al* 1986). More recently Hoeks *et al* (1990) reported a different approach which consists of selecting and memorising an M-line perpendicular to the vessel from a B-mode two-dimensional image. Then, performing off-line Doppler processing in selected data windows coinciding with the vessel walls, it permits the sample volumes to track the vessel walls based on the assessed displacement.

In order to relate the internal diameter to arterial pressure, an instantaneous and continuous pressure measurement is needed. As far as we know, the only non-invasive device available which meets all these requirements is a photoplethysmograph based on a method described by Penaz in 1973 (see below).

The body of this paper will deal with the method developed to derive and process the diameter-pressure curves of forearm arteries from the non-invasive measurements of the diameter (ultrasonic echo tracking) and the intraluminal pressure (photoplethysmography at the finger level). The method is then applied to brachial and radial arteries and discussed from a haemodynamic point of view.

Our method promises to be a very useful tool to investigate the arterial system of healthy subjects or patients with various vascular diseases, and to assess the effects of pharmacological therapies.

2. Material and method

2.1. Equipment

An ultrasonic echo tracking device has been developed in collaboration with Asulab SA. Short ultrasonic pulses of 10 MHz centre frequency are generated and detected by means of a strongly focused piezoelectric transducer (6.5 mm diameter, 11 mm focal length). The −10 dB beam width is 0.3 mm at the focus and the depth of field at −10 dB is 5 mm. A stereotaxic arm with micrometric screws allows accurate positioning of the transducer perpendicularly to the vessel. The ultrasonic echoes reflected by the interfaces between blood and both inner anterior and posterior arterial walls are identified on an RF mode display and automatically tracked (figure 1). A time interval averaging technique is used to enhance the initial resolution defined by a 75 MHz clock (corresponding to a spatial depth of 10 μm). Averaging is performed over a number (16 in our case) of time-of-flight

measurements, acquired at a 5 kHz rate. Provided this frequency is asynchronous with the instrument clock, the resolution of the measurement increases with the square root of the number of independent time intervals acquired (Hewlett Packard). The theoretical resolution on the diameter evolution is thus 2.5 μm. This has been confirmed on reference targets in the laboratory.

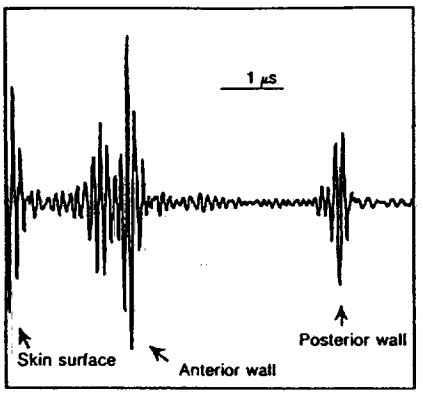

Figure 1. Typical RF echo signal from the anterior and posterior arterial walls.

A commercially available photoplethysmograph (Finapres™) is linked to the system. This apparatus performs non-invasive continuous recording of the pressure at the finger level with a resolution of 0.25 kPa (2 mmHg). With a maximal rate of pressure rise of more than 488 kPa s^{-1} (3600 mmHg s^{-1}), it accurately reproduces the pressure variations. Further description of this instrument is given by Wesseling *et al* (1982 and 1985).

A personal computer performs data acquisition and processing (wall position, arterial pressure) over 300 times per second. A typical recording of the brachial artery diameter is shown in figure 2(*a*), with the corresponding finger arterial pressure shown in figure 2(*b*).

The reproducibility of the measurement of the radial artery diameter has been assessed by Mooser *et al* (1988). These authors have carried out 7 separate determinations of the arterial diameter in 10 subjects over a 4 h period, repositioning the transducer before each reading. In a given individual, the standard error from the mean diastolic diameter varies between 30 μm and 200 μm. These variations include both the actual fluctuations in arterial diameter during the day and the potential positioning error.

The high reproducibility of the diameter-pressure curve measurement has also been reported (Perret *et al* 1990b), where 10 volunteers were measured during two sessions which took place at the same time of the day within a nine day period. The mean compliance-pressure curves obtained for the two sessions could be superimposed.

2.2. Material

A group of five healthy male subjects aged 21 to 30 was used to demonstrate the developments presented here. Measurements were performed at Lausanne University Hospital. For each volunteer, 3 to 5 measurements were recorded on the radial artery at the wrist and on the brachial artery at the elbow.

2.3. Method

Each subject was studied in the supine position after resting at least 30 min, with the right forearm extended and secured comfortably on a splint. The plethysmograph was positioned

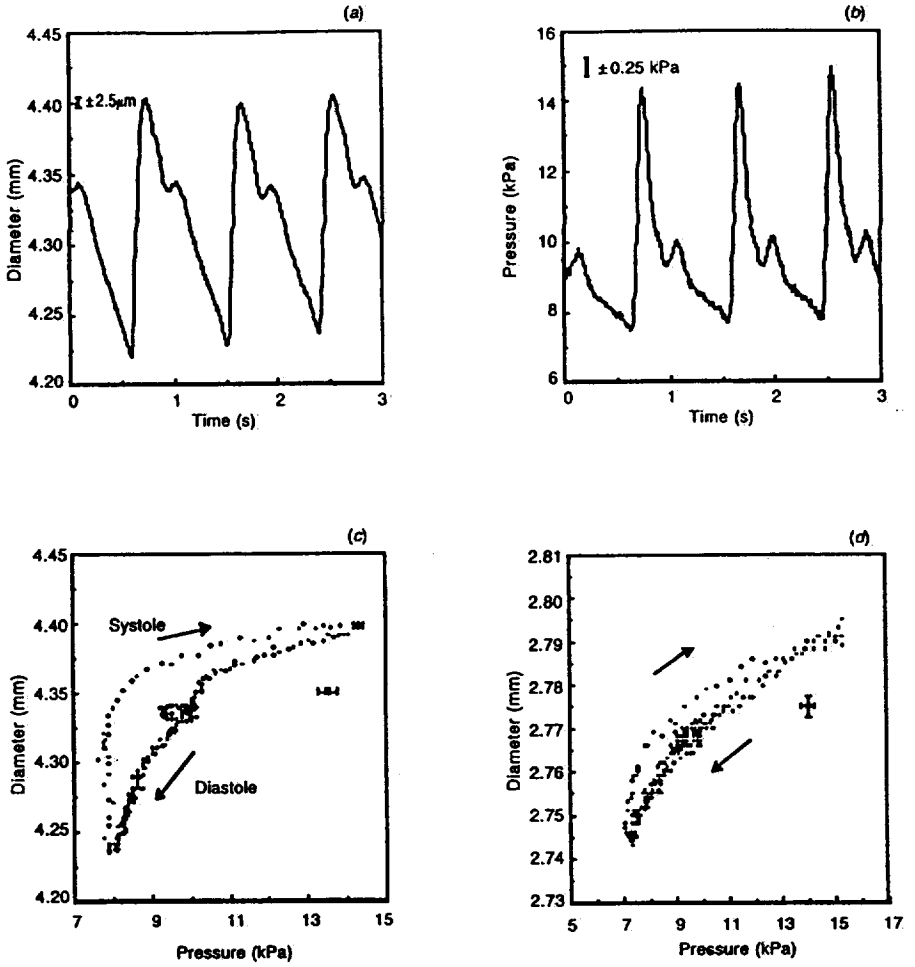

Figure 2. (*a*) Typical recording of the internal diameter changes in the brachial artery. The vertical bar indicates the measurement error of the diameter variations. (*b*) Simultaneous pressure signal recorded by the Finapres. The vertical bar indicates the measurement error of the pressure. (*c*) Diameter-pressure curve obtained by combining the diameter and pressure recordings from (*a*) and (*b*). (*d*) Typical diameter-pressure relationship obtained when the diameter is recorded on the radial artery. All figures, subject no. 3.

on the middle finger. A gel was applied between the transducer and the skin surface, and care was taken not to exert any pressure on the skin. Stereo Doppler mode was used as a help in positioning the probe perpendicularly to the arterial axis. After switching the transducer to pulse-echo, both echoes from the inner arterial wall were visualised and their amplitude maximised by fine positioning using the micrometric screws. The small width of the ultrasonic beam and this positioning technique ensure that it is really the full inner diameter that is measured and not a chord. Note that a deviation of 5° from the perpendicular to the vessel only produces 0.5% error on the diameter.

3. Diameter-pressure relationship

3.1. Background

Due to the complex polyphasic structure of their walls, blood vessels exhibit a marked non-linear viscoelastic behaviour. The elastic modulus of these vessels thus depends strongly on the strain state and therefore on the intraluminal pressure and exhibits frequency dependent properties.

Much work has been reported to determine the relationship between the diameter (or the cross-section) of arteries and the arterial pressure, assuming purely elastic wall material. Most of the reported models are deduced from experimental data (van Loon *et al* 1977, Meister 1983, Langewouters *et al* 1984, Powalowski and Pensko 1985). Other relationships have been obtained within the theory of elasticity, assuming an exponential stress-strain behaviour of the arterial wall material (Simon 1971, Ghista *et al* 1978). A more complex approach based on statistical mechanics and taking into account the polyphasic and elastomeric nature of the vessel wall has also been reported (King 1946, Niederer 1974, Oddou 1980).

Some authors have reported diameter-pressure measurements performed at the same site (e.g. Milnor 1989). Their data were obtained from *in vitro* or invasive *in vivo* experiments in which the diameter was given by displacement gauges directly attached to the vessel wall, and the pressure by intraluminal sensor. Their result showed the diameter lagging with respect to the pressure, with a phase angle increasing sharply between 0 Hz and 2 Hz, where it was about 0.1 radian. Above 2 Hz it increases only slightly with frequency (Bergel 1961, Anliker *et al* 1968). Viscoelastic models that match the measured data over a sufficiently wide range of frequencies are scarce and involve complex pressure-area relationships (Holenstein *et al* 1980).

By measuring simultaneously the diameter and the pressure of an artery, assuming negligible viscoelasticity, we were then able to choose a model which best fits the diameter-pressure curve obtained for each subjet studied. Using the least-square method to compare different relationships, it appears that the function proposed by Langewouters *et al* (1984) approximates our data best (see figure 3(*b*) below). This is shown in table 1, where the

Table 1. Comparison between different diameter-pressure relationships proposed in the literature: (1) Langewouters *et al* 1984, (2) van Loon *et al* 1977, (3) Vander Werff 1974, (4) Powalowski and Pensko 1985, (5) Kivity and Collins 1974 (6) Hayashi *et al* 1980. The residual mean square of the regression is calculated for one measurement of each five healthy subjects. The mean value for the group is reported in the last column.

Fitted model	Residual Mean Square × 10^{-6}					
	Subject no.					Mean
	1	2	3	4	5	
(1) $S = a_1\left[\frac{\pi}{2} + \tan^{-1}\left(\frac{p - a_2}{a_3}\right)\right]$	4.7	3.3	2.3	2.2	5.1	3.5
(2) $S = a_1 + a_2[1 - \exp(a_3.p)]$	4.3	3.5	2.7	3.1	5.4	3.8
(3) $S = a_1\left[1 + tgh\left(\frac{p}{a_2}\right)\right]$	9.2	4.7	9.9	6.3	5.6	7.1
(4) $p = a_1.\exp(a_2.S)$	9.1	8.0	6.2	5.7	15.4	8.9
(5) $p = a_1.S^5 + \frac{a_2}{S}$	5.7	7.2	11.9	5.1	16.5	9.3
(6) $p = a_1.\exp(a_2.D)$	18.3	9.1	18.3	13.1	16.4	15.0

residual mean square of the regression for different models is reported. The comparison is performed on one diameter pressure measurement of each five subjects including the hysteresis elimination procedure described below. The a_i denote the unknown parameters of the models. The residual mean square is the sum of squares of deviations divided by the number of data points, with the least-square estimates substituted for the parameters.

The model chosen expresses the relationship between the pressure p and the cross-sectional area S by using an arctangent function and three optimal-fit parameters:

$$S = \alpha\left[\frac{\pi}{2} + \tan^{-1}\left(\frac{p-\beta}{\gamma}\right)\right], \quad S = \frac{\pi d^2}{4} \tag{1}$$

where d is the arterial internal diameter assuming a cylindrical vessel. The three parameters α, β and γ fully characterise the diameter-pressure curve. They have, however, no direct physical meaning since they are not linked to any characteristic value of the wall material.

Figures 2(*c*) and 2(*d*) show typical diameter-pressure curves obtained respectively on the brachial and radial arteries. These plots confirm the marked non-linear behaviour of the artery; the vessel wall gets stiffer with increasing strain. In addition, we observe a hysteresis between the systolic and the diastolic parts of the cardiac cycle. Both the finite distance between the two sites of measurement and viscoelasticity of the wall could cause a hysteresis to appear. The observed hysteresis shows the pressure lagging with respect to the diameter. If viscoelastic properties were predominant (pressure leading diameter), the hysteresis would be in the opposite direction. We conclude that the hysteresis is mainly due to the delayed pressure at the finger compared to the forearm diameter variation. Since the separation between the pressure and diameter measurement sites is smaller for the radial artery than for the brachial artery, the observed delay and hysteresis are correspondingly smaller also (figures 2(*c*) and 2(*d*)). The loop observed during the diastolic phase reflects the dicrotic notch signal.

Assuming negligible viscoelasticity, the hysteresis is thus an experimental artefact that has to be corrected before calculating the mechanical properties of the artery. We have therefore developed a model based on haemodynamic considerations, which allows us to suppress the hysteresis and to build up a diameter-pressure curve accounting for the fact that the diameter and the pressure are measured at different sites.

3.2. Elimination of the hysteresis

The method described here is based on four hypotheses which are presented below, and discussed in the following section.

Assuming no viscoelastic behaviour of the vessel wall (first hypothesis), the local diameter-pressure relationship is only a function of α, β and γ:

$$d(p) = d(p,\alpha,\beta,\gamma) \tag{2}$$

The local pulse wave velocity is given by (second hypothesis):

$$c(p) = \left(\frac{S}{\varrho}\frac{\partial p}{\partial S}\right)^{1/2} \tag{3}$$

where ϱ is the blood density (e.g. Pedley 1980). After interpolation of the diameter-pressure recording in order to obtain a constant density of points over the cardiac cycle, the general equation (2) is fitted on the diameter-pressure curve. The pulse wave velocity can then be temporarily calculated for each pressure level using equation (3). This is, however, an

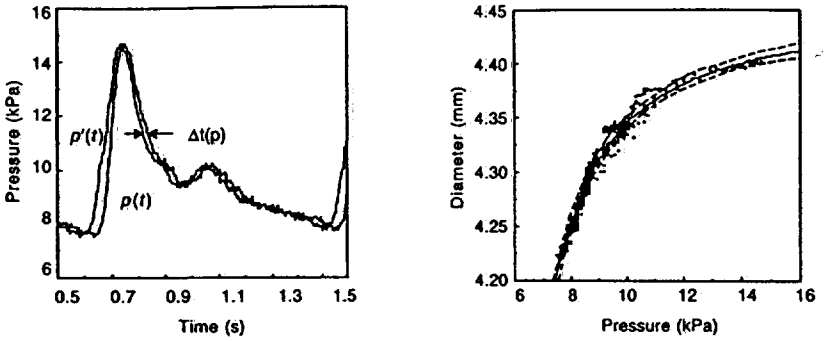

Figure 3. (*a*) Comparison of the recorded pressure signal at the finger level, $p(t)$, with the corrected curve obtained after the data processing $p'(t)$. (*b*) Arctangent model fitted by non-linear regression to the corrected diameter-pressure curve of a brachial artery. Dashed lines represent corresponding 95% confidence limits. Both figures, subject no. 3.

approximation, since it is determined from data with artefactual dispersion. The pulse wave transit time Δt is then calculated using (third hypothesis):

$$\Delta t(p) = \frac{\Delta z}{c(p)} \tag{4}$$

where Δz is the distance between the diameter and the pressure measurement sites. It is then supposed that this time of travel (which is a function of pressure) only modifies the shape of the pressure wave but not its amplitude (fourth hypothesis).

The last step is to apply selectively the pre-calculated negative delay to the finger pressure signal in order to estimate a corrected pressure waveform at the position where the diameter was measured (figure 3(*a*)). With this corrected pressure signal, $p'(t) = p(t + \Delta t)$, a new diameter-pressure curve is constructed. The method is improved by optimisation of the distance Δz or by successive iterations. In fact, the process is restarted from the corrected diameter-pressure curve, till this curve exhibits no more measurable hysteresis. Note that the final Δz values (about 20 cm for the brachial artery and 8 cm for the radial artery) are near the *in vivo* estimated length of the vessel. Figure 3(*b*) illustrates the successful suppression of the hysteresis by this method. Thus, the corrected diameter-pressure curve is considered as representative of the elastic behaviour of the artery at the site where the diameter is measured.

The shape of the corrected diameter-pressure curve is close to the diastolic part of the original curve (compare figures 2(*c*) and 3(*b*)). This is not due to the higher density of points during diastole which has been compensated but can be explained within the same hypotheses. For a fixed value of the diameter, the pressure difference δp between the recorded data and the corrected pressure at the diameter measurement site may be expressed as (figure 4):

$$\delta p = p(t) - p(t + \Delta t) \tag{5}$$

Expanding to first order (since Δt is small compared to the cardiac cycle), it yields

$$\delta p = \frac{\partial p}{\partial t} \Delta t + \theta(\Delta t^2) \tag{6}$$

Thus, at the first order, δp is proportional to the time derivative of the pressure. Due to the shape of the pressure wave in the peripheral arteries, this slope is much higher during systole than during diastole, especially at low pressure. Therefore δp is higher during systole (δp_1 in figure 4) than during diastole (δp_2 in figure 4). This explains why the corrected relationship is close to the points recorded during the diastolic part of the cardiac cycle.

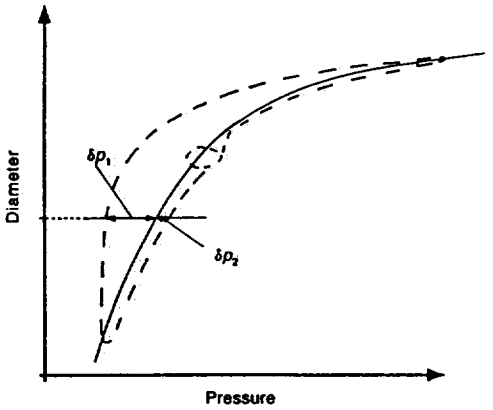

Figure 4. Typical diameter-pressure curve obtained by measuring the diameter at the brachial artery and the pressure at the finger (dashed line). Diameter-pressure relationship after suppression of the hysterisis (solid line).

3.3. Validity of the hypotheses

The four hypotheses on which the method is established will be reviewed and discussed in this section.

The first concerns the viscoelastic response of the brachial and radial arteries (muscular arteries of medium size). In order to estimate the importance of the viscoelasticity of a similar vessel, we have measured the internal diameter of a digital artery with the Finapres placed on the adjacent finger. This allowed us to obtain a diameter-pressure curve without artefactual hysteresis (figure 5). No viscoelastic behaviour can be detected with our resolution. This is somehow in contradiction with the external diameter-pressure loops obtained *in vitro* on a segment of human finger arteries by Langewouters *et al* (1988). Only the markedly different measurement conditions can explain this discrepancy. In any case, assuming a phase lag between diameter and pressure of 0.1 radian (see section 3.1.) at 10 Hz (the foot of the wave is mainly determined by the higher harmonics), a time delay of 1.5 ms due to viscoelasticity is predicted. This is negligible compared with the typical 25 ms delay applicable to the finger pressure signal for eliminating the hysteresis (brachial artery, see the foot of the pressure pulse in figure 3(*a*)).

The second assumption consists in calculating the pulse wave velocity using equation (3), which neglects blood velocity. It expresses, within a one-dimensional theory, the propagation speed of a pressure disturbance relative to the fluid at rest (Pedley 1980). The peak blood velocity reported for the radial artery is about 0.3 m s^{-1} (Casty 1980) and we obtain typical pulse wave velocities of 20 m s^{-1} at 13.3 kPa (100 mmHg) (figure 6(*a*)). It therefore seems reasonable to neglect the contribution of the blood velocity (about 1.5% of the pulse wave velocity).

A third hypothesis has been used to calculate the pressure wave transit time. Although we know from arterial haemodynamics that the pulse wave velocity increases towards periphery, equation (4) assumes a mean pulse wave velocity over the distance separating the

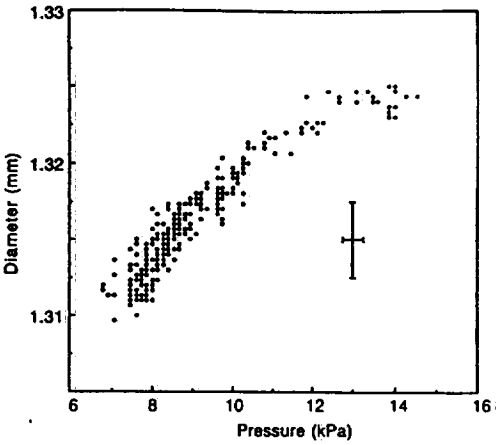

Figure 5. Diameter-pressure curve of a digital artery. The transducer and the cuff are placed on adjacent fingers. The vertical and horizontal bars are corresponding measurement errors associated with each data point.

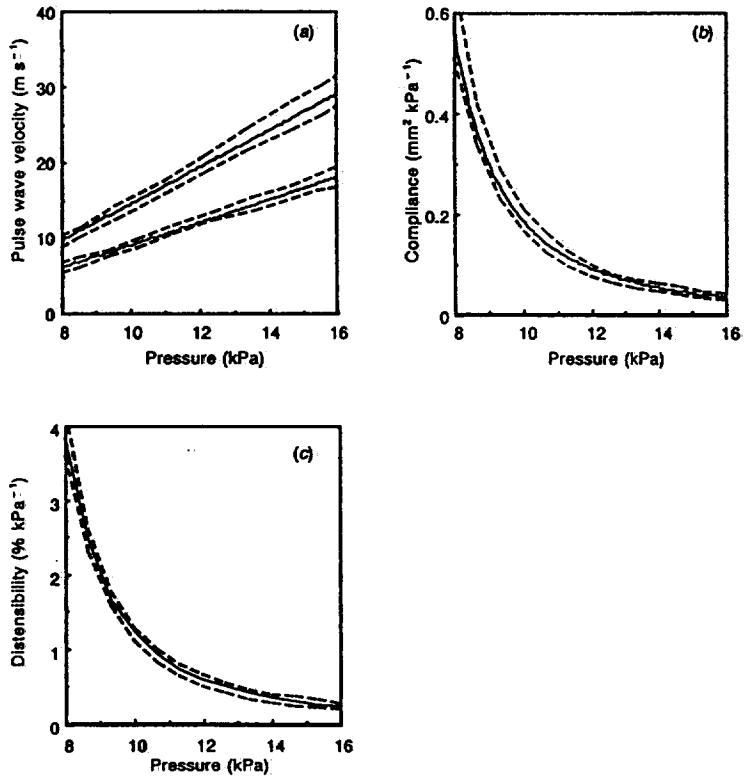

Figure 6. Mechanical parameters calculated from diameter-pressure curves of a healthy subject no. 3 (23 y). Dashed lines are corresponding 95% confidence limit calculated on the three optimal fit parameters determined by non-linear regression on the model. (*a*) Typical pulse wave velocity curves obtained for the brachial (lower curve) and radial (upper curve) arteries. (*b*) Compliance-pressure curve for the brachial artery. (*c*) Distensibility-pressure curve for the brachial artery.

two sites of measurement. The recent models of the arterial tree take into account the stiffening of the vessel wall with increasing distance from the heart. For example, Stettler *et al* (1981) used the following expression for the pulse wave velocity,

$$c(p,z) = c(p).(g_1 + g_2 z) \tag{7}$$

where z is the distance to the heart and g_1 and g_2 are constants. Rigorously, equation (4) should then be replaced by

$$\Delta t(p) = \int_{z}^{z+\Delta z} \frac{dz}{c(p,z)} \tag{8}$$

Using equation (7) for the pulse wave velocity, integrating and expanding to the first order, equation (8) yields,

$$\Delta t(p) = \frac{\Delta z}{c(p)}\left(\frac{1 - [\Delta z g_2/(g_1 + z g_2)]}{2(g_1 + z g_2)}\right) + \theta(\Delta z^2) \tag{9}$$

Thus, equation (9) expresses $\Delta t(p)$ as equation (4) times a multiplicative factor given in the large brackets. Since this factor is independent of pressure, and since the actual separation Δz is of no concern in our approach, a fictitious separation $\Delta z'$ can be considered (defined as Δz times the large bracket term). The $\Delta z'$ value is scanned heuristically until the artefactual hysteresis is minimised; although the resulting value cannot be interpreted as the actual separation, the corresponding transit time Δt is valid (to a first order approximation).

The fourth hypothesis is certainly the most questionable. We assume that the pressure wave amplitude is not modified during its travel from the forearm to the finger. But it is known that the evolution of the geometric and elastic wall properties along the arterial tree and the reflected waves modify the pulse shape and amplitude. Systolic peaking and steepening accompanied by diminution of the diastolic level is commonly observed when the pressure pulse moves towards periphery (Milnor 1989). This seems however to have negligible effect in our case; a good estimate of the pressure evolution between our sites of measurement has been found in papers studying the Finapres (Wesseling *et al* 1982, 1985, van Egmond *et al* 1985, Imholz *et al* 1988). These authors essentially compare the systolic and diastolic pressures obtained with the finger cuff and with intra-arterial catheters. All mention small discrepancies between the two measurement methods. On the average, both systolic and diastolic pressures are lower when measured at the finger level. However, this reduction is no more than 5% of the intra-arterial nominal pressure. Some important inter-individual variations are nevertheless reported. Furthermore, the elastic properties, such as compliance, will be slightly affected since they imply the pressure in a differential form.

We can thus estimate that the obtained diameter-pressure curves are really representative of both radial and brachial arteries, and that the approximations considered are especially justified for the radial artery, which is close to the finger.

4. Assessment of mechanical properties

The short protocol described in section 2.2. was undertaken in order to illustrate the method developed to obtain the diameter-pressure curves of peripheral arteries.

Since the arterial wall has non-linear behaviour, its elasticity depends on the transmural pressure. Treating the vascular wall as homogeneous and isotropic, an incremental modulus has been proposed (Peterson *et al* 1960) to describe the mechanical properties of the vessel

wall material. A simpler and more practical approach, particularly in clinical medicine, consists of using elastic parameters such as compliance and distensibility which can be derived directly from the diameter-pressure curve. Such parameters are very practical since they do not require wall thickness measurement, which is difficult to obtain non-invasively. Furthermore, these parameters express the dynamic wall response to the pressure pulse and therefore control the blood flow.

4.1. Diameter-pressure curve

It has been verified that the artefactual hysteresis observed in the diameter-pressure curves can be suppressed by appropriate time delay removal in all our data. Figure 7 shows a corrected diameter-pressure curve for the brachial artery of each subject. The internal diameter evolution is plotted against pressure for one cardiac cycle.

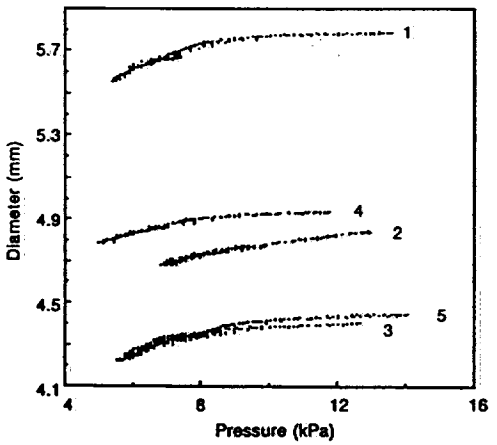

Figure 7. Diameter-pressure curve for the brachial artery of five subjects. One cardiac cycle is depicted.

4.2. Compliance-pressure curve

The compliance C, which is controlled by the elasticity of a vessel in the circumferential direction, is given by

$$C(p,z) = \left(\frac{\partial S(p,z)}{\partial p}\right)_z \tag{10}$$

The cross-sectional area of the vessel is considered as a function of the pressure and the distance from the heart. Using this definition and the chosen model for the artery equation (2), the following analytical form can be obtained for the local arterial compliance:

$$C = \frac{\alpha}{\gamma} \cdot \frac{1}{1 + [(p - \beta)/\gamma]^2} \tag{11}$$

Once the diameter-pressure curve has been fitted to equation (2) (figure 3(*b*)), equation (10) allows us to build the corresponding compliance-pressure curve (figure 6(*b*)). The 95% confidence limits presented in figures 3(*b*) and 6 are computed from the confidence ellipsoid in the three parameters α,β,and γ calculated by non-linear regression (Press *et al* 1987).

The method developed provides dynamic compliance values for the whole range of pulse pressure. Hasson *et al* (1984) and Megerman *et al* (1986) have already emphasised the necessity of obtaining these curves in order to compare different vessels more meaningfully. For example, arterial compliance was measured in two subjects with two different approaches. One method was based only on extreme values of pressure and cross-section during systole and diastole (mean compliance). The other method relied on our continuous compliance curve approach. Using the extreme values only, the compliance values of these two subjects appear similar (i.e. 0.165 $mm^2\ kPa^{-1}$ or 0.022 $mm^2\ mmHg^{-1}$, table of figure 8); but once their compliance-pressure curves are established (figure 8) it clearly appears that the dynamic behaviour of these vessels is different.

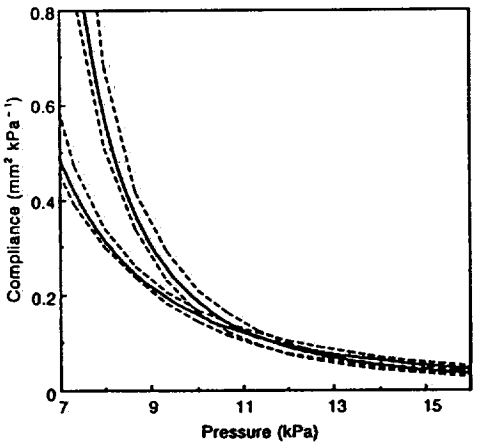

Figure 8. Compliance-pressure curves for the brachial artery of subjects 3 (upper curve) and 4 (lower curve). Dashed lines represent 95% confidence limits.

	Pressure		Section	
Subject	Syst.	Diast.	Syst.	Diast.
3	14.7	7.6	15.22	14.05
4	13.7	7.1	19.15	18.05

Much work has already been carried out to evaluate non-invasively arterial compliance or distensibility (equal to the compliance divided by the cross-section). The different approaches were: using the pulse-wave velocity (e.g. Smulyan *et al* 1984); analysing the diastolic pressure decay (Finkelstein *et al* 1988); measuring electrical impedance (Shimazu *et al* 1985); or by plethysmograhy (Westling *et al* 1984). These methods offer a more global estimate of arterial compliance at the cost of their inability to determine arterial compliance as a direct function of blood pressure. The systolo-diastolic excursion of the natural pressure pulse is used to obtain the volume distensibility (analogue to mean compliance, see above) and an external cuff is required to vary the mean pressure level in order to estimate the pressure dependance. Although these methods are not similar to ours, a good qualitative agreement can be found, especially when accounting for the high intra- and inter-individual variability of the forearm arteries properties (due to the important muscular component of their wall). More extensive comparison would require complex corrections for the measurement sites, the subjects age, the pressure level, etc.

Figure 9 shows the compliance-pressure curves obtained for the brachial and radial arteries of each subject. Despite important inter-individual variations, the different stiffnesses of the two vessels are clearly depicted. The compliance is more than twice as high for the brachial artery as for the radial artery. This is related to the 3% increase of the brachial artery diameter during systole compared with that of the radial artery of less than 1%.

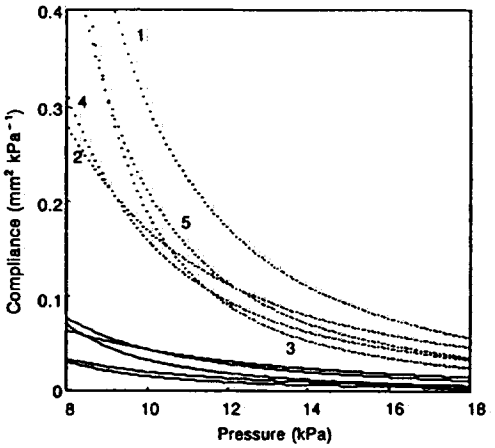

Figure 9. Compliance-pressure curves for the brachial (···) and radial (——) arteries of five healthy subjects.

4.3. Pulse wave velocity-pressure curve

The most common methods used to estimate the pulse wave velocity take a characteristic feature of the arterial pulse wave (pressure, velocity, etc.) and determine the time interval between its appearance at two points a known distance apart along the artery. This procedure is relatively simple but suffers from two major inconveniences. Firstly, it is difficult to implement when a local estimate of the pulse wave velocity is sought, because it involves measuring very short time intervals; and secondly, the non-linear propagation characteristics of the large amplitude pressure waves generated by the heart and the presence of reflections shed some doubt on the validity of these methods, which ignore these effects.

Three different approaches were used to overcome these problems. Anliker *et al* (1968) measured the transit time of short trains of small sine waves generated externally. They reported velocities rising from 4 to 6 m s^{-1} during systole in the dog carotid artery. The other approach consists of determining the true propagation coefficients of the pulse wave by using three simultaneous recordings of pressure flow or diameter at at least two sites (Reuderink *et al* 1988). Pulse wave velocities obtained by this method for the dog femoral and carotid arteries have values ranging between 8 and 12 m s^{-1} at frequencies above 4 Hz.

The third approach consists of determining the diameter-pressure curve of the vessel studied and calculating the pulse wave velocity with equation (3). Typical velocities obtained by this method are depicted in figure 6(*a*). They appear as a smooth first order function of pressure over the physiological pressure range. No similar study has been found in the literature for the forearm arteries. Busse *et al* (1979) used this method to measure the velocities in the carotid arteries of patients . They reported very similar curves with a comparable increase between the diastolic and systolic values but, unfortunately, did not mention any absolute value.

Finally, the relatively high velocities obtained in the present study, ranging from 10 m s^{-1} to 25 m s^{-1} for the radial artery, are not surprising. The increase in pulse wave velocity toward the periphery has been confirmed by a number of studies (Milnor 1989). For comparison, McDonald (1974) reported wave velocities of 8.5 m s^{-1} determined by the transit time of the foot of the pressure pulse between the human brachial and radial arteries, which corresponds to our 10 m s^{-1}.

5. Conclusions

The device and the analysis method presented here provide a non-invasive dynamic measurement of the diameter-pressure relationship of forearm arteries. Its high sampling rate and accuracy allow selection of a three-parameter arctangent model to describe the relationship between the internal diameter and the distending pressure of the brachial and radial arteries. The shape of the recorded curves confirms the marked non-linear response of the the arterial wall material.

Based on these curves, the elastic behaviour of arteries can be obtained at physiological distending pressures. It allows us to follow changes in arterial elasticity resulting independently of passive changes caused by variation in arterial pressure. We have shown that arterial compliance cannot be characterised by a single value representative of the whole range of pressure. Furthermore, when measuring any elastic arterial parameter, it is absolutely necessary to measure it as a function of blood pressure.

In fact, the vessel wall thickness should preferably be measured, in order to characterise completely the strain state of the artery. We are currently studying the possibility of deriving this parameter from the RF echo signal. This will allow us to develop and test more complete rheological models, accounting for the complex polymeric structure of the wall material.

The limitation of our method to forearm arteries is solely linked to the required pressure measurement. The Finapres seems to be the only device currently available that is able to measure arterial pressure continuously and non-invasively. If a toe cuff is developed for this apparatus, we could study the leg arteries using the same approach. However, the pressure wave evolution along the vascular bed prevents us applying the proposed method to more proximal arteries (cerebral arteries for example).

The method presented in this article provides three parameters (equation (2)) which fully describe the elastic properties of the forearm arteries. It makes it possible to perform statistical evaluation of arterial behaviour measured in different haemodynamic conditions. The influences of different factors on these parameters can then be systematically assessed (Mooser *et al* 1988, Perret *et al* 1988, 1989, 1990a). For example, one can study pharmacological therapies which may have a protective effect on the cardiovascular system by acting more or less selectively on arterial compliance (Perret *et al* 1990b). This new method therefore promises to be a useful tool to investigate non-invasively the arterial system of healthy subjects or patients with various vascular diseases and may be important for the prevention, diagnosis and treatment of these diseases.

References

Anliker M, Histand M B and Ogden E 1968 Dispersion and attenuation of small artificial pressure waves in the canine aorta *Circ. Res.* **23** 539-51

Arndt J O, Klauske J and Mersch F 1968 The diameter of intact carotid artery in man and its change with pulse pressure *Pflugers Arch.* **301** 230-40

Bergel D H 1961 The dynamic elastic properties of the arterial wall *J. Physiol.* **156** 458-69

Busse R, Schabert A, Summa Y, Bumm P and Wetterer E 1979 The mechanical properties of exposed human common carotid arteries *in vivo Basic Res. Cardiol.* **74** 545-54

Casty M 1980 Differenzierung zwischen normalen und pathologischen Stromungsverhaltnissen im arteriellen Kreislauf mittels gepulstem Ultraschall *PhD thesis* no. 6626 ETH Zurich

Eriksen M 1987 Noninvasive measurement of arterial diameters in humans using ultrasound echoes with prefiltred waveforms *Med. Biol. Eng. Comput.* **25** 189-94

Finkelstein S M, Collins V R and Cohn J N 1988 Arterial vascular compliance response to vasodilators by Fourier and pulse contour analysis *Hypertension* **12** 380-7

Ghista D N, Jayaraman G and Sandler H 1978 Analysis for the noninvasive determination of arterial properties and for transcutaneous continuous monitoring of arterial blood pressure *Med. Biol. Eng. Comput.* **16** 715-26

Groves D H, Powalowski T and White D N 1982 A digital technique for tracking moving interfaces *Ultrasound Med. Biol.* **8** 185-90

Hasson J E, Megerman J and Abbott W M 1984 Post-surgical changes in arterial compliance *Arch. Surg.* **119** 788-91

Hayashi K, Handa H, Nagasawa S and Okumura A 1980 Stiffness and elastic behaviour of human intracranial and extracranial arteries *J. Biomech.* **13** 175-84

Hewlett Packard *Understanding Frequency Counter Specifications* Application Note 200-4 pp 26-9

Histand M B and Anliker M 1973 Influence of flow and pressure on wave propagation in the canine aorta *Circ. Res.* **32** 524-9

Hoeks A P G, Brands P J, Smeets F A M and Reneman R S 1990 Assessement of the distensibility of superficial arteries *Ultrasound Med. Biol.* **16** 121-8

Hokanson D E, Mosersky D J and Summer D S 1972 A phased-locked echo tracking system for recording arterial diameter changes *in vivo J. Appl. Physiol.* **32** 728-33

Holenstein R, Niederer P and Anliker M 1980 A viscoelastic model for use in predicting arterial pulse waves *J. Biomed. Eng.* **102** 318-25

Imholz B P M, Van Montfrans G A, Settels J J, Van der Hoeven G M A, Karemaker J M and Wieling W 1988 Continuous non-invasive blood pressure monitoring: reliability of Finapres device during the Valsalva manoeuvre *Cardiovasc. Res.* **22** 390-7

Imura T, Yamamoto K, Kanamori K, Mikami T and Yasuda H D 1986 Noninvasive ultrasonic measurement of the elastic properties of the human abdominal aorta *Cardiovasc. Res.* **20** 208-14

King A L 1946 Pressure-volume relation for cylindrical tubes with elastomeric walls: the human aorta *J. Appl. Phys.* **17** 501-5

Kivity Y and Cellins R 1974 Nonlinear wave propagation in viscoelastic tubes: application to aortic rupture *J. Biomech.* **7** 67-76

Langewouters G J, Wesseling K H and Goedhard W J A 1984 The static elastic properties of 45 human thoracic and 20 abdominal aortas *in vitro* and the parameters of a new model *J. Biomech.* **17** 425-35

Langewouters G J, Zwart A, Busse R and Wesseling K H 1988 Pressure-diameter relationships of segments of human finger arteries *Clin. Phys. Physiol. Meas.* **7** 43-55

McDonald D A 1974 *Blood Flow in Arteries* (Baltimore: Edward Arnold) pp 389-419

Megerman J, Hasson J E, Warnock F, L'Italien G J and Abbott M 1986 Noninvasive measurements of nonlinear arterial elasticity *Am. J. Physiol.* **250** 181-8

Meister J J 1983 Mesure par échographie Doppler et modélisation théorique de l'effet de troubles cardiaques sur la pression et le débit artériels *PhD thesis* no 504 Swiss Federal Institute of Technology, Lausanne

Milnor W R 1989 *Hemodynamics* (Baltimore: Williams and Wilkins) pp 225-59

Mooser V, Etienne J D, Farine P A, Monney P, Perret F, Cecchini M, Gagnebin E, Bornoz C, Tardy Y, Arditi M, Meister J J, Leuenberger C E, Saurer E, Mooser E, Waeber B and Brunner H R 1988 Noninvasive measurement of internal diameter of peripheral arteries during cardiac cycle *J. Hypertension* **6** S179-81

Niederer P 1974 A molecular study of the mechanical properties of arterial vessel walls *Z. Angew. (Math.) Phys.* **25** 565-77

Oddou C 1980 Microrhéologie des élastomeres et du tissu pariétal artériel *J. Biophys. Med. Nucl.* **4** 277-83

Pedley T J 1980 *The Fluid Mechanics of Large Blood Vessels* (Cambridge: Cambridge University Press) pp 72-125

Penaz J 1973 Photoelectric measurement of blood pressure, volume and flow in the finger *Digest 10th Int. Conf. Med. Biol. Eng. Dresden* pp 104

Perret F, Mooser V, Waeber B, Mooser E, Nussberger J and Brunner H R 1988 Postischemic dilatation of the radial artery in normotensive volunteers *Angiology: Strategy for Diagnosis and Therapeutics* ed H Boccalon (Paris: John Libbey Eurotext) pp 25-6

——— 1989 Effect of cold pressor test on the internal diameter of the radial artery *Am. J. Hypertension* **2** 727-8

Perret F, Mooser V, Waeber B, Tardy Y, Meister J J, Nussberger J and Brunner H R 1990a Acute effect of cigarette smoking on the radial artery diameter (submitted for publication)

——— 1990b Evaluation of the effect of β-adrenoceptor blockade, calcium entry blockade and ACE inhibitor on arterial compliance of normotensive volunteers (submitted for publication)

Peterson L, Jensen R and Parnel J 1960 Mechanical properties of arteries *in vivo Circ. Res.* **8** 622-39

Powalowski T and Pensko B 1985 A noninvasive ultrasonic method for the blood flow and pressure measurements to evaluate the haemodynamic properties of the cerebro-vascular system *Arch. Acoust.* **10** 303-14

Press W H, Flannery B P, Teukolsky S A and Vetterling W T 1987 *Numerical Recipes: the Art of Scientific Computing* (Cambridge: Cambridge University Press) pp 521-38

Reuderink P, Sipkema P and Westerhof N 1988 Influence of geometric taper on the derivation of the true propagation coefficient using a three point method *J. Biomech.* **21** 141-53

Shimazu H, Fukuoka M, Ito H and Yamakoshi K 1985 Noninvasive measurement of beat-to-beat vascular viscoelastic properties in human fingers and forearms *Med. Biol. Eng. Comput.* **23** 43-7

Simon B R 1971 Large deformation analysis of arterial cross-section *Basic Eng.* **93** 138-46

Smulyan H, Vardan S, Griffiths A and Gribbin B 1984 Forearm arterial distensibility in systolic hypertension *J. Am. Coll. Cardiol.* **3** 387-93

Stettler J C, Niederer P and Anliker P 1981 Theoretical analysis of arterial haemodynamics including the influence of bifurcations *Ann. Biomed. Eng.* **9** 145-64

Vander Werff T J 1974 Significant parameters in arterial pressure and velocity development *J. Biomech.* **7** 437-47

van Egmond J, Hasenbos M and Crul J F 1985 Invasive versus non-invasive measurement of arterial pressure *Br. J. Anaesth.* **57** 434-44

van Loon P, Klip W and Bradley E L 1977 Length-force and volume-pressure relationships of arteries *Biorheology* **14** 181-201

Wesseling K H, De Wit B, Settels J J and Klawer W H 1982 On the indirect registration of finger blood pressure after Penaz *Funkt. Biol. Med.* **1** 245-50

Wesseling K H, Settels J J, Van Der Hoeven G M A, Nijboer J A, Butjin M W T and Dorlas J C 1985 Effects of peripheral vasoconstriction on the measurement of blood pressure in a finger *Cardiovasc. Res.* **19** 139-45

Westling H, Jansson L, Jonson B and Nilsen R 1984 Vasoactive drugs and elastic properties of human arteries *in vivo*, with special reference to the action of nitroglycerine *Eur. Heart J.* **5** 609-16

Genetic Hypertension. Ed J. Sassard. Colloque INSERM/John Libbey Eurotext Ltd. © 1992, Vol. 218, pp. 281-283

Arterial wall distensibility in hypertensive rats

Daniel Hayoz, Michel Niederberger, Blaise Rutschmann, Hans R. Brunner and Bernard Waeber

Division d'Hypertension, Centre Hospitalier Universitaire Vaudois, Lausanne, Switzerland

Introduction

The purpose of our study was to determine whether vascular alterations induced by chronic hypertension modify mechanical properties of the arteries. Vascular smooth muscle cell hypertrophy and extracellular matrix modifications in the media are responsible for arterial wall thickening (1-4). It is today possible to measure continuously in the anesthetized rat the internal diameter of the carotid artery simultaneously with intra-arterial pressure using a new non-invasive device (5). In the present study we measured the mechanical behavior of the common carotid artery of 16-week-old spontaneously hypertensive rats (SHR) treated for 6 weeks with either the ACE inhibitor captopril or the arteriolar dilator hydralazine. Treated and untreated rats were compared to normotensive controls (WKY rats).

Methods

Ten 16-week old normotensive male rats (WKY) and 30 age- and sex-matched spontaneously hypertensive rats (SHR) were used. The SHR were allocated to 6 week treatments with either captopril (n = 10), hydralazine (n = 9) or vehicle (tap water; n = 10). The drugs were administered in drinking water (captopril, 25 mg/30 ml of water, hydralazine, 5 mg/30 ml of water).

Anesthesia was induced with ether and then maintained with fluothane (1.5%). The right external carotid artery was cannulated with a catheter (PE 50) filled with a heparinized 0.9% NaCl solution. Intra-arterial pressure and heart rate were monitored using a computerized data acquisition system (6). The internal diameter of the left external carotid artery was measured at the same time using an A-Mode ultrasonic echo-tracking device (5). Ten successive diameter-pressure recordings were obtained for each animal in a five minute period. The apparatus allows measurements of the internal carotid artery diameter variations with a precision close to one micron. This degree of resolution is made possible by oversampling (5000 arterial diameter measurements per second) and averaging 16 consecutive values. For the recordings, a 10-MHz probe is positioned perpendicularly over the artery without direct contact with the skin. The Doppler technique is used for guidance of the probe and an ultrasonic gel is employed for signal transduction.

The simultaneous and continuous acquisitions of internal arterial diameter and blood pressure are processed on line to compute a diameter (or cross-section) -pressure relationship. The latter is

subsequently converted into a distensibility-pressure curve. This curve fits best with an arctangent function first described by Langwouters (7).
Arterial cross-sectional distensibility (D) is the inverse of the Peterson elastic modulus, and represents the arterial compliance normalized for the cross-section (s). [$D = (1/s) * \partial$ cross-section/∂ pressure]
Data are reported as means ± SEM. A one way analysis of variance was used to compare the baseline characteristics of the experimental groups. Differences were considered significant for p values < 0.05. Statistical analysis of compliance-pressure and distensibility-pressure curves were done using a multivariate analysis based on Hotelling T2 considering compliance values at three arbitrarily defined blood pressures in the range of measured values.

Results

Under halothane anesthesia, captopril- and hydralazine-treated hypertensive rats and WKY normotensive controls displayed overlapping blood pressures (Figure 1), allowing statistical comparisons between the distensibility-pressure curves. Vehicle-treated SHR exhibited clearly higher blood pressure values. There was no significant difference in heart rate between the 4 groups of animals (SHR: Vehicle = 324 ± 11, captopril = 348 ± 22 and hydralazine = 318 ± 12 b/min; WKY = 316 ± 21 b/min). Left ventricular mass adjusted to total body weight was significantly ($p<0.01$) reduced in treated-SHR in comparison to untreated SHR (3.19 ± 0.11 g/kg) (Table 1).

	WKY	SHR		
	Vehicle	Vehicle	Captopril	Hydralazine
Systolic BP (mm Hg)	169±2***	218±2	170±5***	182±3***
Diastolic BP (mm Hg)	135±2***	176±3	137±5***	151±2***
Heart rate (bpm)	316±21	324±11	348±22	318±12
Left ventricular mass per kg (g/kg)	2.41±0.03**	3.19±0.11	2.51±0.05**	2.68±0.06**

Mean ± SEM *p<0.05 **p<0.01 ***p<0.001 versus SHR vehicle

Table 1

Hemodynamic parameters and lefet ventricular mass of the different groups of rats under anesthesia

Figure 1. shows the cross-sectional distensibility as a function of intra-arterial blood pressure recorded synchronously in the controlateral carotid artery. There was no statistically significant difference in the distensibility-pressure curves between the treated SHR and the normotensive controls, although distensibility tended to be enhanced by the two antihypertensive agents. Because of the absence of overlapping blood pressures between untreated SHR and WKY animals, the distensibility-pressure curves cannot be subjected to statistical analysis. These curves appear however to represent the direct continuation of one another.

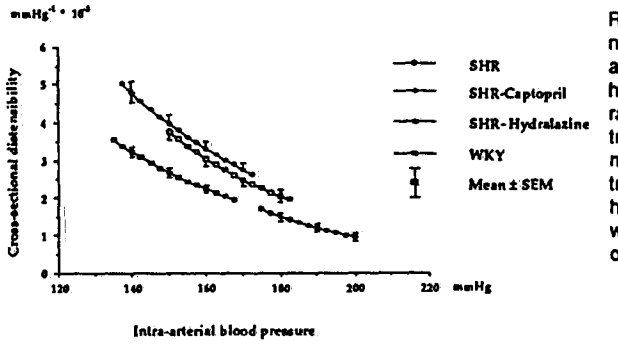

Legend Figure 1

Relationships between cross-sectional distensibility of the carotid artery and intra-arterial pressure established in spontaneously hypertensive rats (SHR) and normotensive controls (WKY). The 16-week old animals were studied after a 6 week treatment with either captopril or hydralazine administered in drinking water. Untreated animals received only water.

Discussion

This study performed in intact young spontaneously hypertensive rats shows the impact of drug-induced blood pressure reductions on distensibility-pressure curves using a new ultrasound A-Mode echotracking device. The two drugs, the ACE inhibitor captopril and the arterial dilator hydralazine, were equally effective in lowering blood pressure but, as anticipated, ACE inhibition with captopril led to a more pronounced regression of cardiac hypertrophy (8,9).

The major advantage of our technique is derived from the fact that the arterial diameter and the intra-arterial pressure are recorded continuously over the entire pulse pressure range. The arterial distensibility can therefore be related to each pressure actually measured in these animals. The determinations were performed at the carotid artery, a typical elastic artery. By this approach no significant difference was found between captopril- or hydralazine-treated hypertensive rats and their normotensive untreated WKY counterparts, although a trend towards an increased distensibility was apparent after treatment. Moreover, the distensibility-pressure curves established in untreated hypertensive animals appeared to be the direct extension of the corresponding curves determined in WKY rats. These data may seem rather surprising since there is general agreement that arterial wall thickening, already present in young SHR, is associated with increased stiffness (10). They are however in agreement with previous observations made using the same echotracking system in patients with essential hypertension and in normotensive subjects (11). In this clinical setting also, the hypertensive disorder did not result a decrease in arterial distensibility, at least as assessed at the level of the radial artery, a medium-size muscular artery.

The experiments reported here were carried-out in rather young rats treated for only a few weeks. Further studies involving older hypertensive animals are needed first to ensure whether long-term blood pressure control changes the mechanical properties of the arterial wall and secondly to relate mechanical behavior with morphometric analysis.

References

1. Warshaw DM, Mulvany MS et al., (1979): Mechanical and morphological properties of arterial resistance vessels in young and old spontaneous hypertensive rats. Circ Res; 45: 250-259.
2. Chobanian AV, Prescott MF et al., (1984): The effects of hypertension on the arterial walls. Exp Mol Pathol; 41: 153-169.
3. Folkow B. (1982) : Physiological aspects of primary hypertension. Physiol Rev; 62: 347-504.
4. Hart MN, Heistad DDet al., (1980): Effect of chronic hypertension and sympathetic denervation on wall/lumen ratio of cerebral vessels. Hypertension; 2: 419-423.
5. Tardy Y, Meister JJ et al., (1991): Non-invasive estimate of the mechanical properties of peripheral arteries from ultrasonic and photoplethysmographic measurements. Clin Phys Physiol Meas; 12: 39-54.
6. Flückiger JP, Gremaud G et al., (1989): Measurement of sympathetic nerve activity in the unanesthetized rat. J Appl Physiol; 67: 250-255.
7. Langwouters GJ, Wesseling KH et al., (1984): The static elastic properties of 45 human thoracic and 20 abdominal aortas in vitro and the parameters of a new model. J Biomechanics; 17: 425-435.
8. Sen S, Tarazi RC et al., (1980): Effect of converting enzyme inhibitor (SQ 14,225) on myocardial hypertrophy in spontaneously hypertensive rats. Hypertension; 2: 169-176.
9. Freslon JL, Giudicelli JF. (1983): Compared myocardial and vascular effects of captopril and dihydralazine during hypertension development in spontaneously hypertensive rats. Br J Pharmac; 80: 533-543
10. Michel JB, Salzmann JL et al., (1990): Effect of hypertension and vasodilator treatment on arterial wall structure. In: Atkinson J., Capdeville C. Zannad F., eds: Coronary and cerebrovascular effects of antihypertensive drugs. Cambridge, Transmedica; 205-218.
11. Perret F, Hayoz D et al., (1990): Arterial compliance : is it necessarily decreased in hypertensive patients. 13th Scientific Meeting of the International Society of Hypertension Montréal, Canada.; Abst: S82 P3.17.

Glucose tolerance and insulin secretion in essential hypertension after treatment with an angiotensin converting enzyme inhibitor

Donatella Santoro, Andrea Natali, Alfredo Quinones Galvan, Antonio Masoni, Paolo Gazzetti and Eleuterio Ferrannini

Journal of Hypertension 1991, 9 (suppl 6):S406–S407

Keywords: Essential hypertension, glucose tolerance, insulin secretion, angiotensin converting enzyme inhibition, blood pressure.

Introduction

A wealth of epidemiological evidence confirms the clinical observation that essential hypertension is frequently associated with abnormalities of glucose metabolism such as impaired glucose tolerance and overt non-insulin-dependent diabetes. Insulin is the principal regulator of carbohydrate metabolism, and an alteration in either its secretion or action can impair glucose homeostasis. Recently, insulin resistance has been demonstrated in untreated essential hypertension [1,2] and one study has reported that this metabolic abnormality can be partially reversed by treatment with an angiotensin I converting enzyme (ACE) inhibitor [3]. This observation implicates the renin–angiotensin–aldosterone system in the control of carbohydrate metabolism through effects on insulin secretion, insulin sensitivity or both.

To our knowledge, no data are available on the influence of chronic ACE inhibition on insulin secretion. The present study was therefore undertaken to assess glucose tolerance and insulin secretion in untreated hypertensive patients before and after chronic ACE inhibition.

Methods

The study group consisted of 15 ambulatory patients (one woman and 14 men, mean age 48 ± 2 years, body mass index 26.1 ± 0.4 kg/m^2) with essential hypertension (blood pressure 150 ± 3/105 ± 1 mmHg). The experimental protocol was designed as an open trial, in which 12 weeks of active therapy were preceded by 4 weeks of single-blind, placebo run-in.

Each patient underwent an oral glucose tolerance test once at the end of the 1-month placebo period (week 0) and then after 4, 8 and 12 weeks of active treatment with cilazapril (5 mg/day). During the oral glucose tolerance tests, venous blood was drawn twice basally (at −30 and 0 min) and then at 30-min intervals during the 2 h following the ingestion of 75 g glucose for the measurement of plasma glucose, insulin and potassium concentrations. Fasting plasma aldosterone was assayed only during weeks 0 and 12.

Glucose tolerance was quantified as the incremental (above the basal value) glucose area under the time–concentration curve (calculated by trapezoidal integration). The insulin secretory response to glucose was analysed by plotting, for each individual test, the insulin increments against the respective glucose increments, and then fitting a linear regression to the data. The slope of this regression line reflects the sensitivity of insulin release to glucose stimulation.

Results

A significant fall in blood pressure (12 ± 4/15 ± 3 mmHg) was achieved after the first month of ACE inhibition; this change was sustained for the following 8 weeks. At week 12, the mean decrease was 13 ± 3/17 ± 2 mmHg. The body mass index remained stable.

Fasting plasma glucose and insulin levels did not change significantly during the study. The mean incremental glucose areas were 282 ± 30, 290 ± 29, 269 ± 35, and 230 ± 31 mmol/l.120 min, respectively, at baseline and during weeks 4, 8 and 12. The reduction was statistically different only between the baseline and the final test ($P < 0.03$ by Wilcoxon's signed rank test). Figure 1 shows the mean insulin/glucose slopes for the four sequential tests. In weeks 8 and 12, but not week 4, the mean slopes were significantly

From the Metabolism Unit of the CNR Institute of Clinical Physiology, Pisa, Italy.

Requests for reprints to: Dr Eleuterio Ferrannini, CNR Institute of Clinical Physiology, Via Savi 8, 56100 Pisa, Italy.

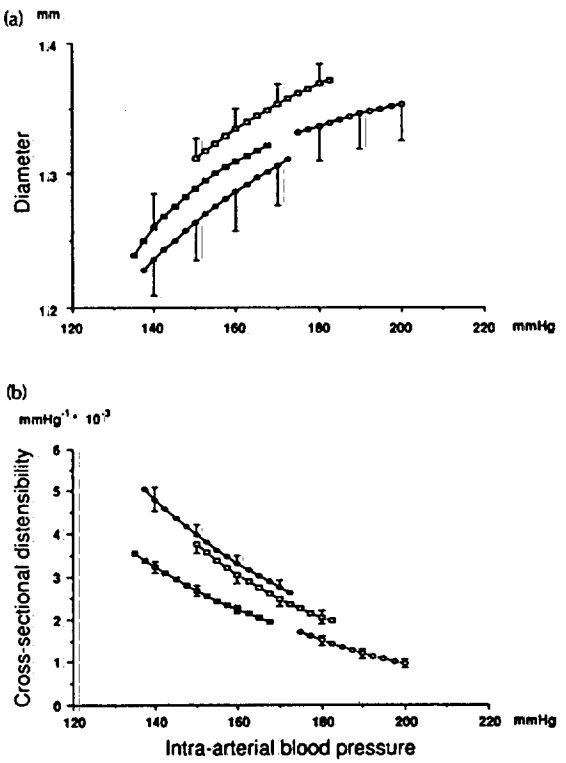

Fig. 1. (a) Relationships between the internal diameter of the carotid artery and intra-arterial pressure in spontaneously hypertensive rats (SHR) and normotensive controls (WKY) and (b) cross-sectional distensibility–pressure curves derived from (a). The 16-week old SHR were studied after 6 weeks of treatment with either captopril (●) or hydralazine (□) administered in drinking water. Untreated SHR (○) or WKY (■) drank water alone. Means ± s.e.m.

displayed overlapping blood pressures (Fig. 1), allowing statistical comparisons to be made between the diameter–pressure and distensibility–pressure curves. Vehicle-treated SHR exhibited clearly higher blood pressure values. There was no significant difference in heart rates between the four groups of animals (SHR: vehicle 324 ± 11, captopril 348 ± 22 and hydralazine 318 ± 12 beats/min; WKY 316 ± 21 beats/min). Left ventricular mass adjusted to total body weight was significantly ($P < 0.01$) reduced in the treated SHR (captopril, 2.51 ± 0.05 g/kg; hydralazine, 2.68 ± 0.06 g/kg) in comparison with untreated SHR (3.19 ± 0.11 g/kg). There was no statistically significant difference in the diameter–pressure curves (Fig. 1a) or the distensibility–pressure curves (Fig. 1b) between the treated SHR and the WKY controls, although distensibility tended to be enhanced by the two antihypertensive agents. Because the blood pressure values for the untreated SHR did not overlap those of the WKY rats, the diameter–pressure and distensibility–pressure curves cannot be subjected to statistical analysis. These curves appeared, however, to represent a direct continuation of one another.

Discussion

The present study is the first description, in intact SHR, of the impact of drug-induced blood pressure reductions on diameter–pressure and distensibility–pressure curves. The two drugs used were equally effective in lowering blood pressure but, as expected, the ACE inhibitor gave the best regression of cardiac hypertrophy. The major advantage of the new measurement device used in the present study is that the arterial diameter and the intra-arterial pressure are recorded continuously over the entire pulse–pressure range, so that diameter and distensibility can be related to each pressure measurement. We found no clear-cut difference between the captopril- or hydralazine-treated hypertensive rats and their normotensive WKY controls. The diameter–pressure and distensibility–pressure curves of the untreated SHR appeared to be a direct extension of the curves in the WKY rats. These data, albeit surprising, are in accord with our previous observations in humans using the same echotracking system (manuscript submitted for publication). In the clinical setting also, the hypertensive disorder did not result in a decrease in arterial distensibility, at least as assessed at the level of the radial artery, a medium-size muscular artery. The experiments reported here were carried out in rather young rats treated for only a few weeks. Further studies involving older hypertensive animals treated for longer periods are needed to ascertain whether long-term elevations in blood pressure change the mechanical properties of the arterial wall.

References

1. FOLKOW B: Physiological aspects of primary hypertension. *Physiol Rev* 1982, 62:347–504.
2. WARSHAW DM, MULVANY MS, HALPERN W: Mechanical and morphological properties of arterial resistance vessels in young and old spontaneous hypertensive rats. *Circ Res* 1979, 45:250–259.
3. CHOBANIAN AV, PRESCOTT MF, HAUDENSCHILD CC: The effects of hypertension on the arterial walls. *Exp Mol Pathol* 1984, 41:153–169.
4. TARDY Y, MEISTER JJ, PERRET F, BRUNNER HR, ARDITI M: Non-invasive estimate of the mechanical properties of peripheral arteries from ultrasonic and photoplethysmographic measurements. *Clin Phys Physiol Meas* 1991, 12:39–54.
5. PERRET F, MOOSER V, HAYOZ D *ET AL.*: Evaluation of arterial compliance–pressure curves: effect of antihypertensive drugs. *Hypertension* 1991, 18 (suppl II):II77–II83.
6. FLÜCKIGER JP, GREMAUD G, WAEBER B *ET AL.*: Measurement of sympathetic nerve activity in the unanesthetized rat. *J Appl Physiol* 1989, 67:250–255.
7. LANGWOUTERS GJ, WESSELING KH, GOEDHARD WJA: The static elastic properties of 45 human thoracic and 20 abdominal aortas *in vitro* and the parameters of a new model. *J Biomech* 1984, 17:425–435.

Neither hydralazine nor captopril significantly shifts carotid artery distensibility–pressure curves determined in intact spontaneously hypertensive rats

Michel Niederberger, Daniel Hayoz, Blaise Rutschmann, Yanik Tardy*, Jürg Nussberger, Bernard Waeber and Hans R. Brunner

Journal of Hypertension 1991, 9 (suppl 6):S404–S405

Keywords: Spontaneously hypertensive rat, Wistar–Kyoto normotensive rat, cross-sectional distensibility.

Introduction

Chronic hypertension is associated with arterial wall thickening [1] due primarily to hypertrophy of the vascular smooth muscle cells [2] and perhaps partly to an increase in the extracellular matrix components of the arterial media [3]. These structural changes may modify the mechanical properties of the vessels. A new non-invasive device allows continuous measurement of the internal diameter of the carotid artery simultaneously with intra-arterial pressure in the anesthetized rat [4,5]. In the present study, we assessed the mechanical properties of the common carotid artery of 16-week-old spontaneously hypertensive rats (SHR) treated for 6 weeks with either captopril or hydralazine, in comparison with untreated SHR and normotensive Wistar–Kyoto rats (WKY).

Methods

We used 10 16-week-old male WKY and 30 age- and sex-matched SHR. The SHR were either treated for 6 weeks with captopril (25 mg/30 ml drinking water; n = 10) or hydralazine (5 mg/30 ml drinking water, n = 9) or were untreated (tap water; n = 10). On the study day, anesthesia was induced with ether and maintained with 1.5% fluothane. The right external carotid artery was cannulated with a catheter (PE 50; Portex, London, UK) filled with a heparinized 0.9% NaCl solution. Intra-arterial pressure and the heart rate were monitored with a computerized data-acquisition system [6]. The internal diameter of the left external carotid artery was measured at the same time using an A-Mode ultrasonic echo-tracking device [4] which allows a precision close to 1 μm, obtained by oversampling (5000 arterial diameter measurements per s) and averaging 16 consecutive values. For the recordings, a 10-MHz probe was placed perpendicularly over the artery without direct skin contact. The Doppler technique was used to guide the probe and an ultrasonic gel was used for signal transduction.

The simultaneous acquisition of arterial diameter and blood pressure measurements was processed on-line to compute a diameter (or cross-section)–pressure relationship, which was converted into compliance–pressure and distensibility–pressure curves. These curves fit best with an arctangent function [7]. Cross-sectional compliance (C), in the case of a cylindrical vessel, is given by $C = \delta s/\delta p$, where δs is the change in cross-section and δp is the change in blood pressure. Arterial cross-sectional distensibility (D) is the inverse of the Peterson elastic modulus, i.e. the compliance value normalized for the cross-section (s). It is defined by $D = (1/s) \times \delta s/\delta p$.

A one-way analysis of variance was used to compare the general baseline characteristics of the experimental groups. $P < 0.05$ was considered significant. Data are reported as means ± s.e.m. For the statistical analyses of the compliance–pressure and distensibility–pressure curves a multivariate analysis was used, based on Hotelling T2 taking compliance values at three arbitrarily defined blood pressures in the range of measured values.

Results

Under halothane anesthesia, the captopril and hydralazine-treated SHR and WKY normotensive controls

From the Division of Hypertension, Centre Hospitalier Universitaire Vaudois, Lausanne, and *Department of Physics, Swiss Federal Institute of Technology, Ecublens, Switzerland.

Sponsorship: This was was supported by grants from the Swiss National Science Foundation, the Cardiovascular Research Fund and the Swiss Association of Cigarette Manufacturers.

Requests for reprints to: Dr Bernard Waeber, Division d'Hypertension, CHUV, Rue Pierre Decker, 1011 Lausanne, Switzerland.

−20/−13 mmHg after 2 h, $P < 0.01$; −13/−9 mmHg after 3 h, $P < 0.01$) and increased the E/A ratio after 2 h (1.16 ± 0.3, $P < 0.05$) and 3 h (1.26 ± 0.3, $P < 0.05$). No change in ventricular dimensions and heart rate was observed.

After chronic therapy we found a further increase in the E:A ratio in 10 responder patients (Table 1). The left ventricular mass index shows a significant reduction in comparison with basal values ($P < 0.05$) after 6 and 12 months of therapy.

The echo-Doppler measurements of hypertensive patients at the end of treatment did not show statistically significant differences in comparison with those of normotensive subjects.

Discussion

Acute verapamil administration produced a significant increase in flow velocity in protodiastole and decreased flow velocity in telediastole. These modifications resulted in a significant increase, after 2 and 3 h, in the E:A ratio. This suggests a redistribution of transmitral flow (when compared with both basal and placebo recordings) in favour of the rapid filling phase. From a hemodynamic point of view, the main variation was the afterload reduction, since the ventricular dimensions and the heart rate were unchanged.

The second part of the study showed that chronic administration of verapamil can maintain and potentiate the modifications of the Doppler parameters observed in the acute phase, producing a further increase in the E:A ratio.

With respect to morphological changes, we observed a significant reduction in the left ventricular mass, as a consequence of the decreased thickness of the interventricular septum and of the posterior wall. At the end of the study period values for both ventricular filling and myocardial mass of hypertensive patients were not significantly different from those of normotensive subjects. This indicates that effective blood pressure control by verapamil can normalize the mild and early morphological and functional changes present in hypertensives without definite left ventricular hypertrophy [6].

References

1. Messeru FM: Antihypertensive therapy. Going to the heart of the matter. *Circulation* 1990, 81:1128–1135.
2. Trimarco B, Wikstrand J: Regression of cardiovascular structural changes by antihypertensive treatment. *Hypertension* 1984, 6 (suppl III):III150–III157.
3. Sahn DJ, De Maria A, Kisslo J, Weyman A: Recommendations regarding quantitation in M-mode echocardiography: results of a survey of echocardiographic measurements. *Circulation* 1978, 58:1071–1083.
4. Devereux RB, Casale PN, Kligfield P, *et al.*: Performance of primary and derived M-mode echocardiographic measurements for detection of left ventricular hypertrophy in necropsied subjects and in patients with systemic hypertension, mitral regurgitation and dilated cardiomyopathy. *Am J Cardiol* 1986, 57:1388–1393.
5. Spirito P, Maron BJ: Doppler echocardiography for assessing left ventricular diastolic function. *Ann Intern Med* 1988, 109:122–126.
6. Smith VE, White WB, Meeran MK, Karimeddini MK: Improved left ventricular filling accompanies reduced left ventricular mass during therapy of essential hypertension. *J Am Coll Cardiol* 1986, 8:1449–1454.

Table 1. Echocardiographic and Doppler parameters in normotensive, control and in hypertensive patients before and after verapamil administration.

		Hypertensive patients		
	Controls (n = 12)	Placebo (I) (n = 12)	Acute study (II) (n = 12)	Chronic study (III) (n = 10)
Left ventricular diastolic diameter (mm)	49.8 ± 2.9	50.6 ± 3.0	50.4 ± 3.1	50.5 ± 3.7
Interventricular septum (mm)	8.6 ± 0.9	10.0 ± 0.9	10.1 ± 0.9	9.1 ± 1.1*†
Posterior wall (mm)	8.5 ± 0.6	9.8 ± 1.0	9.9 ± 1.1	8.8 ± 0.8*†
Left ventricular mass index (g/m²)	91 ± 11	118 ± 16	117 ± 18	100 ± 17**‡
E (cm/s)	71.2 ± 13.1	65.9 ± 8.9	69.8 ± 9.8*	70.1 ± 10.0*
A (cm/s)	50.2 ± 14.0	64.8 ± 9.2	58.1 ± 16.0*	52.6 ± 12.0**†
E:A	1.51 ± 0.3	1.08 ± 0.2	1.26 ± 0.3*	1.49 ± 0.3**‡

Means ± s.d. E, peak mitral flow velocity in protodiastole; A, peak mitral flow velocity in telediastole; E:A, ratio between the two velocities; *$P < 0.05$, **$P < 0.01$, versus I; †$P < 0.05$, ‡$P < 0.01$, versus II.

BURSTEIN, C.
Lab. de Technologie des enzymes
Université de PARIS 7

BIOS 175 MARQUE SET

Biosensors & Bioelectronics 8 (1993) 000-000

Detection of heavy metal salts with biosensors built with an oxygen electrode coupled to various immobilized oxidases and dehydrogenases

Jean-Charles Gayet, Ahmed Haouz, Annette Geloso-Meyer & Claude Burstein*

Université Paris 7, Laboratoire de Technologie des Enzymes et des Biomembranes, Tour 54, 2 place Jussieu, F-75251 Paris cédex 05, France

(Received 15 June 1992; revised version received and accepted 1 October 1992)

Abstract: Immobilized oxidases were bound on the surface of an affinity membrane and mounted on an oxygen electrode. These biosensors were used for heavy metal salt measurements. After immobilization of the enzymes, first order kinetics of inactivation were observed. Surface immobilization increases the sensitivity by a factor of 10, compared to reticulation of the enzyme in a gelatin matrix.

After immobilization, 50% inactivation was observed with 20 μM $HgCl_2$ for L-glycerophosphate oxidase and 50 nM for pyruvate oxidase. Restoration of activity after $HgCl_2$ treatment is feasible, but neither complete nor reproducible. To reuse the biosensor, L-lactate dehydrogenase (LDH) from rabbit muscle in solution was coupled to immobilized L-lactate oxidase (insensitive to heavy metal salts). LDH (particularly inexpensive) was replaced after each measurement. The I_{50} in phosphate buffer was 1 μM for $HgCl_2$ and 0·1 μM for $AgNO_3$; with other heavy metal salts, no inhibition was observed below 500 μM. In Tris buffer, the I_{50} was 10 μM for $CdCl_2$ and $ZnCl_2$, 50 μM for Pb-acetate and 250 μM for $CuSO_4$.

The use of different enzymes and buffers may allow measurement of specific heavy metal salts.

Keywords: heavy metal salt determination, enzyme electrode, enzyme immobilization, biosensor

* To whom correspondence should be addressed.

1. INTRODUCTION

Heavy metal compounds are well known for their toxicity in the environment, polluting air, water and food. Various biological effects have been described (Webb, 1966*a*; MacGregor & Clarkson, 1974). At the molecular level, these toxic compounds decrease the activity of certain enzymes.

The effect of heavy metals seems to involve the thiol groups of proteins. Fixation of the heavy metal on these thiol groups may explain their noxious effect (Webb, 1966*b*).

Various techniques requiring very expensive instrumentation (such as flame spectrophotometry or polarography) are available to measure ~~mercuric~~ salt concentrations precisely. A simpler and more rapid test is often required in the field. Control of contamination of air, water and food depends on simple, rapid and multiple assays.

Some authors have already evaluated the use of immobilized enzyme probes for the determination of enzyme inhibitors (Mattiasson *et al.*, 1978; Tran-Minh, 1985; Fukano & Chiba, 1988).

In our laboratory, we have previously designed biosensors with immobilized oxidases in gelatin film (Zapata-Bacri & Burstein, 1988). Our aim was to develop a new biosensor sensitive to toxic compounds, using immobilized enzymes on the surface of a film tightly bound to an oxygen electrode. In this paper, the effects of heavy metal salts below 500 μM on enzyme activity were chosen as a model for measuring pollution with biosensors. Heavy metal salt concentrations were determined with immobilized oxidases or dehydrogenases coupled to immobilized oxidases.

2. MATERIALS AND METHODS

Enzymes and substrates were purchased from Sigma (except for L-lactate dehydrogenase from rabbit muscle, from Boehringer).

All lyophilized enzymes were dissolved in 50 mM potassium phosphate buffer, pH 7·0, and stored at −20°C. We used various buffers at different pHs (Table 1) depending on the assay:

- 100 mM potassium phosphate buffer, pH 6·5–7·6;
- 100 mM sodium malate buffer, pH 5·0–5·6;
- 100 mM glycine–NaOH buffer, pH 8·1; and
- 100 mM sodium succinate buffer, pH 3·8.

All measurements were performed with the Clark electrode (Gilson type) in 2 ml of buffer thermostatted at 30°C. Concentrations are in final molarity. Because oxygen measurements allow for turbid or colour mixtures without interference, samples were added without any pretreatment (except dilution, when necessary).

2.1. Oxygen consumption measurements

Oxygen consumption was measured amperometrically at −700 mV *vs* SCE with a Clark electrode. 100% oxygen saturation (240 μM) was obtained in buffer saturated with bubbling air at 30°C. 0% oxygen was obtained with glucose oxidase and 100 mM glucose, a substrate concentration high enough to consume the oxygen completely in 10 s.

2.2. Measurements of enzyme in solution

The Clark electrode was covered with a naked polypropylene membrane. 1 μl of enzyme was introduce into the thermostatted cell at 30°C. Oxygen consumption was measured against time after addition of a specific substrate in high enough concentration to obtain V_{max}. 1 U enzyme gives 1 μmol of oxidized substrate per min.

2.3. Enzyme immobilization

2.3.1. Reticulation in gelatin film

Enzyme immobilization was carried out by mixing, at 40°C, 0·5 ml of the appropriate buffer (see Table 1) containing 10 units of enzyme and 0·5 ml of a 10% aqueous gelatin solution (~~250~~ Blooms, bone gelatin from Rousselot, France). The mixture was gently agitated at 40°C for 2 min and poured rapidly onto a glass plate covered with a gas-selective hydrophobic film (6 μm thick polypropylene from Bollore Inc, Paris, France). One ml of mixture was spread on 40 cm² and solidified spontaneously after 5 min at 4°C. The film was further polymerized at 0°C by covering it with 2·5% aqueous glutaraldehyde, freshly prepared, for 6 min. The film was washed three times with a large volume of appropriate buffer containing 50 mM lysine, to remove unreacted glutaraldehyde.

The enzyme film was stored in buffer or dry at 4°C and remained active for at least 6 months. The film was peeled off the glass plate and cut into small (1 cm²) squares which were attached to the active part of a Clark electrode with a

TABLE 1 Sensitivity of oxidases and dehydrogenases to 50 μM $HgCl_2$. Immobilized oxidases or dehydrogenases (on the surface of UltraBind film) were incubated with 50 μM $HgCl_2$ for 2 min at the indicated pH, in the following buffers: (a) 10 mM sodium malate; (b) 100 mM potassium phosphate; (c) 100 mM glycine/NaOH; (d) 100 mM sodium succinate; (e) 10 mM sodium phosphate containing 700 μM TPP, 10 μM FAD, 5 mM $MgSO_4$ and 100 mM KCl.

Enzymes	*EC*	*pH (buffer)*	*Sensitivity to $HgCl_2$ (50 μM)**
Oxidases:			
L-amino-acid, *Crotalus atrox* (venom)	1.4.3.2	6·5 (b)	−
ascorbate, *Cucurbita* species	1.10.33	5·6 (a)	−
glucose, *Aspergillus niger*	1.1.3.4	5·0 (a)	−
L-glycerophosphate, *Pediococcus* species	1.1.3.21	8·1 (c)	−
L-glycerophosphate, *Streptococcus thermophilus*	1.1.3.21	7·0 (b)	+
L-lactate, *Pediococcus* species	1.13.12.4	7·0 (b)	−
oxalate, barley seedlings	1.2.3.4	3·8 (d)	−
pyruvate, *Pediococcus* species	1.2.3.3	7·0 (e)	+
sulphite, chicken liver	1.8.3.1	7·5 (b)	−
L-tyrosine, mushroom	1.14.18.1	6·5 (b)	−
Dehydrogenases:			
alcohol, equine liver	1.1.1.1	8·8 (c)	−
L-lactate, rabbit muscle	1.1.1.27	7·0 (b)	+
L-lactate, lobster tail	1.1.1.27	6·5 (b)	−
glucose, *Bacillus megaterium*	1.1.1.47	7·6 (b)	−

* + sensitive; − insensitive.

rubber ring (Fig. 1). The average yield of enzyme immobilization was 50%. After the oxygen probe was mounted a 500-fold signal amplification was observed, presumably due to the proximity of the enzyme to the sensitive part of the Clark electrode, resulting in confinement of oxygen on the biosensor.

2.3.2. Covalent binding on affinity membrane

Surface immobilization of enzymes was carried out with affinity membranes (UltraBind US 450 from Gelman Sciences Inc, Ann Arbor, USA).

The surface of the affinity membrane presents (according to Gelman) activated aldehyde groups which react covalently with the amine groups of the protein added. The membrane was mounted on the oxygen electrode above a polypropylene film (Fig. 1). The enzyme (1 unit in 1 μl of 50 mM phosphate buffer, pH 7·0) was added in front of the platinum cathode (diameter 0·2 mm). The affinity membrane was dried completely with a hair dryer (cold air flow) for 2 min. The film was treated for 3 min with 10 μl of 0·1% glutaraldehyde to secure the enzyme to the surface of the film. The yield of immobilization was between 1 and 10%; signal amplification was also observed (about 500-fold). Functioning enzyme films are stable for at least 8 h. In storage, the film was stable for at least 15 days at 4°C in buffer or dry.

2.3.3. Immobilized enzyme measurements

The film with the immobilized enzyme was attached with a rubber toroidal ring to the active part of the Clark electrode, the polypropylene film facing the platinum electrode and the immobilized enzyme facing the measurement cell (Fig. 1). The assay was performed similarly to soluble enzyme. Rinsing three times with 2 ml buffer allows the restoration of 100% oxygen saturation of the electrode. The immobilized enzyme remains on the sensor and can be reutilized.

The initial velocity can be measured in less than 10 s. Restoration of 100% oxygen saturation may take 1–2 min.

3. RESULTS AND DISCUSSION

Heavy metal salt inhibition or inactivation was tested with various oxidases and dehydrogenases,

bios55175p 19-02-93 16:15:40

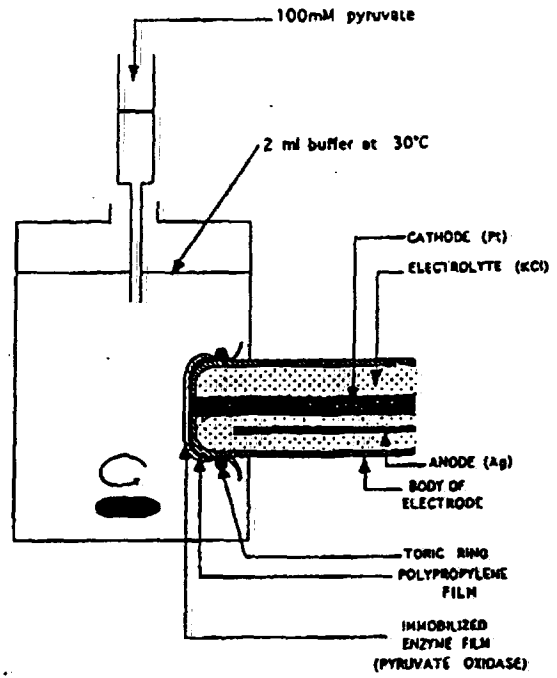

Fig. 1. Biosensor for pyruvate. The oxygen sensor is a Clark electrode, allowing the measurement of oxygen concentration by an amperometric method. If a film of immobilized oxidase (for example, pyruvate oxidase) is tightly bound (with a toric ring) to the sensitive tip above the polypropylene film, a biosensor for pyruvate is obtained.

in solution, reticulated in gelatin film or covalently bound to the surface of an affinity membrane.

Mercury salts appear to be the most potent inhibitors, compared to other heavy metal salts. They were chosen for screening for sensitive oxidases.

After immobilization on the surface of an affinity membrane, oxidases were inactivated and were either sensitive or resistant to 50 μM $HgCl_2$ (Table 1).

Three enzymes (sensitive to $HgCl_2$) were most extensively studied: L-glycerophosphate oxidase (from *Streptoccocus thermophilus*), pyruvate oxidase (from *Pediococcus* species) and L-lactate dehydrogenase (from rabbit muscle) coupled to lactate oxidase (from *Pediococcus* species). Lactate oxidase from *Pediococcus* species, insensitive to $HgCl_2$, was chosen for coupling to L-lactate dehydrogenase.

3.1. Effects of mercuric chloride on L-glycerophosphate oxidase

Initial velocities obtained with the enzyme in solution were measured at various substrate concentrations in the presence of different concentrations of $HgCl_2$. For L-glycerophosphate oxidase, reversible noncompetitive inhibition was observed; K_M and K_I values are reported in Table 2.

After immobilization, either in a gelatin film or on the surface of an affinity membrane, first-order kinetics of irreversible inactivation were obtained as a function of $HgCl_2$ concentration. Results are presented in Fig. 2. This allowed us to determine the 50% inhibition I_{50}: 200 μM for gelatin film, 20 μM for UltraBind and 1 μM for the enzyme in solution.

It was found that surface immobilization increases the sensitivity to $HgCl_2$ as compared with immobilization in a gelatin matrix.

Immobilization of L-glycerophosphate oxidase on the surface of an UltraBind membrane provides a sensitive biosensor for $HgCl_2$.

TABLE 2 $HgCl_2$ inhibition of L-glycerophosphate oxidase, pyruvate oxidase and L-lactate dehydrogenase in solution. Initial velocity was measured at various substrate concentrations in the absence or presence of a fixed concentration of $HgCl_2$. K_M and K_I values were determined by Lineweaver and Burk plots.

Enzymes	*Inhibition*	K_M (mM)	K_I (μM)
L-glycerophosphate oxidase, *Streptococcus thermophilus*	noncompetitive	12 ± 1	1·0 ± 0·2
pyruvate oxidase, *Pediococcus* species	mixed	5·0 ± 0·5	20 ± 2
L-lactate dehydrogenase, rabbit muscle, versus NADH	competitive	0·1 ± 0·2	10 ± 1

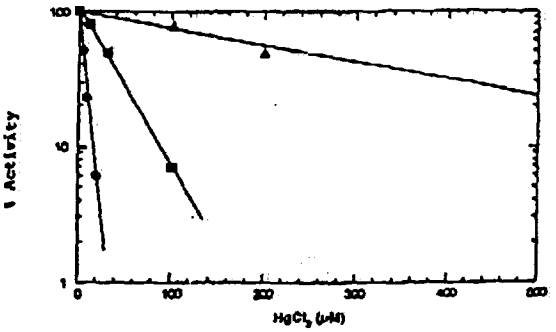

Fig. 2. Effects of various $HgCl_2$ concentrations on L-glycerophosphate oxidase: ●, enzyme in solution; ■, enzyme immobilized at the surface of an affinity membrane (UltraBind); ▲, enzyme immobilized in gelatin. $HgCl_2$ treatment lasted 2 min at 30°C in 0·1 M phosphate, pH 7·0.

3.2. Restoration of activity of immobilized L-glycerophosphate oxidase

After inactivation, mercuric salt could not be removed in three washings with 2 ml of buffer. It was found that addition of 10 mM ethylenediamine tetraacetic acid (EDTA) in buffer was only able to stop the mercuric salt effect, without restoring the activity. In the absence of EDTA, bound $HgCl_2$ remained in the enzymatic film.

To restore activity of the biosensor, 25 mM Dithiothreitol (DTT) in buffer was added in preliminary experiments. However, even after extensive washing of the enzyme film, the sensitivity to mercuric salt was not completely restored, suggesting that some DTT remained in the film. Better results were obtained if, after mercuric salt treatment, successively 10 mM EDTA and only 25 μM DTT were added (Table 3). Under these conditions, the biosensor can be reused for several successive $HgCl_2$ determinations. The restoration of activity takes about 10 min but was not always 100%. This reuse allowed several assays with the same biosensor.

TABLE 3 Inactivation by $HgCl_2$ of L-glycerophosphate oxidase immobilized at the surface of an affinity membrane, and restoration of activity by EDTA plus DTT. The reagents were successively removed by three washings with 2 ml of buffer after each treatment.

Reagents successively added to L-glycerophosphate oxidase biosensor	*% activity*
none	100
50 μM $HgCl_2$	44
10 mM EDTA	40
10 mM EDTA + 25 μM DTT	95
50 μM $HgCl_2$	50

3.3. Effects of mercuric chloride on pyruvate oxidase

In solution, pyruvate oxidase showed mixed reversible inhibition with mercury salt towards pyruvate (Fig. 3). K_M and K_I values are reported in Table 2.

With pyruvate oxidase immobilized at the surface of an affinity membrane, the mercuric salt showed first-order kinetics of irreversible inactivation versus inhibitor concentration.

As shown in Table 4, the inhibition of pyruvate oxidase by mercuric chloride was similar for enzyme both in solution and immobilized. Sensitivity to mercuric chloride was increased by decreasing either the content of Mg^{2+} and TPP in the buffer or the amount of immobilized enzyme. Similar results were described by Tran-Minh (1985): decreasing the amount of urease increased inhibition by fluoride ions. The mixed inhibition kinetics with soluble enzyme and the higher sensitivity to mercuric salt observed on the biosensor with pyruvate oxidase, compared with the other enzymes, suggest the involvement of an —SH group near the active site, as described by Koland & Gennis (1982).

With a decrease in the amount of TPP and

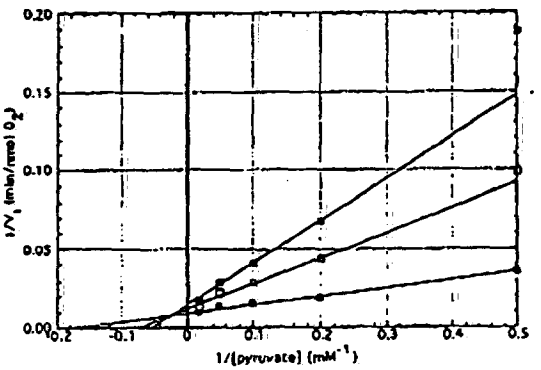

Fig. 3. Mixed inhibition of pyruvate oxidase in solution by $HgCl_2$. Initial velocity (v_i) was measured at various concentrations of substrate with or without a constant amount of ● $HgCl_2$ = 0; □, $HgCl_2$ = 20 mM; ■, $HgCl_2$ = 50 μM.

TABLE 4 Effects of $HgCl_2$ on pyruvate oxidase. Enzyme activity was measured in solution, immobilized in a gelatin film and on an UltraBind film. Low amount of enzyme: 5 μg of pyruvate oxidase on the UltraBind membrane instead of 22 μg in the standard assay. Low mg^{2+} and TPP: buffer containing 45 μM TPP and 0·5 mM $MgSo_4$ compared to standard buffer containing 700 μM TPP and 5 mM $MgSO_4$. Washing of the enzyme immobilized on UltraBind with 10 mM EDTA was necessary to remove TPP and Mg^{2+}.

Pyruvate oxidase	*μM $HgCl_2$ giving 50% inhibition I_{50}*
in solution	10
immobilized in gelatin	25
immobilized on UltraBind film	10
low amount immobilized on UltraBind	0·5
immobilized on UltraBind with low Mg^{2+} and TPP	0·1
low amount immobilized on UltraBind with low Mg^{2+} and TPP	0·05

Mg^{2+} in the buffer and the amount of enzyme, I_{50} for $HgCl_2$ decreased to 50 nM (Table 4).

3.4. Restoration of activity of immobilized pyruvate oxidase

During mercuric salt inactivation of pyruvate oxidase on an affinity membrane, three washings (with phosphate buffer containing Mg^{2+} and TPP) were sufficient to stop inactivation and restore nearly complete activity. Regeneration with buffer containing Mg^{2+} and TPP is possible because of the involvement of an —SH group near the active site. We have found that Mg^{2+} and TPP were sufficient to compete with $HgCl_2$ for the —SH group, allowing nearly complete restoration of enzyme activity. This restoration takes about 10 min and was not obtained if TPP was removed from the washing buffer. Presumably, TPP complexes the $HgCl_2$ and restores an active —SH group. Restoration was not always complete, but it allowed several assays with the pyruvate biosensor.

3.5. Heavy metal salt inhibition of L-lactate dehydrogenase in solution

The reaction of L-lactate dehydrogenase from rabbit muscle (LDH) in solution was initiated by addition of pyruvate and NADH. Pyruvate was transformed to L-lactate by LDH. Immobilized L-lactate oxidase from *Pedioccocus* species (LOD), an enzyme insensitive to heavy metal salts, oxidized the L-lactate, and oxygen consumption was measured.

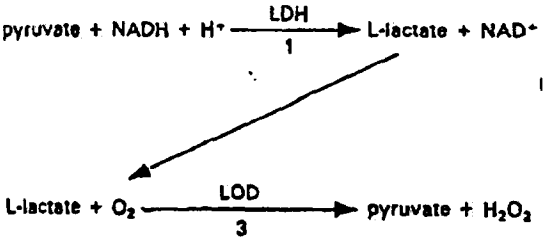

Fig. 4.

After each incubation with heavy metal salts and measurement of L-lactate dehydrogenase inhibition, the LDH in solution in the thermostatted cell was removed by washing. The results are presented in Table 5. LDH was very sensitive to $HgCl_2$ and $AgNO_3$ (I_{50} was respectively 1 and 0·1 μM) when assayed in 0·1 M phosphate buffer, pH 7·0, but sensitive to other heavy metal salts only when tested in 0·1 M Tris–HCl buffer, pH 9·0. The decreasing order of sensitivity was $AgNO_3 > HgCl_2 > CdCl_2$, $ZnCl_2 >$ Pb-acetate $> CuSO_4$.

If a mixture of different heavy metal salts has

TABLE 5 Inhibition of L-lactate dehydrogenase in solution by various heavy metal salts. L-lactate dehydrogenase in solution was coupled with immobilized L-lactate oxidase bound to a Clark electrode. L-lactate dehydrogenase was inhibited by various heavy metal salts. The inactivation was measured, in 0·1M phosphate, pH 7·0 or 0·1 M Tris, pH 9·0 buffer, after 5 min incubation with the heavy metal salts. Remaining activity was determined by addition of 10 mM pyruvate and 1 mM NADH.

Heavy metal salts	*μM giving 50% inhibition*	
	Buffer: Phosphate, 0·1 M, pH 7·0	*Tris–HCl, 0·1 M, pH 9·0*
$HgCl_2$	1	1
$AgNO_3$	0.1	0.1
$CdCl_2$	>500	10
$ZnCl_2$	>500	10
Pb-acetate	>500	50
$CuSO_4$	>500	250

to be determined, $HgCl_2$ can be measured with pyruvate oxidase, $AgNO_3$ with L-lactate dehydrogenase in phosphate buffer, the other heavy metal salts being detected with L-lactate dehydrogenase in Tris–HCl buffer (Table 5).

3.6. Restoration of L-lactate dehydrogenase

It is more convenient to use LDH in solution because it is 10 times more sensitive to $HgCl_2$ or $AgNO_3$ than when immobilized at the surface of UltraBind. Furthermore, when immobilized LDH was used, after inhibition with $HgCl_2$ or $AgNO_3$ it was difficult to restore 100% activity reproducibly. Finally, the very low price of LDH (100 times cheaper than LOD) allows the use of fresh LDH in solution for each assay.

4. CONCLUSIONS

In this paper, detection of heavy metal salts with biosensors is described.

The best detection limit (10 nM $HgCl_2$) was obtained with pyruvate oxidase. This concentration is the maximum tolerated for mercury compounds in drinking water. It is, respectively, 10 and 100 times lower than those obtained with urease by Tran-Minh (1985) and by Mattiasson *et al.* (1978). Good detection of mercury compounds still requires at least 10-fold better sensitivity than this.

The coupling of enzymes allowed the use of dehydrogenases with an oxygen electrode. The restoration of activity after heavy metal salt treatment was not reproducible enough to reuse the same probe many times. We found that it was better to use a mixed biosensor with all enzymes insensitive to heavy metal salt in the immobilized state, and the sensitive enzyme in solution, so that it can be renewed easily for each measurement. Furthermore, enzymes in solution were more sensitive than immobilized enzymes.

Our laboratory is studying organo-metallic compounds soluble in the aqueous phase. Tests in organic solvents may also give interesting results and new applications.

Many problems of metal salt toxicity could be solved by the use of this kind of biosensor because it is possible to perform simple, rapid and multiple assays in the field. Those biosensors designed for heavy metal salt determinations could be used because of the specificity of the sensitive enzymes for heavy metal salt contaminants in medicine, food or the environment.

For each application, research and development will be necessary.

ACKNOWLEDGEMENTS

This work was supported by L'Université Paris 7, Paris (France), Les Fabriques de Tabac Réunies, Neuchâtel (Switzerland) and La Lyonnaise des Eaux, Le Pecq (France).

REFERENCES

Fukano, S. & Chiba, M. (1988). Inhibition mechanisms of δ-aminolevulinic acid dehydratase by heavy metal. I. Application of the immobilized enzyme. *Nippon Eiseigaku Zasshi*, 43(2), 651–8.

Koland, J.G. & Gennis, R.B. (1982). Identification of active site cysteine residue in *E. coli* pyruvate oxidase. *J. Biol. Chem.*, 257(11), 6023–7.

MacGregor, J.T. & Clarkson, T.W. (1974). Distribution, tissue binding and toxicity of mercurials. In: *Protein–Metal Interactions*, ed. M. Friedman, Plenum Press, New York, pp. 463–503.

Mattiasson, B., Danielsson, B., Hermansson, C. & Mosbach, K. (1978). Enzyme thermistor analysis of heavy metal ions with use of immobilized urease. *FEBS Lett.* 85(2), 203–6.

Tran-Minh, C. (1985). Immobilized enzyme probes for determining inhibitors. *Ion-Selective Electrode Rev.*, 7, 41–75.

Webb, J.L. (1966*a*). *Enzyme and Metabolic Inhibitors*, Vol. II, Academic Press, New York. pp. 729–986.

Webb, J.L. (1966*b*). *Enzyme and Metabolic Inhibitors*, Vol. II. Academic Press, New York. pp. 635–53.

Zapata-Bacri, A.M. & Burstein, C. (1988). Enzyme electrode composed of the pyruvate oxidase coupled to an oxygen electrode. *Biosensors*, 3, 227–37.

for measurements of pyruvate in biological media.

L-Lactate oxidase immobilized on the surface of a film bound to an oxygen electrode was used for assays of L-lactate dehydrogenases and various NAD(H)-dependent dehydrogenases and their substrates.

Ahmed HAOUZ, Annette GELOSO-MEYER and Claude BURSTEIN.

Laboratoire de Technologies des Enzymes et des Biomembranes. Hall de Biotechnologies. Tour 54. Université Paris 7. 2, place Jussieu. 75251 Paris Cedex 05.

Summary

Coimmobilization of L-lactate oxidase (LOD) and L-lactate dehydrogenase (LDH) on the surface of an affinity membrane tightly bound to an oxygen electrode permits recycling of L-lactate and pyruvate and lowers the detection limit of their assays to 10 nM.

For a better quantification of L-lactate dehydrogenase measurements, the lactate biosensor was built with immobilized L-lactate oxidase. L-lactate dehydrogenase was added in solution. This permits very easy measurements of L-lactate dehydrogenase. The detection limit of LDH was 1 IU/l.

In the case of inactivation by various heavy metal compounds, this technique allows one to use the same L-lactate biosensor many times, by renewing L-lactate dehydrogenase for each assay. Organomercurial (PHMB) measurement is described as an example. 10 μM PHMB could be detected.

Furthermore, the biosensor with coimmobilized lactate oxidase and lactate dehydrogenase permits a rapid screening of numerous dehydrogenases in solution for their sensitivity to various heavy metal substances.

Coupling coimmobilized LOD + LDH with an extra NAD(H)-dependent dehydrogenase allows the measurements of all dehydrogenases, their substrates and NAD^+, with a Clark electrode. Moreover, this coupling recycles NAD^+ and permits the use of dehydrogenases in bioreactors.

Key words : enzyme immobilization, biosensors, bioreactors, coupling and recycling, NAD(H)-dependent dehydrogenase, detection of PHMB, detection of L-lactate and LDH.

Introduction

Immobilization of enzyme was often considered a prerequisite for industrial utilization in bioreactors (preparative techniques) or biosensors (analytical devices). Immobilization in most cases stabilizes enzyme activities. Furthermore, the solid state of the enzyme allows easy reuse. These properties decrease the cost utilization of the catalysts and permit the industrial spread of these enzyme technologies.

Concerning biosensors, the multiplicity of available probes is great. Various sensors can be used (amperometric, voltametric, optic, ...). For each enzyme, a new biosensor can be designed. 10,000 metabolic reactions are catalysed by 10,000 specific enzymes. Furthermore, the same reaction can be catalysed by enzymes from various sources : microbial, animal or vegetal. Even in one animal the enzymes from different tissues (muscle, heart, liver) present different kinetic constants (K_M, V_M, optimum pH) and different properties (stability). This diversity may explain the difficulties encountered when comparing the data of various scientific papers (Schmidt 1991).

The use of one type of sensor is valuable if it covers the utilization of a large number of enzymes. We have chosen the Clark electrode which is an oxygen sensor (amperometric method). This electrode is easy to use. All oxidases using oxygen as cosubstrate can be used to construct a biosensor. Crude extracts, turbid or colored, can be measured without pretreatment.

For some needs, depending on the field of use, the assay may not be sensitive enough. Coupling an oxidase and the corresponding dehydrogenase amplifies the signal by a factor between 10 and 4,000, as described in the literature (Schmidt 1991). We have chosen the coupling of L-lactate oxidase (LOD) and L-lactate dehydrogenase (LDH), which seems to give the best results. Furthermore, in the present paper, by coupling LOD + LDH to an extra NAD(H)-dependent dehydrogenase, we show the possibility of measuring, with a Clark electrode, all dehydrogenases, their substrates and NAD^+.

Materials and Methods

Most of the enzymes and substrates were purchased from Sigma, except alcohol dehydrogenase (from yeast), L-lactate dehydrogenase (from rabbit muscle) and NAD^+, purchased from Boehringer.

Buffer and pH depended on the enzyme used in the assay:

- 0.1 M phosphate, pH 6.5 or 7.0, for L-lactate oxidase (LOD) and L-lactate dehydrogenase (LDH), glucose and L-glutamate dehydrogenase ;
- 0.1 M glycine-NaOH, pH 9.5, for L-malate dehydrogenase ;
- 0.1 M glycine-NaOH, pH 8.6, for alcohol dehydrogenase ;
- 0.1 M Tris, pH 8.0, for L-α-glycerophosphate dehydrogenase.

oxygen consumption measurements

Oxygen consumption was measured amperometrically at - 700 mV, with a Clark electrode covered with a polypropylene film (6 μM thick from Bollore Inc., Paris, France). This hydrophobic film protects the electrode against various soluble contaminations. Buffer saturated with air at 30°C gave 100% oxygen concentration (240 μM). 0% oxygen was obtained with glucose oxidase in solution plus saturated substrate (addition of 100 mM glucose). The assay lasts less than 10 sec. The assay was performed in 2 ml.

Measurements of enzymes in solution

The Clark electrode was covered with the polypropylene film. Soluble oxidases or oxidase + dehydrogenase were added with their substrates and oxygen consumption was measured versus time in 2 ml of buffer at 30°C.

If enzyme activities were to be measured, substrate concentration [S] was 10 K_M to obtain V_M. If substrate concentrations were to be measured, [S] was < $K_M/3$ to obtain a pseudolinearity with substrate concentrations.

The detection limit was the lowest amount of substrate easily detected in our conditions (about $K_M/100$).

Activities of dehydrogenases alone were tested in solution by measuring the variation of absorption of NADH at 340 nm.

Enzyme immobilization

Enzymes were bound covalently on the surface of an affinity membrane (UltraBind US 450, from Gelman Sciences Inc., Ann Arbor - USA).

The surface of the affinity membrane presents, according to Gelman, activated aldehyde groups which react covalently with some of the amino groups of the protein (NH_2 at ε position of lysine). The membrane was tightly bound with a toroidal ring to an oxygen electrode above the polypropylene film as shown in Fig. 1. Enzymes (0.1 to 1 IU) in less than 5µl of 0.05 M phosphate buffer pH 7.0 were added in front of the platinum cathode. The affinity membrane was dried with a hair dryer (cold air flow) for 1 min. The enzyme was more tightly bound to the surface by treatment with 0.1% to 0.5% glutaraldehyde in cold water, for 1 min. The film was washed 3 times with 0.1 M phosphate buffer pH 7.0 to remove excess glutaraldehyde. The immobilized enzyme faced the buffer (2 ml) thermostatted at 30°C (Fig.1).

The overall preparation takes less than 5 min.

Functioning enzymes were stable for at least a week. With dehydrogenases, better results can be obtained by addition during immobilization of 10 mM NAD^+, which protects these enzymes.

Respiratory chain from *E. coli* membranes.

E. coli was broken with a French press at 20,000 PSI (approximatively 1600 bars). Unbroken bacteria and cell wall fragments were discarded in the pellet after 20 min centrifugation at 15,000 rpm. Inverted membrane vesicles were collected in the pellet after 3 hours centrifugation at 50,000 rpm.

The vesicles were stored at -80°C in 10 mM phosphate buffer, pH 7.0. 10 µg of protein were immobilized either in 5% gelatin reticulated with 1% glutaraldehyde for 2 min (according to Burstein *et al.* 1984) or at the surface of a nylon membrane (Ioprodyne PALL-Corporation, New York) without any addition of glutaraldehyde.

Immobilized enzyme measurements

The assay was started by addition of the substrate. The assay lasts less than 10 sec. The film was washed 3 times with 2 ml of the appropriate buffer, for approximately 2 min to restore 100% oxygen saturation and the biosensor can be reused every 2 min. The average error was less than 10%.

Results

Recycling of L-lactate and pyruvate

When L-lactate oxidase (LOD) was coimmobilized with L-lactate dehydrogenase (LDH), the addition of pyruvate + NADH initiated the formation of L-lactate, which is oxidized by L-lactate oxidase according to the following equations :

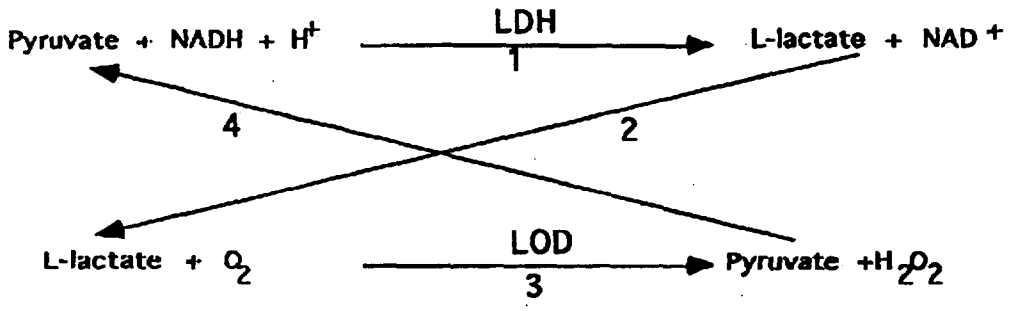

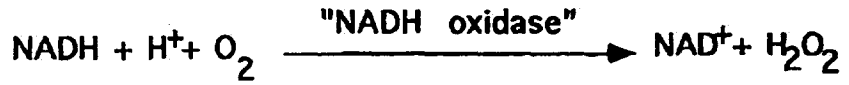

The two chemical reactions are coupled, the net reaction is an apparent "NADH oxidase". This allows the assay of pyruvate, L-lactate and NADH. Kinetic results are presented in Table 1. Only L-lactate and pyruvate are recycled, allowing a detection limit of 10 nM.

When a low amount of L-lactate (1 μM) was added (Fig. 2,A), the measured signal of oxygen consumption was very low. All the L-lactate was consumed and transformed into pyruvate within a few seconds (one cycle of L-lactate oxidation). Further addition of 15 mM NADH (Fig. 2,B) initiates the recycling of L-lactate. The 1μM pyruvate produced by LOD after L-lactate addition, is now transformed into L-lactate by LDH. L-lactate was recycled about 200 times until oxygen was completely consumed in the measurement cell (2 ml). The reaction mixture was removed from the measurement cell (Fig. 2,C) and reoxygenated by vigourous agitation, before reintroduction into the measurement cell. Without any further addition, oxygen consumption resumed until anaerobiosis was once more attained. L-lactate was again recycled 200 times. Oxygenation was repeated (Fig. 2,C). After

5-fold reoxygenation, L-lactate was recycled 1,000 times (it can continue until all the NADH is consumed).

An amplification of L-lactate measurements of 4,000 was observed. The detection limit of the assay was decreased from 40 μM to 10 nM (Table 1).

NADH was not recycled (Table 1).

ASSAYS OF L-LACTATE DEHYDROGENASE WITH THE LOD BIOSENSOR.

The UltraBind film is saturated with 20 μg of protein facing the electrode. Furthermore, only the enzyme facing the cathode (0.2 cm diameter) is functional. The spot of the enzyme deposited has a higher diameter, part of the enzyme is lost.

A mixed biosensor with immobilized LOD and LDH in solution is much easier to handle. As shown in Fig. 3, a linear relationship between V_M and LDH concentration was obtained. 1 IU/l was the detection limit. A small background was observed, due presumably to nonspecific binding of a small amount of substrate or enzyme to the film.

USE OF COUPLED DEHYDROGENASES FOR MEASUREMENTS OF HEAVY METAL COMPOUNDS

Dehydrogenases are considered to be very sensitive to heavy metal compounds. They are a good tool for measuring a variety of heavy metal compounds.

For instance we have measured with an LOD biosensor combined with soluble LDH the sensitivity to organomercurials (PHMB). In preliminary experiments we screened for the most sensitive LDH. Amongst the LDHs, available in the Sigma catalog (7 tested), LDH from rabbit muscle was the most sensitive; in contrast, LDH from lobster tail was completely resistant. LDH inactivation is pseudo order 1 (Fig. 4). The plot $k_{obs} = f(I)$ allows the measurement of PHMB (Fig. 4). LDH from rabbit muscle was sensitive to 10 μM organomercurials at pH 7.0. To restore the activity, before the next assay, it was found particularly easy to remove the sensitive LDH in solution by washing the biosensor.

LDH is not protected by NADH against PHMB inactivation. The cysteine reacting with PHMB seems to be different from the SH reacting with $HgCl_2$. This latter inactivation was protected by NADH. PHMB does not reach the same site as $HgCl_2$, probably because of steric hindrance. The NAD(H)-

dependent dehydrogenase assay is described in more detail in the following paragraph.

To test the sensitivity to mercurials of various NAD(H)-dependent dehydrogenases in solution, with a Clark electrode, LOD from Pediococcus species was used coimmobilized with LDH from lobster tail, these two enzymes being insensitive to mercurials.

ASSAYS OF DEHYDROGENASES WITH LOD + LDH COIMMOBILIZED.

As shown above, LOD coimmobilized with LDH results in an apparent "NADH oxidase".

If "NADH oxidase" is coupled to a dehydrogenase such as alcohol dehydrogenase, the following equations can be written :

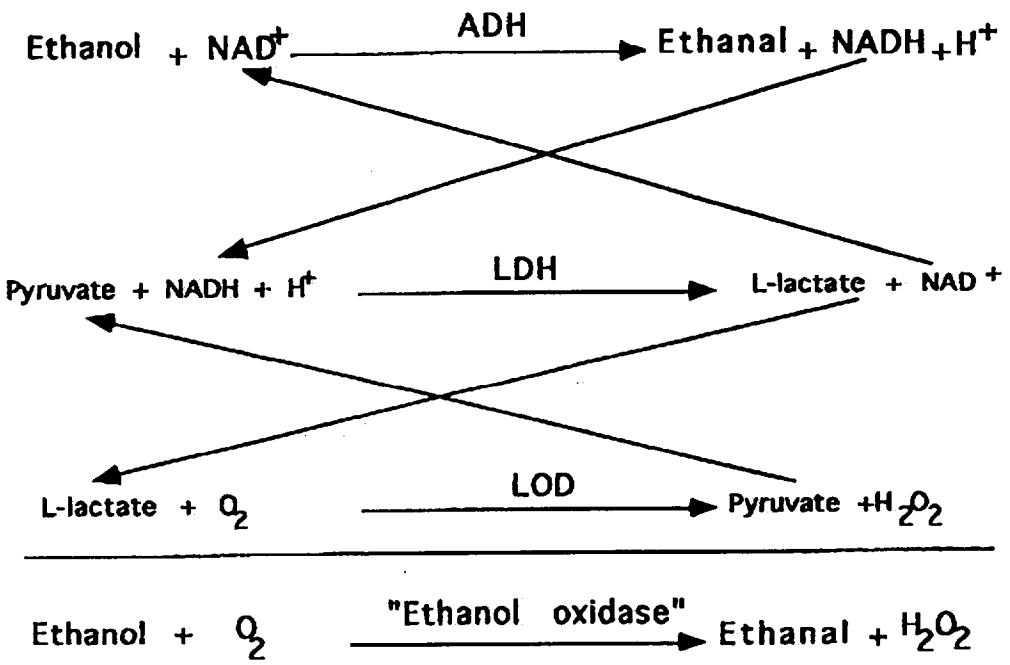

the net reaction is an apparent "ethanol oxidase". NAD^+ is recycled. Thus, the coupling of these 3 reactions allows the assay of NAD(H)-dependent ethanol dehydrogenase and its substrate and recycling of NAD^+ with 50 nM as detection limit.

If alcohol dehydrogenase is replaced by another dehydrogenase in the presence of its specific substrate, analogous reactions can be produced, as for example for L-α-glycerophosphate, L-malate, glucose and L-glutamate.

The five dehydrogenases can be successively immobilized with LOD + LDH and are easily utilized on an oxygen probe. Results are presented in Table 2.

We previously described (Burstein *et al.* 1981) the use of the immobilized respiratory chain as "NADH oxidase". The respiratory chain immobilized in gelatin reticulated with 1% glutaraldehyde gave no more than 0.06 µmol./min O_2 consumed. In contrast, the two lactate enzymes as described above (Table 1) allowed us to reach 2 µmol./min O_2 consumed. The respiratory chain from *E. coli* when immobilized (by adsorption instead of covalent fixation) at the surface of the nylon membrane (loprodyne from Pall) gave 3 µmol./min O_2 consumed. The respiratory chain may also be used as "NADH oxidase" immobilized at the surface of a nylon film in absence of glutaraldehyde.

The use of a mixed biosensor with immobilized LOD + LDH or the respiratory chain and a dehydrogenase in solution permits the quantitative assay of all dehydrogenases with an oxygen electrode. It is more difficult to prepare the respiratory chain than to buy LOD + LDH. The respiratory chain contains many other dehydrogenases (succinate, lactate, malate, glycerophosphate...); as described by Burstein *et al.* 1984, these dehydrogenases may disturb the assays.

CONCLUSIONS

The use of UltraBind allows the covalent fixation of the enzymes on the surface of the film. The immobilization technique takes less than 5 min. No extra dialysis membrane (which may limit the diffusion of substrates) is needed to maintain the enzyme at the surface of the film.

The instrument needed for the assay is small and inexpensive and may be used in the field. The amount of enzyme per biosensor is 1 IU (which is much less than the utilization in the literature which is between 40 IU and 1000 IU). The assay time is particulary short (less than 10 sec) compared to 10 to 30 min.

In this paper, we have shown that chemical coupling of reactions performed by coimmobilized L-lactate oxidase and L-lactate dehydrogenase allows 4,000-fold recycling of L-lactate and pyruvate. This recycling was already described by Scheller *et al.* in 1985, using a thermistor. The use of a Clark electrode and UltraBind film make the biosensor much easier to build. The oxygen electrode described by Mizutani (1983 and 1985), Schubert (1985) and Wollenberger (1987) gave results with lower performances than ours, probably due to the immobilization technique.

We have used the L-lactate amplification to miniaturize the assay of L-lactate and pyruvate in one drop of blood, without preliminary treatment, in 10 sec. A routine test is now accessible for intensive care or in sport medicine, for example.

We have tried the coupling of other oxidases and corresponding dehydrogenases (alcohol or glucose). The amplification observed was never as good as with L-lactate. Similar results were presented by Ollson *et al.* (1986) for alcohol and Schubert *et al.* (1985) for glucose. The differences of amplification observed may be the result of various equilibrium constants for each reaction considered. With glucose oxidase, the product of the reaction, gluconolactone, is quickly hydrolysed to form gluconate. This reaction impairs the recycling.

These coupled assays of LOD + LDH allow the measurement of L-lactate and LDH in cell culture. When cells are alive they excrete L-lactate. When cells are dying or injured, they liberate L-lactate dehydrogenase. The use of LDH measurements was described as a marker of cell injury and death by Mizutani (1985) and more recently by Legrand *et al.* (1992). The assay in the latter paper was performed by a Boehringer test kit, which is much less

convenient than the biosensor proposed in the present paper. The assay of LDH in solution with the LOD biosensor permits an easy test of a healthy cell culture. These measurements need to be generalized. Automatized, they will solve monitoring of cells in culture. Clinical control is also feasible in acute myocardial infection, congestive heart disease, pernicious anemia, coronary artery disease or hepatitis.

Coupling a NAD(H)-dependent dehydrogenase with "NADH oxidase" permits the transformation of dehydrogenase reactions (3,000 enzymes are dehydrogenases among the 10,000 enzymes supposed to exist) into oxidase reactions (allowing the use of the oxygen probe).
In the case of a bioreactor, the use of coimmobilized LOD + LDH or the immobilized respiratory chain may solve the problem of recycling NAD^+ for dehydrogenase utilization and permits a new generation of bioreactors using NAD(H)-dependent dehydrogenases which were not utilizable because of the cost of the cofactor.

The detection limit for PHMB was found to be 10 μM. This is far too high to be used for determination of mercuric compounds in drinking water (the norm is 10 nM). In a recent paper, Gayet *et al* (1993) showed that the use of pyruvate oxidase allows one to reach this value for $HgCl_2$. A 10-fold more sensitive assay is still needed. One way is to screen various dehydrogenases in solution. The use of immobilized LOD + LDH allowed the screening of soluble dehydrogenases sensitive to various heavy metal compounds : in medicine, food industry and environmental problems.

Acknowledgements:

This work was supported by Bertin "et Cie", Plaisir (France), "les Fabriques de Tabac Réunies", Neuchâtel (Suisse), "La Lyonnaise des Eaux", Le Pecq (France) et "L'Université Paris 7", (France).

REFERENCES

Burstein, C., Ounissi, H., Legoy, M.D., Gellf, G. and Thomas, D. "Recycling of NAD+ using coimmobilized alcohol dehydrogenase and *E. coli* ". (1981) *Applied Biochemistry and Biotechnology* 6, 329-338.

Burstein, C., Adamowicz, E., Boucherit, K. Rabouille, C. and Romette, J-L. "Immobilized respiratory chain activities from *Escherichia coli* utilized to measure D- and L-lactate, succinate, L-malate, 3-glycerophosphate, pyruvate, or NAD(P)H." (1986) *Applied Biochemistry and Biotechnology* 12, 1-15.

Legrand, C., Bour, J.M., Jacob, C., Capiaumont, J., Martial, A., Marc, A., Wudtke, M., Kretzmer, G., Demangel, C., Duval, D. and Hache, J. "Lactate dehydrogenase (LDH) activity of the number of dead cells in the medium of cultured eukaryotic cells as marker." (1992) *Journal of Biotechnology* 25, 231-243.

Mizutani, F., Sakasi, K. and Shimura, Y. "Sequential determination of L-lactate and lactate dehydrogenase with immobilized enzyme electrode." (1983) *Anal. Chem.* 55, 35-38.

Mizutani, F., Yamanaka, T., Tanabe, Y. and Tsuda, K. "An enzyme electrode for L-lactate with a chemically amplified response." (1985) *Analytica Chimica Acta* 177, 153-166.

Scheller, F., Siegbahn, N., Danielsson, B. and Mosbach, K. "High-sensitivity enzyme thermistor determination of L-lactate by substrate recycling." (1985) *Anal. Chem.* 57, 1740-1743.

Schmidt, H.L., Schuhmann, W., Scheller, F.W. and Schubert, F. "Specific features of biosensors." (1991) *Chemical and Biochemical Sensors*, VCH, Weinheim 3, 719-817.

Schubert, F., Kirstein, D., Schröder, K.L. and Scheller, F.W. "Enzyme electrodes with substrate and co-enzyme amplification." (1985) *Analytica Chimica Acta* 169, 391-396.

Figure 1. Biosensor composed with an oxygen electrode covered with a film of immobilized L-lactate oxidase.

The hydrophobic polypropylene film, facing the electrode, permits only gas (oxygen) to flow through.

The enzyme immobilized on the UltraBind film is facing the measurement cell. The assay was performed by addition of 20 mM L-lactate at 30°C in 2 ml of 0.1 M phosphate buffer at pH 7.0.

Figure 2. Recording of oxygen consumption with LOD and LDH coimmobilized on the surface of the UltraBind film.

In A, 1 μM L-lactate is introduced,

in B, 15 mM of NADH is introduced,

in C, complete oxygen consumption is observed, followed by reoxygenation (the 2 ml of reaction mixture was removed from the cell and violently mixed with a vortex before reintroduction in the cell). Reoxygenation was repeated in C.

Figure 3. Titration curve of LDH measurements with a biosensor (oxygen electrode + LOD immobilized).

LDH was introduced in solution and rinsed for each measurement.

Assay was performed by simultaneous addition of 15 mM NADH and 2 mM pyruvate in 0.1 M phosphate buffer at pH 6.5.

Figure 4. Kinetics of PHMB inactivation of soluble rabbit muscle LDH, incubated at 30°C with various amount of PHMB (◇ 10 μM, □ 25μM, × 50μM, ■ 75μM). The activity of LDH was measured with the LOD biosensor as described in Fig. 3.

Table 1. Kinetic results obtained with LOD and LDH coimmobilized on a Clark electrode, as described in Fig. 3.

After each measurement, the substrates are rinsed.

L-lactate without recycling was measured in the absence of NADH.

K_M and V_M were determined from a Lineweaver-Burk plot.

Table 2. Kinetic results obtained with various immobilized dehydrogenases coupled to immobilized LOD + LDH.

Table 1.

assay of	K_M mM	V_M µmol./min of O_2 consumed	During recycling Detection limit nM	Without recycling Detection limit nM
L-lactate	2	18	10	40,000
pyruvate	0.2	10	10	40,000
NADH	3	2	5,000	5,000

Table 2.

dehydrogenase E.C	Source of enzyme	pH of Buffer	K_M (mM) specific substrate	K_M (mM) NAD^+	V_M µmol./min of O_2 consumed	Detection limit µM of specific substrate
alcohol 1.1.1.1	baker yeast	8.6	3	1.0	2.0	20
L-α-glycerophosphate 1.1.1.8	rabbit muscle	8.0	14	0.07	3.7	70
L-malate 1.1.1.37	pigeon breast	9.5	26	0.13	2.8	150
glucose 1.1.1.47	Bacillus megaterium	7.0	10	0.05	8.0	100
L-glutamate 1.4.1.3	beef liver	7.3	5	0.5	5.5	50

Fig.1

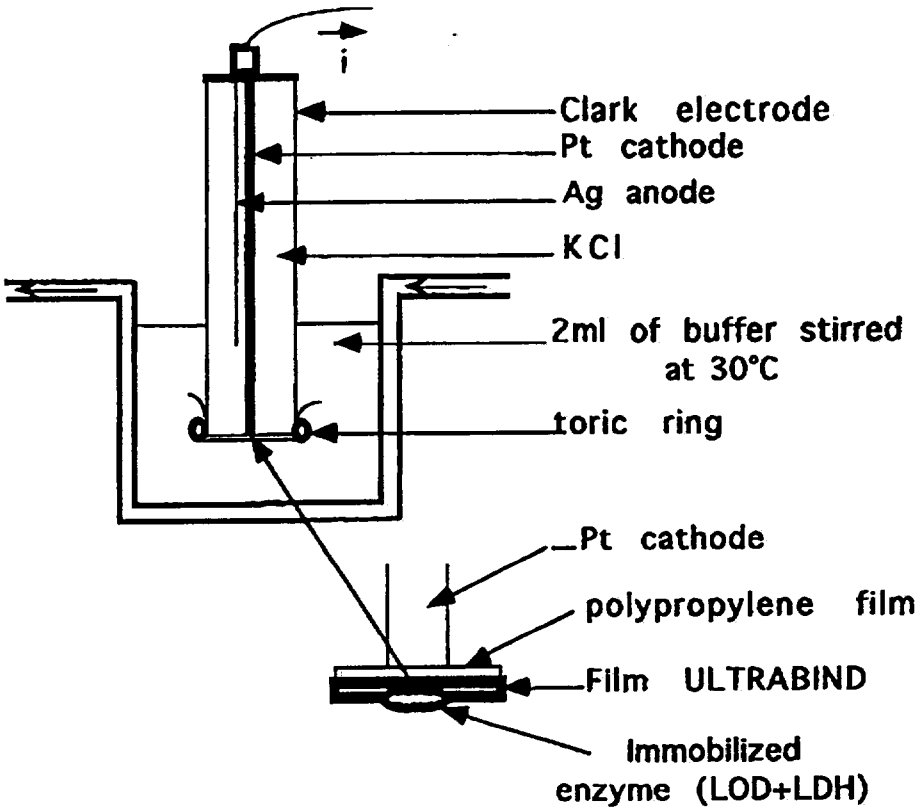

Fig. 2

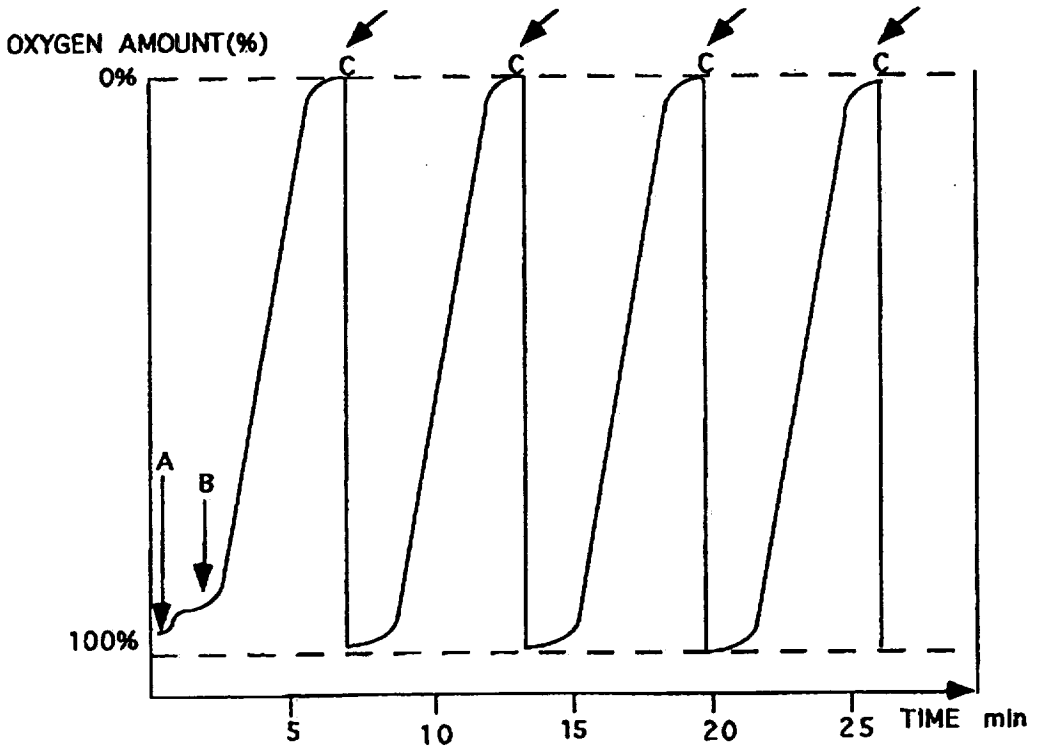

2023252048

Fig. 3

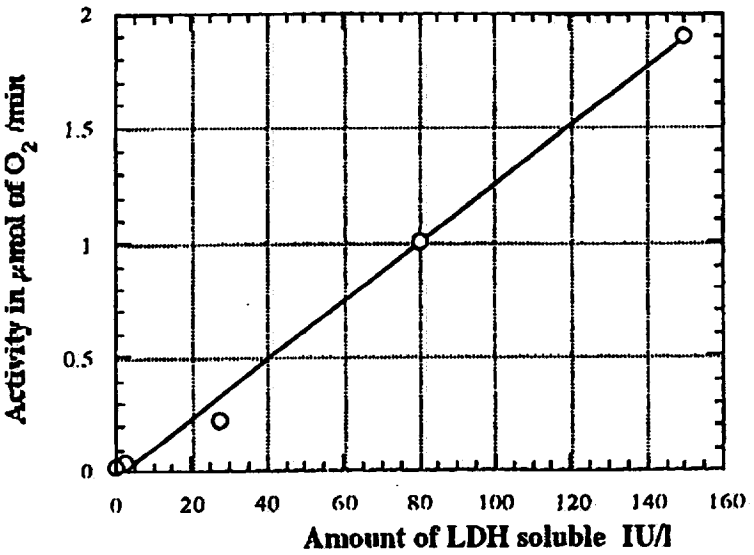

Fig. 4

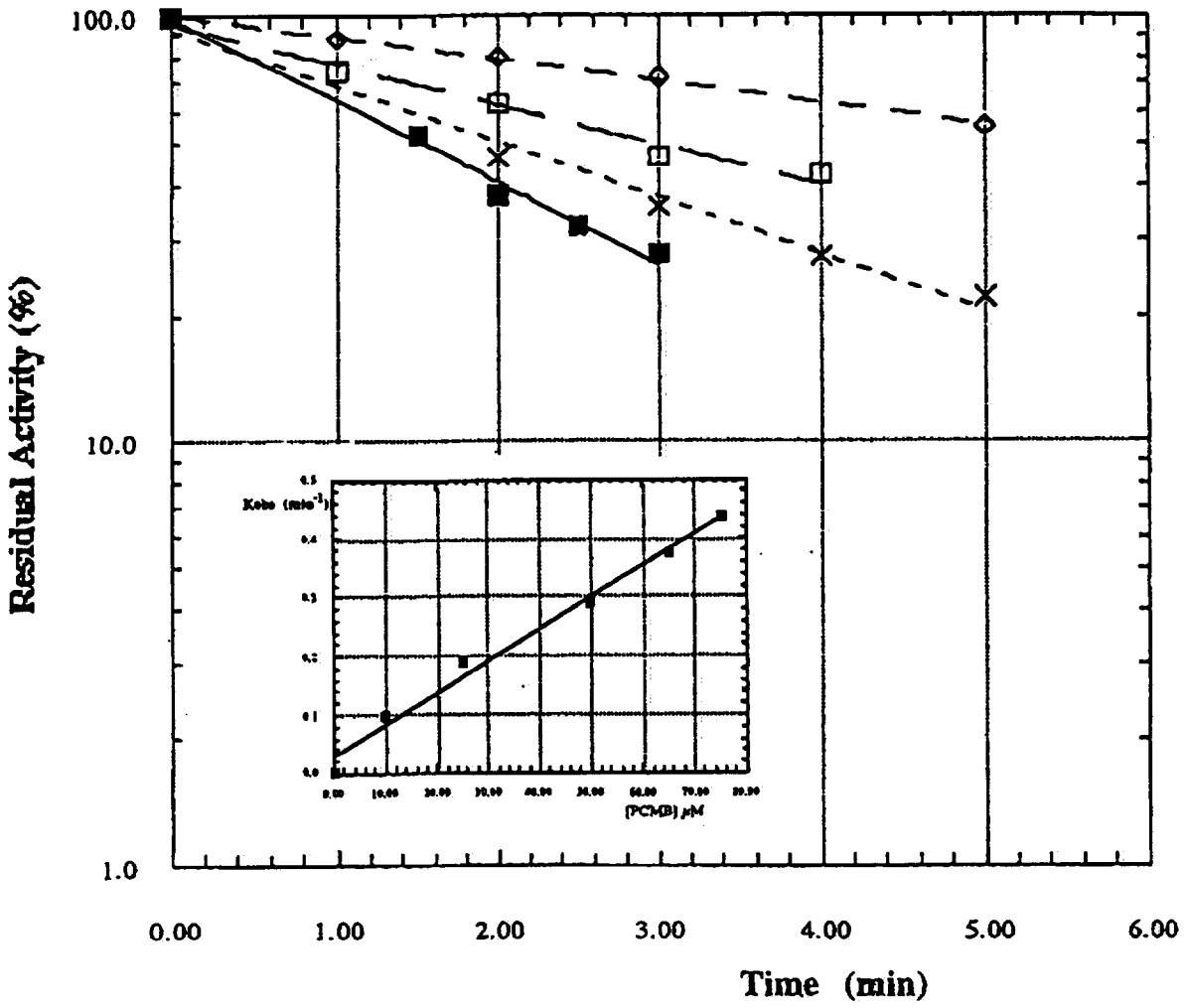

CABOCHE, J.

In Prof. J.M. BESSON's group.
Laboratory of Neurochemistry - Anatomy
University of Paris 6.

Dr. J. Caboche, University of Paris, France

1. Title : Parallel Decrease of Glutamic Acid Decarboxylase and Preproenkephalin in the Rat Striatum Following chronic Treatment with a Dopaminergic D1 Antagonist and D2 Agonist.

   Source : J. Neurochem. 1991, 56, 428-435.

   Authors : Caboche, J., Vernier, P., Julien, J.F., Rogard, M., Mallet, J. & Besson, M.J.

2. Title : Rôle de la Nicotine dans la Régulation des ARN Messagers codant pour la Préproenképhaline dans le Striatum du Rat.

   Source : Sem. Hôp. Paris, 1992, 68, N° 36-37, 1296-1297.

   Authors : Caboche, J., Rogard, M. & Besson, M.J.

RÔLE DE LA NICOTINE DANS LA RÉGULATION DES ARN MESSAGERS CODANT POUR LA PRÉPROENKÉPHALINE DANS LE STRIATUM DU RAT

J. CABOCHE, M. ROGARD, M.J. BESSON

CABOCHE J., ROGARD M., BESSON M.J. — Rôle de la nicotine dans la régulation des ARN messagers codant pour la préproenképhaline dans le striatum du rat. **Sem Hôp Paris**, 1992, **68**, n° 36-37, 1296-1297.

RÉSUMÉ : Les taux d'ARN messagers (ARNm) codant pour la préproenképhaline (PPE), précurseur de l'enképhaline, et la glutamique acide décarboxylase (GAD), enzyme de biosynthèse du GABA, ont été mesurés par la technique d'hybridation *in situ*, dans le noyau caudé-putamen et le noyau accumbens du rat, après des traitements chroniques avec de la nicotine (injection sous-cutanée quotidienne, 0,35 mg/kg, pendant 15 jours). L'injection chronique de nicotine produit une augmentation significative des taux d'ARNm codant pour la PPE dans le noyau caudé (+23 %, $p<0,01$), et le noyau accumbens (+32 %, $p<0,005$), par comparaison aux taux d'ARNm PPE mesurés chez des rats contrôles. Aucune modification des taux d'ARNm GAD n'a été décelée. Cette étude pose le problème important du rôle de la nicotine dans la régulation génique sélective de l'enképhaline dans le striatum de rat, rôle pouvant s'exercer par des récepteurs nicotiniques postsynaptiques.

MOTS-CLÉS : Nicotine. — ARN messagers. — Glutamique acide décarboxylase. — Préproenképhaline. — Striatum. — Noyau accumbens. — Dopamine.

La nicotine exerce un rôle important au niveau du système nerveux central dans l'addiction au tabac chez l'homme (Clarke, 1987 [2]). Chez le rat, des substances addictives telles que l'amphétamine et la cocaïne exercent leur action en activant le système dopaminergique du cerveau, et plus particulièrement le système DA mésolimbique (Fibiger et Phillips, 1987 [4]). De même, il a été montré que la nicotine a un effet stimulateur sur la libération de dopamine (DA), plus important dans le noyau accumbens, structure cible du système DA méso-striatal, mais aussi dans le noyau caudé-putamen, zone de projection de la voie DA nigro-striatale (Imperato et al., 1986 [6]).

Le but de notre étude était de voir si l'injection chronique de nicotine pouvait, soit par son rôle facilitateur sur la libération de DA, soit par un effet direct sur les neurones striataux, réguler l'activité des neurones striataux. Nous avons choisi pour cela d'analyser, par la technique d'hybridation in situ, les taux d'ARN messagers (ARNm) codant pour les précurseurs de deux des neurotransmetteurs du striatum : la préproenképhaline (PPE) précurseur de l'enképhaline et la glutamique acide décarboxylase (GAD) enzyme de biosynthèse du GABA.

Des rats mâles ont été injectés quotidiennement, par voie sous-cutanée, à l'aide de (−) nicotine di (+) tartrate (Sigma) (0,35 mg/kg) ou de NaCl 9 ‰ (rats contrôles). Après 15 jours de traitement les rats ont été perfusés par voie intracardiaque à l'aide de paraformaldéhyde à 2 %, puis des coupes frontales de 10 µm d'épaisseur de toute l'extension rostro-caudale du striatum ont été préparées. Ces coupes ont été mises en présence de sondes ADN complémentaires (ADNc) marquées au ^{35}S, et spécifiques des ANRm codant pour la PPE ou la GAD.

Après exposition de ces lames sur film autoradiographique, les signaux d'hybridation obtenus avec les sondes ^{35}S-ADNc-PPE et -GAD, ont été quantifiés à l'aide d'un système d'analyse d'images informatisé (IMSTAR, France). Nos résultats montrent que les taux d'ANRm-PPE augmentent de façon significative dans le noyau caudé (+26 %, $p < 0,01$) et le noyau accumbens (+32 %, $p < 0,005$) chez les rats traités de façon chronique à l'aide de nicotine, par comparaison avec leur contrôle (n = 4 rats

Laboratoire de Neurochimie-Anatomie, IDN, Université Paris 6, 9, quai St-Bernard, 75005 PARIS.

pour chaque groupe). En revanche, aucune régulation des ARNm-GAD n'a été trouvée, dans ces deux régions.

La nicotine semble donc produire une activation sélective des neurones ENK dans l'ensemble du striatum, noyau caudé-putamen et noyau accumbens se traduisant par une augmentation de l'expression des ARNm codant pour le précurseur de l'ENK : la PPE. Des augmentations d'ARNm-PPE d'amplitude similaire ont été retrouvées après une interruption de la transmission DA par administration d'un neuroleptique. A l'inverse, la stimulation des récepteurs DA (principalement des DA-D_2) induit une réduction des taux d'ARNm-PPE (Caboche et al., 1991 [1] ; Giraud et al., 1991 [5]). L'administration chronique de nicotine ayant un effet opposé à celui obtenu par stimulation des récepteurs DA, il ne semble pas que les augmentations d'ARNm-PPE observées dans cette étude résultent de l'action facilitatrice de la nicotine sur les récepteurs DA. Nos résultats suggèrent au contraire une action directe de la nicotine sur les neurones ENK striataux. De fait, dans le striatum, il semble que les récepteurs nicotiniques ne soient pas exclusivement localisés sur les fibres DA puisqu'après lésion des neurones DA les sites de fixation de la ^{3}H-nicotine ne disparaissent pas complètement (Clarke and Pert, 1985 [5]). Comme il est maintenant établi que le Ca^{2+} intervient dans la régulation du gène de la PPE (Van Nguyen et al., 1990 [7]), l'augmentation des taux d'ARNm-PPE produite par le traitement chronique avec de la nicotine, pourrait être due à une entrée de Ca^{2+} consécutive à l'activation des récepteurs nicotiniques.

En ce qui concerne l'absence de modifications des taux d'ARNm-GAD après administration chronique de nicotine, plusieurs hypothèses peuvent être émises pour tenter d'interpréter ce résultat :

1) si l'on admet l'existence des récepteurs nicotiniques sur les neurones striataux, il est possible que la stimulation de ces récepteurs soit dépourvue d'effet sur la régulation du gène de la GAD ;

2) la nicotine en favorisant la libération de DA peut provoquer une régulation opposée des ARNm-GAD dans les deux principales sous-populations de neurones striataux efférents. En effet ces sous-populations qui expriment préférentiellement soit les récepteurs DA-D2 (couplés négativement à l'adényl cyclase), soit les récepteurs DA-D1 (couplés positivement à cet enzyme) sont régulés différentiellement (inhibition ou activation) par la DA. L'analyse globale après radioautographie sur film ne permettant pas de déceler ces régulations différentielles, une analyse au niveau cellulaire permettra d'élucider ce point.

En conclusion, certains de ces effets addictifs de la nicotine pourraient résulter d'une activation de la synthèse de l'ENK au niveau du striatum et plus précisément dans les régions limbiques de cette structure système.

DISCUSSION

Pr McLEOD

J'avais une curiosité en regardant votre poster sur les durées d'action de la nicotine. Y-a-t-il une raison particulière pour faire ces injections pendant 15 jours ? Est-ce que cela fait partie d'un plan ou est-ce qu'il y en aura d'autres...

J. CABOCHE

Absolument. Pour l'instant, nous avons commencé des traitements chroniques vu les données de la littérature. Il semble maintenant qu'un traitement plus court puisse permettre d'obtenir une telle régulation et il conviendra de voir si ces modulations dureront après cessation du traitement.

J.C. ORSINI

Courte durée ça signifie combien ?

J. CABOCHE

3 heures.

RÉFÉRENCES

1. CABOCHE J., VERNIER P., JULIEN J.F., ROGARD M., MALLET J., BESSON M.J. — Parallel decrease of glutamic acid decarboxylase and preproenkephalin in the rat striatum following chronic treatment with a dopaminergic D1 antagonist and D2 agonist. *J Neurochem*, 1991, *56*, 428-435.
2. CLARKE P.B.S. — Nicotine and smoking : a perspective from animal studies. *Psychopharmacology*, 1987, *92*, 135.
3. CLARKE P.B.S., PERT A. — Autoradiographic evidence for nicotine receptors on nigrostriatal and mesolimbic dopaminergic neurons. *Brain Research*, 1985, *348*, 355-358.
4. FIBIGER H.C., PHILLIPS A.G. — Role of catecholamine transmitters in brain reward systems : implications for the neurobiology of affect. *In* : ENGEL J., ORELAND L. — *Brain Reward Systems and Abuse*, p. 61. Eds J. Engel and L. Oreland, New York, Raven Press, 1987.
5. GIRAUD P., KOWALSKI C., BANNON M.J., EIDE L.E., CUPO A., OLIVER C., HERY F. — Utilisation des sondes d'ARN messager pour l'étude de la biosynthèse des enképhalines dans le striatum. *Encéphale*, 1989, *15*, 111-115.
6. IMPERATO A., MULAS A., DI CHIARA G. — Nicotine preferentially stimulates dopamine release in the limbic system of freely moving rats. *European J Pharmacol*, 1986, *132*, 337-338.
7. VAN NGUYEN T., KOBIERSKI L., COMB M., HYMAN S.E. — The effect of depolarization on expression of the human proenkephalin gene is synergistic with cAMP and dependent upon a cAMP-inducible enhancer. *J. Neuroscience*, 1990, *10*, 2825-2833.

CERUTTI, P.A.

Dept. of Carcinogenesis
Swiss Experimental Cancer Research Institute
Lausanne

Reprinted from Biochemistry, 1991, 30.

The Balance between Cu,Zn-Superoxide Dismutase and Catalase Affects the Sensitivity of Mouse Epidermal Cells to Oxidative Stress†

Paul Amstad, Alexander Peskin,‡ Girish Shah,§ Marc-Edouard Mirault,∥ Rémy Moret, Irène Zbinden, and Peter Cerutti*

Department of Carcinogenesis, Swiss Institute for Experimental Cancer Research, 1066 Epalinges, Lausanne, Switzerland
Received March 8, 1991; Revised Manuscript Received June 6, 1991

ABSTRACT: Oxidants are toxic, but at low doses they can stimulate rather than inhibit the growth of mammalian cells and play a role in the etiology of cancer and fibrosis. The effect of oxidants on cells is modulated by multiple interacting antioxidant defense systems. We have studied the individual roles and the interaction of Cu,Zn-superoxide dismutase (SOD) and catalase (CAT) in transfectants with human cDNAs of mouse epidermal cells JB6 clone 41. Since only moderate increases in these enzymes are physiologically meaningful, we chose the following five clones for in-depth characterization: CAT 4 and CAT 12 with 2.6-fold and 4.2-fold increased catalase activities, respectively, SOD 15 and SOD 3 with 2.3-fold and 3.6-fold increased Cu,Zn-SOD activities, respectively, and SOCAT 3 with a 3-fold higher catalase activity and 1.7-fold higher Cu,Zn-SOD activity than the parent JB6 clone 41. While the increases in enzyme activities were moderate, the human cDNAs were highly expressed in the transfectants. As demonstrated for the clone SOD 15, this discordance between message concentrations and enzyme activities may be due to the low stability of the human Cu,Zn-SOD mRNA in the mouse recipient cells. According to immunoblots the content of Mn-SOD was unaltered in the transfectants. While the activities of glutathione peroxidase were comparable in all strains, the concentrations of reduced glutathione (GSH) were significantly lower in SOD 3 and SOD 15. This decrease in GSH may reflect a chronic prooxidant state in these Cu,Zn-SOD overproducers. The Cu,Zn-SOD overproducers SOD 15 and SOD 3 were hypersensitive to the formation of DNA single-strand breaks, growth retardation, and killing by an extracellular burst of superoxide plus H_2O_2 while the CAT overproducers were protected relative to the parent clone JB6 clone 41. The double transfectant SOCAT 3 was well protected from oxidant damage because of its increased content in CAT, which counterbalances the increase in Cu,Zn-SOD. The inducibility of the growth-competence-related protooncogene c-*fos* was decreased in all transfectants, albeit probably for different reasons. We conclude that H_2O_2 represents the major intracellular oxidant on the pathways to DNA single-strand breakage and cytotoxicity and that the hypersensitivity of Cu,Zn-SOD transfectants is mostly due to the overproduction of H_2O_2. The balance of SOD and CAT plus glutathione peroxidase is more important for overall sensitivity than the level of Cu,Zn-SOD alone. Growth stimulation may occur when cells are protected from excessive oxidant toxicity but only when a sufficient oxidant signal remains to activate the necessary growth pathways.

Oxidants are ubiquitous in our aerobic environment and are formed in situ in tissues and cells by normal metabolism and the metabolism of certain xenobiotics. They are always toxic and produce macromolecular damage. At the same time oxidants can serve as (patho)physiological signals in growth and differentiation (Cerutti, 1985; Crawford et al., 1988; Shibanuma et al., 1988; Murrel et al., 1990; Cerutti & Trump, 1991). The sensitivity of cells to oxidants is attenuated by low molecular weight antioxidants and antioxidant enzymes. The biochemistry of the most important enzymes [i.e., superoxide dismutases (SOD),[1] catalase (CAT), GSH peroxidases (GPx), GSH reductase, and GSH *S*-transferases] has been studied in detail [see Cerutti et al. (1988)]. However, the physiological role of a single antioxidant enzyme in situ in the cell is only poorly understood because of complex interactions and interrelationships between the individual components. Complete deficiency in SOD sensitizes *Escherichia coli* (Natvig et al., 1987) and *Drosophila* (Phillips et al., 1989) to oxidative stress, and in several instances an increase in intracellular SOD was protective (Krall et al., 1988; Kyle et al., 1988; Elroy-Stein et al., 1986). However, there are remarkable exceptions. For example, a large increase in Fe- or Mn-SOD sensitized *E. coli* to paraquat toxicity (Scott et al., 1987; Bloch & Ausubel, 1986), and inactivation of Cu,Zn-SOD in human fibroblasts increased their growth rate (Michiels et al., 1988). There was no proportionality between the degree of resistance to paraquat and the complement of transfected Cu,Zn-SOD in HeLa cells. Cells with high complements were less protected and contained increased levels of peroxidized lipid (Elroy-Stein et al., 1986). Cytotoxic effects prevented the preparation of stable transfectants of bovine adrenocortical cells with human Cu,Zn-SOD (Norris & Hornsby, 1990). These results suggest that a fine

† This work was supported by the Swiss National Science Foundation and the Swiss Association of Cigarette Manufacturers and the Association for International Cancer Research.

* Address correspondence to this author.

‡ Present address: Institute of Developmental Biology, Academy of Science of USSR, Moscow 117808, USSR.

§ On leave from the Biochemistry Division, Bhabha Atomic Research Centre, Bombay 400 085, India.

∥ Present address: Ontogénèse et Génétique Moléculaire, Le Centre Hospitalier de l'Université Laval, 2705 Boulevard Laurier, Québec, G1V 4G2 Canada.

[1] Abbreviations: SOD, superoxide dismutase; CAT, catalase; GPx, selenium glutathione peroxidase; GSH, reduced glutathione; AO, active oxygen; GAPDH, glyceraldehyde-3-phosphate dehydrogenase; X/XO, xanthine/xanthine oxidase; EDTA, ethylenediaminetetraacetic acid; SDS, sodium dodecyl sulfate; $O_2^{\cdot-}$, superoxide anion radical.

0006-2960/91/0430-9305$02.50/0

balance between several antioxidant enzymes determines the physiological and pathophysiological effects of oxidants. It is interesting to note that mouse L-cells, neuroblastoma cells, and NIH 3T3 fibroblasts transfected with human Cu,Zn-SOD possessed a compensatory increase in glutathione peroxidase (GPx) (Ceballos et al., 1988; Kelner & Bagnell, 1990) and that promotable mouse epidermal cells JB6 clone 41) possess a superior antioxidant defense due to a coordinate increase in both Cu,Zn-SOD and CAT (Crawford et al., 1989).

Our present results with stable transfectants of mouse epidermal cells JB6 clone 41 indicate that at comparable levels of GPx the balance between Cu,Zn-SOD and CAT is a determining factor for their sensitivity to a burst of extracellular active oxygen (AO) produced by xanthine/xanthine oxidase (X/XO). Cu,Zn-SOD overproducers were hypersensitive to retardation of growth, cell killing, and DNA strand breakage by AO while CAT overproducers were protected. An increase in Cu,Zn-SOD was tolerated without an increase in oxidant sensitivity when it was counterbalanced by a corresponding increase in CAT in a double transfectant. Both increases in CAT and Cu,Zn-SOD diminished the inducibility of the growth-related protooncogene c-*fos*, albeit probably for different reasons. We propose that cells are stimulated to grow when they are protected from excessive AO toxicity as long as a sufficient AO signal remains to activate the necessary growth pathways.

Materials and Methods

Construction of Expression Vectors Containing Cu,Zn-SOD or CAT and Preparation of Stable Transfectants. The pD_5-*neo* vector containing the adeno 5 major late promoter, the SV40 promoter and enhancer sequences, and the neomycin resistance gene casette was used for the construction of a human Cu,Zn-SOD expression vector. A 600-bp cDNA fragment was removed by *Pst*I digestion from clone pS61-10 (Sherman et al., 1983), and the G- and C-tails were removed with the double-strand exonuclease *Bal*31. *Bam*HI linkers were added to the blunt-ended SOD cDNA fragment before ligation into the unique *Bam*HI site of the pD_5-*neo* vector. Transfection into mouse epidermal JB6 clone 41 cells was according to Chen and Okayama (1987), and resistant clones were selected in medium containing 400 μg/mL geneticin for 9 days. Control cell clones were also prepared which contained only the pD_5-*neo* vector without the SOD cDNA insert.

An expression vector containing complete CAT cDNA was constructed by using the pCAT1 clone of Korneluk et al. (1984), which lacks the 5′ portion coding for 77 amino acids. In order to complement the 5′ portion, the 5′ 450-bp *Pst*I to *Pvu*II fragment of the rat catalase cDNA clone pMJ1010 (Furuta et al., 1986) was inserted into the *Pst*I and *Pvu*II sites of pCAT1. Immediate early promoter sequences of cytomegalovirus (CMV), i.e., 1.2-kb *Pst*I to *Ava*II, were then inserted between the *Pst*I and *Nco*I sites of the vector containing the fused rat–human CAT cDNA. Finally the vector was completed by the insertion of a hygromycin gene resistance casette. For this purpose pSP65–SV40–hygromycin was restricted with *Sal*I and *Hin*dIII, and the ends of the 2.5-kb SV40–hygromycin expression casette were filled in with Klenow enzyme. This blunt-ended fragment was then ligated into the unique *Hpa*I site of the modified pCAT1 plasmid containing fused rat–human CAT cDNA under direction of the CMV promoter.

Growth Conditions and Antioxidant Enzyme Activities for the Parent Strain and Transfectants of JB6 Clone 41 Cells. Mouse epidermal cells JB6 clone 41 originally had been received from Dr. N. Colburn and were cultured in monolayers with 8% fetal calf serum (GIBCO, Grand Island, NY) in MEM supplemented with 50 ng/mL Na_2SeO_3. To the medium of stable CAT transfectants was added 10 μg/mL hygromycin; for stable SOD transfectants 100 μg/mL geneticin was added, and for CAT plus SOD double transfectants both antibiotics were added for routine culturing in order to guard against the loss of the transfected DNAs. These antibiotics were omitted immediately before experiments measuring biological properties. For the determination of CAT and GPx activities, the monolayers were rinsed twice with ice-cold phosphate-buffered saline and the cells collected by scraping with a sterile rubber policeman. The cells were sedimented for 4 min at 1600*g* and processed either for enzyme/protein or for mRNA analyses. For enzyme/protein lysates, cells were resuspended in 50 mM potassium phosphate buffer containing 0.5% Triton X-100 and sonicated (in an ice–water bath) for two 30-s bursts on a Branson sonicator B15 (position 2, continuous setting; Branson Ultrasonics Corp., Danbury, CT) with a 30-s cooling interval. Total protein concentration was determined according to the procedure of Peterson (1977). For CAT and GPx activities, sonicates were first spun 5 min at 800*g* (4 °C). The supernatants were assayed according to the procedures of Clairborne (1985) for CAT activity and Günzler and Flohé (1985) for GPx activity.

For SOD measurements cells were suspended in 100 mM triethanolamine–diethanolamine buffer and homogenized with a Teflon glass Dounce homogenizer. The homogenate was centrifuged at 105000*g* for 1 h (4 °C), and the supernatant was passed through a small Sephadex G25 (coarse) column to remove low molecular weight substances which interfere with the enzyme assay according to the procedure of Paoletti et al. (1986). An aliquot of the eluate was applied onto a 5.5% polyacrylamide gel in order to localize SOD activity according to the procedure of Beauchamp and Fridovich (1971) with the exception that no tetramethylethylenediamine was used for staining. Mn-SOD activity was determined in mitochondrial fractions prepared by differential centrifugation. Mitochondria were disrupted by freezing–thawing in a high ionic strength buffer (0.25 mM sucrose, 0.12 M KCl, 10 mM Tris-HCl, pH 7.4). Mitochondrial membranes were removed by sedimentation at 105000*g* for 1 h, and enzyme activity was measured in the supernatant. Reduced glutathione (GSH) concentration was determined by the monobromobimane method of Cotgreave and Moldeus (1986).

Western Blot Analysis. Total cellular sonicates were prepared in 50 mM potassium phosphate, pH 7.0–0.5% Triton X-100. The sonicates were then mixed with an equal volume of 2× SDS buffer, boiled for 3 min, frozen, boiled again for 3 min, and applied to a 12.5% SDS–polyacrylamide gel. Forty micrograms of protein was applied to each lane and, after electrophoresis, transferred to an Immobilon PVDF membrane (Millipore Corp., Bedford, MA) by electrotransfer. CAT protein concentration was determined after 2 h of prehybridization by overnight incubation with a mixture of rabbit anti-human CAT antibody and rabbit anti-human Mn-SOD antibody at 4 °C. The filter was washed five times followed by hybridization with 100000 cpm/mL ^{125}I-labeled goat anti-rabbit immunoglobulin.

Northern Blot Analysis. Total RNA was prepared according to the procedure of Chirgwin et al. (1979). A total of 10 μg of total RNA was electrophoresed on a 1.4% agarose–formaldehyde gel and then transferred to gene screen membranes. The filters were prehybridized in 50 mM Tris-HCl, pH 7.5, 0.1% sodium pyrophosphate, 1% SDS, 0.2% poly(vinylpyrrolidone), 0.2% Ficoll, 5 mM EDTA, 50% for-

mamide, 0.2% BSA, 1× SSC, and 150 μg/mL denatured salmon sperm DNA at 65 °C for 6 h. For hybridization, 1 × 10^6 cpm/mL of ^{32}P-labeled probe solution was used. The filteres were washed at 65 °C twice for 15 min with 2× standard sodium citrate (SSC)–0.1% SDS and twice for 15 min with 0.1× SSC–0.1% SDS. The probe was a transcript of an SP65 recombinant containing in the antisense direction a cDNA fragment of human Cu,Zn-SOD (450-bp *Alu* to *Taq*) (Sherman et al., 1983).

The stability of Cu,Zn-SOD mRNAs transcribed from the endogenous and transfected genes, respectively, was estimated by using actinomycin D in the parent strain JB6 clone 41 and the SOD transfectant SOD 15. Actinomycin D (5 μg/mL) in DMSO was added to cultures which were approximately 80% confluent and growth continued for 2, 4, 6, 8, and 10 h before the preparation of total RNA according to Chirgwin et al. (1979) and Northern blotting using a ^{32}P-labeled riboprobe as described above.

Induction of c-*fos* by AO treatment in JB6 clone 41 and in the antioxidant gene transfected clones was determined as described previously (Crawford et al., 1988) in monolayer cultures grown for 24 h in only 0.25% fetal calf serum. The cultures were exposed to AO generated by 20 μg/mL X and 2.0 μg/mL XO (obtained from Boehringer Mannheim) for 30 min. The production of $O_2^{\cdot-}$ was determined spectrophotometrically by the reduction of cytochrome. The rate of $O_2^{\cdot-}$ release was close to linear during the first 15 min at 0.45 nmol of $O_2^{\cdot-}$/min and had decreased to less than 0.2 nmol/min of this value after 30 min. Cells were harvested and total RNA was prepared for Nothern blotting as described above. The probe was prepared by the transcription of an SP6 recombinant containing a 685-bp *Sal*I to *Pst*I fragment of v-*fos* (Van Beveren et al., 1986).

RNase Protection Analysis of CAT Expression. RNase protection analysis was used to demonstrate the presence of human CAT message in the transfectants CAT 4 and SOCAT 3. For this purpose the SP65 recombinant described above containing in the antisense direction the 1250-bp *Hin*dIII to *Pvu*II human CAT cDNA insert was linearized with *Xho*I, and a ^{32}P-labeled riboprobe of 468 nucleotides was prepared according to the procedure of Melton et al. (1984). The probe was passed through a spin column and precipitated with 2 M ammonium acetate and 2.5 volumes of ethanol. The pellet was washed with 75% ethanol–25% 0.1 M sodium acetate, pH 5.7, dried under vacuum, and dissolved in 100 μL of hybridization buffer (80% formamide–40 mM Pipes, pH 6.4–400 mM NaCl–1 mM EDTA).

Total cellular RNA (10 μg), prepared as described above, was taken up in 30 μL of hybridization buffer, and 5 × 10^5 cpm of the CAT riboprobe was added. After the mixture was heated for 15 min to 85 °C and incubated overnight at 45 °C, 300 μL of RNase buffer (10 mM Tris-HCl, pH 7.8–5 mM EDTA–300 mM NaCl) containing 40 μg/mL RNase A and 2 μg/mL RNase T1 was added, and the samples were incubated for 30 min at 30 °C. The RNase was then inactivated by the addition of 10 μL of 20% SDS and 50 μg of proteinase K for 15 min at 37 °C. The RNA was extracted with 400 μL of phenol–chloroform–isoamyl alcohol and the aqueous layer transferred to a centrifuge tube containing 10 μg of tRNA. The RNA was taken up in 2 M ammonium acetate and precipitated with an equal volume of 2-propanol and the pellet washed once with 75% ethanol before it was dried under vacuum. The RNA was then dissolved in 5 μL of gel loading buffer (80% formamide–40 mM Tris–borate, pH 7.5); the sample was heated to 85 °C for 10 min and loaded in a buffer consisting of 89 mM Tris–89 mM boric acid–2 mM EDTA onto a 5% denaturing polyacrylamide gel [19:1 acrylamide: bis(acrylamide)] which was run for 3 h at 50 W. The dried gel was then exposed to an X-ray film.

Southern Blot Analysis. DNA was extracted, restricted with *Bam*HI, and electrophoresed in 0.8% agarose gels. The DNA was transferred to nitrocellulose essentially as described by Southern. The filters were hybridized with a nick-translated 450-bp probe removed by *Hin*dIII/*Eco*RI from an SP65 vector containing a 450-bp *Alu*I to *Taq*I human Cu,Zn-SOD cDNA fragment (Sherman et al., 1983). As expected, only the SOD-transfected clones showed a band at approximately 0.5 kb for the transfected gene in addition to a double band at approximately 10 kb for the endogenous mouse gene, which is present in all cell clones. From a comparison of the intensities of the bands for the transfected and the endogenous gene, we estimate that the SOD transfectants contain no more than one to two copies of the tranfected human SOD gene (data not shown). For CAT a nick-translated probe was prepared by using a 1250-bp fragment removed by *Hin*dIII and *Eco*RI from an SP64 construct containing a 1250-bp *Hin*dIII to *Pvu*II fragment of human CAT cDNA (Korneluk et al., 1984). The blots contain two clearly separated bands at approximately 1.8 kb for the transfected human CAT gene in transfected clones and a band at approximately 10 kb for the mouse CAT gene in all cell clones. Ratios of densitometer readings for the bands attributed to the transfected over the endogenous CAT gene indicate that the transfectants contain two to three human CAT copies per cell (data not shown).

Growth Properties, DNA Synthesis Capacity, and Colony-Forming Ability of Antioxidant Gene Transfected JB6 Cells in the Presence and Absence of Oxidant Stress. For the determination of the effect of AO on the growth of the parent JB6 clone 41 cells and the antioxidant gene transfected clones, 10^5 cells were plated into 10-cm Petri dishes in MEM supplemented with 8% serum and 50 ng/mL Na_2SeO_3 and allowed to grow for 2 days before treatment with X/XO at the indicated doses. Without changing the culture medium the cells were harvested at the indicated times by trypsinization, and their number was counted in a hemocytometer (Muehlematter et al., 1988). For the determination of the survival of colony-forming ability, 500 cells for each strain were plated into 6-cm Petri dishes and allowed to grow for 14 h under the usual culture conditions. The cultures were then treated without medium change with increasing doses of X/XO (0.5–1.75 μg/mL XO and 10 μg/mL X). Control cultures received only 10 μg/mL X. Growth was then continued for 7 days without medium change when the colonies were fixed with methanol and stained with 2% crystal violet and counted.

DNA Single-Strand Breakage. DNA single-strand breakage was measured by the alkaline elution method of Kohn et al. (1976) as described previously (Muehlematter et al., 1988). JB6 cells were seeded at low density in Petri dishes and cultured as described above. After 12 h they were labeled in their DNA by the addition of [^{14}C]thymidine over a period of 48 h. Subsequently, the cultures were grown in fresh medium containing nonradioactive thymidine for 12 h. Before treatment with active oxygen generated by X/XO, fresh medium supplemented with 8% fetal calf serum was added. Following treatment for 30 min, the medium was removed and the cells were scraped and collected directly on the filters used for alkaline elution.

Results

Transfection of Mouse Epidermal Cells JB6 Clone 41 with Human Cu,Zn-SOD, CAT, or Both Enzymes. JB6 clone 41

Table I: Activities of Antioxidant Enzymes in Transfected JB6 Clone 41 Cells[a]

cell strain	CAT (units/mg of protein)	SOD (units/mg of protein)	SOD/CAT	GPx (units/mg of protein)	GSH (nmol/10^6 cells)
JB6 cl 41	5.6 ± 1.1 (5)	21 ± 6 (11)	3.8	33 ± 4 (4)	2.6 ± 0.3 (4)
SOD 15	6.7 ± 1.1 (3)	48 ± 14 (11)	7.2	45 ± 5 (4)	1.5 ± 0.1 (4)
SOD 3	4.8 ± 1.2 (2)	76 ± 9 (5)	15.8	45 ± 5 (4)	0.9 ± 0.1 (4)
CAT 4	14.5 ± 1.7 (4)	27 ± 3 (5)	0.5	45 ± 8 (4)	2.7 ± 0.1 (4)
CAT 12	23.6 ± 1.2 (4)	23 ± 4 (4)	1.0	35 ± 11 (4)	3.9 ± 0.2 (4)
SOCAT 3	17.2 ± 4.3 (*n*)	36 ± 6 (8)	2.1	26 ± 5 (4)	3.9 ± 0.2 (4)

[a] Cells were grown in monolayer cultures and extracted when confluency was approximately 80%. Values for enzyme activities are given in units per milligram of protein cell extract; means ± SD are listed; values in parentheses represent the number of independent determinations used for these calculations. Units are defined as follows: catalase, micromoles of H_2O_2 consumed per minute; SOD, amount of SOD inhibiting the rate of control NADH oxidation by 50%; GPx, nanomoles of NADPH oxidized per minute at 1 nM GSH. The values for reduced glutathione are nanomoles per 10^6 cells.

cells were transfected with expression vectors containign cDNA of human Cu,Zn-SOD and a neomycin resistance casette or fusion rat–human cDNA of CAT and a hygromycin resistance casette, respectively. Several transfectants in each series were grown in mass culture, and SOD, CAT, and glutathione peroxidase (GPx) activites were determined in lysates. Representative transfectants with a moderate increase in the particular antioxidant enzyme were chosen for detailed characterization on the molecular and cellular level.

CAT 4 was transfected in a second round with the human Cu,Zn-SOD expression vector, and neomycin/hygromycin resistant clones were selected. A particular clone, SOCAT 3, with moderate levels of both human Cu,Zn-SOD and CAT, was chosen for in-depth investigation.

Expression of Human Cu,Zn-SOD mRNA and Rat–Human CAT mRNA in JB6 Transfectants. Stationary mRNA concentrations were determined by using transcripts from SP65 recombinants containing cDNA fragments of human Cu,-Zn-SOD and human CAT cDNA, respectively. The Northern blots under high stringency conditions in Figure 1A show the messages for endogenous mouse Cu,Zn-SOD and transfected human Cu,Zn-SOD, which possess different lengths in the clones SOD 3, SOD 15, and SOCAT 3. CAT 4 and a pD5-*neo* transfected clone serve as controls. It is evident that the amount of stationary mRNA is severalfold higher for the transcripts of the transfected than for the endogenous Cu,-Zn-SOD gene in SOD 3 and SOCAT 3. A rough measure of the level of expression of the transfected gene can be obtained by comparison with the amount of message transcribed from the corresponding endogenous gene. In order to distinguish the endogenous mouse CAT mRNA from the transfected rat–human CAT mRNA, we performed the RNase protection experiment shown in Figure 1B. A 468-nucleotide transcript was prepared from an SP6 recombinant which contained in the antisense direction a 1200-bp human CAT cDNA fragment reaching from the *Pvu*II site to the *Hin*dIII site and which was linearized with *Xho*I. Correspondingly, a 486-nucleotide RNA fragment was protected from RNase digestion in the transfectants CAT 4, CAT 12, and SOCAT 3 but not in the parent clone 41. In contrast, a short fragment of approximately 100 nucleotides was protected in all clones and originates from the endogenous mouse CAT message. As noted for the Cu,Zn-SOD transfectants, it is evident that the transcripts from the transfected CAT gene are more abundant than those originating from the endogenous gene.

The stabilities of the endogenous mouse SOD and transfected human SOD mRNAs were compared in clone SOD 15 in an experiment with the transcriptional inhibitor actinomycin D. The Northern blots are shown on Figure 2. Transcripts of the gene for glyceraldehyde-3-phosphate dehydrogenase (GAPDH) were measured as reference. Our results indicate a much lower stability for the human Cu,Zn-SOD message

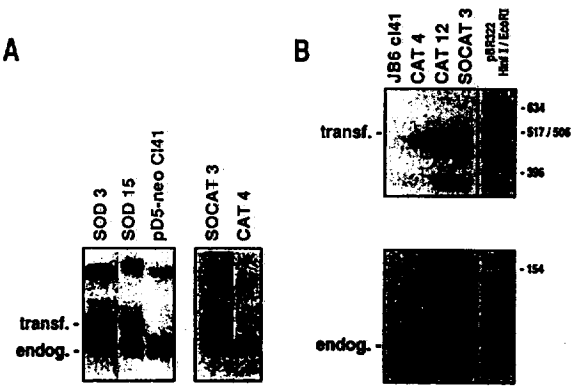

FIGURE 1: Expression of endogenous and transfected Cu,Zn-SOD and CAT genes in transfectants of JB6 clone 41. (A) The concentrations of endogenous mouse message and message transcribed from transfected human cDNA for Cu,Zn-SOD were measured by Northern blotting of total RNA extracted from monolayer cultures of the stable transfectants SOD 3, SOD 15, and SOCAT 3. For comparison, corresponding Northern blots were also performed for the parent JB6 clone 41, for CAT 4, and for cells which had been transfected with the pD$_5$-*neo* vector which did not contain a cDNA insert. A labeled transcript of an SP65 recombinant containing in the antisense direction a cDNA fragment of human Cu,Zn-SOD was used as the probe and is described under Materials and Methods. (B) The expression of transfected and endogenous CAT mRNA in parent clone 41, CAT 4, CAT 12, and SOCAT 3 was determined in RNase protection experiments. Total cellular RNA was hybridized with a 468-nucleotide ^{32}P-labeled riboprobe transcribed from an SP65 recombinant containing in antisense direction an insert of human CAT cDNA and digested with RNases A and T1. The protected RNA was isolated and separated by gel electrophoresis and the dried gel exposed to an X-ray film as outlined under Materials and Methods.

transcribed from the transfected gene than for the endogenous mouse message.

Levels of Antioxidant Enzymes in JB6 Clone 41 Transfectants. CAT, SOD, and GPx activities as well as concentrations of reduced glutathione were measured in lysates of the parent clone 41 and the antioxidant gene transfectants and are given in Table I. It is evident that CAT 4 possesses 2.6-fold and CAT 12 4.2-fold higher CAT activities than the parent clone 41. In SOD 15 the total SOD activity is 2.3-fold and in SOD 3 3.6-fold above the parent JB6 cells while CAT levels are essentially unaltered. In SOCAT 3 the total SOD activity is 1.7-fold higher than in the parent clone 41 and 1.3-fold higher than in CAT 4 from which it was derived. No significant differences were observed in the GPx activities between all six cell strains. In contrast, the concentrations of reduced GSH were lower in SOD 15 and SOD 3 (see Table I) while total glutathione levels were comparable (data not shown).

Mn-SOD activity was determined in soluble mitochondrial preparations of the parent clone 41 and CAT 4 and found to

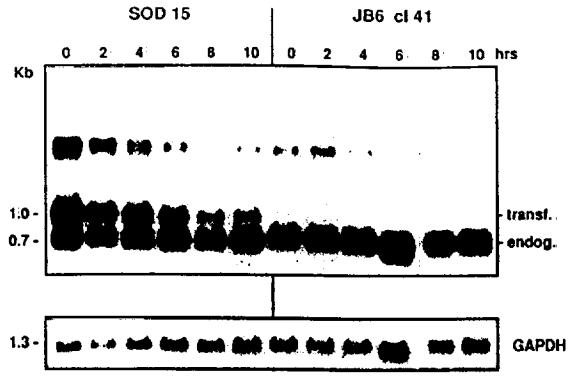

FIGURE 2: Stability of Cu,Zn-SOD mRNA transcribed from the transfected human Cu,Zn-SOD cDNA and from the endogenous Cu,Zn-SOD gene, respectively. Monolayer cultures were treated with 5 μg/mL actinomycin D and total RNA prepared after the indicated duration of growth for Nothern blotting with a human Cu,Zn-SOD riboprobe as described in the legend to Figure 1.

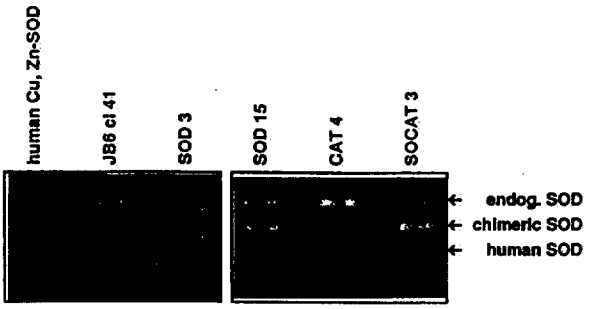

FIGURE 3: SOD activity gel of extracts of the parent JB6 clone 41 and its transfectants. Cellular homogenates were centrifuged at high speed, and the supernatant was passed through a Sephadex G25 column as described under Materials and Methods. Aliquots of the eluates were applied to a 5.5% PAGE, and the SOD activity was localized as described by Beauchamp & Fridovich (1971).

be 10–15-fold lower than Cu,Zn-SOD in both clones. Mn-SOD protein levels were estimated by immunoblotting (see below).

A SOD activity gel is shown in Figure 3. Because of its higher mobility human Cu,Zn-SOD can be readily distinguished from endogenous mouse Cu,Zn-SOD. Since Cu,-Zn-SOD is a dimer, the band between the two activities most probably represents the mouse–human heterodimer. It is evident that the SOD-transfected clones SOD 3, SOD 15, and SOCAT 3 contain active human Cu,Zn-SOD.

The presence of human CAT protein in CAT 4, CAT 12, and SOCAT 3 was demonstrated by immunoblotting with rabbit anti-human CAT antibody. The immunoblots in Figure 4 show double bands for the CAT transfectants which correspond to human and mouse CAT, which cross-reacts with the antibody. The parent clone 41, SOD 15, and SOD 3 show single bands. Indeed, the filters had been reacted simultaneously with a mixture of rabbit anti-CAT and rabbit anti-human Mn-SOD antibodies. The high-mobility band in all cell clones corresponds to endogenous mouse Mn-SOD, which cross-reacts with the latter antibody. According to these data all six cell clones contained comparable amounts of Mn-SOD.

Susceptibility to DNA Strand Breakage upon Exposure to Superoxide plus Hydrogen Peroxide. We measured the induction of DNA single-strand breaks (alkali-labile sites) in four representative cells strains, i.e., parent, SOD 15, CAT 4, and SOCAT 3, at two doses of $O_2^{\cdot-}$ plus H_2O_2 produced extracellularly by 40/3 and 40/4 μg/mL X/XO by the al-

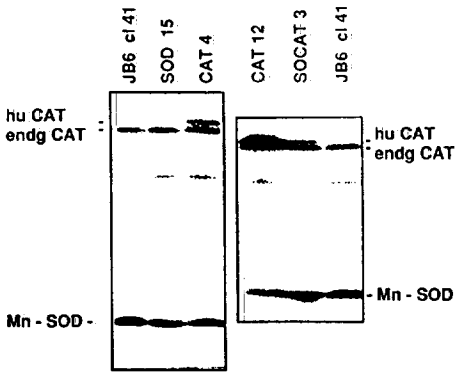

FIGURE 4: Immunoblots for CAT and Mn-SOD in sonicates of the parent JB6 clone 41 and its transfectants. Boiled cellular sonicates were separated on 12.5% SDS–PAGE and electrotransferred to a PVDF membrane. CAT and Mn-SOD proteins were determined by the reaction with a mixture of rabbit anti-human CAT antibodies and rabbit anti-human Mn-SOD antibodies. The immune complexes were made visible by the reaction with ^{125}I-labeled goat anti-rabbit immunoglobulin G, followed by autoradiography (for experimental details, see Materials and Methods).

kaline elution method. From Figure 5 we can derive the following order of decreasing susceptibilities: SOD 15 > parent > CAT 4 ≃ SOCAT 3. Our data indicate that H_2O_2 is the major intracellular oxidant species which ultimately leads to DNA breakage by an extracellular burst of $O_2^{\cdot-}$ plus H_2O_2 but give no information on the mechanism of break formation.

Growth Properties and DNA Synthesis Capacity of Antioxidant Gene Transfectants in the Presence and Absence of Oxidant Stress. Growth curves were determined for the parent clone 41 and the antioxidant gene transfectants. Monolayer cultures were established by plating 10^5 cells into 10-cm Petri dishes and cell numbers counted after different lengths of growth. The results shown on Figure 6A are for routine culture conditions in an atmosphere of 5% CO_2. With the exception of CAT 4 with a slightly higher growth rate, the parent clone and the transfectants possess similar growth potentials. Addition of 15 or 25 μg/mL xanthine to the culture medium did not affect growth. Panels B and C of Figure 6 show growth curves under oxidative stress generated extracellularly by X/XO, which produces a mixture of $O_2^{\cdot-}$ and H_2O_2. Two doses were used in order to magnify strain differences between the SOD transfectants and the parent strain (Figure 6B) and the CAT transfectants and the parent strain (Figure 6C), respectively. Monolayer cultures were treated 2 days after plating when they reached a density of (4–6) × 10^5 cells per 10-cm Petri dish. After 6 h 15/1.5 μg/mL X/XO (initial rate of $O_2^{\cdot-}$ production of 0.45 nmol/min) had destroyed 81% of the parent clone, 68% of SOCAT 3, 89% of SOD 15, and 94.4% of SOD 3. While the surviving cells of the parent clone and SOCAT 3 possessed normal growth potential, the remaining cells of SOD 15 and SOD 3 failed to grow. Our results indicate that the increase in Cu,Zn-SOD in SOD 15 and SOD 3 resulted in sensitization to oxidative stress and that this sensitization was eliminated in SOCAT 3 by a compensatory increase in CAT. A large difference in sensitivity between the parent and CAT transfectants becomes apparent at a higher dose of X/XO of 25/2.5 μg/mL. Under these conditions 93% of the parent cells were killed within 6 h as compared to 65% for CAT 12 and 51% for CAT 4. Cells which survived the initial toxicity possessed normal growth properties. Qualitatively similar results were obtained at low doses for the survival of colony-forming ability although the quantitative differences between the six cell strains were less

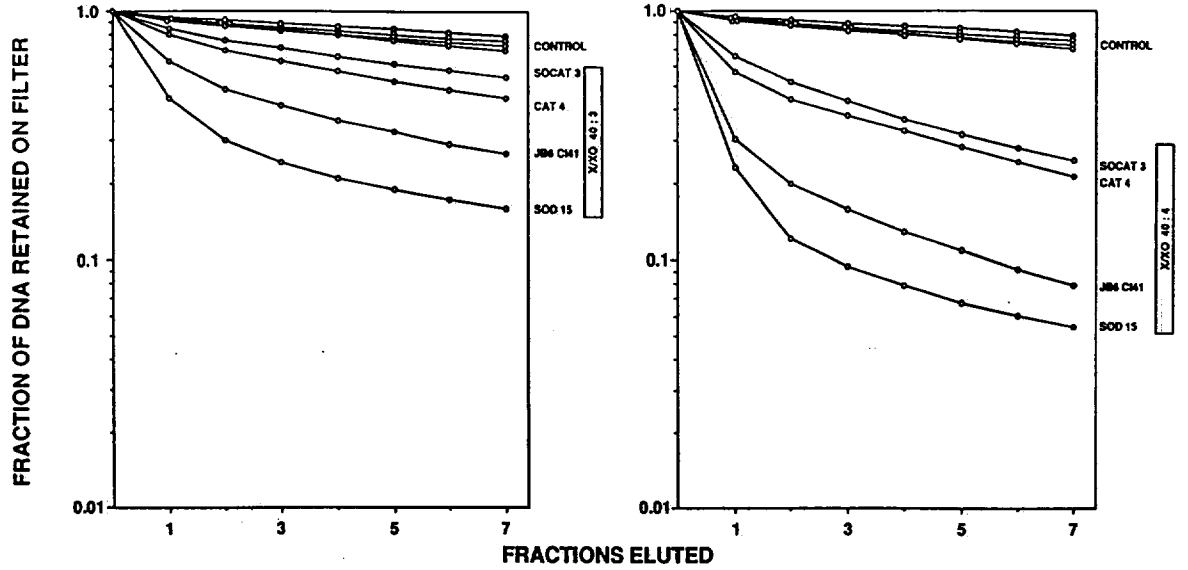

FIGURE 5: Active oxygen induced DNA strand breakage in the parent JB6 clone 41 and the transfectants SOD 15, CAT 4, and SOCAT 3. Monolayer cultures were labeled in their DNA with [^{14}C]thymidine. Before treatment with 40/3 μg/mL X/XO (left side) or 40/4 μg/mL X/XO (right side), respectively, fresh medium supplemented with 8% fetal calf serum was added. Following treatment for 30 min the medium was removed, and the cells were scraped and collected on the filters used for alkaline elution.

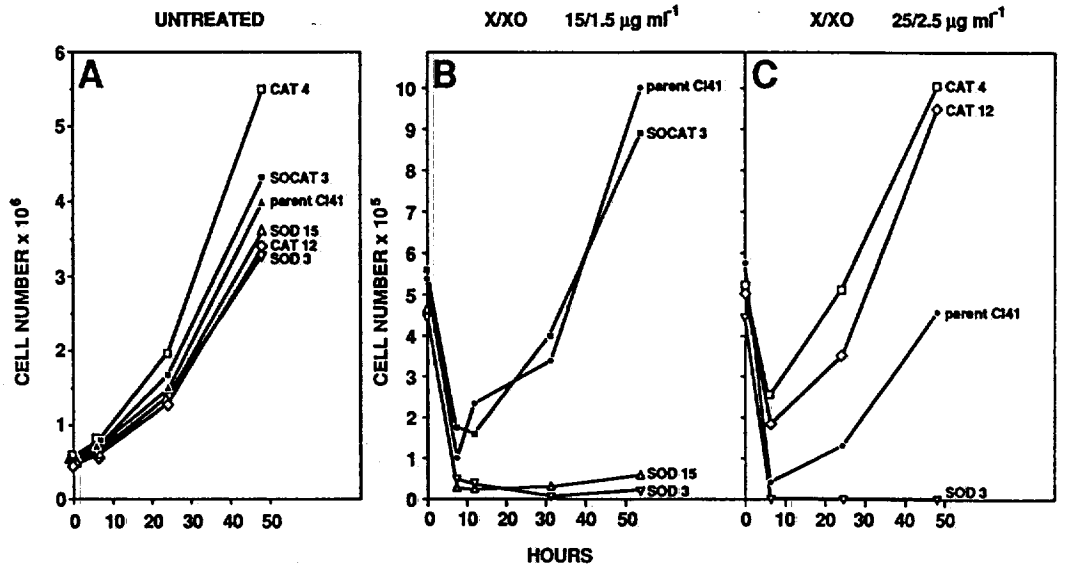

FIGURE 6: Growth curves of the parent JB6 clone 41 and its transfectants under routine culture conditions and following exposure to an extracellular oxidative burst. (A) Monolayer cultures containing (4–6) × 10^5 cells per 10-cm Petri dish were grown in an atmosphere of 5% CO_2 for the indicated lengths of time and cell numbers determined following trypsinization. (B) Monolayer cultures at the indicated cell density were exposed to an extracellular burst of AO produced by 15 μg/mL X and 1.5 μg/mL XO, and growth continued for increasing lengths of time before harvesting and determination of cell numbers. (C) Monolayer cultures at the indicated cell density were exposed to an extracellular burst of AO produced by 25 μg/mL X and 2.5 μg/mL XO, and growth continued for increasing lengths of time before determination of cell numbers (see Materials and Methods).

pronounced than for the growth data reported above (results not shown).

The effect of oxidant stress on the DNA synthesis capacity of the antioxidant gene transfectants was assessed by measuring the incorporation of [^{3}H]thymidine in a 1-h pulse into acid-insoluble material at different lengths of time after exposure to an extracellular oxidative burst. The results were analogous to the growth curves, the relative resistance of the four cell strains being CAT 4 > SOCAT 3 > parent clone 41 ≫ SOD 15. From the protective capacity of intracellular CAT in CAT 4 and CAT 12 and the fact that additional CAT prevented hypersensitivity due to increased levels of Cu,Zn-SOD in SOCAT 3, we conclude that H_2O_2 is mostly responsible for the cytocidal action of an extracellular burst of $O_2^{\cdot-}$ plus H_2O_2.

Inducibility of c-fos mRNA by Oxidant Stress in Antioxidant Gene Transfectants. The induction of growth-competence-related genes is a necessary prerequisite for growth stimulation. The immediate early gene c-*fos* is a prototype in this regard, and we have shown previously that its transcription is induced in JB6 cells by oxidants (Crawford et al., 1988; Muehlematter et al., 1989). Therefore, we compared the increase in stationary concentration of c-*fos* mRNA following AO treatment in the antioxidant gene transfectants.

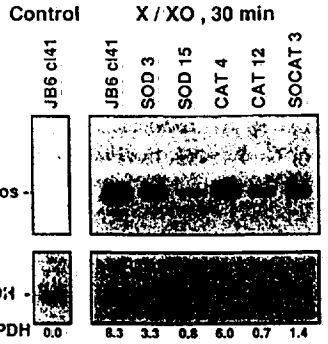

FIGURE 7: Induction of c-*fos* message by an extracellular oxidative burst in the parent JB6 clone 41 and its transfectants. Partially serum-starved monolayer cultures were exposed to AO generated by 20 μg/mL xanthine and 2 μg/mL xanthine oxidase, and growth continued for 30 min before the preparation of total RNA. A labeled transcript of an SP6 recombinant containing in the antisense direction a fragment of v-*fos* DNA was prepared in order to probe the Northern blots. After exposure to an X-ray film the stripped filters were rehybridized with a probe for rat glyceraldehyde-3-phosphate dehydrogenase (GAPDH). The autoradiograms of the blots were evaluated by densitometry, and the values for the ratios of c-*fos* mRNA/GAPDH mRNA are listed in the lower portion of the figure.

Figure 7 shows Northern blots with ratios of densitometer readings relative to the reference gene GAPDH. The following order of decreasing inducibility of c-*fos* (c-*fos*/GAPDH) was observed (after 30 min of AO treatment generated by 20 μg/mL X plus 2.0 μg/mL XO): parent clone 41 (8.3) > CAT 4 (6.0) > SOD 3 (3.3) > SOCAT 3 (1.4) > SOD 15 (0.8) = CAT 12 (0.7). While the absolute values for the ratios of c-*fos*/GAPDH varied, the same order of c-*fos* inducibility for the different strains was observed in several experiments.

Discussion

The cellular antioxidant defense is composed of multiple low molecular weight components and several enzymes. Because these molecules interact, complement, interfere, or even compete with each other and act at different sites in the cell, the elucidation of their respective roles is a difficult task. Our present work focuses on the interrelationship of Cu,Zn-SOD and CAT in the protection of mouse epidermal cells JB6 from an extracellular burst of $O_2^{\cdot-}$ plus H_2O_2. This form of oxidant stress mimics the action of phagocytic leukocytes in inflammation which produce a large amount of AO close to the surface of the target cell (Nathan et al., 1979; Simon et al., 1981; Sinet, 1982). We prepared cells with moderate increases in Cu,Zn-SOD, CAT, or both enzymes because only at moderate increases is a condition created which is physiologically meaningful. SOCAT 3 cells with concomitant increases in both Cu,Zn-SOD and CAT were prepared by consecutive transfections with expression vectors containing different antibiotic selection markers rather than cotransfection. Only this more laborious approach allows the unambiguous evaluation of the effects of the introduction of the second antioxidant enzyme, i.e., Cu,Zn-SOD, on the cellular resistance to oxidative stress.

Clones SOD 3 and SOD 15 contain one to two copies of human Cu,Zn-SOD cDNA and clones CAT 4 and CAT 12 two to three copies of CAT cDNA under the direction of strong transcriptional promoters; the double transfectant SOCAT 3, which is derived from CAT 4, contains in addition to CAT cDNA one to two copies of human Cu,Zn-SOD cDNA. From the Northern blots it is evident that the cDNAs are well expressed in the transfectants. However, the high mRNA concentrations do not result in equal increases in enzyme activities. For example, a ratio of 7 of human Cu,Zn-SOD mRNA over endogenous mouse Cu,Zn-SOD mRNA only results in a 3-fold higher total SOD activity in clone SOD 3. These discrepancies may be due to low stability of the Cu,Zn-SOD mRNAs transcribed from the transfected human cDNAs. This is demonstrated in clone SOD 15 in Figure 2 in an experiment with the transcriptional inhibitor actinomycin D. RNase protection analysis of RNA from CAT 12 and CAT 4 indicates a ratio of 4 and 3, respectively, for mRNA transcribed from the transfected gene relative to mRNA from the endogenous gene. These ratios reflect well the increases in CAT activities in these clones relative to parent cells (see Figure 1 and Table I).

Expression of human Cu,Zn-SOD in SOD 15, SOD 3, and SOCAT 3 did not affect significantly CAT activities which remained on the level of the respective parents, i.e., JB6 clone 41 and CAT 4. Similarly, increased CAT activities in CAT 4 and CAT 12 had no major effect on their SOD activities. Judging from the immunoblots shown in Figure 4, neither the expression of human Cu,Zn-SOD nor that of CAT altered the amounts of Mn-SOD protein, and no major differences in Mn-SOD activity were detected in mitochondrial preparations of CAT 4 reltive to the parent clone 41. Similarly, no significant differences were observed in GPx activity for all six cell strains studied in this work. In contrast to our findings, human Cu,Zn-SOD transfectants of mouse L-cells, neuroblastoma cells, and NIH 3T3 fibroblasts possessed increased GPx activities (Ceballos et al., 1988; Kelner & Bagnell, 1990) as did trisomy 21 human fibroblasts with three copies of the Cu,Zn-SOD gene (Sinet, 1982). The concentrations of reduced glutathione were comparable in the parent clone, CAT 4, CAT 12, and SOCAT 3. The fact that they were significantly lower in SOD 3 and SOD 15 may reflect a situation of chronic oxidative stress in these strains.

It is evident from our results that increases in Cu,Zn-SOD and CAT had opposite effects on the sensitivity of JB6 cells to killing, growth inhibition, and the formation of DNA single-strand breaks by an extracellular burst of AO. However, the balance between Cu,Zn-SOD and CAT plus GPx may be more important for sensitivity to AO than the absolute amount of a single antioxidant enzyme. Indeed, at comparable levels of GPx the most sensitive strains SOD 15 and SOD 3 have high ratios of SOD/CAT of 7.2 and 15.8 while the resistant strains CAT 4 and CAT 12 have low ratios of 0.5 and 1.0, respectively (see Table I). Taken together, our data suggest that H_2O_2 represents a major intracellular AO species on the pathways to cytotoxicity and DNA single-strand breakage. However, our results do not imply that DNA is the immediate target for attack by H_2O_2 or its radical derivatives (Cantoni et al., 1989). Sensitization by excess Cu,Zn-SOD appears to be a consequence of overproduction of H_2O_2.

A small extracellular burst of AO can stimulate rather than inhibit the growth of fibroblasts (Zimmerman & Cerutti, 1984; Shibanuma et al., 1988; Murrel et al., 1990) and epidermal cells. In particular, we observed that X/XO stimulated the growth of promotable JB6 clone 41 but not of nonpromotable JB6 clone 30 (Muehlematter et al., 1988). Interestingly, both CAT and Cu,Zn-SOD levels were coordinately increased 2–3-fold on the mRNA and enzyme levels in clone 41 relative to clone 30 (Crawford et al., 1989). At an equal dose, AO induced the growth-competence-related protooncogene c-*fos* more efficiently in the nonpromotable clone 30 (Crawford et al., 1988). The reason for this apparent paradox may be that cells are stimulated to grow when they are protected from excessive AO toxicity as long as a sufficient AO signal remains

to activate the necessary growth pathways. Despite the opposite effects of additional CAT and Cu,Zn-SOD on cytotoxicity by AO, the inducibility of c-*fos* is reduced in both types of transfectants. However, the reasons for the decrease in c-*fos* induction are probably quite different for CAT and Cu,Zn-SOD transfectants. The former are well protected from excessive H_2O_2 toxicity, but at the same time the signal which results in c-*fos* induction is attenuated. We had shown previously that H_2O_2 rather than $O_2^{\cdot-}$ represents the active species for the induction of the translocation to the plasma membrane of protein kinase C (Larsson & Cerutti, 1989) and that CAT rather than SOD inhibited S6 phosphorylation by X/XO in JB6 cells (Larsson & Cerutti, 1988). In contrast, increases in Cu,Zn-SOD levels alone augment the intracellular formation of H_2O_2, and toxic effects on components of the signal transduction pathways may predominate. It should be noted that in the X/XO system used in our work a large amount of $O_2^{\cdot-}$ plus H_2O_2 is generated close to the cell surface. Superoxide may penetrate the membrane sufficiently for dismutation by cytosolic Cu,Zn-SOD. Therefore, enhanced oxidative damage in SOD 15 and SOD 3 may occur preferentially at the plasma membrane. Peroxidatic activity of Cu,Zn-SOD (Hodgson & Fridovich, 1975) may contribute to the peroxidation of membrane lipids. Induction of c-*fos* and other immediate early genes is necessary for the acquisition of growth competence in many types of cells, but it is by no means sufficient for growth stimulation. Oxidants are bound to affect multiple pathways which participate in positive and negative growth regulation. Therefore, it is not astonishing that no simple relationship was observed between the inducibility of c-*fos* and growth response to oxidants for the SOD and CAT transfectants studied in this work.

Our results imply that H_2O_2 is the major damaging species as well as the trigger for pathophysiological reactions for an extracellular burst of AO produced by X/XO (Simon et al., 1981; Link & Riley, 1988). Similarly, the toxic effects of activated inflammatory leukocytes can be mostly attributed to H_2O_2 (Nathan et al., 1979; Simon et al., 1981; Thomas et al., 1986). Evidently epidermal cells such as JB6 are poorly protected from a large extracellular flux of H_2O_2 in part because CAT is located mostly in peroxysomes and the contribution of cytosolic SeGPx is only minor (Michiels et al., 1988). Any further increase in H_2O_2 by excess Cu,Zn-SOD only aggravates toxicity. Reduction of Fe^{III} by $O_2^{\cdot-}$ which might be diminished by SOD does not appear to contribute in a major way to toxicity (Kyle et al., 1988). It should be appreciated that the contributions of CAT and Cu,Zn-SOD to antioxidant defense could be quite different under normoxic conditions or when AO is generated intracellularly. For example, in most cell systems a moderate increase in cytoplasmic SOD was protective against redox-cycling drugs such as paraquat (Elroy-Stein et al., 1986; Krall et al., 1988).

Acknowledgments

We thank Dr. A. Baret for supplying antibodies against human catalase and manganese superoxide dismutase and Drs. Y. Groner, R. Gravel, and T. Hashimoto for cDNAs of human Cu,Zn-superoxide dismutase and human and rat catalase, respectively.

Registry No. SOD, 9054-89-1; CAT, 9001-05-2; GPx, 9013-66-5; reduced glutathione, 70-18-8.

References

Beauchamp, B., & Fridovich, I. (1971) *Anal. Biochem. 44*, 276–287.

Bloch, C., & Ausubel, F. (1986) *J. Bacteriol. 168*, 795–798.

Cantoni, O., Sestili, P., Cattabeni, F., Bellomo, G., Pou, S., Cohen, M., & Cerutti, P. (1989) *Eur. J. Biochem. 182*, 209–212.

Ceballos, I., Delabar, J., Nicole, A., Lynch, R., Hallewell, R., Kamoun, P., & Sinet, P. (1988) *Biochim. Biophys. Acta 949*, 58–64.

Cerutti, P. (1985) *Science 227*, 375–381.

Cerutti, P., & Trump, B. (1991) *Cancer Cells 3*, 1–7.

Cerutti, P., Fridovich, I., & McCord, J., Eds. (1988) *Oxy-Radicals in Molecular Biology and Pathology*, pp 493–507, Alan R. Liss, Inc., New York.

Chen, C., & Okayama, H. (1987) *Mol. Cell. Biol. 7*, 2745–2752.

Chirgwin, J., Przbyla, A., MacDonald, R., & Rutter, W. J. (1979) *Biochemistry 18*, 5294–5299.

Clairborne, A. (1985) Catalase activity, in *Handbook of Methods for Oxygen Radical Research* (Greenwald, R., Ed.) pp 283–284, CRC Press, Boca Raton, FL.

Cotgreave, I., & Moldeus, P. (1986) *J. Biochem. Biophys. Methods 13*, 231–249.

Crawford, D., Zbinden, I., Amstad, P., & Cerutti, P. (1988) *Oncogene 3*, 27–32.

Crawford, D., Amstad, P., Yin Foo, D., & Cerutti, P. (1989) *Mol. Carcinog. 2*, 136–143.

Elroy-Stein, O., Bernstein, Y., & Groner, Y. (1986) *EMBO J. 5*, 615–622.

Furuta, S., Hayashi, H., Hijikata, M., Miyazawa, S., Osumi, T., & Hashimoto, T. (1986) *Proc. Natl. Acad. Sci. U.S.A. 83*, 313–317.

Günzler, W., & Flohé, L. (1985) Glutathione peroxidase, in *Handbook of Methods for Oxygen Radical Research* (Greenwald, R., Ed) pp 285–290, CRC Press, Boca Raton, FL.

Hodgson, E., & Fridovich, I. (1975) *Biochemistry 14*, 5299–5303.

Kelner, M., & Bagnell, R. (1990) *J. Biol. Chem. 265*, 10872–10875.

Kohn, K., Erickson, L., Ewig, R., & Friedman, C. (1976) *Biochemistry 15*, 4629–4637.

Korneluk, R., Quan, F., Lewis, W., Guise, K., Willard, H., Holmes, M., & Gravel, R. (1984) *J. Biol. Chem. 259*, 13819–13823.

Krall, J., Bagley, A., Mullenbach, G., Hallewell, R., & Lynch, R. (1988) *J. Biol. Chem. 263*, 1910–1914.

Kyle, M., Nakae, D., Sakaida, I., Micadei, S., & Farber, J. (1988) *J. Biol. Chem. 263*, 3784–3789.

Larsson, R., & Cerutti, P. (1988) *J. Biol. Chem. 263*, 17452–17458.

Larsson, R., & Cerutti, P. (1989) *Cancer Res. 49*, 5627–5632.

Link, E., & Riley, P. (1988) *Biochem. J. 249*, 391–399.

Melton, D., Krieg, P., Rebagliati, M., Maniatis, T., Zinn, K., & Green, M. (1984) *Nucleic Acids Res. 12*, 7035–7056.

Michiels, C., Raes, M., Azchary, M. D., Delaive, E., & Remacle, C. (1988) *Exp. Cell Res. 179*, 581–589.

Muehlematter, D., Larsson, R., & Cerutti, P. (1988) *Carcinogenesis 9*, 239–245.

Muehlematter, D., Ochi, T., & Cerutti, P. (1989) *Chem.-Biol. Interact. 71*, 339–352.

Murrel, G., Francis, M., & Bromley, L. (1990) *Biochem. J. 265*, 659–665.

Nathan, C., Silverstein, S., Brükner, S., & Cohn, Z. (1979) *J. Exp. Med. 149*, 100–113.

Natvig, D., Imlay, K., Touati, D., & Hallewell, R. (1987) *J. Biol. Chem. 262*, 14697–14701.

Norris, K., & Hornsby, P. (1990) *Mutat. Res. 237*, 95–106.
Paoletti, F., Aldinucci, D., Mocali, A., & Caparrini, A. (1986) *Anal. Biochem. 154*, 536–541.
Peterson, G. (1977) *Anal. Biochem. 83*, 346–356.
Phillips, J., Campbell, S., Michaud, D., Charbonneau, M., & Hilliker, A. (1989) *Proc. Natl. Acad. Sci. U.S.A. 86*, 2761–2765.
Scott, M., Meshnik, S., & Eaton, J. (1987) *J. Biol. Chem. 262*, 3640–3645.
Sherman, L., Dafni, N., Lieman-Hurwitz, J., & Groner, Y. (1983) *Proc. Natl. Acad. Sci. U.S.A. 80*, 5465–5469.
Shibanuma, M., Kuroki, T., & Nose, K. (1988) *Oncogene 3*, 17–21.
Simon, R., Scoggin, C., & Patterson, D. (1981) *J. Biol. Chem. 256*, 7181–7186.
Sinet, P. (1982) *Ann. N.Y. Acad. Sci. 396*, 83–94.
Thomas, M., Shirley, P., Hedrick, C., & DeChatelet, L. (1986) *Biochemistry 25*, 8042–8048.
Van Beveren, C., van Straaten, F., Curran, T., Müller, T., & Verma, I. (1983) *Cell 32*, 1241–1255.
Zimmerman, R., & Cerutti, P. (1984) *Proc. Natl. Acad. Sci. U.S.A. 81*, 2085–2087.

Proc. Natl. Acad. Sci. USA
Vol. 89, pp. 890–894, February 1992
Biochemistry

Genotypic analysis of mutations in *Taq* I restriction recognition sites by restriction fragment length polymorphism/polymerase chain reaction

MARTHA S. SANDY, SUSANNA M. CHIOCCA, AND PETER A. CERUTTI

Department of Carcinogenesis, Swiss Institute for Experimental Cancer Research, CH-1066 Épalinges/Lausanne, Switzerland

Communicated by J. Edwin Seegmiller, September 27, 1991

ABSTRACT **Point mutations in somatic cells play a role in the etiology of several classes of human pathologies. Experimental procedures are required that allow the detection and quantitation of such mutations in disease-related genes in tissue biopsy samples without the need for the selection of mutated cells. We describe the genotypic analysis of single base pair mutations in the *Taq* I endonuclease recognition sequence TCGA, residues 2508–2511 of exon 2 of the human c-H-*ras1* gene, by the restriction fragment length polymorphism/polymerase chain reaction (RFLP/PCR) approach. The high thermostability of *Taq* I endonuclease allows the continuous removal of eventual residual wild-type sequences during the thermocycling of the PCR and reduces polymerase errors in the final RFLP/PCR product to a minimum. As few as five copies of a mutant standard containing two base pair changes in the chosen *Taq* I site could be rescued from 10^8 copies of wild-type DNA. *Taq* I RFLP/PCR holds promise for the monitoring of mutations in biochemical epidemiology.**

Most presently available mammalian mutation systems rely on the isolation of a small fraction of mutated cells with a selectable mutated phenotype. Only mutations in a few genes can be analyzed by this approach, and growing cell cultures have to be used for the *ex vivo* or *in vitro* expansion of mutated cells. Methods are required for the analysis of mutations in disease-related genes and in sequences that are known or suspected to contain mutational hot-spots. Furthermore, mutation analysis should be possible in nondividing tissue biopsy samples. To avoid phenotypic selection, rare mutated DNA sequences have to be detectable in the presence of an enormous excess of homologous wild-type DNA, or they have to be separated by biochemical means. The sensitivity of recent experimental approaches to such "genotypic" mutation analysis (1, 2) is limited by backgrounds that originate from the large excess of wild-type DNA relative to mutated sequences. The restriction fragment length polymorphism/polymerase chain reaction (RFLP/PCR) approach applied here, which measures mutations in restriction enzyme recognition sites, greatly reduces this problem (3, 4). Wild-type recognition sites are cleaved by the corresponding endonuclease, allowing the selective amplification of mutated recognition sequences. The mixtures of amplified mutated fragments are either directly sequenced or cloned in λgt10, and then plaques are analyzed by oligonucleotide hybridization.

We have chosen the *Taq* I restriction recognition sequence TCGA for RFLP/PCR mutation analysis for several reasons. Since the *Taq* I recognition sequence contains the four base pairs, it allows the analysis of all 12 possible single base pair mutations. In addition it contains the CpG dinucleotide sequence. Deamination of cytosine or 5-methylcytosine in CpG dinucleotides appears to represent a major mechanism for the formation of C → T transitions (5–8) in genes related to genetic disease and cancer. The present *Taq* I RFLP/PCR protocol allows the rescue of as few as 5 to 10 mutated copies of *Taq* I site 2508–2511 located in exon 2 of the human c-H-*ras1* protooncogene from 10^8 homologous wild-type sequences.

METHODS

Preparation of Authentic Mutants at *Taq* I Site 2508–2511 of c-H-*ras1*. All 12 possible single base pair mutations in the tetranucleotide TCGA of the *Taq* I recognition sequence (residues 2508–2511) of exon 2 of the human c-H-*ras1* gene were prepared by using synthetic oligonucleotides and a PCR protocol (see Fig. 1 for sequence information). Twelve different 20-mers corresponding to residues 2499–2518 that contained single base changes in the TCGA sequence were used as left-side amplimers. A common right-side amplimer corresponding to nucleotides 2542–2562 plus an 11-nucleotide tail containing an *Eco*RI recognition sequence was used in 12 PCRs with pSVneo-ras1 (9, 10) as template. The amplification conditions were as described below. The 12 resulting 75-base-pair (bp) fragments were used as right-side amplimers in a second round of amplifications with a common left-side amplimer corresponding to residues 2401–2420 plus a 12-nucleotide tail containing an *Eco*RI recognition sequence. The resulting 185-bp fragments were inserted into λgt10. All authentic mutant λgt10 constructs were plaque purified on *Escherichia coli* C600 Hfl.

A mutant standard with two base pair changes in the *Taq* I recognition sequence and two additional upstream mutations was prepared according to the same experimental design, using the 21-mer 5′-TTCCCGTACAACGTGACCTCG-3′ (residues 2498–2518 of c-H-*ras1*; positions of mutations underlined) as right-side amplimer and a 20-mer corresponding to residues 2373–2392 of c-H-*ras1* as left-side amplimer. The left-side amplimer contained a 12-nucleotide tail with an *Eco*RI recognition site. The amplification conditions were as described below. The resulting 157-bp fragment was used as left-side amplimer in a second amplification reaction with a right-side amplimer corresponding to residues 2591–2610 plus a 12-nucleotide tail with an *Eco*RI recognition site. The final 261-bp fragment was cloned in pSP64. This plasmid is referred to as "mutant standard" (pSP64-rasTaqISt). A corresponding wild-type plasmid (pSP64-ras) was constructed by an analogous protocol.

***Taq* I Restriction and Amplification Conditions.** Known amounts of pSP64-rasTaqISt and pSP64-ras were first digested with *Eco*RI to release the 253-bp *ras* inserts and subsequently with *Taq* I endonuclease at 6 units/μl for 2 hr at 65°C. From these stocks eight samples were prepared that

The publication costs of this article were defrayed in part by page charge payment. This article must therefore be hereby marked "*advertisement*" in accordance with 18 U.S.C. §1734 solely to indicate this fact.

Abbreviation: RFLP/PCR, restriction fragment length polymorphism/polymerase chain reaction.

contained the numbers of mutant standard and wild-type *ras* copies indicated in Table 1. The samples were prepared in a total volume of 25 μl of amplification buffer: 2.5 μl containing the DNA, each "amplimer" (see Fig. 1 and below) at 3 μM, 1 mM each of dATP, dCTP, dGTP, and dTTP, 21% (vol/vol) dimethyl sulfoxide, 66.6 mM Tris·HCl at pH 8.8, 16.6 mM ammonium sulfate, 6.7 mM $MgCl_2$, 10 mM 2-mercaptoethanol, 6.7 μM EDTA, and 1.5 units of *Taq* DNA polymerase (Cetus). Under these conditions *Taq* polymerase exhibits relatively high replication fidelity (11). *Taq* polymerase was added to the tubes after an initial melting period of 3 min at 92°C.

PCR cycles 1–15. Outer amplimers—i.e., left-side 20-mer 2373–2392 and right-side 20-mer 2591–2610—were used (see Fig. 1). Each cycle consisted of a melting temperature of 81°C (1.1 min), an annealing temperature of 55°C (0.8 min), and an extension temperature of 65°C (0.3 min). To restrict eventual residual wild-type sequences, *Taq* I endonuclease (1.2 units) was added during the annealing periods of cycles 1, 3, 5, 7, 9, 11, 13, and 15.

PCR cycles 16–25. After the 15th cycle, the dimethyl sulfoxide concentration was reduced to 12% by the addition of dimethyl sulfoxide-free amplification mixture. The 16th cycle was begun with an initial melting period of 3 min at 92°C, after which 1.5 units of *Taq* polymerase was added to each tube. Each cycle consisted of a melting temperature of 91°C (0.8 min) and an annealing temperature of 57°C (0.4 min). After 25 cycles 4 units of *Taq* I endonuclease was added to each tube, and the mixtures were incubated for 30 min at 65°C.

PCR cycles 25–50. After the 25th cycle 3-μl aliquots of the amplification mixtures were removed and diluted 121-fold. The amplification was continued under the conditions outlined above with a new, nested, pair of amplimers—i.e., left-side 20-mer 2401–2420 and right-side 21-mer 2542–2562 at 4 μM final concentrations. These amplimers contained in addition 5′ tails with *Eco*RI recognition sequences to facilitate cloning in λgt10 (see Fig. 1). After the 50th cycle 6 units of *Taq* I endonuclease was added and digestion was allowed to proceed for 1 hr at 65°C.

Purification of Amplified DNA and Cloning in λgt10. The amplification mixtures were purified on Qiagen-5 tips (Qiagen; Chatsworth, CA) and the DNA was precipitated with isopropyl alcohol after the addition of 1 μg of *E. coli* tRNA as carrier. DNA aliquots were ligated to λgt10 arms as outlined by the supplier (Promega). The phage DNA was packaged (Packagene, Promega) and used to infect *E. coli* C600 Hfl. Plaques were lifted onto colony/plaque screens (NEF-978, New England Nuclear). At least two independent packagings were carried out and 1–3 × 10^3 plaques on 10–15 Petri dishes were analyzed for each experimental condition.

Oligonucleotide Plaque Hybridization. Specific probes were prepared according to standard conditions by end-labeling of oligonucleotide 20-mers (residues 2499–2518) corresponding to the wild-type sequence of c-H-*ras1*, mutant standard containing 4 base changes, and oligomers containing all 12 possible single base mutations in the tetranucleotide TCGA of *Taq* I recognition site 2508–2511. The colony/plaque screens were hybridized overnight with the radioactive probes at 54°C in 5× SSPE (1× SSPE is 0.18 M NaCl/10 mM sodium phosphate, pH 7.4/1 mM EDTA)/0.3% SDS. Selective washing temperatures between 60°C and 63°C were employed to exclude nonspecific hybridization.

DNA Sequencing. For sequencing, the purified amplification mixtures or authentic plasmid constructs with wild-type or mutant inserts were enriched for the negative strands by using a 21-mer (residues 2542–2562) as single amplimer. This product was then directly sequenced by the extension of a primer complementary to nucleotides 2441–2461 (5′-CTGGCTGCACGCACTGTGGAA-3′; see Fig. 1) with a Sequenase primer extension kit (United States Biochemical). The four lanes of the sequence autoradiograms representing the four nucleotides were scanned with a densitometer (Hirschmann Elscript 400).

RESULTS

RFLP/PCR of *Taq* I Site 2508–2511 of c-H-*ras1*: Continuous *Taq* I Restriction During Amplification. We tested the capacity of our RFLP/PCR protocol to rescue a few copies of *Taq* I mutant standard from a large excess of c-H-*ras1* DNA. For this purpose we constructed a mutant standard plasmid, pSP64-rasTaqISt, with a 238-bp insert corresponding to residues 2373–2610 of exon 2 of human c-H-*ras1* but that contained two mutations in the *Taq* I recognition site 2508–2511—i.e., ACGT instead of wild-type TCGA, and in addition wild-type C residue 2503 and A residue 2498 5′ upstream of this site were replaced by G and T, respectively. The corresponding wild-type construct pSP64-ras contained the analogous 238-bp wild-type insert (Fig. 1). These plasmids were digested with *Eco*RI to release the *ras* inserts and then exhaustively digested with *Taq* I endonuclease, and mixtures were prepared that contained 5, 10, 100, or 1000 copies of the mutant standard and 10^8 copies of the wild-type DNA (see Table 1). A 185-bp fragment containing the *Taq* site 2508–2511 was amplified by PCR. Conditions were chosen for the first 15 PCR cycles that allowed the continuous *Taq* I endonuclease restriction of eventual residual wild-type sequences (see Fig. 1 and *Methods*).

Quantitation of Rescued Mutant Standard and *Taq* Polymerase-Induced Single Base Pair Changes by Oligonucleotide Plaque Hybridization. The four mixtures of amplified *ras* fragments containing increasing initial copy numbers of mutant standard were cloned in λgt10. Plaques were analyzed with 14 specific 20-mer probes (residues 2499–2518) corresponding to the sequence of the mutant standard, wild type, and the 12 possible single base pair mutations in the *Taq* I site 2508–2511. Only a small fraction of plaques (<0.1%) contained wild-type *ras* sequence 2499–2518 in the four amplification mixtures. This result indicates that wild-type sequences at the *Taq* I site 2508–2511 had been almost completely restricted by the repeated *Taq* I endonuclease digestions used in our protocol. As few as 5 initial copies of

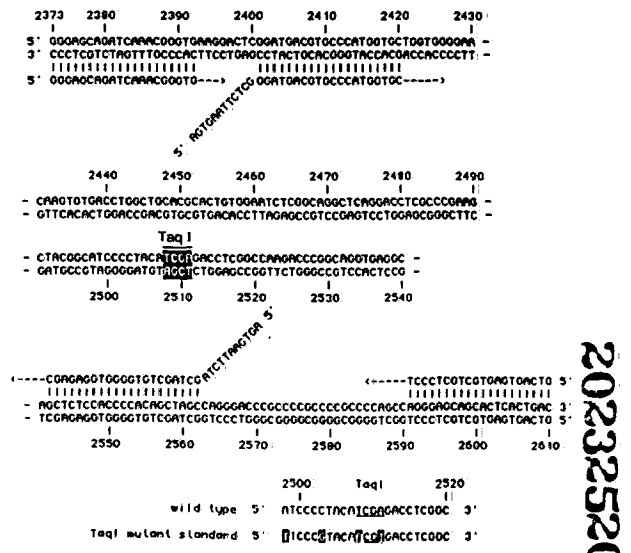

FIG. 1. RFLP/PCR mutagenesis of *Taq* I site 2508–2511 of exon 2 c-H-*ras1*: Sequence information.

mutant standard could be rescued from 10^8 copies of homologous wild-type sequence giving rise to 5.1 ± 2.8% of the identified λ plaques. The fraction of identified plaques containing the mutant standard sequence increased with increasing input copy number and was 8.5 ± 2.6 for 10 initial copies, 43.8 ± 7.0 for 100 initial copies, and 80.3 ± 18.2 for 1000 initial copies (Fig. 2). The total fractions of plaques that could be identified with the 14 oligonucleotide probes varied from 63% to 74%, leaving approximately ⅓ of the plaques unidentified. Direct sequencing of DNA from several plaques by primer extension (see below) indicated that they contained amplimer multimers, small deletions and insertions affecting the *Taq* I site 2508–2511, and also single base pair changes in this site that had escaped detection by oligonucleotide hybridization.

Since the mutant standard contains two additional mutated sites upstream, single base pair mutations in the selected *Taq* I site do not affect the frequency of mutant standard plaques detected by oligonucleotide hybridization. In contrast, the sensitivity with which a particular base pair change can be detected in the *Taq* I site 2508–2511 depends on the frequency with which this particular mutation is produced by polymerase infidelity on residual unrestricted wild-type templates. As shown in Fig. 2, we have determined the relative abundances of all 12 possible *Taq* polymerase-induced single base pair mutations in the selected *Taq* I site 2508–2511. For all four initial mutant standard/wild-type DNA mixtures that were analyzed in detail *Taq* polymerase-induced errors occurred in the following order of decreasing frequency: A → G (TCGG) >> T → C (CCGA) > T → A (ACGA) = G → A (TCAA) > C → T (TTGA) > A → T (TCGT) > G → T (TCTA). The abundance of mutant standard DNA affected the magnitude of the fractions of single base pair mutations but not their relative importance. It is evident that *Taq* polymerase preferentially induces transitions at A·T base pairs and that the error frequencies are sequence dependent. We conclude that 10 copies of mutagen-induced single base pair mutations in *Taq* I site 2508–2511 should be readily detectable in the presence of 10^8 copies of wild-type DNA by the *Taq* I RFLP/PCR protocol except for transitions involving A·T base pairs, which represent frequent *Taq* polymerase errors.

Sequence Analysis of *Taq* I RFLP/PCR Products by Primer Extension. The *Taq* I RFLP/PCR products were subjected to direct sequencing by the extension of a 21-mer (corresponding to residues 2441–2461). Fig. 3 gives the results for wild-type DNA, for the RFLP/PCR product from the initial mixture containing 10^3 copies of *Taq* I mutant standard, and for authentic *Taq* I mutant standard DNA. The presence of the mutant standard in the RFLP/PCR product is readily discernible in the sequence shown in the center of Fig. 3, where bands for residues T2498, G2503, A2508, and T2511 are visible that are absent from the wild-type sequence shown to the left. The four lanes of the autoradiograms for each sequence were scanned with a densitometer. The tracings are shown in Fig. 4 for the RFLP/PCR product of the initial mixture containing 10^3 copies of mutant standard and 10^8 copies of wild-type sequence. Peaks are discernible for the residues indicated above that are specific for the mutant standard sequence.

Band intensities for individual residues vary for sequences of unique DNA fragments, probably due to conformational restraints. However, these variations are reproducible. Therefore, we normalized our data relative to the intensities of two representative residues for each lane. For example, we determined the ratios 2[G2503/(G2496 + G2518)]. These normalized values for the band intensities of residues G2503 in comparison with those obtained with wild-type and authentic mutant standard DNA are direct measures for the mutant standard and wild-type content of the RFLP/PCR product, respectively. The data summarized in Table 1 (columns 2–5) show that as few as 5 initial copies of mutant standard can be measured and that the band intensities of mutant standard residue G2503 increase with increasing initial copy number, while the band intensities of wild-type residue C2503 decrease correspondingly.

The band intensities for residues 2508 and 2511 of the *Taq* I site were analyzed in an analogous manner on the sequence

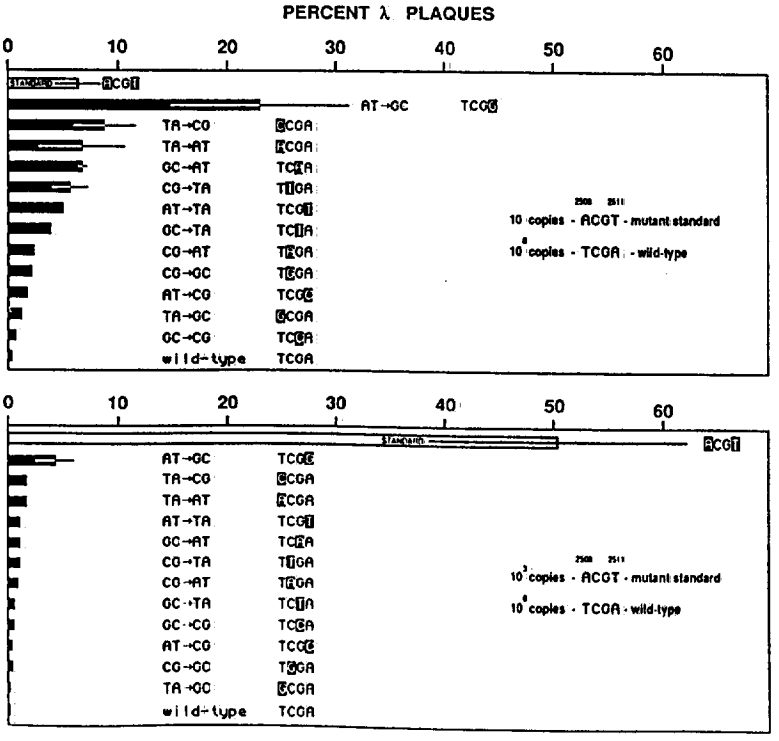

FIG. 2. Analysis of RFLP/PCR products originating from mixtures initially containing 10 (*Upper*) or 1000 (*Lower*) copies of mutant standard and 10^8 copies of wild-type DNA. The RFLP/PCR products were cloned in λgt10, the phage was plated on *E. coli* C600 Hfl, and the plaques were analyzed for their content of mutant standard, *Taq* polymerase-induced single base pair mutations and wild-type DNA by hybridization with 14 specific oligonucleotide probes. The data represent means of four Petri dishes containing in total 1219 or 1160 plaques (*Upper* and *Lower*, respectively). Individual plaques hybridized only with a single probe. The histograms show the percent plaques containing a particular mutation relative to the total plaques on a particular Petri dish. Error bars indicate standard deviations.

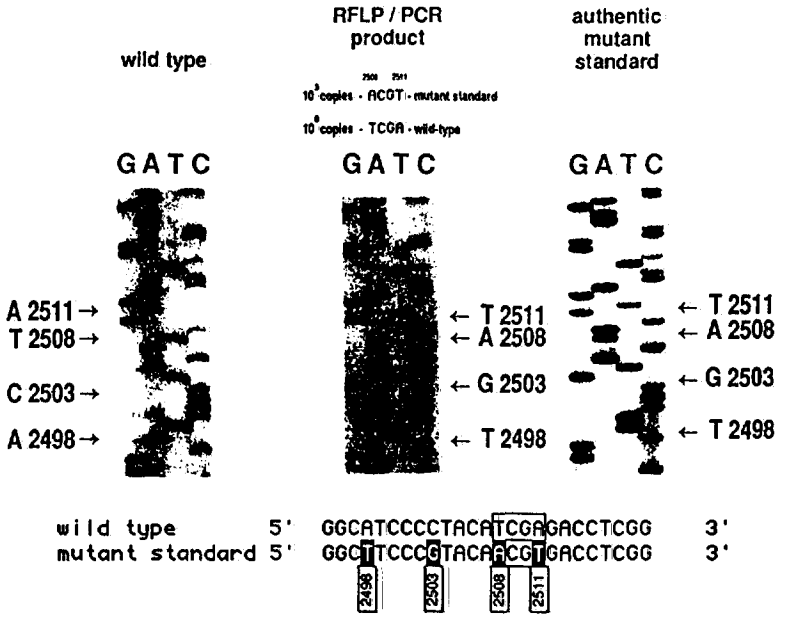

FIG. 3. Direct sequencing of RFLP/PCR product by primer extension. The center sequence derives from the RFLP/PCR product of the initial mixture containing 10^3 copies of mutant standard and 10^8 copies of wild-type DNA; the left sequence derives from authentic wild-type DNA and the right sequence, from authentic mutant standard DNA. The negative strands were sequenced by the extension of a primer complementary to residues 2441–2461. The mutated residues in the mutant standard are indicated in the center and right sequences and the corresponding wild-type residues, in the left sequence.

autoradiograms and the data are given in columns 6–13 of Table 1. There is good agreement for the contents in wild-type residues T2508 and A2511 for each individual RFLP/PCR product, and their contents decrease with increasing initial copy number of mutant standard. This decrease is compensated for by a corresponding increase in the content of A2508 that originates from the mutant standard. Densitometric measurements of mutant standard residue T2511 are less accurate because this residue gives rise to a low-intensity band. It should be noted that a signal for G2511, which represents the most abundant *Taq* polymerase-induced mutation, A·T → G·C in the *Taq* I site, was visible in the RFLP/PCR product originating from initially 5 copies of mutant standard and 10^8 copies of wild-type DNA (data not shown). We conclude that direct sequencing by primer extension of the *Taq* I RFLP/PCR products allows the detection of the more abundant mutations.

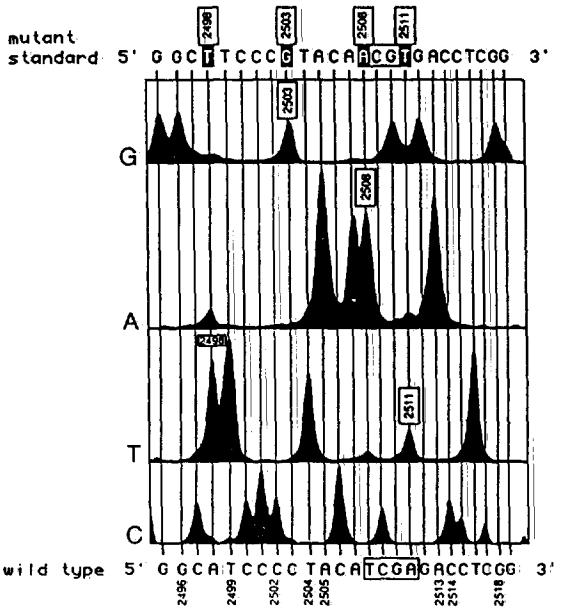

FIG. 4. Densitometer tracings of the sequence of the RFLP/PCR product resulting from initially 10^3 copies of mutant standard and 10^8 copies of wild-type DNA (shown in Fig. 3). The peaks originating from residues specific for mutant standard and the positions of wild-type residues that served for data normalization are indicated.

DISCUSSION

The RFLP/PCR protocol for analysis of genotypic mutations measures mutations in restriction enzyme recognition sequences. This allows the efficient enrichment of mutated over wild-type sequences by exhaustive restriction with the corresponding endonuclease followed by the selective amplification of the uncut sequences by PCR. We had explored the feasibility of this approach in studies of *Pvu* II site 1727–1732 and *Msp* I site 1695–1698 of exon 1 of the human c-H-*ras1* gene. As few as 10 copies of *Pvu* II mutant standard with two base pair changes in the recognition sequence and a third mutation upstream of the site could be rescued by the RFLP/PCR procedure from 10^8–10^9 wild-type sequences (3, 4).

The *Taq* I RFLP/PCR protocol described here allowed the efficient rescue of mutant standard that contains two base pair replacements in the *Taq* I site 2508–2511 and two additional changes 5′ upstream of this site from a large excess of wild-type DNA. Plaque hybridization as well as sequencing allowed the determination of the mutant standard content of RFLP/PCR mixtures originating from the initial mixtures of only 5 copies of mutant standard and 10^8 copies of wild-type DNA. Highest reproducibility was observed for the content of G2503, which is specific for the mutant standard, and the corresponding wild-type residue, C2503, by direct sequencing (see Table 1). Residue 2503 is located 5′ upstream of the *Taq* I site 2508–2511 and mutations at this residue are not selected. Therefore, sequences containing wild-type C2503 must be mutated in *Taq* I site 2508–2511.

The capacity of the RFLP/PCR protocol to rescue single base pair mutations is limited by the amount of residual unrestricted wild-type DNA that is present during PCR because of the limited fidelity of the polymerase, in particular of *Taq* polymerase, used in the reaction (4, 10–13). The high thermostability of *Taq* I endonuclease allows the continuous restriction of eventual residual wild-type DNA during amplification. Less than 0.1% of the plaques resulting from the

Table 1. Quantitation of mutant standard in RFLP/PCR product by direct sequencing (c-H-*ras1* exon 2 *Taq* I site 2508–2511)

	WT C2503		MS G2503		WT T2508		MS A2508		WT A2511		MS T2511	
No. of copies	OD (n = 2)	% of WT	OD (n = 3)	% of MS	OD (n = 3)	% of WT	OD (n = 3)	% of MS	OD (n = 2)	% of WT	OD (n = 2)	% of MS
All WT	0.84 ± 0.02	100	0.022 ± 0.02	2.5	0.74 ± 0.01	100	—	—	0.53 ± 0.06	100	—	—
All MS	—	—	1.36 ± 0.03	100	—	—	0.88 ± 0.02	100	—	—	0.37 ± 0.02	100
5 MS + 10^8 WT	0.66 ± 0.06	78	0.095 ± 0.015	7	—	—	—	—	—	—	—	—
10 MS + 10^8 WT	0.60 ± 0.03	71	0.225 ± 0.025	17	0.44 ± 0.04	59	0.11 ± 0.05	12	0.32 ± 0.04	61	0.19 ± 0.05	51
10^2 MS + 10^8 WT	0.37 ± 0.01	44	0.555 ± 0.005	41	0.21 ± 0.07	28	0.34 ± 0.07	39	0.17 ± 0.02	32	0.20 ± 0.12	54
10^3 MS + 10^8 WT	0.10 ± 0.10	12	1.04 ± 0.14	76	0.09 ± 0.02	12	0.66 ± 0.03	75	0.07 ± 0.005	14	0.33 ± 0.04	89

WT, wild type; MS, mutant standard. From left to right, columns labeled OD give means of densitometer readings (see Fig. 4; n = number of sequences read) expressed as the following ratios: for WT C2503, 2[C2503/(C2502 + C2514)]; for MS G2503, 2[G2503/(G2496 + G2518)]; for WT T2508, 2[T2508/(T2499 + T2504)]; for MS A2508, 2[A2508/(A2505 + A2513)]; for WT A2511, 2[A2511/(A2505 + A2513)]; and for MS T2511, 2[T2511/(T2499 + T2504)]. The adjacent columns give the percent nucleotide content relative to the WT or authentic MS for each nucleotide.

Taq I RFLP/PCR product contained the wild-type sequence. In contrast, the percentages of wild-type plaques in the *Pvu* II site 1727–1732 and in the *Msp* I site 1695–1698 RFLP/PCR products of the c-H-*ras1* gene were in the range of 14–23% and 35–40%, respectively (4).

Even in the *Taq* I RFLP/PCR system a few copies of uncut wild-type DNA remain, and mutations are produced experimentally due to *Taq* polymerase infidelity. By far the most frequent *Taq* polymerase error according to plaque hybridization was A·T 2511 → G·C (TCGG), followed by T·A 2508 → A·T (ACGA). This agrees with published work, in which A·T → G·C transitions were reported to be the most frequent *Taq* polymerase errors (11–14). However, RFLP/PCR analysis of two independent restriction sites in exon 1 of c-H-*ras1* revealed different spectra of *Taq* polymerase errors. The predominant *Taq* mutations in the internal tetranucleotide of *Pvu* II site 1727–1732 were C·G 1730 → G·C (AGGT) and, at lower frequency, C·G 1730 → A·T (AGAT), while the predominant *Taq* mutations at the two G residues of *Msp* I site 1695–1698 were G·C 1698 → T·A (CCGT) and, at lower frequency, G·C 1698 → A·T (CCGA) (4). It appears that *Taq* polymerase fidelity depends more on sequence context than on the base pair that is being replicated. The mutant standard content of the RFLP/PCR product originating from a known number of initial copies allows an estimate of the sensitivity of the *Taq* I RFLP/PCR protocol for specific base pair changes. For some mutations with low *Taq* polymerase backgrounds—e.g., T·A 2508 → G·C (GCGA) and G·C 2510 → C·G (TCCA) (see Fig. 2)—it should be possible to rescue as little as one copy of these mutants in the presence of 10^9 wild-type sequences. For the *Msp* I site 1695–1698 the transversion G·C → T·A at base pair 1698 represents the most frequent *Taq* polymerase error. Nevertheless, 100 copies of this single base pair mutation could be rescued from 10^8 copies of wild-type DNA (4).

The sensitivity of mutant quantitation in the RFLP/PCR product by cloning and plaque hybridization is high, but the procedure is laborious and costly. The data in Table 1 indicate that quantitative sequence analysis was capable of measuring single base pair mutations in the *Taq* I site 2508–2511 originating from minimally 10–100 initial copies of mutant standard plus 10^8 copies of wild-type DNA. Modification of the PCR conditions and the use of polymerases with lower error rates (14) might further increase the overall sensitivity of RFLP/PCR mutation analysis and allow its application to the measurement of spontaneous and xenobiotic-induced somatic mutations in disease related genes in humans (15–19).

This work was supported by the Swiss National Science Foundation, the Swiss Association of Cigarette Manufacturers, and the Association for International Cancer Research.

1. Rossiter, B. & Caskey, C. T. (1990) *J. Biol. Chem.* **265**, 12753–12756.
2. Cariello, N., Keohavong, P., Kat, A. & Thilly, W. (1990) *Mutat. Res.* **231**, 165–176.
3. Zijlstra, J., Felley-Bosco, E., Amstad, P. & Cerutti, P. (1990) in *Mutagens and Carcinogens in the Diet*, ed. Pariza, M. W. (Wiley/Liss, New York), pp. 187–200.
4. Felley-Bosco, E., Pourzand, C., Zijlstra, J., Amstad, P. & Cerutti, P. (1991) *Nucleic Acids Res.* **19**, 2913–2919.
5. Ehrlich, M., Zhang, X. Y. & Inamdar, N. (1990) *Mutat. Res.* **238**, 277–286.
6. Cooper, D. & Youssoufian, H. (1988) *Hum. Genet.* **78**, 151–155.
7. Hollstein, M., Sidransky, D., Vogelstein, B. & Harris, C. (1991) *Science* **253**, 49–53.
8. Barker, D., Schafer, M. & White, R. (1984) *Cell* **36**, 131–138.
9. Parada, L., Tobin, C., Shih, C. & Weinberg, R. (1982) *Nature (London)* **297**, 474–478.
10. Capon, D., Chen, E., Levinson, A., Seeburg, P. & Goeddel, D. (1983) *Nature (London)* **302**, 33–37.
11. Eckert, K. & Kunkel, T. (1990) *Nucleic Acids Res.* **18**, 3739–3743.
12. Tindall, K. & Kunkel, T. (1988) *Biochemistry* **27**, 6008–6013.
13. Saiki, R., Gelfand, D., Stoffel, S., Scharf, S., Higuchi, R., Horn, G., Mullis, K. & Erlich, H. (1988) *Science* **239**, 487–491.
14. Keohavong, P. & Thilly, W. (1989) *Proc. Natl. Acad. Sci. USA* **86**, 9253–9257.
15. Mendelsohn, M. & Albertini, R., eds. (1989) *Mutation and the Environment, Part C: Somatic and Heritable Mutation, Adduction and Epidemiology* (Wiley/Liss, New York).
16. Bos, J. L. (1988) *Mutat. Res.* **195**, 255–271.
17. Baker, S. J., Fearon, E. R., Nigro, J. M., Hamilton, S. R., Preisinger, A. C., Jessup, J. M., van Tuinen, P., Ledbetter, D. H., Barker, D. F., Nakamura, Y., White, R. & Vogelstein, B. (1989) *Science* **244**, 217–221.
18. Nigro, J. M., Baker, S. J., Preisinger, A. C., Jessup, J. M., Hostetter, R., Cleary, K., Bigner, S., Davidson, N., Baylin, S., Devilee, P., Glover, T., Collins, F., Weston, A., Modali, R., Harris, C. & Vogelstein, B. (1989) *Nature (London)* **342**, 705–708.
19. Takahashi, T., Nau, M., Chiba, I., Birrer, M., Rosenberg, R., Vinocour, M., Levitt, M., Pass, H., Gazdar, A. & Minna, J. (1989) *Science* **246**, 491–494.

Proc. Natl. Acad. Sci. USA
Vol. 89, pp. 5331–5335, June 1992
Genetics

Genotypic analysis of *N*-ethyl-*N*-nitrosourea-induced mutations by *Taq* I restriction fragment length polymorphism/polymerase chain reaction in the c-H-*ras1* gene

SUSANNA M. CHIOCCA, MARTHA S. SANDY, AND PETER A. CERUTTI

Department of Carcinogenesis, Swiss Institute for Experimental Cancer Research, 1066 Epalinges/Lausanne, Switzerland

Communicated by Gerald N. Wogan, February 26, 1992

ABSTRACT **In genotypic mutation analysis DNA sequence changes are determined without the *in vivo* or *in vitro* selection of phenotypically altered cells. We have studied the induction of base-pair changes by *N*-ethyl-*N*-nitrosourea in *Taq* I endonuclease recognition site 2508–2511 (TCGA) of the c-H-*ras1* gene in human fibroblasts by the restriction fragment length polymorphism/polymerase chain reaction (RFLP/PCR) method. This site contains the four bases, and all 12 possible single base-pair changes can be monitored. The transition of guanine to adenine at position 2510 was the major mutation detected by λ plaque oligonucleotide hybridization and quantitative sequence analysis of the RFLP/PCR products. It involves the G residue of the CpG sequence of the coding strand. Data calibration with an internal mutant standard indicates that absolute frequencies for this transition lie in the range of 4–12 × 10^{-7}. The present study documents the capacity of the RFLP/PCR approach to measure mutagen-induced base-pair changes in a specific gene sequence without the selection of a phenotypically altered cell.**

Somatic mutations participate in the etiology of numerous human pathologies and their detection represents an important goal in molecular epidemiology. Only a minute fraction of cells harbors a particular mutation in the earliest stages of the development of a disease and the mutation only rarely gives rise to a selectable altered phenotype. Although the type of mutations that are induced by a particular mutagen can be defined in model systems, the actual mutability of a particular nucleotide sequence is expected to vary substantially for different genetic loci. Factors that affect the mutability are local chromatin structure and sequence context, the transcriptional state of the gene, its replication schedule, and the repairability of the mutagen-induced lesions. A case in point is the spectrum of base-pair mutations found in the tumor suppressor gene p53 in human tumors. The existence of five hypermutable domains in this gene may be dictated by protein function. However, the type and exact location of the mutations and the choice of the mutated domain were found to be organ and tumor specific (1). This suggests that different mutagens and factors that modulate mutability are involved in the different tumor progenitor cells. For the identification of endogenous and environmental mutagens that play a causative role in the formation of particular mutations in disease-related target genes, "genotypic" mutation analysis is required; this allows the quantitation of specific mutated sequences without the need for the *ex vivo* or *in vitro* selection or expansion of phenotypically altered cells (2–4).

In search of approaches allowing genotypic mutation analysis we have applied the restriction fragment length polymorphism/polymerase chain reaction (RFLP/PCR) approach to the determination of base-pair mutations induced by the ethylating agent *N*-ethyl-*N*-nitrosourea (ENU) in *Taq* I site 2508–2511 of exon 2 of the human c-H-*ras1* gene. In the RFLP/PCR method mutations are determined in restriction recognition sequences. Wild-type (wt) recognition sequences are cleaved and the resistant mutated sequences are selectively amplified by PCR (3, 5, 6). ENU was chosen because it induces preferentially base-pair changes of the type found as background mutations in the *HPRT* gene in the human (7) and because its mutational specificity is well known (8–10). Analysis of the *Taq* I recognition sequence TCGA allows the detection of all 12 possible base-pair changes. Furthermore, it contains the CpG dinucleotide, which appears to be hypermutable, presumably because of the deamination of cytosine or 5-methylcytosine (11–13). *Taq* I RFLP/PCR has the experimental advantage that residual wt sequences can be continuously removed during the thermocycling in PCR because of the high thermostability of *Taq* I endonuclease. The present study documents the capacity of the RFLP/PCR approach to measure mutagen-induced base-pair changes in a specific gene sequence without the selection of a phenotypically altered cell.

MATERIALS AND METHODS

Cell Culturing and Mutagen Treatment. Monolayers of human foreskin fibroblasts (type 3229) were cultured in Dulbecco's modified Eagle medium (DMEM) supplemented with 10% fetal calf serum. The monolayers were treated with 4 mM (experiment 1) or 2 mM (experiments 2–4) ENU. After 30 min of incubation the treatment medium was replaced with fresh DMEM supplemented with 10% fetal calf serum. The cells were harvested after 48 hr in experiments 1 and 4 and after 72 hr in experiments 2 and 3. Treatment of line 3229 human foreskin fibroblasts with 2 mM ENU had only a minor effect on cell growth during the 72-hr expression period. For example, 2.3 × 10^6 cells per Petri dish expanded to 8.5 × 10^6 cells during 72 hr in the untreated controls but expanded to 7 × 10^6 cells following ENU treatment. On the other hand, colony-forming ability (mean ± SD) was reduced to 45.7% ± 3.2% by 2 mM ENU and to 19.2% ± 4.0% by 4 mM ENU.

Preparation of DNA Enriched in c-H-*ras1* Sequences. Bulk DNA was prepared by the guanidine isothiocyanate procedure according to Chirgwin *et al.* (14) and restricted in aliquots of 120–140 μg with 3 units of *Bam*HI per μg. The restricted DNA was separated by electrophoresis (1% agarose gels in 40 mM Tris base/20 mM sodium acetate/1 mM Na_2EDTA adjusted to pH 7.2). Gel slices containing DNA from approximately 6.5 to 9.4 kilobases (kb) were removed and the DNA was electroeluted in a Biotrap apparatus (15). The recovery of c-H-*ras1* sequences in enriched preparations was determined by Southern blotting. A nick-translated 6.6-kb c-H-*ras1* fragment released by *Bam*HI from pSVneo-

The publication costs of this article were defrayed in part by page charge payment. This article must therefore be hereby marked "*advertisement*" in accordance with 18 U.S.C. §1734 solely to indicate this fact.

Abbreviations: ENU, *N*-ethyl-*N*-nitrosourea; RFLP/PCR, restriction fragment length polymorphism/polymerase chain reaction; MS, mutant standard; wt, wild-type.

ras1 (16) served as probe (17). Only DNA preparations were used for *Taq* I RFLP/PCR analysis for which the recovery of c-H-*ras1* sequences was >60%.

***Taq* I RFLP/PCR of Recognition Site 2508–2511 of Exon 2 of c-H-*ras1*.** Aliquots of DNA enriched in 6.6-kb *Bam*HI fragments of c-H-*ras1* containing 1–2 × 10^7 copies of this gene from ENU-treated and untreated cells were digested with *Bgl* I. *Bgl* I digestion produces a 365-base-pair (bp) fragment (residues 2274–2638) containing *Taq* I site 2508–2511. This restriction was performed to obtain fragments of comparable lengths for genomic *ras* DNA mutated in *Taq* I site 2508–2511 (i.e., 365 bp) and *Eco*RI-digested mutant standard (MS) plasmid pSP64-rasTaqISt (i.e., 238 bp plus two 8-bp *Eco*RI tails), which are contained in the amplification mixture. The genomic DNA was then exhaustively digested with an excess of *Taq* I for 4 hr at 65°C. To each of the restricted genomic DNA preparations were added 10 copies of *Eco*RI-digested MS pSP64-ras-TaqISt. Construction of the MS plasmid, which contains 4-bp changes relative to wt in the *ras* sequence 2373–2610, 5′-TTCCCGTACAACGTGA-3′ (note: mutations are underlined; 2-bp changes are located in the *Taq* I site 2508–2511), the amplification protocol with repeated digestion with *Taq* I endonuclease, purification of the RFLP/PCR product, cloning into λgt10, and conditions for the direct sequencing of the RFLP/PCR product have been described (6). The four lanes of the sequence autoradiograms representing the four nucleotides were scanned with a densitometer (Hirschmann Elscript, model 440). Comparison of the normalized peak areas to the corresponding data from authentic wt, mutant, or MS DNA allowed determination of the composition of the RFLP/PCR products (see Tables 1 and 2).

2508 2511

RESULTS AND DISCUSSION

Genotypic mutation analysis by RFLP/PCR determines mutations in restriction sequences. Only mutated sites that have become resistant to cleavage by the corresponding endonuclease are amplified by PCR (3, 5). In the *Taq* I RFLP/PCR protocol, residual wt sequences that might be further amplified are continuously removed during the thermocycling by multiple additions of the thermostable *Taq* I endonuclease. We measured ENU-induced base-pair changes in *Taq* I site TCGA 2508–2511 of exon 2 of c-H-*ras1*. We first prepared DNA enriched in c-H-*ras1* containing 1–2 × 10^7 copies of this gene from ENU-treated and untreated human foreskin fibroblasts by gel electrophoresis. To these preparations of genomic DNA were added 10 copies of a MS containing 2-bp changes in the *Taq* I site 2508–2511 and two additional changes 5′ to this site (6). The DNA samples were exhaustively digested with *Taq* I endonuclease and a 162-bp fragment containing *Taq* I site 2508–2511 was amplified by PCR with continued digestion by *Taq* I endonuclease (see Fig. 1 legend). The *Taq* I RFLP/PCR products of four independent experiments were analyzed for their content in wt sequence, single base-pair mutations, and MS by cloning into λgt10. Plaque hybridization with a specific oligonucleotide probe did not reveal the presence of wt DNA in any of the RFLP/PCR products. It is evident that wt sequences had been completely restricted by the repeated *Taq* I digestions before, during, and after amplification.

ENU Induces the Transition of Guanine to Adenine at Position 2510 (G-2510 to A-2510) in *Taq* I site 2508–2511 of c-H-*ras1*. Fig. 1 shows a typical result for hybridization of λ plaques with mutant A-2510 20-mer (residues 2499–2518) containing A instead of G at position 2510. In this particular experiment the total number of plaques varied from 182 to 241 on the four Petri dishes originating from DNA from untreated cells (Fig. 1 *Upper*) and from 162 to 201 for DNA from ENU-treated cells (Fig. 1 *Lower*). It is evident that ENU treatment induced the transition G-2510 → A-2510. Quantitative plaque hybridization data from three independent experiments are given in Table 1 (columns 4 and 7). The A-2510 content of the RFLP/PCR product from untreated cells varied from 4.6% to 7.2% and from ENU-treated cells from 17.6% to 23.1%, corresponding to a 2.5- to 3.8-fold increase. When 10^8 copies of authentic wt c-H-*ras1* DNA from pSVneo-ras1 was processed by the same RFLP/PCR protocol, 6.6% of the resulting λ plaques contained the A-2510 mutation (see Table 1). Since this value is comparable to that for DNA from untreated cells it is likely that these background A-2510 mutations are introduced experimentally by *Taq* polymerase (5, 18–21).

The A-2510 mutant content of the RFLP/PCR products was estimated independently by direct sequencing using a 21-mer corresponding to residues 2441–2461 as primer. For comparison, authentic wt c-H-*ras1* DNA and authentic mutant A-2510 DNA were sequenced in parallel. The middle panels in Fig. 2 show representative sequences derived from RFLP/PCR products of experiment 2. For DNA from untreated and ENU-treated cells alike, the wt 2508–2511 sequence TCGA predominates, but only in the latter is a band for A-2510 visible next to wt residue G-2510. As expected, only the A-2510 band is visible in the sequence of the authentic mutant A-2510 shown on the right-hand panel.

The sequence autoradiograms were quantitatively evaluated by densitometry and the tracings for the G and A lanes are shown in Fig. 3. It is well known that band intensities in a particular lane obtained by primer extension depend on the position of the residues in the sequence, presumably because of conformational restraints of the DNA. However, these differences in band intensities are reproducible. Therefore, we normalized our data in each lane relative to reference residues located outside of the *Taq* I site 2508–2511 (see also ref. 6). As indicated in Table 1, we used residues A-2505 and A-2513 for the normalization of the intensities of mutant A-2510. The content of the RFLP/PCR products in mutant A-2510 was computed in reference to data from the sequence of authentic mutant A-2510 DNA. The data from four inde-

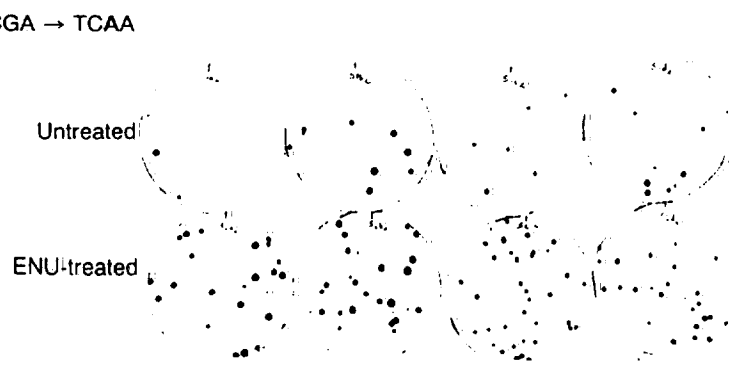

FIG. 1. Quantitation of ENU-induced G-2510 → A-2510 mutation in *Taq* I site 2508–2511 of c-H-*ras1* of DNA from human fibroblasts by RFLP/PCR analysis: hybridization of λ plaques with A-2510 mutation-specific oligonucleotide probe. (*Upper*) RFLP/PCR product from DNA of untreated control cultures. (*Lower*) RFLP/PCR product from DNA of ENU-treated cultures.

Table 1. Quantitation of ENU-induced G-2510 to A-2510 transition in RFLP/PCR products by sequence analysis and λ plaque hybridization

	Untreated cells			ENU-treated cells*		
	A-2510 content		% TCΔA	A-2510 content		% TCΔA
	Mean†	%‡	λ plaques§	Mean†	%‡	λ plaques§
Authentic mutant A-2510	0.94 ± 0.16	100		0.94 ± 0.16	100	
Experiment						
1	0.067 ± 0.016	7.1 ± 1.7	7.2 ± 1.6	0.139 ± 0.056	14.8 ± 5.9	17.7 ± 2.6
2	0.056 ± 0.023	5.9 ± 2.4	7.1 ± 0.8	0.243 ± 0.091	25.8 ± 9.7	23.1 ± 0.1
3	0.083 ± 0.012	8.8 ± 1.3	—	0.233 ± 0.052	24.8 ± 5.5	—
4	—	—	4.6 ± 1.0	0.243 ± 0.022	25.8 ± 2.3	17.6 ± 2.0
wt¶ c-H-*ras1*	0.052 ± 0.002	5.5 ± 0.2	6.6 ± 0.8	0.052 ± 0.002	5.5 ± 0.2	6.6 ± 0.8

*Treatment with 4 mM ENU in experiment 1 and with 2 mM ENU in experiments 2–4.
†Means ± standard deviations of normalized densitometer readings of two or three sequences: 2(A-2510/A-2505 + A-2513).
‡Percent A-2510 content relative to authentic mutant A-2510 DNA.
§Percent of total identified plaques containing TCΔA, means ± standard deviations; data from ≈1000 plaques on four Petri dishes for each experimental condition.
¶For RFLP/PCR product of 10^8 copies of wt c-H-*ras1* DNA.

pendent experiments are listed in Table 1 (columns 2, 3, 5, and 6). The A-2510 mutant content of the RFLP/PCR products from untreated cells was in the range from 5.9% to 8.8%, whereas the values for ENU-treated cells varied from 14.8% to 25.8%. It is evident that there is good agreement between the data obtained by direct sequencing and plaque hybridization with the exception of experiment 4, where plaque hybridization yielded a significantly lower value. Sequence analysis of the RFLP/PCR product of 10^8 copies of wt c-H-*ras1* DNA indicates the presence of 5.5% of the A-2510 mutant. As discussed above for the plaque hybridization data, it appears likely, therefore, that A-2510 mutants in DNA from untreated cells originate from *Taq* polymerase errors (5, 18–21).

Although analysis of the RFLP/PCR products by direct sequencing is rapid and economical, its sensitivity varies with the intensity of the band of the residue of interest. For a residue with good signal strength in the authentic mutant DNA such as A-2510, we estimate that the limit mutant content for which reliable data can be obtained lies between 5% and 10%. Because of the need to add MS to the genomic DNA for the estimation of absolute mutation frequencies (see below), the bands for A-2508 and T-2511 can arise either from MS or from single base-pair changes at these positions. This problem can be resolved by restriction of the MS sequence 2508–2511 ACGT with *Mae* II in the RFLP/PCR product before sequencing. We conclude that direct sequencing can replace laborious cloning into λ and plaque hybridization at least for major base-pair mutations.

Our results agree with the mutational specificity of ENU reported in the literature. It induced preferentially G·C → A·T transitions in the *HPRT* gene in mouse cells and in shuttle vectors in human cells (7–10). Although A·T → T·A transversions represent the second most frequent base-pair change induced by ENU in most mammalian and bacterial systems, this mutation predominates in the activation of the *neu* protooncogene in ENU-induced tumorigenesis in the mouse brain (22, 23). We did not observe ENU-induced A·T → T·A transversions in *Taq* I site 2508–2511 in the present work (see Fig. 4).

Rare Mutations, Spontaneous Mutations, and *Taq* Polymerase Errors. In the present experiments the starting DNA for RFLP/PCR analysis contained 1–2 × 10^7 copies of the c-H-*ras1* gene. Therefore, rare mutations with frequencies in the range of 1–10 × 10^{-7} and below might be observed only in part of the experiments. This may be the case for the transversion C → A-2509. From the histogram in Fig. 4, which shows the content of the RFLP/PCR product in all 12 possible single base-pair mutations in *Taq* I site 2508–2511 for experiment 2, it is evident that the content of C → A-2509 mutation is much higher in DNA from ENU-treated than untreated cells. Though this result was reproducible for repeated λ packaging of the cloned DNA followed by independent plaque analysis, it was only observed in experiment 2. In the other experiments (experiments 1, 3, and 4) the content in the A-2509 mutation was comparable for DNA from ENU-treated and untreated cells and ranged from 2% to

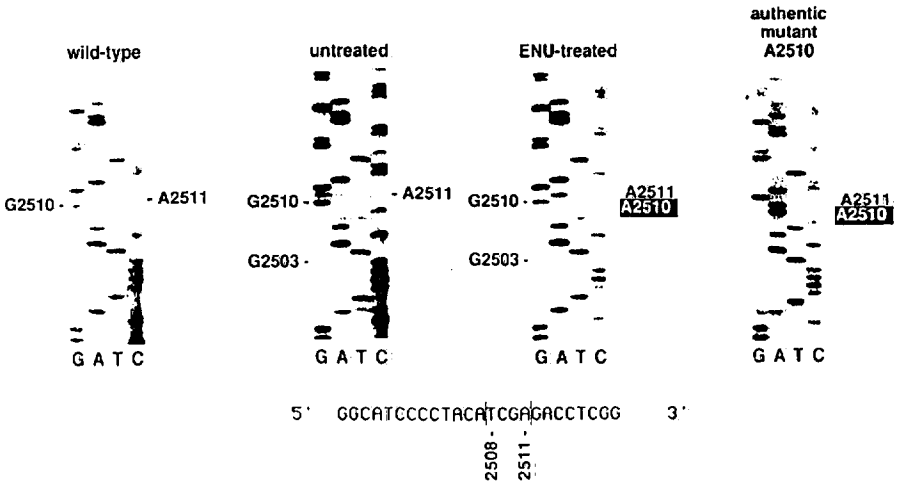

FIG. 2. Direct sequencing of amplified fragments containing *Taq* I site 2508–2511 of c-H-*ras1* from DNA of ENU-treated and untreated human fibroblasts (middle panels). Sequences of the corresponding fragments of wt and authentic mutant A-2510 c-H-*ras1* DNA are shown on the left and right sides, respectively. The purified *Taq* I RFLP/PCR products were enriched for the negative strands by amplification with *Taq* polymerase using a single amplimer corresponding to residues 2542–2562. These DNA preparations were directly sequenced by extension of a primer complementary to nucleotides 2441–2461 (5'-CTGGCTGCACGCACTGTGGAA-3') with a Sequenase primer extension kit (United States Biochemical).

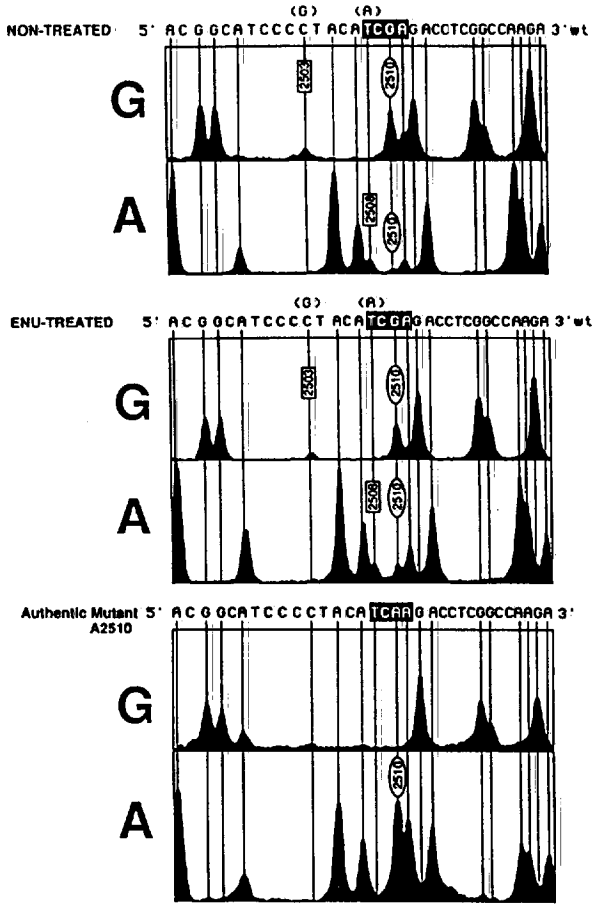

FIG. 3. Densitometer tracings of the G and A lanes of the sequences shown in Fig. 2. The site of the major ENU-induced transition G-2510 → A-2510 is indicated (encircled) as are the residues G-2503 and A-2508 (boxed-in), which are specific for the MS. Comparison of the normalized peak areas to the corresponding data from authentic wt, mutant, or MS DNA allowed determination of the composition of the RFLP/PCR products (see Tables 1 and 2).

5%. Separate experiments indicate that the C → A-2509 transversion is only rarely induced by *Taq* polymerase (6).

The histogram in Fig. 4 also shows a relatively high percentage of C → T-2509 transitions. The T-2509 mutant content varied from 8.4% to 11.5% in the RFLP/PCR products from untreated cells of three independent experiments and was moderately increased in the samples from treated cells to 14.3–16.2%. Its relatively high content in DNA from untreated cells suggests that it might represent a spontaneous mutation in addition to being weakly induced by ENU. The C → T-2509 transition is only induced with moderate frequency by *Taq* polymerase (6). Similar contents of DNA from treated and untreated cells were also measured for the A → G-2511 mutation. However, this transition represents the predominant *Taq* polymerase error at *Taq* I site 2508–2511 (6). Indeed, weak bands for residue G-2511 are visible on the sequences and their densitometer tracings in Figs. 2 and 3. The low band intensity for wt A-2511 in the sequence of the RFLP/PCR product from untreated cells is probably due to its high MS content (30%) relative to the RFLP/PCR product from ENU-treated cells (16.5%).

Absolute Frequency of the ENU-Induced G-2510 → A-2510 Transition in *Taq* I Site 2508–2511 of c-H-*ras1*. Plaque hybridization or direct sequencing discussed above measures the mutant composition of the RFLP/PCR product but neither procedure allows conclusions about the absolute

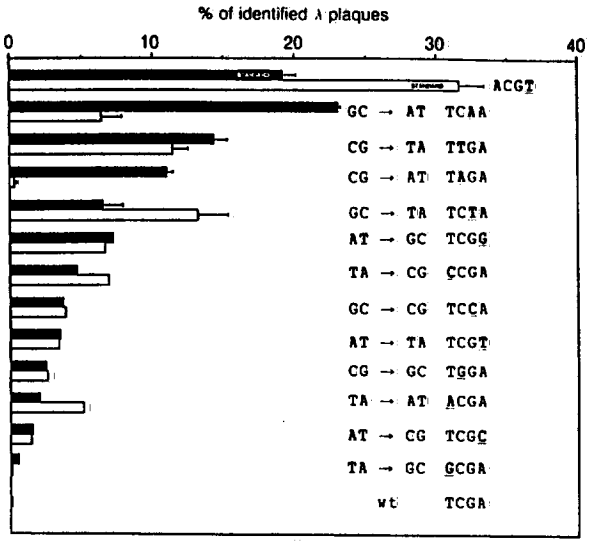

FIG. 4. Composition of the *Taq* I RFLP/PCR product from DNA of untreated fibroblasts plus MS (□) and ENU-treated human fibroblasts plus MS (■) in the 12 possible base-pair mutations, MS, and wt in *Taq* I site 2508–2511 of c-H-*ras1*. Data are from experiment 2 for λ plaque hybridization with 14 specific oligonucleotide probes as described in the legend to Fig. 1. For each experimental condition 1000–1700 plaques on four to eight Petri dishes were analyzed. Error bars indicate standard deviations.

frequencies of mutations in the cellular DNA preparations. The unknown efficiency of cloning into λgt10 precludes quantitation. Therefore, we have calibrated our measurements by the addition of 10 copies of MS at the onset of the experiment. The MS consists of a 238-bp fragment that is homologous to the wt *ras1* sequence (residues 2372–2610) but contains 4-bp changes. Two changes are located in the *Taq* I site 2508–2511 (ACGT) and render the fragment resistant to *Taq* I cleavage, and two additional changes are located 5′ upstream of this site. The fraction of MS copies found in the RFLP/PCR allows calibration of the data and estimation of absolute mutation frequencies. The MS contents were measured by plaque hybridization with a MS-specific oligonucleotide probe as well as by direct sequencing, and good agreement was observed between the two analytical methods (see Table 1 for A-2510 mutation). For quantitative sequence measurements we used the MS-specific residue G-2503. Since G-2503 is located upstream of the *Taq* I site 2508–2511, ENU- or *Taq* polymerase-induced mutations at this site are not selected. Therefore, the normalized intensity of the band for G-2503 directly allows determination of the MS content of the RFLP/PCR product (see Figs. 2 and 3). The signals for residues G-2496 and G-2516 were used for normalization and the normalized intensity for G-2503 in the sequence of authentic MS DNA was used as the 100% reference value.

Table 2 lists means from plaque hybridization and sequencing for the MS and A-2510 mutant contents of the RFLP/PCR products of DNA from ENU-treated cells. The original data for the A-2510 contents are given in Table 1. The means of the MS contents were determined in an analogous fashion. It should be recalled that the MS contents of the RFLP/PCR products result from the initial addition of 10 copies of MS to the c-H-*ras1*-enriched cellular DNA containing 1–2 × 10^7 copies of this gene (see Fig. 1 legend). The copy number of a particular mutation in the cellular DNA and its content in the RFLP/PCR product are not related in a simple fashion. Therefore, mutation frequencies can only be estimated when the contents of MS and of the mutation in question are in the same range. As is evident from Table 2, this is the case for the

Table 2. ENU-induced G-2510 to A-2510 mutation frequency per c-H-*ras1* gene copy

Exp.	% MS*	% A-2510 mutation†	Initial *ras1* copies	A-2510 mutation frequency
1	19.5	16.2	2.0×10^7	4×10^{-7}
2	16.5	24.4	1.7×10^7	9×10^{-7}
3	10.0	25.0	1.7×10^7	—
4	18.5	21.7	1.0×10^7	12×10^{-7}

*Means of MS contents of RFLP/PCR products obtained by plaque hybridization and direct sequencing using MS-specific residue G-2503.

†Means of A-2510 mutant contents of RFLP/PCR products from Table 1 obtained by plaque hybridization and direct sequencing.

ENU-induced G → A-2510 transition in experiments 1, 2, and 4. For these experiments G → A-2510 transition frequencies of $4–12 \times 10^{-7}$ per c-H-*ras1* gene are calculated. These values are probably overestimates since there is no simple procedure for their correction for G → A-2510 transitions in DNA from untreated cells (see Table 1).

It is conceivable that some lesions, in particular ethylated thymine, persist in the DNA after the 72-hr expression time used in our experiments. These persistent lesions could give rise to misincorporation during the first rounds of PCR amplification by *Taq* polymerase. Persistent ethylated thymine lesions would give rise to mutations at A·T base pairs. The fact that the ENU-induced mutations in our experiments involved only G·C base pairs argues against this possibility.

CONCLUDING REMARKS

Maximal sensitivity of the RFLP/PCR method depends on the completeness of the restriction of wt sequences and the fidelity of the polymerase used in the PCR (19–23). Although no wt DNA could be detected in *Taq* I RFLP/PCR products, the fact that *Taq* polymerase errors were detected indicates that a few residual wt sequences must have been present at the onset of the amplification reaction. The error frequency of *Taq* polymerase used in our experiments depends on the base pair that is being replicated as well as on sequence context. For *Taq* I site 2508–2511 the error rates were highest for A·T pairs in the coding and noncoding strands—i.e., A → G-2511 >> T → A-2508 (6). Correspondingly, mutagen-induced changes are detected with lowest sensitivities at these base pairs. In contrast, the G → A-2510 transition, which represents the major ENU-induced mutation in our present experiments, corresponds to a moderate *Taq* polymerase error. Under these conditions ENU induced a 2.5- to 3.8-fold increase in the A-2510 mutant content of the RFLP/PCR products relative to DNA from untreated cells. For this particular G → A-2510 transition the sensitivity of the *Taq* I RFLP/PCR protocol is in the range of 5–10 mutant copies in 10^7 c-H-*ras1* genes. In our hands replacement of *Taq* polymerase by Vent (New England Biolabs), T4, or T7 polymerase did not yet yield superior results. Although replication errors per base pair for these polymerases have been reported to be lower (21), the contents of the RFLP/PCR products in other undesirable side products increased relative to *Taq* polymerase. Although our present work documents the capacity of the RFLP/PCR protocol to measure ENU-induced base-pair changes in the *Taq* I recognition sequence 2508–2511 of c-H-*ras1* in cultured human cells, the principle of the RFLP/PCR approach is applicable to any restriction recognition site in any gene of known sequence. Hereditary disease with mutations in *Taq* I restriction sites include hemophilias due to factor VIII (24) and factor X (25) deficiencies. The RFLP/PCR method holds promise for the determination of rare somatic mutations in disease-related genes in molecular epidemiology (26, 27).

We thank Dr. P. Amstad for many valuable suggestions during the course of this work and Miss I. Zbinden for excellent technical assistance. This work was supported by the Swiss National Science Foundation, the Swiss Association of Cigarette Manufacturers, and the Association for International Cancer Research.

1. Hollstein, M., Sidransky, D., Vogelstein, B. & Harris, C. (1991) *Science* 253, 49–53.
2. Rossiter, B. & Caskey, C. T. (1990) *J. Biol. Chem.* 265, 12753–12756.
3. Zijlstra, J., Felley-Bosco, E., Amstad, P. & Cerutti, P. (1990) in *Mutagens and Carcinogens in the Diet*, ed. Pariza (Wiley-Liss, New York), pp. 187–200.
4. Mendelsohn, M. & Albertini, R., eds. (1989) *Mutation and the Environment* (Wiley-Liss, New York), Part C.
5. Felley-Bosco, E., Pourzand, C., Zijlstra, J., Amstad, P. & Cerutti, P. (1991) *Nucleic Acids Res.* 19, 2913–2919.
6. Sandy, M., Chiocca, S. & Cerutti, P. (1992) *Proc. Natl. Acad. Sci. USA* 89, 890–894.
7. Recio, L., Cochrane, J., Simpson, D., Skopek, T., O'Neill, J., Nicklas, J. & Albertini, R. (1990) *Mutagenesis* 5, 505–510.
8. Eckert, K., Ingle, C., Klinedinst, D. & Drinkwater, N. (1988) *Mol. Carcinog.* 1, 50–56.
9. Richardson, K., Richardson, F., Crosby, R., Svenberg, J. & Skopek, T. (1987) *Proc. Natl. Acad. Sci. USA* 84, 344–348.
10. Giphart-Gassler, M., Groenewegen, A., den Duek, H., van de Putte, P. & Tasseron-de Jong, J. (1989) *Mutat. Res.* 214, 223–232.
11. Ehrlich, M., Zhang, X. Y. & Inamdar, N. (1990) *Mutat. Res.* 238, 277–286.
12. Cooper, D. & Youssoufian, H. (1988) *Hum. Genet.* 78, 151–155.
13. Barker, D., Schafer, M. & White, R. (1984) *Cell* 36, 131–138.
14. Chirgwin, J., Przybyla, A., McDonald, R. & Rutter, W. (1979) *Biochemistry* 18, 5294–5299.
15. Göbel, U., Maas, R. & Clad, A. (1987) *J. Biochem. Biophys. Methods* 14, 245–260.
16. Parada, L., Tobin, C., Shih, C. & Weinberg, R. (1982) *Nature (London)* 297, 474–478.
17. Davis, L., Dibner, M. & Battey, J., eds. (1986) *Basic Methods in Molecular Biology*, (Elsevier, New York).
18. Eckert, K. & Kunkel, T. (1990) *Nucleic Acids Res.* 18, 3739–3744.
19. Tindall, K. & Kunkel, T. (1988) *Biochemistry* 27, 6008–6013.
20. Saiki, R., Gelfand, D., Stoffel, S., Scharf, S., Higuchi, R., Horn, G., Mullis, K. & Erlich, H. (1988) *Science* 239, 4877–4891.
21. Keohavong, P. & Thilly, W. (1988) *Proc. Natl. Acad. Sci. USA* 86, 820–823.
22. Peratoni, A., Rice, J., Reed, C., Watani, M. & Wenk, M. (1987) *Proc. Natl. Acad. Sci. USA* 84, 6317–6321.
23. Sukumar, S. & Barbacid, M. (1990) *Proc. Natl. Acad. Sci. USA* 87, 718–722.
24. Gitschier, J., Wood, W., Shuman, M. & Lawn, R. (1986) *Science* 232, 1415–1416.
25. Watzke, H., Lechner, K., Roberts, H., Reddy, S., Welsch, D., Friedman, P., Mahr, G., Jagadeeswaran, P., Monroe, D. & High, K. (1990) *J. Biol. Chem.* 265, 11982–11989.
26. Marx, J. (1991) *Science* 253, 612–616.
27. Ashby, J. & Monod, R. (1991) *Nature (London)* 352, 185–186.

[CANCER RESEARCH 52, 3952–3960, July 15, 1992]

Mechanism of c-*fos* Induction by Active Oxygen[1]

Paul A. Amstad, Georg Krupitza, and Peter A. Cerutti[2]

Department of Carcinogenesis, Swiss Institute for Experimental Cancer Research, Lausanne, Switzerland

ABSTRACT

We have compared the mechanisms of the transcriptional induction of c-*fos* in mouse epidermal cells JB6 (clone 30) by an extracellular burst of active oxygen of the type produced by inflammatory phagocytes to induction by serum and phorbol ester. All three inducers elicit a characteristic immediate early response of c-*fos* which is inhibited by the protein kinase inhibitor H7 but enhanced by the protein synthesis inhibitor cycloheximide. Experiments with stable transfectants containing *fos* 5′ upstream regulatory sequences linked to an HSV-tk-chloramphenicol-acetyl-transferase reporter construct indicate that the joint dyad symmetry element-AP-1 motifs exert the most potent enhancer effect in response to active oxygen as well as serum. It is concluded that the different signal transduction pathways used by these inducers converge to the same 5′ regulatory sequences of c-*fos*.

In contrast to these common features only active oxygen induction of c-*fos* required the poly-ADP-ribosylation of chromosomal proteins. The inhibitors of ADP-ribose transferase benzamide and 3-amino-benzamide suppressed the elongation of the c-*fos* message and the *de novo* synthesis of nuclear factors, among them c-Fos and c-Jun, which bind to the *fos*-AP-1 motif *in vitro* only following stimulation with active oxygen. No active oxygen-induced change was observed in the protein complex which binds to an oligonucleotide containing the SIF and dyad symmetry element motifs *in vitro*. The presence of Fos and Jun proteins was detected in this complex. Only active oxygen, but not serum or phorbol ester, induces DNA breakage. We propose that poly-ADP-ribosylation is required because it participates in the repair of DNA breaks which interfere with transcription. We observed that Fos protein is weakly poly-ADP-ribosylated in response to active oxygen, but the functional role of this modification remains unclear.

INTRODUCTION

Growth promotion by oxidants is observed with cultured human and mouse fibroblasts as well as epidermal cells (1–5). It is expected to play a role in inflammation, fibrosis, and tumorigenesis (6–8). Indeed, oxidants trigger (patho)physiological reactions which resemble those induced by growth and differentiation factors. For example, AO[3] activates the phosphorylation of the ribosomal subunit S6 (9) and causes the membrane translocation of protein kinase C as well as its activation (10). The fact that low doses of oxidants can stimulate rather than inhibit cell growth implies that they are capable of reprogramming gene expression, and it was not unexpected to find that they induce the immediate early genes c-*fos* and c-*myc* (2, 4, 11). An increase in the amounts of Fos protein and heterodimer formation with Jun appears to be required for growth stimulation (12) and malignant transformation (13). While the signal transduction pathways which are activated by oxidants appear to have steps in common with growth and serum factors they are expected to be unique in other respects. Only oxidants induce DNA damage, particularly DNA breaks (14), which may affect transcription because of changes in chromatin conformation. DNA containing breaks also serves as a cofactor for the activation of ADPR transferase (15). Since this enzyme is located in the nucleus and accomplishes the posttranslational poly-ADP-ribosylation of chromosomal proteins it may represent an important link between DNA damage and oxidant-induced modulation of gene expression (6, 8).

We report that AO is a moderate transcriptional inducer of c-*fos* in mouse epidermal cell line JB6, which depends on the joint DSE/AP-1 enhancer elements in the 5′ upstream regulatory sequences for induction. Poly-ADP-ribosylation of chromosomal proteins is required for the transcriptional induction of c-*fos* and for the consecutive increase in Fos and Jun proteins which bind to the *fos* AP-1 oligonucleotide *in vitro* in response to AO but not to serum or phorbolester. It is likely that poly-ADP-ribosylation is necessary for the efficient elongation of the *fos* message because it participates in the repair of DNA strand breaks. Fos protein itself is weakly poly-ADP-ribosylated in response to AO, but the role of this posttranslational modification remains unclear.

MATERIALS AND METHODS

Cell Cultures and Treatment. Mouse epidermal cell line JB6 clone 30 (from Dr. N. Colburn) was cultured in monolayers at 37°C and 5% CO_2 using MEM containing 8% fetal calf serum. Seventy to eighty % confluent monolayers were starved for 24 h by growth in MEM containing only 0.25% fetal calf serum prior to exposure to a mixture of O_2^- plus H_2O_2 produced extracellularly by 20 μg/ml xanthine and 2 μg/ml xanthine oxidase (X/XO). Cycloheximide dissolved in ethanol (35 μM), benzamide (1 mM), 3-aminobenzamide (1 mM), and H7 (50 μM) from a 50 mM stock solution made up in 50% aqueous dimethyl sulfoxide were added 5 min before the X/XO treatment when indicated.

Isolation of RNA, Northern Blot Analysis, and Nuclear Runoff Transcription. Monolayers were washed twice with cold phosphate-buffered saline, and RNA was isolated after cell lysis with guanidinium thiocyanate (16). Ten-μg aliquots of RNA were electrophoresed on 1.4% agarose-formaldehyde gels (16) and transferred to gene screen membranes. The filters were prehybridized in 50% formamide, 50 mM Tris-HCl (pH 7.5), 0.1% sodium pyrophosphate, 1% SDS, 0.2% polyvinylpyrolidone, 0.2% Ficoll, 5 mM EDTA, 0.2% bovine serum albumin, 1× standard saline citrate (150 mM NaCl, 15 mM Na-citrate, pH 7), and 150 μg/ml denatured salmon sperm DNA at 65°C for 4 h. Hybridization was carried out with 1×10^6 cpm/ml of ^{32}P-labeled antisense riboprobes at 65°C for 16 h. The riboprobes were SP6 recombinants with a 1.5-kilobase insert containing exon 1 of c-*fos* *Hin*dIII to *Eco*RI fragment from pc-*fos*-(mouse)-3; (17), a 685-base pair *Sal*I to *Pst*I fragment of v-*fos* (18) containing sequences of exons 3 and 4 of c-*fos*; or a 1400-base pair *Pst*I fragment of rat glyceraldehyde-3-phosphate dehydrogenase (19), respectively. The filters were then washed at 65°C twice for 15 min with 2× standard saline citrate-0.1% SDS and twice for 15 min with 0.1× standard saline citrate-0.1% SDS. Nuclear runoff transcription of the c-*fos* and glyceraldehyde-3-phosphate dehydrogenase genes from AO-treated and control cells was measured as described by Crawford *et al.* (2).

Received 2/6/92; accepted 5/7/92.

The costs of publication of this article were defrayed in part by the payment of page charges. This article must therefore be hereby marked *advertisement* in accordance with 18 U.S.C. Section 1734 solely to indicate this fact.

[1] Supported by the Swiss National Science Foundation and the Swiss Association of Cigarette Manufacturers [illegible] International Cancer Research.

[2] To whom requests for reprints should be addressed, at Department of Carcinogenesis, Swiss Institute for Experimental Cancer Research, CH. Des Boveresses 155, 1066 Epalinges/Lausanne, Switzerland.

[3] The abbreviations used are: AO, active oxygen; ADPR, 2′-monophosphoadenosine 5′-diphosphoribose; MEM, minimum essential medium; DSE, dyad symmetry element; mAB, monoclonal antibody; CAT, chloramphenicol-acetyltransferase; CRE, cyclic AMP-responsive element; FCS, fetal calf-serum; SDS, sodium dodecyl sulfate; HSV-tk, herpes simplex virus-thymidine kinase.

Nuclear Extracts for Gel Retardation Experiments. Oxidant-treated or control monolayer cultures on 15-cm Petri dishes were rinsed twice with cold phosphate-buffered saline, and the cells were lysed directly on the plate on ice in 1 ml buffer containing 10 mM 4-(2-hydroxyethyl)-1-piperazinethanesulfonic acid (pH 7.9), 1 mM EDTA, 60 mM KCl, 1 mM phenylmethylsulfonyl fluoride, and 0.5% NP-40. After 5 min, the lysates were collected with a rubber policeman, centrifuged at 800 × *g* and washed once in 0.5 ml of the same buffer from which NP-40 was omitted and then resuspended in 0.1 ml 0.25 M Tris-HCl (pH 7.8), 60 mM KCl, and 1 mM phenylmethylsulfonyl fluoride. The nuclei were lysed by 3 cycles of freezing (−78°C for 5 min) and thawing (37°C for 5 min). The lysates were cleared by centrifugation at 8800 × *g* for 15 min at 4°C and used in the gel retardation experiments described below.

Oligonucleotide Probes. (*a*) A synthetic DNA fragment was prepared which contained the *fos*-AP-1 consensus sequence:

5'-AGCTTGCTGCGTCAGCCGGATC-3'
TCGAACGACGCAGTCGGCCTAG

(*b*) Oligonucleotide −345 to −269 contains the mouse 5' upstream c-*fos* sequence from *Alu*I site −345 to *Hpa*II site −269 (18). The 5' end of the fragment is joined to a 32-nucleotide non-*fos* linker, and the 3' end is joined to a 14-nucleotide non-*fos* linker. The −345 to −295 sequence contains the SIF element and the major portion of the DSE (−312 to −295). Again the 5' end is joined to a 32-nucleotide non-*fos* linker, and the 3' end is joined to a 12-nucleotide non-*fos* linker.

(*c*) A DNA fragment (−313 to −292)

5'-GGATGTCCATATTAGGACATCT-3'
CCTACAGGTATAATCCTGTAGA

containing the DSE (−312 to −293) with no flanking sequences was prepared synthetically and used in oligonucleotide competition experiments.

Gel Retardation Conditions. The DNA fragments described above were ^{32}P-labeled using the Klenow fragment of DNA polymerase I. The labeled oligonucleotides were purified from unincorporated nucleotides by chromatography on a Sephadex G-50 column and ethanol precipitation.

Aliquots of nuclear extracts (5 μg protein) were preincubated for 5 min at 25°C in a total volume of 20 μl of a buffer containing 10 mM 4-(2-hydroxyethyl)-1-piperazinethanesulfonic acid (pH 7.9), 60 mM KCl, 1 mM EDTA, 4% Ficoll, 2 μg polydeoxyinosinic-cytidylic acid, and 5 mM dithiothreitol (20). They were then reacted with 20,000 cpm (0.15 ng) of end-labeled, double-stranded oligonucleotide probe for 30 min at 25°C. After 30 min at room temperature the samples were subjected to electrophoresis on 4% polyacrylamide gels in 0.25× Tris-borate-EDTA (89 mM Tris, 89 mM borate, 2 mM EDTA). The gels were fixed in 10% acetic acid:30% methanol for 30 min prior to drying and autoradiography. In oligonucleotide competition experiments nuclear extracts were preincubated with a 300-fold molar excess of the corresponding unlabeled oligonucleotide before the addition of the radioactive oligonucleotide probe.

For the characterization of oligonucleotide binding proteins by immunocompetition nuclear extracts were preincubated in the buffer described above for 15 min at 25°C before the addition of anti-c-Fos antibody, anti-c-Jun antibody, or nonimmune rabbit serum. After incubation for 16 h at 4°C the samples were reacted with the ^{32}P-labeled oligonucleotide probe for 30 min at 4°C and then analyzed by gel electrophoresis as described above. The anti-Fos 456 antibody had been raised in a rabbit and is directed against a peptide corresponding to amino acids 151–292 of mouse c-Fos (Medac Molecular Biology, Hamburg, Germany). Mouse monoclonal antibodies against NH_3-terminal c-Fos peptide 4–17 (mAB_{4-17}), COOH-terminal Fos peptide 359–378, and c-Myc peptide 43–55 were purchased from Microbiological Associates Inc./National Cancer Institute (Bethesda, MD); anti-c-Jun 48–4 is a polyclonal rabbit antibody raised against the 82 COOH-terminal amino acids of avian c-Jun. This antibody was the generous gift of Dr. M. C. Frame (21). Mouse monoclonal antibody against poly-ADPR was a gift of Dr. A. Belcredi (OF2S-Austria; Ref. 22). Normal rabbit serum was obtained from Nordic Immunology (Tilberg, the Netherlands). Our experimental conditions are a modification of the method described in (23).

CAT Vector Constructs with 5' Regulatory Sequences of c-*fos*, Preparation of Stable Transfectants, and RNAse Protection Assay. Different segments of the 5' upstream regulatory sequences of mouse c-*fos* were cloned into the pBLCAT$_4$ vector (24). This vector contains the HSV-tk promoter sequence from residues −109 to +51 linked to the structural gene of bacterial CAT. The cloning sites used in our constructs consist of a *Bam*HI site at the HSV-tk promoter residue −109 and a *Hind*III site 27 residues upstream. The following plasmids were prepared which contain the major enhancer elements DSE (−313 to −293), AP-1 (−292 to −285), and CRE (−63 to −57): (*a*) p(DSE/AP-1-CRE)tk-CAT containing the mouse c-*fos* upstream sequence from 5' −345 (*Alu*I) to −18 (*Alu*I); (*b*) p(DSE/AP-1)tk-CAT containing the *fos* segment 5' −345 (*Alu*I) to −269 (*Hpa*II); (*c*) p(DSE)tk-CAT containing the *fos* segment 5' −345 (*Alu*I) to −295 (*Fok*I); (*d*) p(AP-1)-tk-CAT containing the synthetic *fos* oligonucleotide 5' −292 to −285; (*e*) p(CRE)tk-CAT containing the *fos* segment 5' −126 (*Hind*II) to −18 (*Alu*I); (*f*) p*fos*-CAT contained the full-length upstream sequence of mouse c-*fos* from −641 (*Hind*III) to +109 (*Acc*I) cloned into the *Hind*-III site of pSVO-CAT. In contrast to the constructs described above the *fos* upstream sequences and the endogenous *fos* promoter are directly linked to the *CAT* gene.

Stable transfectants of JB6 (C130) cells were prepared by cotransfection of the above plasmid constructs at a 50-fold excess with pSV_2*neo* according to the calcium phosphate precipitation protocol of Chen and Okayama (25). After selection for 10 days in complete culture medium containing 200 μg/ml G418 the resistant colonies (approximately 100/15-cm-diameter Petri dish) were pooled by trypsinization, and the cultures were expanded in antibiotic-free medium. Cell pools of each stable CAT transfectant were frozen for later use. According to this protocol effects of the integration site on the expression of the constructs are averaged out. The inducibility of c-*fos* promoter-CAT constructs by AO (generated by 20 μg/ml X plus 2 μg/ml XO) and 20% FCS was determined in the serum-starved (24 h in medium containing only 0.25% FCS), stable transfectants using the RNase protection assay. The preparation of the ^{32}P-labeled CAT-RNA probe and the extraction of total RNA 1 h after treatment were as described by Angel *et al.* by (26).

Preparation of Nonhistone Nuclear Proteins and Determination of FOS-poly-ADP ribosylation by Western Blotting. Cells were cultured in monolayers as described above. At 70% confluency the cells were pooled and replated at 5 × 10^5 cells/dish and grown to 80% confluency in MEM containing 8% FCS and 0.25 μCi/ml of [^{3}H]leucine. The medium was replaced by MEM supplemented with 0.25% FCS, and cell growth continued for 24 h. The cultures were then exposed to an extracellular burst of AO produced by 40 μg/ml X and 4 μg/ml XO. When indicated, benzamide (0.1 mM) was added 15 min before the AO treatment. After a 60-min exposure to AO, the cells were scraped with a rubber policeman, and for each experimental condition the contents of 15 dishes (15 cm diameter) were pooled for the preparation of nuclear proteins. Nuclei were prepared as described previously. Nuclear pellets were treated with ice-cold 5% perchloric acid for 2 h, and the acid-insoluble pellets which contain nonhistone proteins were washed twice with 5% perchloric acid, 99% ethanol (−20°C) and acetone (−20°C). The air-dryed pellet was dissolved in 4 ml of a pH 6.5 buffer containing 6 M guanidium chloride, 50 mM sodium phosphate, and 5 mM mercaptoethanol and centrifuged for 16 h at 4°C with a SW 60 rotor at 210,000 × *g*.

The poly-ADP-ribosylated proteins contained in the high-speed supernatant were separated by affinity chromatography on PBA 30 phenylboronate agarose as described previously (27). The affinity-purified, poly-ADP-ribosylated material was electrophoresed on 3% stacking and 7% running polyacrylamide gels according to the method of Holtlund *et al.* (28). The sizes of the applied fractions were adjusted according to their [^{3}H]leucine content. After the development of the gels the proteins were electrotransferred overnight (0.3 mA, 15 V, 4°C) to nitrocellulose filters in a pH 6.8 buffer containing 150 mM glycine, 20

mM Tris base, 0.2% SDS, and 15% methanol according to the method of Towbin *et al.* (29). The filters were washed with distilled water and saturated overnight at 4°C on a rocker platform with 10 mM Tris buffer, pH 7.4, containing 1 × Denhardt's solution, 100 mM $MgCl_2$, 0.1% Triton X-100, and 0.5% bovine serum albumin. Fos antibodies (fos mAB_{4-17} or fos $mAB_{359-378}$) were then added in the same buffer, and the incubation was continued for 12 h under the same conditions. The filters were then washed four times with Tris-buffered saline before the addition of 10^5 cpm ^{125}I-labeled sheep anti-mouse Ig and incubated overnight at 4°C. All immunoblots were developed by autofluorography using presensitized Amersham X-ray hyperfilm MP.

RESULTS

Transcriptional Induction of c-*fos* by Active Oxygen is Suppressed by Inhibitors of Protein Kinases and ADPR Transferase. As reported previously (2) an extracellular burst of AO generated by xanthine/xanthine oxidase (X/XO; 20 μg/ml X and 2 μg/ml XO) rapidly increases the rate of transcription of c-*fos*, c-*myc* exons 1 and 3, and β-actin in serum-starved mouse epidermal cell line JB6 (C130). The Northern blots in Fig. 1*A* show that preincubation of the cultures with the protein kinase C plus protein kinase A inhibitor H7 (50 μM) suppressed the increase in the stationary c-*fos* message concentration which is otherwise observed at 15 min and 60 min following AO treatment. The ADPR transferase inhibitors benzamide (1 mM) and 3-amino-benzamide (1 mM) had a similar effect. Maximal inhibition of 67% was observed for benzamide 60 min after treatment. In contrast, ADPR-transferase inhibitors had no effect on the accumulation of c-*fos* message following treatment with phorbolester (20 ng/ml) or serum (20% fetal calf serum; Fig. 1*B*).

Nuclear runoff experiments were performed with probes containing the exon 1 sequence and the sequences of exons 3 and 4, respectively, in order to evaluate the effect of ADPR transferase inhibition on message elongation. Fig. 2 shows that benzamide inhibited the formation of long messages much more strongly than of short messages containing only exon 1 in response to AO (Fig. 2, *left*). In contrast, benzamide had only a minor effect on transcriptional elongation in response to phorbol ester (Fig. 2, *right*) and serum (data not shown). Only AO induces DNA strand breaks (14) and the poly-ADP ribosylation of structural and functional chromosomal proteins in mouse and human epidermal cells (27, 30). Poly-ADP-ribosylation is required for the efficient resealing of DNA breaks.

Fos Protein is Poly-ADP-ribosylated in Response to Treatment with Active Oxygen. Extracellularly generated AO causes DNA strand breakage in JB6 cells and stimulates the poly-ADP-ribosylation of chromosomal proteins (14). We explored whether Fos protein itself serves as a poly-ADPR acceptor. Our experimental design for the analysis of the poly-ADP-ribosylation nonhistone nuclear proteins has been described previously (27, 31). In short, in order to facilitate quantitation and sampling total cellular proteins in monolayer cultures were prelabeled with [^3H]leucine. Poly-ADP-ribosylated, acid-insoluble nuclear proteins were isolated by affinity chromatography on phenylboronate PBA-30 columns and analyzed by immunoblotting with monoclonal antibodies raised against the NH_2-terminal peptide 4–17 or the COOH-terminal peptide 359–378 of Fos, respectively. The immunoblot with anti-fos $mAB_{359-378}$ reproduced in Fig. 3*A* (*Lane 3*) shows two strong bands at M_r 58,000 to 60,000 and M_r 65,000 to 70,000 in the fraction of poly-ADP-ribosylated nuclear proteins which were retained by phenylboronate from cells which had been treated with AO for 15 min. Only weak bands are discernible 60 min after AO treatment (Fig. 3*A*, *Lane 5*). Poly-ADP-ribosylation of Fos protein was completely suppressed by the addition of the ADPR-transferase inhibitor benzamide (Fig. 3*A*, *Lanes 4* and *6*; 100 μM benzamide added 15 min before AO treatment). *Lane 7* in Fig. 3*A* shows the mobility of unmodified Fos protein contained in the nuclear protein fraction which was not absorbed by phenylboronate. Analogous results with anti-Fos mAB_{4-17} are shown

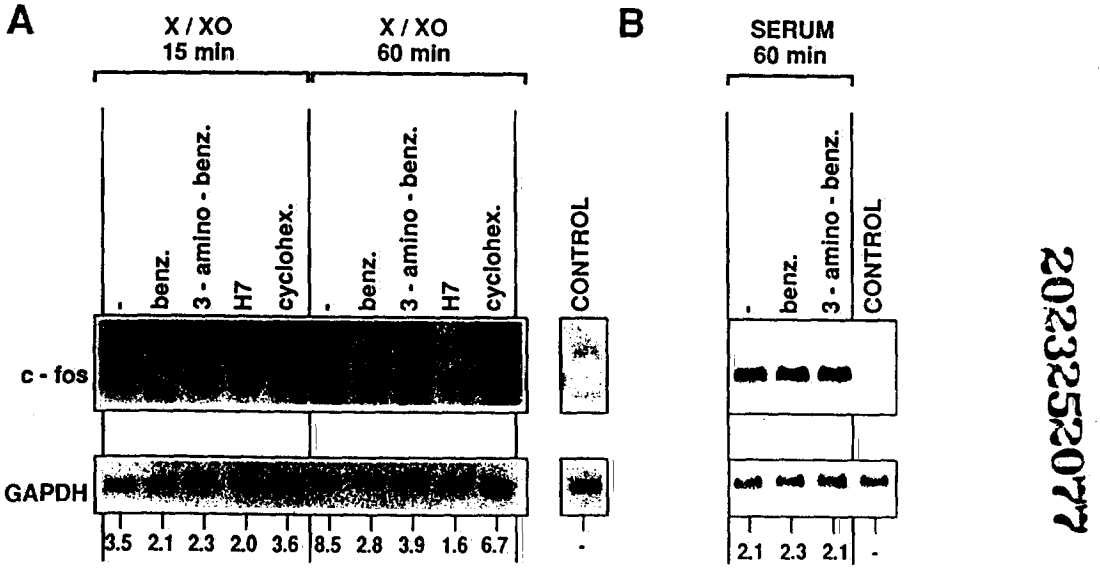

Fig. 1. Inhibition of c-*fos* induction by AO in mouse epidermal cells by inhibitors of ADPR transferase and protein kinases. In *A*, serum-starved JB6 (C130) cells were preincubated for 5 min with benzamide (1 mM), 3-amino-benzamide (1 mM), H7 (50 μM), or cycloheximide (35 μM) before treatment with AO generated by 20 μg/ml X and 2 μg/ml XO. Total RNA was extracted at the indicated times, and its content in c-*fos* message was determined by Northern blotting with a v-*fos* probe (685 base pairs from *SalI* to *PstI*). In *B*, serum-starved JB6 (C130) cells were preincubated for 5 min with benzamide (1 mM) or 3-amino-benzamide (1 mM) as indicated before treatment with 20% FCS. The experimental conditions were as described above.

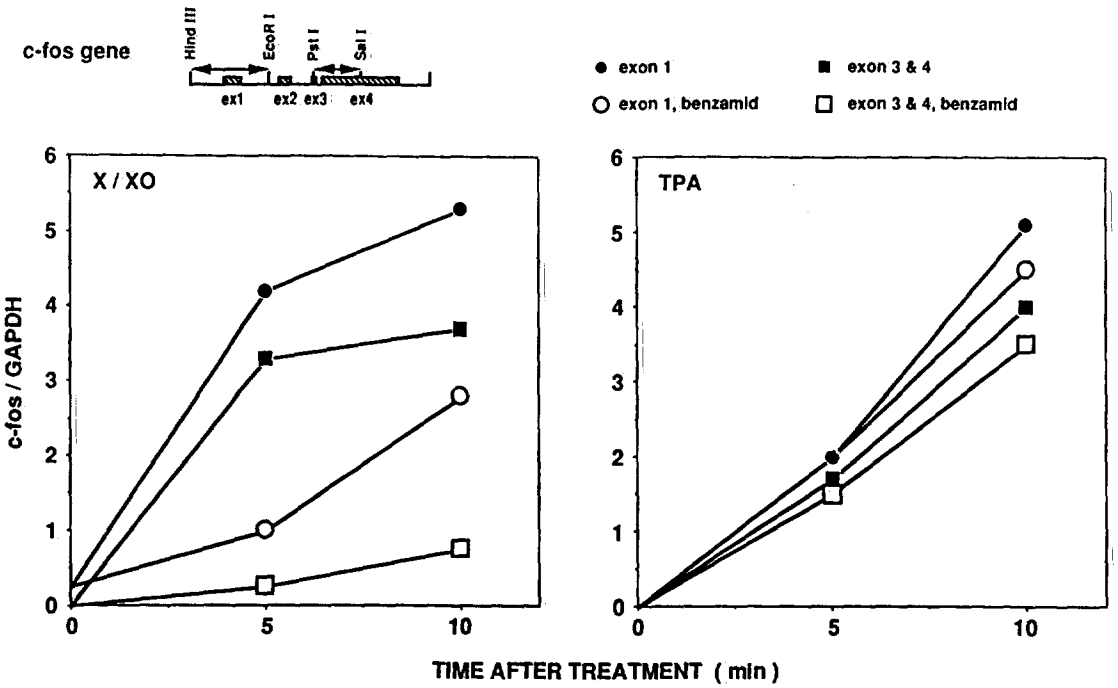

Fig. 2. Effect of inhibitor of ADPR transferase on message elongation in nuclear runoff transcription. Serum-starved JB6 (C130) cells were treated with AO (*left*) or phorbol ester (20 ng/ml) in the presence or absence of the ADPR transferase inhibitor benzamide (1 mM). Nuclear runoff transcription was performed as described previously (2) using as probes linearized SP6 plasmid DNA with a 1.5-kilobase insert containing exon 1 of a c-*fos* fragment (*Hind*III to *Eco*RI) from pc-*fos*(mouse)-3 (17) or a 685-base pair v-*fos* fragment (*Sal*I to *Pst*I) with sequences of exons 3 and 4 of c-*fos* (18).

in Fig. 3*B*. Only a single band at M_r ~63,000 is visible in the immunoblot of phenylboronate adsorbed proteins after 15 min AO treatment (Fig. 3*B*, *Lane 3*). As expected, poly-ADP-ribosylation decreased the mobility of Fos protein due to an increase in molecular weight and changes in ionic behavior. The extent of Fos substitution with poly-ADPR chains after 15 min of AO treatment is estimated to be only a few percent. The number of poly-ADPR chains per protein and their length remain undefined since phenylboronate indiscriminately retains all poly-ADP-ribosylated proteins. When nuclear extracts from AO-treated cells were predigested with snake venom phosphodiesterase no poly-ADP-ribosylated proteins were retained by the phenylboronate column which could be detected by Western blotting with anti-Fos antibody. No poly-ADP-ribosylation of Fos was detected when serum-starved JB6 cells were treated with phorbol ester (data not shown).

The Joint DSE/AP-1 Enhancer Motifs Are Required for c-*fos* Induction by Active Oxygen. Serum-starved JB6 cells which had been stably transfected with plasmids containing different segments of the c-*fos* 5′ upstream regulatory region linked to a CAT reporter construct were exposed in parallel to a burst of AO or 20% fetal calf serum. CAT-RNA concentrations were then measured 1 h after treatment by the RNAse protection method. The data in Fig. 4 show that AO was a much weaker inducer than serum but that the relative inducibility was comparable for both agents for all six constructs investigated. The strongest induction was observed for the complete c-*fos* upstream sequence and the *fos* promoter (−641 to +109) rather than the HSV-tk promoter contained in all the other constructs. Inducibility was 50% (for AO) and 65% (for serum) lower for a construct containing the segment −345 to −18 linked to a tk-promoter-CAT reporter construct. Slightly higher inducibility was observed for a shortened construct containing the segment −345 to −269 linked to tk-CAT. The −345 to −18 segment includes the SIF, DSE, AP-1, and cyclic AMP responsive regulatory elements, while the segment −345 to −269 only contains SIF, DSE, and AP-1. It is concluded that the sequences downstream from −269 do not exert a major enhancer activity in response to either agent. A construct with segment −345 to −295 which lacks two base pairs at the 3′ end of the DSE and the AP-1 element was still induced but with lower efficiency. It follows that the joint DSE-AP-1 motifs exert the most potent enhancer effect. Constructs containing only the AP-1 octanucleotide (−292 to −285) or the CRE (−126 to −18) were only weakly induced or not induced by either agent. The fact that the relative inducibility of all six constructs was the same for AO and serum is documented by the ratios of the densitometer readings for each construct (Fig. 4, *right ordinate*). We conclude that AO and serum use the same regulatory motifs in the 5′ upstream region of the c-*fos* gene.

Active Oxygen Increases the Amounts of Fos and Jun Proteins in Nuclear Extracts which Bind to the Fos AP-1 Element *in Vitro*. Mobility shift experiments with nuclear preparations from AO-treated cells were carried out with a radioactive oligonucleotide probe containing the *fos*-AP-1 octanucleotide (corresponding to residues −292 to −285 of the mouse c-*fos* 5′ upstream region) flanked by nonspecific sequences. As shown in Fig. 5 a single but broad shifted band is discernible on the autoradiograms. The results in Fig. 5 (*left*, *Lane 1* relative to *Lane 5*) indicate that AO treatment for 30 min increased factor binding. This increase was not observed when the cells were AO treated in the presence of benzamide, H7, or cycloheximide. It is concluded that the activation of protein kinases, ADPR transferase, and *de novo* protein synthesis are required for the AO-induced increase in factor binding. The data in Fig. 5 (*middle*) indicate that c-Fos and c-Jun are among the factors which bind to *fos* AP-1. Nuclear extracts from AO-treated cells were preincubated with polyclonal rabbit antibody raised against

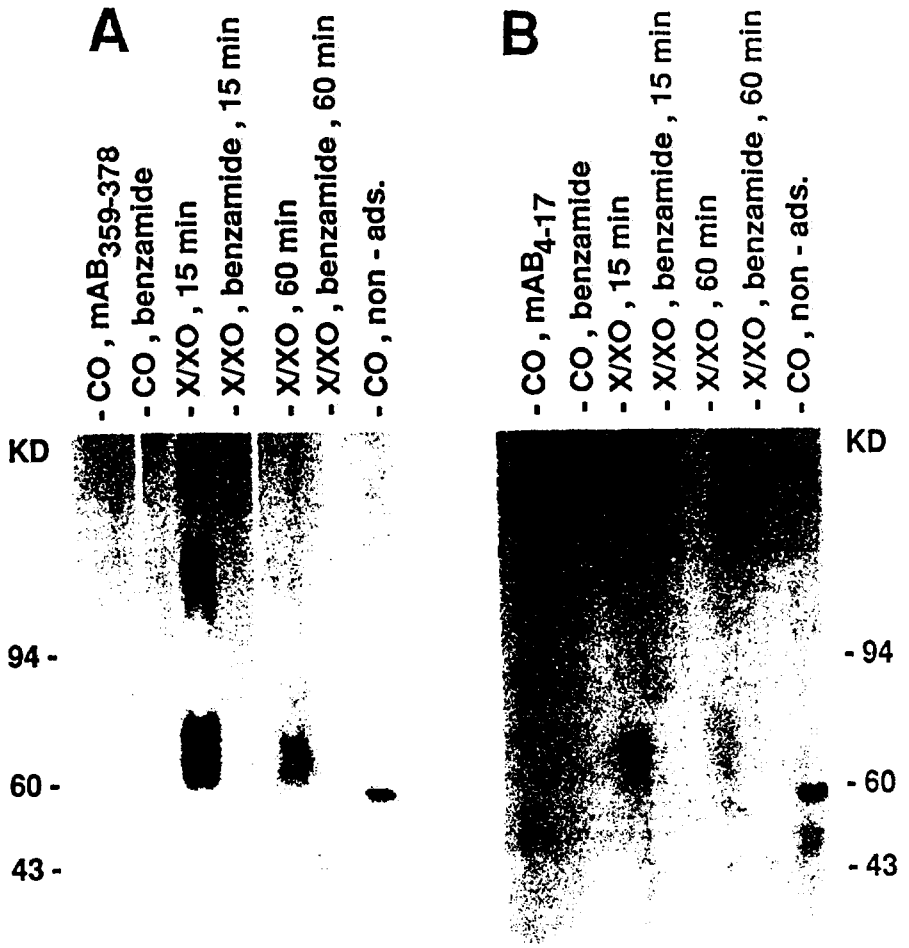

Fig. 3. Poly-ADP-ribosylation of c-Fos in response to active oxygen. Serum-starved JB6 (C130) cells were treated with AO generated by X/XO for the indicated length of time in the presence or absence of the ADPR transferase inhibitor benzamide (1 mM). Nuclear nonhistone proteins were then prepared, and poly-ADP-ribosylated proteins were separated by affinity chromatography on phenylboronate agarose PBA30. The proteins which were retained by the boronate column were eluted, and their Fos protein content was estimated by Western blotting (27) as described in "Materials and Methods." Aliquots of the flowthrough material which was not absorbed by the column were analyzed as controls. In *A*, the filter was reacted with a monoclonal antibody ($mAB_{359-378}$) raised against COOH-terminal Fos peptide 359–378. In *B*, the filter was reacted with a monoclonal antibody (mAB_{4-17}) raised against the NH_3-terminal Fos peptide 4–17. The filters were then washed and incubated with ^{125}I-labeled sheep anti-mouse Ig and exposed to X-ray film for autofluorography.

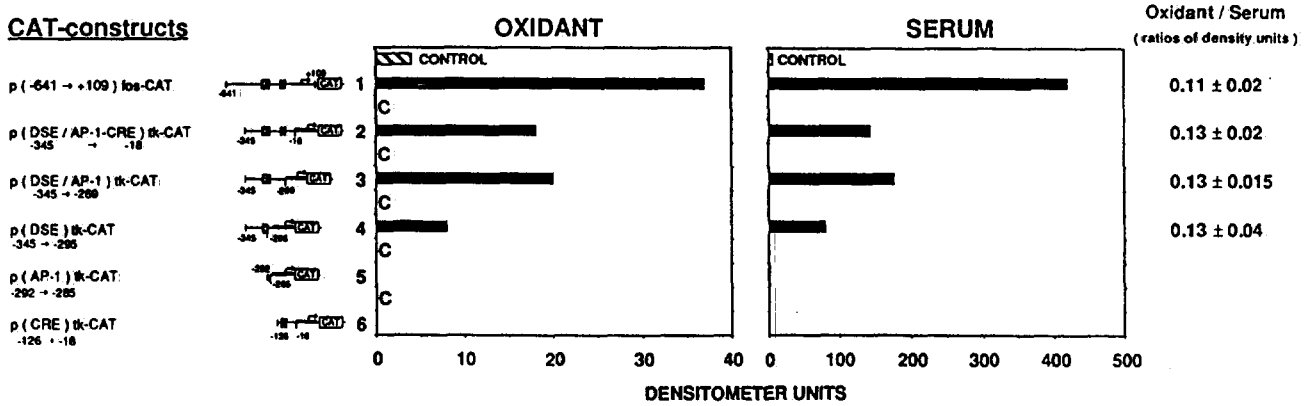

Fig. 4. The joint DSE/AP-1 motifs serve as major enhancers for c-*fos* induction by active oxygen and serum. Stable transfectants of JB6 (C130) cells were prepared with constructs containing segments of the mouse c-*fos* 5′ upstream regulatory sequences linked to a HSV-tk-CAT reporter molecule (*left*). In contrast, the transfectant p(−641 → +109) *fos*-CAT contained the entire c-*fos* upstream sequence as well as the c-*fos* promoter directly linked to the *CAT* gene. The transfectants were serum-starved and treated in parallel either with AO produced by X/XO or 20% fetal calf serum for 1 h. Total RNA was then extracted, and its content in CAT RNA was determined by the RNAse protection method (26) and as described in "Materials and Methods." The intensities of the bands of the autoradiograms were measured with a densitometer, and the inducibility of the constructs is expressed in arbitrary units. *Right*, column gives means of ratios of the densitometer readings with SD, for AO induction over serum induction from three independent experiments.

amino acids 151–292 of mouse c-Fos or a polyclonal rabbit antibody raised against the 82 carboxy-terminal amino acids of avian c-Jun, respectively, before the addition of the radioactive oligonucleotide probe. It is evident that the addition of these antibodies abolished factor binding (Fig. 5, *middle*, *Lanes 2* and *4*). Preincubation of nuclear extracts from AO-induced cells with a monoclonal antibody against poly-ADPR chains did not affect the mobility shift (data not shown). This result indicates that none of the proteins which bind *in vitro* to *fos*-AP-1 is heavily poly-ADP-ribosylated. Analogous results were obtained with nuclear extracts prepared 60 min following stimulation with serum (Fig. 5, *right*).

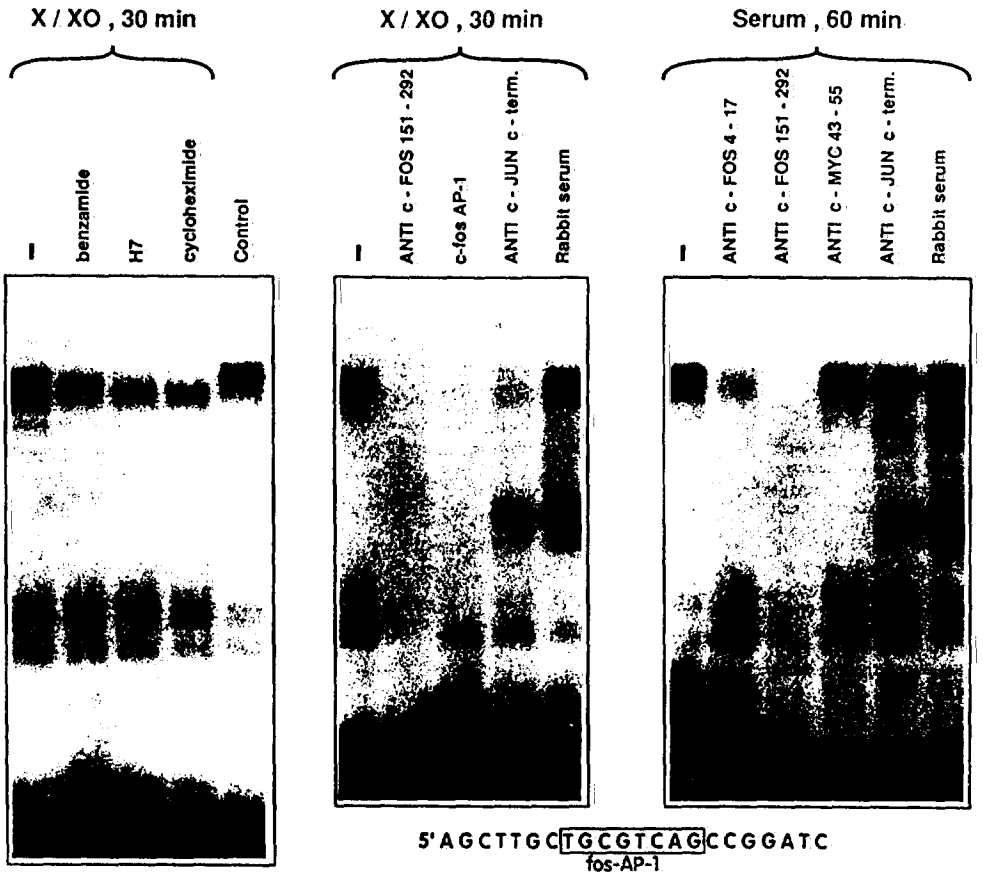

Fig. 5. Mobility shift of a probe containing the *fos*-AP-1 octanucleotide motif with nuclear extracts from JB6 (C130) cells. Nuclear extracts were prepared at the indicated times following treatment of serum-starved cells with AO produced by X/XO or 20% fetal calf serum, respectively. The extracts were reacted with the ^{32}P-labeled *fos*-AP-1 oligonucleotide probe, the samples were electrophoresed on 4% polyacrylamide gels, and the films were evaluated by autoradiography. As indicated (*left*), the cell cultures were preincubated for 5 min with benzamide (1 mM), H7 (50 μM), or cycloheximide (35 μM) before treatment with AO. Nuclear extracts from AO-treated cells (*middle*) were preincubated with polyclonal rabbit antibodies against peptide 151–292 of the mouse c-Fos protein (*Lane 2*) or the 82 COOH-terminal aminoacids of the avian c-Jun protein (*Lane 4*), or rabbit preimmune serum (*Lane 5*), respectively, before reaction with the ^{32}P-labeled probe. In order to document the specificity of the interaction, nuclear extracts were preincubated with a 300-fold molar excess of the corresponding unlabeled oligonucleotide before adding the radioactive probe (*Lane 3*). Nuclear extracts from serum-treated cells (*right*) were preincubated as indicated with the antibodies described above (*Lanes 3* and *5*) before the reaction with the radioactive probe. Additional samples were preincubated with monoclonal antibodies raised against the NH_3-terminal Fos peptide 4–17 (*Lane 2*) and mouse c-Myc peptide 43–55 (*Lane 4*), respectively.

Active Oxygen Treatment Does Not Change the Protein Complement in Nuclear Extracts which Binds to an Oligonucleotide Containing the SIF and DSE Motifs *in Vitro*. Mobility shift experiments with nuclear extracts from controls and AO-treated cultures were carried out with an oligonucleotide containing the c-*fos* sequences −345 to −295 joined to non-*fos* linkers. This oligonucleotide contains the SIF element (32) and the DSE (33) shortened by 2 base pairs on the 3′ end (−312 to −295). It is evident from Fig. 6 that AO treatment for 30 min had no effect on the complement of proteins which bound to this oligonucleotide *in vitro*. The specificity of factor binding to the above probe was explored in competition experiments with excess nonradioactive oligonucleotides (Fig. 6, *left*). An excess of oligonucleotide −345 to −295 eliminated all radioactive bands (Fig. 6, *left*, *Lane 3*). Interestingly, an excess of the 22-mer oligonucleotide −313 to −292 which corresponds to the DSE sequence eliminated all minor bands and weakened the major low-mobility band, (Fig. 6, *left*, *Lane 4*), while an excess of 22-mer containing the *fos*-AP-1 nonanucleotide sequence had no effect on the banding pattern (Fig. 6, *left*, *Lane 5*). These results indicate that the multiple proteins which bind to the sequence −345 to −295 *in vitro* require the DSE for their interaction. In order to characterize at least some of the proteins which bind to the oligonucleotide −345 to −295 the nuclear extracts from AO-treated cells were preincubated with antibodies raised against c-Fos, c-Jun, and c-Myc peptides before the reaction with the radioactive oligonucleotide probe. The results given in Fig. 6 (*right*) indicate that three different anti-Fos antibodies almost completely prevented protein binding to the −345 to −295 probe (*Lanes 3* and *4*) or gave rise to a supershifted low-mobility band (*Lane 5*), indicating that c-Fos is present in the protein complex formed by nuclear extracts of AO-treated cells and untreated controls alike (data not shown). Similarly, pretreatment with anti-c-Jun antibody gave rise to an additional supershifted low-mobility band (*Lane 2*), suggesting that c-Jun is also present in the protein complex. We also reacted the nuclear extracts with a monoclonal antibody raised against poly-ADPR chains. This antibody did not affect the mobility shift (*Lane 8*), indicating that none of the binding proteins is heavily poly-ADP-ribosylated.

DISCUSSION

Our experiments indicate that the transcriptional induction of c-*fos* by AO in many aspects resembles induction by phorbol ester or serum, *i.e.*, rapid induction and down-regulation, and

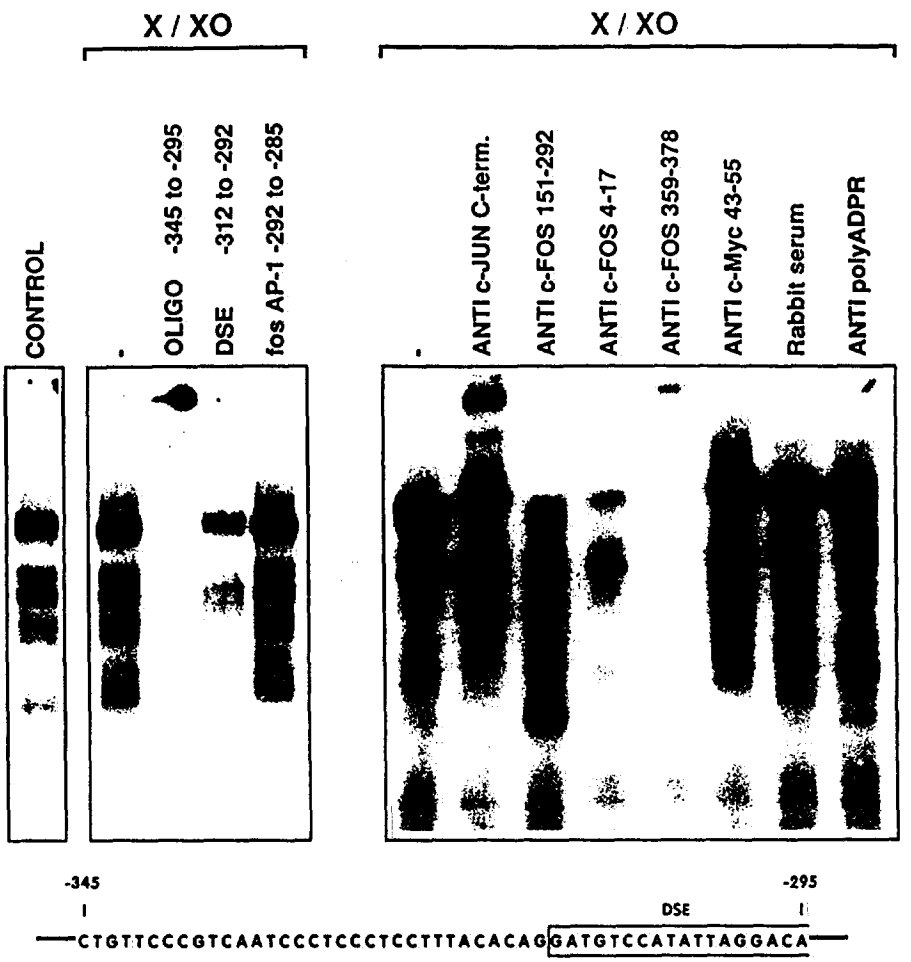

Fig. 6. Mobility shift of *fos* oligonucleotide −345 to −295 containing the SIF and DSE motifs with nuclear extracts from active oxygen-treated JB6 (C130) cells. Nuclear extracts were prepared from cells which had been treated with AO for 30 min. The nuclear extracts were preincubated (*left*) with a 300-fold molar excess of the indicated oligonucleotides before the addition of the radioactive oligonucleotide containing the c-*fos* upstream sequences −345 to −295. The nuclear extracts were preincubated (*right*) with the indicated antibodies described in Fig. 5. In addition, monoclonal antibodies raised against the COOH-terminal Fos peptide 359–378 (*Lane 5*) or against poly-ADPR chains (*Lane 8*) were used.

suppression by inhibitors of protein kinases. However, only transcriptional induction by AO is suppressed by inhibitors of ADPR transferase, indicating a requirement for the poly-ADP-ribosylation of chromosomal proteins.

A comparison of the inducibility with AO and serum of stable transfectants with CAT-reporter constructs containing 5′ upstream regulatory sequences of c-*fos* indicates that both inducers require the joint DSE/AP-1 motifs for efficient induction. Similarly, it was reported that short-wavelength UV light, phorbol ester, and platelet-derived growth factor all required the serum-responsive element (−319 to −300) for efficient induction in NIH-3T3 cells (24). While these agents at least in part use different peripheral signal transduction pathways they all converge to common genetic mechanisms for the transcriptional activation of c-*fos*.

Our mobility shift experiments indicate increased binding of Fos and Jun to the *fos*-AP-1 octanucleotide after 30 min of treatment with AO or serum. Similarly, increased binding of Fos and Jun to the collagenase TPA-responsive element which is closely related to the *fos*-AP-1 sequence has been reported for nuclear extracts from phorbol ester-treated (26, 34) and UVC-treated cells (20). This increase in Fos and Jun was suppressed when cells were treated with AO in the presence of inhibitors of ADPR transferase, protein kinases, and protein synthesis. From these results we propose that posttranslational poly-ADP-ribosylation and phosphorylation of as-yet unidentified proteins are required for the *de novo* synthesis of Fos, Jun, and possibly other regulatory proteins. Of course, our results do not imply that increased Fos and Jun binding to *fos*-AP-1 occurs *in vivo*. Although our present work concentrates on c-*fos*, it should be noted that AO also induces c-Jun in JB6 (C130) cells according to nuclear runoff transcription experiments.[4] Induction of c-Jun has also been observed in Hela cells in response to H_2O_2 (35).

Reports in the literature suggest that newly synthesized Fos and Jun proteins participate in the down-regulation of c-*fos*. Transient transfection experiments with CAT constructs in Fos-overproducing cells indicate that the DSE rather than the *fos*-AP-1 motif is mostly involved in down-regulation (36). Indeed, our mobility shift experiments indicate the presence of Fos and Jun in the protein complex which interacts with the DSE *in vitro* since preincubation of nuclear extracts with anti-Fos antibodies prevented the binding of proteins to the *fos* upstream fragment −345 to −295 or caused the formation of supershifted high-molecular-weight protein complexes (see Fig. 6, *right*). Binding of factors to this fragment required the presence of the DSE sequence, since an excess of a 22-mer DSE oligonucleotide essentially prevented their interaction with the −345 to −295 probe. It cannot be decided whether the complement of Fos which is associated with the protein complex which binds to DSE changes upon exposure to AO, since our mobility shift data reveal no difference between extracts from controls

[4] G. Shah, P. Amstad, and P. Cerutti, unpublished observations.

and treated cells. Other inducers of c-*fos* in several types of cells did not cause a discernible change in protein binding to DSE, according to mobility shift experiments and *in vivo* footprinting (37).

It has been reported that the oxidation of specific cystein residues in the basic domains of Fos and Jun decreases heterodimer formation and their capacity to bind to the human metallothionein II AP-1 element *in vitro* (21, 38). Therefore, it was conceivable that AO treatment of cells results in the oxidation of Fos and Jun *in situ* and consequently decreases their capacity to bind to their enhancer motifs. When we omitted the preincubation of nuclear extracts with 5 mM dithiothreitol before the reaction with the *fos*-AP-1 probe the complement of Fos and Jun which bound to the oligonucleotide *in vitro* was greatly diminished. However, this reduction in binding capacity was observed for extracts from AO-treated and serum-treated cells alike. Therefore, our experiments do not indicate whether the direct oxidation of Fos and Jun in cells exposed to AO plays a role in the transcriptional regulation of c-*fos*. Examples of proteins the activity of which may be regulated by the redox state include the oxy-R encoded protein in bacteria (39), heat shock factor in *Drosophila* (40), iron-responsive element binding protein in mammalian cells (41), and protein kinase C (10).

The requirement for poly-ADP-ribosylation of chromosomal proteins represents a unique feature of AO which is not shared by other inducers of c-*fos*. Our results suggest two major alternatives for the role of poly-ADP-ribosylation. According to the first, the poly-ADP-ribosylation of chromosomal proteins might activate or derepress the initiation of c-*fos* transcription. The observed poly-ADP-ribosylation of Fos itself could play such a role. However, the level of FOS modification was low, and no evidence was obtained for the presence of poly-ADP-ribosylated Fos in the protein complexes which bound to *fos* enhancer elements *in vitro*. Preincubation of nuclear extracts from AO-treated cells with antibody raised against poly-ADPR chains had no effect on factor binding to *fos*-AP-1 or to the DSE-containing oligonucleotide −345 to −295. While the available antibody is highly specific for poly-ADPR it possesses only moderate affinity. Therefore, low substitution with poly-ADP-ribose might not be revealed by our experiments. It should be noted that the poly-ADP-ribosylation of nonhistone proteins other than Fos has been reported (15). For example, topoisomerase I and ADPR transferase are poly-ADP-ribosylated in JB6 cells in response to AO (27). In addition to these functional chromosomal proteins histones and high-mobility group proteins are poly-ADP-ribosylated (30), and their modification might affect transcription because of changes in chromatin conformation.

Alternatively, DNA breaks may exert a long-range effect on chromatin conformation, which is incompatible with efficient message elongation. AO but not phorbol ester or serum produces DNA breaks (14). It is interesting to note that after AO treatment the rate of transcription of exons 3 and 4 was considerably lower than for exon 1 (see Fig. 2, *left*). We propose that poly-ADP-ribosylation is required for efficient c-*fos* induction because it participates in the resealing of DNA breaks (15). Therefore, inhibition of break repair by benzamide or 3-aminobenzamide potentiates their effect on transcription.

REFERENCES

1. Zimmerman, R., and Cerutti, P. Active oxygen acts as a promotor of transformation in mouse embryo fibroblast C3H/10T1/2/C18. Proc. Natl. Acad. Sci. USA, *81:* 2085–2087, 1984.
2. Crawford, D., Zbinden, I., Amstad, P., and Cerutti, P. Oxidant stress induces the protooncogenes c-*fos* and c-*myc* in mouse epidermal cells. Oncogene, *3:* 27–32, 1988.
3. Nakamura, Y., Gindhart, T., Winterstein, D., Tomita, I., Seed, J., and Colburn, N. Early superoxide dismutase-sensitive event promotes neoplastic transformation in mouse epidermal JB6 cells. Carcinogenesis (Lond.), *9:* 203–207, 1988.
4. Shibanuma, M., Kuroki, T., and Nose, K. Induction of DNA replication and expression of protooncogenes c-*myc* and c-*fos* in quiescent Balb/3T3 cells by xanthine/xanthine oxidase. Oncogene, *3:* 17–21, 1988.
5. Murrell, G., Francis, M., and Bromley, L. Modulation of fibroblast proliferation by oxygen free radicals. Biochem. J., *265:* 659–665, 1990.
6. Cerutti, P. Prooxidant states and tumor promotion. Science (Washington DC), *227:* 375–381, 1985.
7. Kozumbo, W., Trush, M., and Kensler, T. 1985. Are free radicals involved in tumor promotion? Chem.-Biol. Interact., *54:* 199–207, 1985.
8. Cerutti, P., and Trump, B. Inflammation and oxidative stress in carcinogenesis. Cancer Cells (Cold Spring Harbor), *3:* 1–7, 1991.
9. Larsson, R., and Cerutti, P. Oxidants induce phosphorylation of ribosomal protein S6. J. Biol. Chem., *263:* 17452–17458, 1988.
10. Larsson, R., and Cerutti, P. Translocation and enhancement of phosphotransferase activity of protein kinase C following exposure of mouse epidermal cells to oxidants. Cancer Res., *49:* 5627–5632, 1989.
11. Hollander, M., and Fornace, A. Induction of *fos* RNA by DNA damaging agents. Cancer Res., *49:* 1687–1692, 1989.
12. Mehmet, H., and Rozengurt, E. Regulation of c-*fos* expression in Swiss 3T3 cells: an interplay of multiple signal transduction pathways. Br. Med. Bull., *47:* 76–86, 1991.
13. Schuermann, M., Neuberg, M., Hunter, J., Jenuwein, T., Ryseck, T., Bravo, R. P., and Müller, R. The leucine repeat motif in FOS protein mediates complex formation with JUN/AP-1 and is required for transformation. Cell, *56:* 507–516, 1989.
14. Muehlematter, D., Larsson, R., and Cerutti, P. Active oxygen induced DNA strand breakage and poly ADP-ribosylation in promotable and non-promotable JB6 mouse epidermal cells. Carcinogenesis (Lond.), *9:* 239–245, 1988.
15. Jacobson, M., and Jacobson, E. (eds.). ADP-Ribose Transfer Reactions. New York: Springer-Verlag, 1989.
16. Davis, L., Dibner, M., and Balley, J. Basic Methods in Molecular Biology. New York: Elsevier, 1986.
17. Miller, D., Curran, T., and Verma, I. c-*fos* protein can induce cellular transformation: a novel mechanism of activation of a cellular oncogene. Cell, *36:* 51–60, 1984.
18. Van Beveren, C., Van Straaten, F., Curran, T., Müller, T., and Verma, I. Analysis of FBJ-MuSV provirus and c-*fos* (mouse) gene reveals that viral and cellular *fos* gene products have different carboxy termini. Cell, *32:* 1241–1255, 1983.
19. Piechaczyk, M., Blanchard, J. M., Marty, L. C., Dani, C., Panabieres, F., El Sabouty, S., Fort, P., and Jeanteur, P. Post-transcriptional regulation of glyceraldehyde-3-phosphate-dehydrogenase gene expression in rat tissues. Nucleic Acids Res., *12:* 6951–6963, 1984.
20. Stein, B., Rahmsdorf, H., Steffen, A., Litfin, M., and Herrlich, H. UV-induced DNA damage is an intermediate step in UV-induced expression of human immunodeficiency virus type 1, collagenase, c-*fos* and metallothionein. Mol. Cell. Biol., *9:* 5169–5181, 1989.
21. Frame, M., Wilkie, N., Darling, A., Chudleigh, A., Pintzas, A., Lang, J., and Gillespie, D. Regulation of AP-1/DNA complex formation *in vitro*. Oncogene, *6:* 205–209, 1991.
22. Belcredi, A. Thesis, University of Vienna, 1987.
23. Distel, R., Ro, H-S., Rosen, B., Groves, D. L., and Spiegelman, B. M. Nucleoprotein complexes that regulate gene expression in adipocyte differentiation: direct participation of c-*fos*. Cell, *49:* 835–844, 1987.
24. Büscher, M., Rahmsdorf, H., Litfin, J., Karin, M., and Herrlich, P. Activation of the c-*fos* gene by UV and phorbolester: different signal transduction pathways converge to the same enhancer element. Oncogene, *3:* 301–311, 1988.
25. Chen, C., and Okayama, O. High-efficiency transformation of mammalian cells by plasmid DNA. Mol. Cell. Biol., *7:* 2745–2752, 1987.
26. Angel, P., Imagawa, M., Chiu, R., Stein, B., Imbra, R., Rahmsdorf, H., Jonat, G., Herrlich, P., and Karin, M. Phorbolester-inducible genes contain a common *cis* element recognized by a TPA modulated *trans*-acting factor. Cell, *49:* 729–739, 1987.
27. Krupitza, G., and Cerutti, P. Poly-ADP-ribosylation of ADPR-transferase and topoisomerase I in intact mouse epidermal cells JB6. Biochemistry, *28:* 2034–2049.
28. Holtlund, J., Jemtland, R., and Kristensen, T. Two proteolytic degradation products of calf-thymus poly(ADP-ribose)polymerase are efficient ADP-ribose acceptors. Eur. J. Biochem., *130:* 309–314, 1983.
29. Towbin, H., Stachelin, T., and Gordon, J. Electrophoretic transfer of proteins from polyacrylamide gels to nitrocellulose sheets: procedure and some applications. Proc. Natl. Acad. Sci. USA, *76:* 4350–4354, 1979.
30. Krupitza, G., and Cerutti, P. Poly ADP-ribosylation of histones in intact human keratinocytes. Biochemistry, *28:* 4054–4060, 1989.
31. Adamietz, P., and Rudolph, A. ADP-ribosylation of nuclear proteins *in vivo*. Identification of histone H2B as a major acceptor for mono- and poly(ADP-ribose) in dimethyl sulfate-treated hepatoma AH7974 cells. J. Biol. Chem., *259:* 6841–6846, 1984.

2. Wagner, W., Hayes, T., Hoban, C., and Cochran, B. The SIF binding element confers sis/PDGF inducibility onto the c-*fos* promoter. EMBO J., *9:* 4477–4484, 1990.
33. Greenberg, M., Siegfried, Z., and Ziff, E. Mutation of the c-*fos* gene dyad symmetry element inhibits serum inducibility of transcription *in vivo* and the nuclear regulatory factor *in vitro*. Mol. Cell. Biol., *7:* 1217–1225, 1987.
4. Auwerx, J., and Sassoni-Corsi, P. IP-1: a dominant inhibitor of *Fos/Jun* whose activity is modulated by phosphorylation. Cell, *64:* 983–993, 1991.
35. Devary, Y., Gottlieb, R., Lau, L., and Karin, M. Rapid and preferential activation of the c-*jun* gene during the mammalian UV response. Mol. Cell. Biol., *11:* 2804–2811, 1991.
6. König, H., Ponta, H., Rahmsdorf, U., Büscher, M., Schönthal, A., Rahmsdorf, H., and Herrlich, P. Autoregulation of *fos*: dyad symmetry element is the major target of repression. EMBO J., *8:* 2559–2566, 1989.
37. Herrera, R., Shaw, P., and Nordheim, A. Occupation of c-*fos* serum response element *in vivo* by a multiprotein complex is unaltered by growth factor induction. Nature (Lond.), *340:* 68–70, 1989.
38. Abate, C., Patel, L., Rauscher, F., and Curran, T. Redox regulation of *FOS* and *JUN* DNA binding activity *in vitro*. Science (Washington DC), *249:* 1157–1161, 1990.
39. Storz, G., Tartaglia, L., and Ames, B. Transcriptional regulator of oxidative stress-inducible genes: direct activation by oxidation. Science (Washington DC), *248:* 189–194, 1990.
40. Becker, J., Mezger, V., Courgeon, A. M., and Best-Belpomme, M. Hydrogen peroxide activates immediate binding of a Drosophila factor to DNA heat-shock regulatory element *in vivo* and *in vitro*. Eur. J. Biochem., *189:* 553–558, 1990.
41. Klausner, R., and Harford, J. *Cis-trans* models for post-transcriptional gene regulation. Science (Washington DC), *246:* 870–872, 1990.

A genotypic mutation system measuring mutations in restriction recognition sequences

Emanuela Felley-Bosco, Charareh Pourzand, Jacob Zijlstra+, Paul Amstad and Peter Cerutti*
Department of Carcinogenesis, Swiss Institute for Experimental Cancer Research, 1066 Epalinges/Lausanne, Switzerland

Received March 7, 1991; Revised and Accepted May 15, 1991

ABSTRACT

The RFLP/PCR approach (restriction fragment length polymorphism/polymerase chain reaction) to genotypic mutation analysis described here measures mutations in restriction recognition sequences. Wild-type DNA is restricted before the resistant, mutated sequences are amplified by PCR and cloned. We tested the capacity of this experimental design to isolate a few copies of a mutated sequence of the human c-Ha-ras1 gene from a large excess of wild-type DNA. For this purpose we constructed a 272 bp fragment with 2 mutations in the PvuII recognition sequence 1727 – 1732 and studied the rescue by RFLP/PCR of a few copies of this 'PvuII mutant standard'. Following amplification with Taq-polymerase and cloning into λgt10, plaques containing wild-type sequence, PvuII mutant standard or Taq-polymerase induced bp changes were quantitated by hybridization with specific oligonucleotide probes. Our results indicate that 10 PvuII mutant standard copies can be rescued from 10^8 to 10^9 wild-type sequences. Taq polymerase errors originating from unrestricted, residual wild-type DNA were sequence dependent and consisted mostly of transversions originating at G.C bp. In contrast to a doubly mutated 'standard' the capacity to rescue single bp mutations by RFLP/PCR is limited by Taq-polymerase errors. Therefore, we assessed the capacity of our protocol to isolate a G to T transversion mutation at base pair 1698 of the MspI-site 1695 – 1698 of the c-Ha-ras1 gene from excess wild-type ras1 DNA. We found that 100 copies of the mutated ras1 fragment could be readily rescued from 10^8 copies of wild-type DNA.

INTRODUCTION

Molecular characterization and quantitation of mutations is of fundamental importance to the understanding of evolution, differentiation and the etiology of hereditary disease. The frequent occurrence of single base pair changes in the activation of the ras protooncogenes (1) and in the inactivation of the tumor suppressor gene p53 (2–4) documents the involvement of mutations in human carcinogenesis. Ideally, methods are required which allow it to identify specific DNA sequence changes in *relevant* genes in tissue biopsies. For the elucidation of early pathogenetic processes it is necessary to detect these changes in a minute minority of cells without the clonal expansion of mutated cells *in vivo* or *in vitro* and without the need for the expression of a selectable mutant phenotype (5). To achieve this goal it is necessary to isolate specific mutated DNA sequences from a large excess of homologous wild type DNA by biochemical means. In contrast, all classical 'phenotypic' mutation systems rely on the isolation of a few mutated cells from a large, usually dividing cell population. This limits mutation analysis to a few genes encoding proteins which produce a selectable cellular phenotype.

A number of experimental approaches to 'genotypic' mutation systems have been developed (6). Several are based on Southern- or Northern hybridization often with sequence amplification by polymerase chain reaction (PCR) and in combination with the specific cleavage of hetero-duplexes at mismatched base pairs. Other protocols take advantage of differences in electrophoretic mobilities of hetero-duplexes or of mutated single stranded nucleic acids. The sensitivity of all these approaches are limited by backgrounds which arise from the presence of excess wild-type sequences. The RFLP/PCR approach to genotypic mutation analysis described here greatly reduces this problem. Base-pair (bp) mutations are detected which are located in a restriction recognition sequence and render this site resistant to cleavage by the corresponding endonuclease. The resistant DNA sequence containing the mutated site is amplified by PCR only after wild type DNA has been essentially eliminated by restriction digestion. Amplified DNA is cloned into λgt10 and mutants are quantitated by oligonucleotide plaque hybridization relative to an internal standard. The maximal sensitivity of the RFLP/PCR method is determined by the completeness of the removal of wild-type sequences together with the inherent error-rate at a particular base pair of the polymerase used in the PCR. The RFLP/PCR protocol for genotypic mutation analysis is applicable to any gene of known sequence. It is highly sensitive, but limited to the identification of point mutations (bp-changes, small deletions and insertions)

* To whom correspondence should be addressed

+ Present address: Toxicology Department-ZYMA SA-1260 Nyon, Switzerland

which result in the elimination of restriction sites. We report here results involving bp-changes in the PvuII site 1727–1732 and the MspI site 1695–1698 of exon 1 of the human c-Ha-ras1 gene. The MspI-site 1695–1698 covers 2 bp of codon 12 of c-ras which represents a mutation hot spot in human cancer (1).

METHODS

RFLP/PCR analysis of PvuII-site 1727–1732 of c-Ha-ras1

Preparation of authentic mutants at PvuII-site 1727-1732 of c-Ha-ras1. All 12 possible single bp mutations in the internal tetranucleotide AGCT of the PvuII recognition sequence (residues 1727–1732) of exon 1 of the human c-Ha-ras1 gene were prepared using synthetic oligonuleotides and a PCR protocol (see Figure 1 for sequence information). Twelve different 20-mers corresponding to residues 1719–1738 which contained single base changes in the AGCT sequence were used as left-side amplimers. A common right-side amplimer corresponding to nucleotides 1765–1784 of c-Ha-ras1 plus a 12 nucleotide tail containing an EcoRI recognition-sequence was used in 12 PCR reactions with pSVneo-ras1 as template (note: pSVneo-ras 1 contains the BamHI fragment, residues 1–6453, of human c-Ha-ras1 (7) inserted into the BamHI sites of the SVneo cloning vector). The amplification conditions were as described below. The 12 resulting 78 bp fragments were purified on Quiagen-5 tips as described by the supplier (DIAGEN, KONTRON, Switzerland) and then used as right-side amplimers in a second round of amplifications with a common left-side amplimer corresponding to residues 1646–1665 of c-Ha-ras1 plus a 12 nucleotide tail containing an EcoRI recognition sequence. The resulting 163 bp fragments were purified on Quiagen-5 tips, digested with EcoRI and cloned into λgt10.

All authentic mutant λgt10 constructs were plaque purified on E. coli C600 Hfl. For this purpose plaques were lifted onto colony/plaque screens and probed with mutant specific ^{32}P-end-labeled oligonucleotides. Positive plaques were picked, the phage eluted from the agar and plated onto E. coli C600 Hfl. When confluent lysis had been achieved the phage was collected in 5ml buffer (100mM NaCl, 20 mM Tris.HCl pH 7.4, 10mM $MgSO_4$) and after the addition of 100 μl $CHCl_3$ the suspension was centrifuged at 10'000 rpm for 10 min at 4°C. Mutant phage contained in the supernatant was titered and then stored at 4°C in the presence of 0.3% $CHCl_3$.

A mutant standard with two bp changes in the PvuII recognition sequence and an additional upstream mutation was prepared according to the same experimental design using the 20-mer 5'T-GAGCATCCTGGTGATCCAG (residues 1719–1738 of c-Ha-ras1; positions of mutations underlined) as left-side amplimer and a 20-mer corresponding to the sequence from residue 1888 to 1907 of c-Ha-ras1 as right-side amplimer. The right-side amplimer contains a XbaI recognition site. The amplification conditions were as described below except that the DMSO concentration was only 6%. After 38 cycles the resulting 188 bp fragment was purified on a Quiagen-5 tip and used as right-side amplimer in a second amplification reaction with a left-side amplimer corresponding to residues 1636 to 1655 of c-Ha-ras1 which contains a SmaI site. After purification the final 272 bp fragment was digested with XbaI and SmaI and cloned into pSP64. This plasmid, referred to as 'mutant standard' (pSP64-ras PvuIISt), was used as internal standard in mixtures with pSVneo-ras1.

PvII - restriction and amplification. A stock of pSVneo-ras1 was digested exhaustively with 4U PvuII/μg plasmid DNA in Tris buffer pH 7.5, 10mM $MgCl_2$, 50mM NaCl, 1mM DTE for 3 h at 37°C. To 10^8 copies of restricted pSVneo-ras1 was added 10 or 100 copies of PvuII mutant standard (see above) which had been predigested with XbaI and SmaI in order to release a 272 bp fragment containing the mutated sequence. The samples were prepared in the amplification buffer which was composed of 66.7mM Tris.HCl pH 8.8 (25°C), 6.7mM $MgCl_2$, 16.6mM $(NH_4)_2SO_4$, 1mM each of the 4 dNTPs, 12% DMSO, 1.25 μM of the left-side and right-side amplimers in a final volume of 25 μl. The amplimers used in the first 30 PCR cycles were 20-mers corresponding to the sequences 1646–1665 and 1765–1784 of c-Ha-ras1 (see Figure 1). After addition of 0.5 U of Taq polymerase (from bact. Thermus aquaticus, Cetus, Calif.) the samples were heated initially to 91°C for 4 min followed by 95 sec at 59°C. Consecutive cycles consisted of 85 sec at 91°C and 95 sec at 59°C and were carried out in an Ampligene Apparatus, Moretronic, Switzerland. After 2,4,6 and 8 cycles 1 U PvuII was added and the samples incubated for 10 min at 52°C in order to eliminate any amplified wt-sequence. Amplification was then continued with 0.5 U fresh Taq-polymerase. After the first 8 cycles the amplification was continued without interruption up to 30 cycles when a 1 μl aliquot was withdrawn from each sample and added to 50 μl fresh amplification buffer. The mixtures contained 1.6 μM of clonable amplimers which in addition to the 20-mer sequences described above contained a 12-nucleotide tail with an EcoRI-recognition sequence (see Figure 1). Before the continuation of the amplification for 10 cycles the samples were treated with PvuII for 20 min at 37°C. In independent experiments 10^9 copies of PvuII digested pSVneo-ras1 were mixed with 1 or 1000 copies of mutant standard and processed according to the protocol described above except that PvuII digestions during amplification were omitted.

Purification of amplified DNA and cloning into λgt10. The amplification mixtures were purified on Quiagen-5 tips and the DNA precipitated with isopropanol after the addition of 1 μg E. coli tRNA as carrier. The samples were then treated with EcoRI in order to free the ends of the amplified fragment. After renewed purification on Quiagen-5 tips, precipitation with isopropanol and washing of the precipitates with 75% ethanol 5ng/DNA aliquots were ligated to 500 ng λgt10 arms as outlined by the supplier (Promega Biotec, Madison, WI.) The phage DNA was packaged (Packagene^r, Promega Biotec, Madison, WI.) and E. coli C600 Hfl infected. Plaques were lifted onto colony/plaque screens (NEF-978, New England Nuclear). At least 2 independent packagings were carried out and $1-3\times10^3$ plaques on 10 to 15 Petri-dishes were analyzed for each experimental condition.

Oligonucleotide plaque hybridization. Specific probes were prepared according to standard conditions by end-labeling with gamma-^{32}P-ATP with T4 polynucleotide kinase of oligonucleotide 20-mers corresponding to the wild-type sequence 1719–1738 of c-Ha-ras1, mutant standard containing 3 base changes and oligomers containing all 12 possible single base mutations in the internal tetranucleotide AGCT of PvuII recognition site 1727–1732. The colony/plaque screens to be analyzed were prehybridized for 1 h with 5×SSPE (1×: 10mM Na-phosphate pH 7.4, 1mM EDTA, 0.15M NaCl), 0.3% SDS, 1% milk protein. After rinsing with water the discs were hybridized overnight with the radioactive probes at 54°C in

5×SSPE, 0.3% SDS. After a first wash at room-temperature with 5×SSPE selective washing temperatures between 60 and 63°C were employed in order to exclude non-specific hybridization. The selective washing temperatures were determined with known mixtures of λgt10 stocks containing authentic mutant inserts (for their preparation see above).

RFLP/PCR analysis of MspI-site 1695–1698 of c-Ha-ras1

Preparation of authentic mutant ras1-T1698 with a single base pair substitution in the MspI-site 1695-1698. The c-Ha-ras1 gene with a G→T transversion at residue 1698 of exon 1 had been originally cloned from the EJ human bladder carcinoma line (8). A SmaI fragment (1644–2246) of this gene was cloned into the vector puc 8. From this the XbaI-EcoRI ras fragment 1644–1905 was removed and cloned into the pSP64 vector (9). This vector, referred to below as pSP64-ras1-T1698 was used in the mutant rescue experiments described below.

MspI/HpaII-restriction and amplification. Stocks of pSVneo-ras1 were digested exhaustively with 10U MspI/μg and 2U HpaII/ug plasmid overnight at 37° under the conditions described above for PvuII. pSP64-ras1-T1698 was digested with XbaI-EcoRI in order to release a 261 bp fragment containing the mutated MspI-site 1695–1698 CCGT. Three samples were prepared in the amplification buffer described above except that the DMSO concentration was only 6%: a) 10^8 copies restricted pSVneo-ras1 b) 100 copies restricted pSP64-ras1-T1698 plus 10^8 copies restricted pSVneo-ras1 c) 1000 copies restricted pSP64-ras1-T1698 plus 10^8 copies restricted pSVneo-ras1. The amplimers used in the first 35 PCR cycles were 20-mers corresponding to the sequences 1646–1665 and 1765–1784 of c-Ha-ras1 (see Figure 1). The amplification cycles were as described above. After 2,4,6,8,10,12 and 14 cycles 2U MspI were added and the samples incubated for 10 min at 55° in order to eliminate any residual wild-type sequences. Amplification was then continued after the addition of 0.5U fresh Taq polymerase. After 14 cycles the amplification was continued to 35 cycles without interruption when a 1μl aliquot was withdrawn from each sample and added to 50μl fresh amplification buffer. The amplification was continued with 1.6μM nested clonable left-side amplimer 1673–1692 and clonable right-side amplimer 1765–1784. These amplimers possessed 12-nucleotide 5'-tails containing EcoRI-recognition sequences (see Figure 1). All subsequent steps consisting of purification of the amplified DNA, cloning into λgt10 and oligonucleotide plaque hybridization were as described above for the analysis of mutants in the PvuII-site 1727–1732. The results shown on Figure 5 are derived from 2 independent packagings and 600–1100 plaques on 4 to 6 Petri dishes.

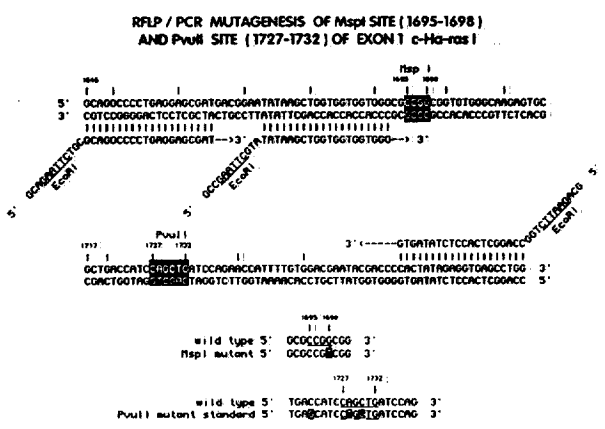

Figure 1. Sequence 1646–1784 of exon 1 of human c-Ha-ras1. The MspI recognition site 1695–1698 and the PvuII recognition site 1727–1732 used in the RFLP/PCR experiments are marked. The sequences of the single base pair mutant pSP64-ras1-T1698 in the MspI-site 1695–1698 and of the PvuII mutant standard SP64-ras-PvuIISt are given in the lower part of the Figure. Only the sequences of the 'clonable' amplimers with 5'-tails containing EcoRI recognition sites are shown.

Radiolabeled amplimer incorporation

In order to compare the efficiency of amplification of mutant standard and wild-type c-Ha-ras1 DNA the 20-mer corresponding to residues 1646–1665 was end-labeled with γ-^{32}P-ATP and T4 polynucleotide kinase under standard conditions. This

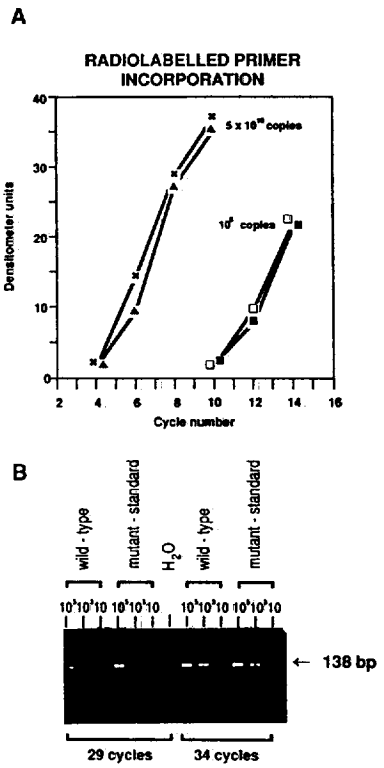

Figure 2. Comparison of amplification efficiencies of the wild-type c-Ha-ras1 sequence 1646–1784 and of the corresponding PvII mutant standard sequence. **A.** Incorporation of 5'-^{32}P-endlabeled left-side amplimer into 138bp amplified fragment with Taq-polymerase. Aliquots were withdrawn at increasing numbers of PCR-cycles and applied on 5% polyacrylamide gels for electrophoretic analysis. The dried gels were exposed to x-ray film for autoradiography and the intensity of the bands at 138bp determined by densitometry. X--X and □-□, 5×10^{10} and 10^8 copies of XbaI/SmaI digested wild-type pSVneo-ras were used as template, respectively; ▲-▲ and ■-■, 5×10^{10} and 10^8 copies of XbaI/SmaI digested mutant standard pSP64-ras PvuIISt were used as template, respectively (see 'Methods'). **B.** Formation of 138bp sequence 1646–1784 by amplification with Taq-polymerase of 10^5, 10^3 and 10 copies of XbaI/SmaI-digested wild-type pSVneo-ras or mutant standard pSP64-ras PvuIISt as templates. After the indicated numbers of PCR- cycles aliquots of the reaction mixtures were electrophoresed on 2% agarose gels and the 138bp band visualized by ethidiumbromide staining (see 'Methods').

radiolabeled oligonucleotide was used as left-side amplimer in a PCR-reaction with a non-radioactive right-side amplimer and 5×10^{10} copies of XbaI and SmaI digested mutant standard pSP64-ras PvuIISt or of XbaI and SmaI digested pSVneo-ras1 as templates, respectively. In a second experiment only 10^8 copies of the template DNAs were used. Amplification conditions were as described above with the exception that no PvuII digestions were performed. Aliquots of the reaction mixtures were withdrawn after increasing numbers of PCR cycles and applied to 5% polyacrylamide gels. After development, the dried gels were exposed to x-ray film for autoradiography. The intensities of the bands at 138 bp corresponding to the expected amplification product were determined by densitometry (Zeineth Scanning densitometer, Biomed Instr., CA.).

RESULTS

Efficiency of amplification of PvuII mutant standard and wild-type sequence 1646–1784 of c-Ha-ras1

In order to calibrate single bp mutations by RFLP/PCR an internal 'PvuII mutant standard' is used with 2 bp-mutations in the chosen recognition sequence. We prepared a mutant standard pSP64-ras PvuIISt with 2 bp changes in the PvuII recognition sequence (1727–1732) and an additional mutation upstream (see Methods and Fig. 1). For the validity of the calibration the amplification efficiencies for mutant standard DNA and mutated sequences (or undigested wt-sequences) from genomic DNA have to be the same. This is demonstrated in Figure 2. The upper portion shows that radiolabeled left-side amplimer (see Figure 1 for sequences) was incorporated into the desired 138 bp fragment with equal efficiency whether mutant standard or wt-sequence served as template. Either 5×10^{10} or 10^8 initial copies of the templates were amplified for 10 or 14 PCR cycles, respectively. The lower portion of Figure 2 compares the amounts of 138 bp fragment synthesized from 10^5, 10^3 and 10 copies of the two templates after 29 and 34 PCR cycles directly by ethidiumbromide staining on a 2% agarose gel. The results indicate comparable amplification efficiencies for PvuII mutant standard- and wt-template also at low numbers of initial copies and high cycle numbers.

Rescue of PvuII mutant standard from excess wild-type sequence 1646–1784 of c-Ha-ras1

The capability of the RFLP/PCR method to rescue a small number of copies of PvuII mutant standard from a large excess of wt sequence was investigated. Mixtures were prepared of 10 and 100 copies of XbaI/SmaI digested mutant standard pSP64-ras PvuIISt with 10^8 copies of exhaustively PvuII digested pSVneo-ras1 and of 1000 copies of mutant standard with 10^9 copies PvuII digested pSVneo-ras1. The mutant standard was restricted with XbaI/SmaI in order to release a 272 bp fragment similar in size to the 256 bp ras-fragment which is liberated by PvuII from pSVneo-ras1 containing a mutation in the PvuII site 1727–1732. The mixtures were amplified with repeated restrictions with PvuII in 30 cycles with 'non-clonable' amplimers and 10 final cycles with amplimers containing tails with EcoRI recognition sequences (see 'Methods' and Figure 1). The 163bp amplified fragments were cloned into λgt10 and plaques were analyzed by oligonucleotide hybridization for their content in wt ras1 sequence 1719–1738 and mutant standard sequence.

The results summarized in Table 1 show that as few as 10 copies of PvuII mutant standard were rescued from 10^8 copies of wt-sequence giving rise to 7.3% of total plaques. Increasing initial copy numbers of PvuII mutant standard gave rise to larger fractions of plaques containing the mutant standard sequence. The fractions of wt-plaques varied from 14 to 23%.

ANALYSIS OF AMPLIFICATION MIXTURE BY λ -PLAQUE HYBRIDIZATION *

Mutant standard	Wild type	Mutant standard % plaques	Wild type % plaques
10	10^8	7.3 ± 0.8	23.3 ± 1.2
100	10^8	13.9 ± 1.3	14.3 ± 1.4
1000	10^9	18.0 ± 1.7	20.4 ± 1.7

* Plaques containing mutant standard or wild-type sequence at the PvuII recognition sequence (# 1727 - 1732). Phage from at least 2 packagings were used and plaques on 10-15 petri dishes were analysed.

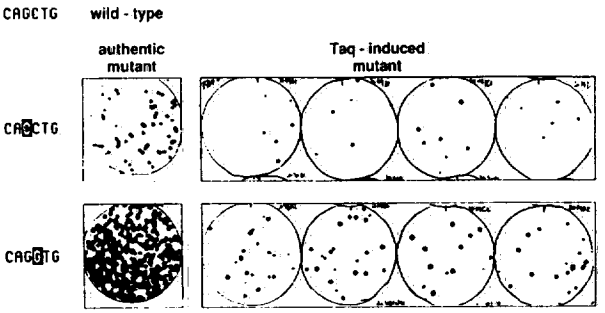

Figure 3. Analysis of λ-plaques for base-pair mutations in PvuII-recognition sequence 1727–1732 of c-Ha-ras1. Mixtures of a few copies of mutant standard pSP64-ras PvuIISt with 10^8 copies of wild-type pSVneo-ras were processed by the RFLP/PCR protocol described in 'Methods'. The amplification product was cloned into λgt10, plaques transferred to plaque screens and analyzed by hybridization with ^{32}-P-end-labeled mutant oligonucleotide probes for Taq-polymerase induced single bp mutations in the PvuII recognition sequence 1727–1732. The selectivity of the washing conditions was ascertained for each mutation with authentic mutant constructs. Upper half, left-side: plaques containing authentic mutant CACCTG; right-side: plaques on 4 plates with same mutation originating from the amplification mixture. Lower half, left-side: plaques containing authentic mutant CAGGTG; right-side: plaques on 4 plates with the same mutation originating from the amplification mixture.

Taq-polymerase errors in PvuII-site 1727–1732 of c-Ha-ras1

Despite exhaustive restriction with PvuII before and during amplification a small amount of intact wt-sequences undoubtedly remains, will be amplified and can give rise to Taq-polymerase errors. Amplified sequences containing Taq-polymerase errors in the PvuII recognition sequence 1727–1732 are resistant to digestion and will be cloned. The ultimate sensitivity of the RFLP/PCR method for a particular bp in the chosen recognition site depends on the error-rate of Taq-polymerase for the replication of this bp. Therefore, we probed λ-plaques resulting from the mixtures of mutant standard with excess wt-sequence for their content of Taq-polymerase induced single bp changes in the internal tetranucleotide AGCT of the PvuII recognition sequence. The plaques were probed with specific oligonucleotides for all 12 possible mutations. Figure 3 shows an example in which discs had been probed for a G→C transversion giving rise to

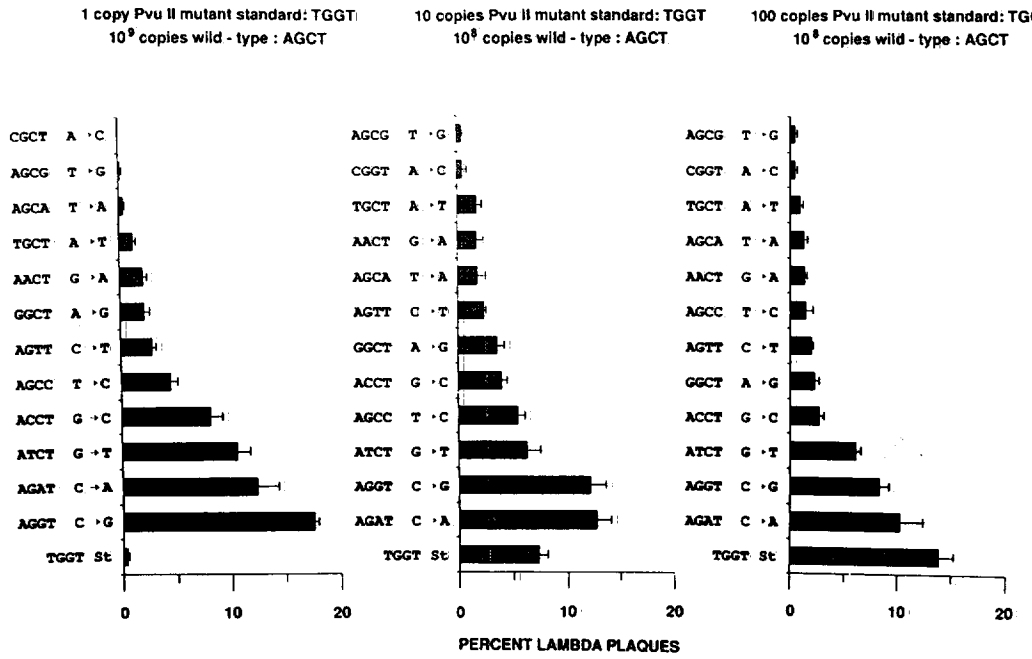

Figure 4. Spectrum of Taq-polymerase induced base-pair mutations in the PvuII-site 1727–1732 of exon 1 of c-Ha-ras1. Mixtures of a few copies of mutant standard pSP64-ras PvuIISt with 10^8 or 10^9 copies of wild-type pSVneo-ras were processed by the RFLP/PCR protocol as described in 'Methods'. λ-plaques were transferred onto plaque screens and analyzed for their content of all 12 possible bp mutations in the internal tetranucleotide AGCT of the PvuII- recognition sequence by hybridization with ^{32}-P-end-labeled oligonucleotide probes. The results represent means from two λ-packagings and 10–15 petri dishes containing 100–200 plaques for each experimental condition. The selectivity of the conditions for each probe was ascertained with authentic mutant constructs. Individual plaques only hybridized with a single probe (see 'Methods').

CACCTG occurring with moderate frequency (upper portion) and a C→G transversion giving rise to CAGGTG which represents a frequent Taq-induced mutation in the PvuII site (lower portion). In all cases the specificity of the probing conditions was ascertained with mixtures of authentic mutant constructs and by assuring that each plaque only hybridized with a single oligonucleotide probe.

Figure 4 compares the frequencies of the 12 possible Taq-polymerase induced bp changes at the internal tetranucleotide A-GCT of the PvuII-site in 3 independent amplification experiments in which 10^9 (Figure 4A) and 10^8 initial copies of wt pSVneo-ras1 (Figure 4B & C) were used, respectively. While there are small quantitative differences the following consensus can be reached for the relative abundance of Taq-induced errors: C→A(AGAT) ≅ C→G(AGGT) > G→T(ATCT). Since the amount of wt-copies which remain undigested during the amplification cycles is not known absolute Taq-error frequencies cannot be derived from our data. In contrast, from a comparison to the data with the mutant standard it is evident that less than 10 copies containing a single bp mutation in the presence of 10^9 copies of wt-sequence can readily be detected for mutations with low Taq-error frequencies, e.g. for A→C(CGCT); T→G(AGCG); T→A(AGCA); A→T(TGCT); G→A(AACT).

Rescue of a single base pair mutation in MspI-site 1695–1698 from excess wild-type c-Ha-ras1 DNA

The rescue of mutant standard such as pSP64-ras PvuIISt with multiple bp changes in a chosen restriction site from excess wt sequences is not affected by Taq-polymerase errors. In contrast, the sensitivity of the detection of single bp mutations is limited by polymerase errors originating from the amplification of residual undigested wt sequences. We assessed the capacity of the RFLP/PCR protocol to rescue a few copies of the c-Ha-ras1 exon 1 fragment 1646–1784 containing a G→T transversion at residue 1698 which is part of the MspI-site 1695–1698 from a large excess of wt c-Ha-ras1 DNA. The chosen mutation affects the middle bp of codon 12 and was detected in the c-Ha-ras1 gene of the EJ human bladder carcinoma line (8) (see Figure 1 for sequence information). Three samples were analyzed by RFLP/PCR (1) 10^8 copies of exhaustively MspI/HpaII digested wt pSVneo-ras1 (2) 100 copies mutant pSP64-ras1-T1698 (XbaI/EcoRI restricted) plus 10^8 copies MspI/HpaII digested pSVneo-ras (3) 1000 copies mutant pSP64-ras1-T1698 (XbaI/EcoRI restricted) plus 10^8 copies MspI/HpaII digested pSVneo-ras1. The samples were amplified with repeated MspI restrictions in 35 cycles with 'non-clonable' amplimers and 10 final cycles with amplimers containing tails with EcoRI recognition sequences (see Figure 1 and Methods). The amplified 136 bp fragments were cloned into λgt10 and plaques analyzed by hybridization with 20-mer oligonucleotides corresponding to the wt c-Ha-ras1 sequence 1688–1707 and with the mutant sequence containing a T-residue at position 1698. From the results shown in Figure 5 it is evident that Taq-polymerase amplification of residual wt ras1 DNA which escaped restriction at the MspI-site 1695–1698 generated 12% λ-plaques with G→T transversions at residue 1698 for the sample containing only 10^8 copies of pSVneo-ras1 at the outset. The percentage of plaques containing G→T transversions at residue 1698 was 23% for the initial mixture of 100 copies mutant pSP64-ras1-T1698 with 10^8 copies of wt pSVneo-ras1 corresponding to a 2 fold increase over

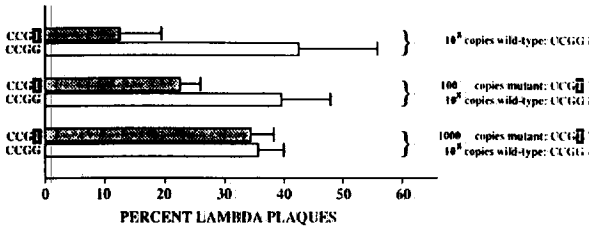

Figure 5. Rescue of a single base pair mutation in the MspI-site 1695–1698 of c-Ha-ras1 from excess wild type DNA. Three samples of c-Ha-ras1 DNA were analyzed by the RFLP/PCR protocol for mutations in the MspI-site 1695–1698: (1) 10^8 copies of exhaustively MspI/HpaII digested pSVneo-ras1 (2) 100 copies of mutant pSP64-ras1-T1698 (xbaI/EcoRI digested) plus 10^8 copies MspI/HpaII digested pSVneo-ras1 (3) 1000 copies mutant pSP64-ras1-T1698 (XbaI/EcoRI digested)plus 10^8 copies MspI/HpaII digested pSVneo-ras1. The conditions for amplification, cloning of the amplified fragments into λgt10 and analysis of plaques by hybridization with ^{32}P-end-labeled wt- and mutant (T1698) oligonucleotide probes are described under 'Methods'. Results are derived from 2 independent packagings and 600–1100 plaques on 4–6 Petri dishes. Error bars represent standard deviations.

the fraction produced by Taq-polymerase infidelity. At 1000 initial copies of mutant pSP64-ras1-T1698 plus 10^8 copies wt pSVneo-ras1 the percentage of mutant plaques had increased to 34%. The Figure also gives the percentage of plaques which contained wt-sequence 1688–1707.

DISCUSSION

The aim of the present work was to test the feasibility to use the RFLP/PCR approach for the development of a genotypic mutation system. Such a system should be capable of measuring low frequency mutations in any gene of known sequence without the need for the phenotypic selection of mutated cells (6). In the RFLP/PCR approach wt-sequences are selectively removed by exhaustive restriction and resistant sequences are amplified by PCR. We have chosen the tetranucleotide AGCT of PvuII recognition site for our studies because it contains all 4 nucleotides. While the composition of the PCR product reflects the initial mixture of mutations it does not allow the estimation of absolute mutation frequencies. Therefore, we are using an internal 'mutant standard' for calibration. We have constructed a mutant standard with 2bp changes in PvuII recognition site and a third mutation upstream. This allows the distinction between λ-plaques containing mutant standard from plaques containing single bp mutations in the final analysis with specific probes. In the present experiments we have used the mutant standard pSP64-ras PvuIISt to evaluate the capacity of the RFLP/PCR protocol to rescue a few copies of mutated sequences in the PvuII site 1727–1732 from a large excess of wt c-Ha-ras1 without interference by Taq-polymerase errors. We have ascertained that mutant standard and wt-sequences are amplified with equal efficiencies (see Figure 2). Our results indicate (Table 1) that 10 copies of mutant standard were readily rescued from 10^8 to 10^9 copies of wt-DNA. While the fraction of mutant standard plaques increased with increasing copy number there is no simple relationship between the two parameters.

In contrast to the rescue of mutant standard the sensitivity of the detection of single bp mutations depends on the frequency of polymerase errors during the replication of a particular bp. Only polymerase errors originating from wt-sequences will interfere since errors in already mutated sequences will give rise to double mutations which are not detected with oligonucleotide probes containing a single altered base. Therefore, the final polymerase error frequencies will depend on the completeness of the removal of wt-sequences by restriction and our protocol employs several steps of restriction before and during amplification. We used conditions for the amplification reaction which were expected to yield relatively low Taq-polymerase errors (10) but retained high amplification efficiency, i.e. Mg^{2+} concentration of 6.7 mM, a total concentrations of dNTPs of 4 mM but a relatively high pH of 8.2 (70°C). The data in Figure 4 attests to the large differences in Taq-polymerase errors depending on the type of bp and the sequence. The replication of G.C bp produced more errors then the replication of A.T bp and transversions were considerably more frequent than transitions. Sequence dependence is indicated by the fact that the C→G transversion (AGGT) was more frequent than the G→C transversion (ACCT) and the C→A transversion (AGAT) more frequent than the G→T transversion (ATCT). Comparison of the three panels in Figure 4 indicates that the fraction of plaques with Taq-polymerase errors did not change significantly when the initial number of wt-copies was increased from 10^8 to 10^9. Under the latter conditions a single copy of mutant standard resulted in 0.3% mutant standard plaques. We estimate that at best RFLP/PCR analysis at PvuII-site 1727–1732 is capable of rescueing 1–5 copies of a single bp mutation from 10^9 copies of c-Ha-ras1 for mutations with low Taq-polymerase error frequencies, e.g. for A→C (CGCT), T→G (AGCG), A→T (TGCT) and T→A (AGCA). It is conceivable that polymerase errors can be further reduced by modifying the amplification conditions (10,11) and consequently that the sensitivity of our RFLP/PCR protocol can be increased.

We have further assessed the sensitivity of the RFLP/PCR protocol for the rescue of a single bp mutation in the MspI-site 1695–1698 of exon 1 of c-Ha-ras1. Unlike the rescue of a doubly mutated standard such as pSP64-ras PvuIISt the capacity to rescue a single bp mutation is limited by backgrounds caused by polymerase errors. The experimental conditions were analogous to the PvuII-site 1727–1732 with the exception that nested 'clonable' left-side amplimer was used for the final 10 PCR cycles. The chosen mutant results from a G→T transversion at bp 1698 which represents the middle bp of codon 12. Mutations in this ras-codon are frequently detected in the DNA from human tumor tissues (1) and the particular G→T transversion studied in the present work had been first detected in the EJ human bladder carcinoma line (8). Our results show that 100 copies of a ras1 fragment containing a mutated MspI-site 1695–1698 with a T-residue in position 1698 could be readily rescued from 10^8 copies of wt ras1 DNA. As expected from the analysis of the PvuII-site 1727–1732 under similar experimental conditions the G→T transversion at bp 1698 represents a relatively frequent Taq-polymerase error. The fraction of plaques containing the T1698 mutation was 12% for the sample composed initially of only wt DNA. This value is comparable to 11% for the frequency of Taq-polymerase induced G→T transversions at bp 1729 in the PvuII-site 1727–1732 for the sample containing initially only 1 copy of PvuII mutant standard but 10^9 copies of wt ras1 DNA.

The predominance of transversions involving G.C bp in our experiments disagrees with published work in which A.T.→G.C

transitions were reported to be the most frequent Taq-polymerase errors (10,11,12,13). Differences in the amplification conditions may be responsible for these discrepancies; e.g. high ratios of concentrations of Mg^{2+}/total dNTPs in several published reports relative to a ratio of 1.7 in the present work; the use of relatively high concentrations of DMSO in our work in contrast to previous authors etc.. It should be stressed that our data does not allow it to calculate absolute error-frequencies for Taq-polymerase because the amount of residual, unrestricted wt-sequence in the amplification mixture cannot be assessed by the RFLP/PCR protocol.

In conclusion, the RFLP/PCR protocol described here allows the analysis of point mutations (bp-changes, small deletions and insertions) in any gene of known sequence without the need to select mutated cells on the basis of an altered phenotype. The method is highly sensitive and relatively simple but limited to mutations which result in the elimination of a restriction site. The experimental design of the RFLP/PCR approach to genotypic mutation analysis has been discussed previously (14,15).

ACKNOWLEDGEMENTS

This work was supported by the Swiss National Science Foundation and th[redacted] Manufacturers [redacted] International Cancer Research.

REFERENCES

1. Bos, J.L. (1988) Mutat. Res. 195, 255–271.
2. Baker, S.J., Fearon, E.R., Nigro, J.M., Hamilton, S.R., Presinger, A.C., Jessup, J.M., van Tuinen, P., Ledbetter, D.H., Barker, D.F., Nakamura, Y., White, R. and Vogelstein, B. (1989) Science 244, 217–221.
3. Nigro, J.M., Barker, S.J., Preisinger, A.C., Jessup, J.M., Hostetter, R., Cleary, K., Bigner, S., Davidson, N., Baylin, S., Devilee, P., Glover, T., Collins, F., Weston, A., Modali, R., Harris C., and Vogelstein, B. (1989) Nature 342, 705–708.
4. Takahashi, T., Nau, M., Chiba, I., Birrer, M., Rosenberg, R., Vinocour, M., Levitt, M., Pass, H., Gazdar, A. and Minna, J. (1989) Science 246, 491–494.
5. See in 'Mutation and the Environment. Part C: Somatic and Heritable Mutation, Adduction and Epidemiology' (1989) (ed.) Mendelsohn, M. and Albertini, R., Wiley-Liss.
6. Rossiter, B. and Caskey, C.T. (1990) J. Biol. Chem. 265, 12753–12756.
7. Parada, L., Tobin C., Shih, C. and Weinberg, R. (1982) Nature 297, 474–478.
8. Capon, D., Chen, E., Levinson, A. Seeburg, P. and Goeddel, D. (1983) Nature 302, 33–37.
9. Salmons, B., Groner B., Friis, R., Muell, D., and Jaggi , R. (1986) Gene 45, 215–220.
10. Eckert, K., and Kunkel, T. (1990) Nucl. Acid. Res. 18, 3739–3743.
11. Keohavong, P. and Thilly, W. (1988) Proc. Natl.Acad. Sci. 86, 820–823.
12. Saiki, R., Gelfand, D., Stoffel, S., Scharf, S., Higuchi, R., Horn, G. Mullis, K. and Erlich, H. (1988) Science 239, 487–491.
13. Tindall, K. and Kundel, T. (1988) Biochemistry 27, 6008–6013.
14. Zijlstra, J., Felley-Bosco, E., Amstad, P. and Cerutti, P. (1990) in 'Mutagens and Carcinogens in the Diet' pp. 187–200 (eds. M. Pariza et al), Wiley-Liss, New York.
15. Parry, J., Shamsher, M., and Skibinski, D., (1990) Mutagenesis 5, 209–212.